Effect of selected Flavonoids and Polyphenols on Key Elements involved in the Regulation of the Glucose/Glycogen Homeostasis and the Wnt Signalling Pathway

Dem Fachbereich Chemie der Technischen Universität Kaiserslautern
zur Verleihung des akademischen Grades
„Doktor der Naturwissenschaften“
eingereichte Dissertation

(D386)

Vorgelegt von
Diplom Lebensmittelchemiker
Yufanyi Ngiewih

Betreuer: **Prof. Dr. G. Eisenbrand**

Kaiserslautern, 2008

Die vorliegende Arbeit entstand zwischen Mai 2004 und Februar 2007 im Fachbereich Chemie, Fachrichtung Lebensmittelchemie und Umwelttoxikologie der Technischen Universität Kaiserslautern.

Eröffnung des Promotionsverfahrens:
Tag der wissenschaftlichen Aussprache: 28.02.2008

Prüfungskommission:

Vorsitzender: **Prof. Dr. Helmut Sitzmann**

1. Berichterstatter: **Prof. Dr. Gerhard Eisenbrand**

2. Berichterstatter: **Prof. Dr. Doris Marko**

The doctor of the future will give no medicine, but will interest her or his patients in the care of the human frame, in a proper diet, and in the cause and prevention of disease.

Thomas A. Edison

US inventor (1847 - 1931)

A

ADP	*Adenosine diphosphate*
AMP	*Adenosine monophosphate*
APC	*Adenomatous polyposis coli*
Arg	*Arginine*
ASEF	*APC stimulated guanine nucleotide exchange factor*
ATP	*Adenosine triphosphate*

B

BGP	*Brain glycogen phosphorylase*
BSβG	*Broad specific β-glycosidase*

C

cAMP	*Cyclic AMP*
CBP	*CREB binding protein*
CK	*Casein kinase*
COMT	*Catechol-O-methyltransferase*
COX-2	*Cyclooxygenase*
CRC	*Colorectal cancer*
CREB	*cAMP responsive element binding protein*
CTNNB1	*β-catenin gene*
CYP	*Cytochrom*

D

Dkk-1	*Dickkopf-1*
DMSO	*Di methylsulfoxideα*
DNA	*Deoxyribonucleic acid*
Dvl	*Dischevelled*

E/F	
ECG	*(-) Epicatechin gallate*
EGCG	*(-) Epigallocatenine-3-gallate*
EphB2/B3	
Fz	*Frizzled*
G	
G-6-P	*Glucose-6-phosphate*
GIT	*Gastrointestinal tract*
GLUT	*Glucose transporter*
GP	*Glycogen phosphorylase*
GPRC	*G-protein coupled receptor*
GS	*Glycogen synthase*
GSK-3	*Glycogen synthase kinase-3*
H	
HEK293	*Human embryonale kidney cells*
HepG2	*Human hepatocyte cancer cell line*
HMG	*High mobility group*
HT29	*Human colorectal cancer cell line*
K/L	
KAPS	*Kinesin super family associated protein*
Lef	*Lymphoid enhancer factor*
LGP	*Liver glycogen phosphorylase*
LGS	*Liver glycogen synthase*
LRP5/6	*Low density lipoproteins receptor protein*
Lys	*Lysine*

M/N

MAP *Mitogen activated protein*

MCT *Monocarboxylate transporter*

MGP *Muscle glycogen phosphorylase*

MGS *Muscle glycogen synthase*

Min *Multiple intestinal neoplasia*

mRNA *Messenger RNA*

MRP *Multidrug related protein*

NOC *N-nitroso compounds*

P

PAPS *3'phospho adenosine 5'phosphosulfate*

PCR *Polymerase chain reaction*

PhK *Phosphorylase kinase*

P13K *Phosphatidyl inositol-3-kinase*

PKA *Protein kinase A*

PKB *Protein kinase B*

PPA1/2 *Protein phosphatase-1/2*

R/ S/T

RNA *Ribonucleic acid*

RT-PCR *Real time polymerase chain reaction*

RXR *Retinoid X receptor*

SAM *S-adenosylmethionine*

SAMP *Serine-alanine-methionine-prolin*

Ser *Serine*

SGLT *Sodium dependent glucose transporter*

Siah

SULT	*Sulfotransferase*
TA	*Transit amplifying cells*
TCF	*T-cell factor*
Thr	*Threonine*
β-Trcp	*β-Transducin repeat containing protein*
U	
UDP	*Uridyl diphosphate*
UDPGT	*UDP glycuronosyl transferase*
W	
WHO	*World health organisation*
Wnt	
Y	
Y, Tyr	*Tyrosine*

1 Introduction

Colorectal cancer is the second most prevalent cancer form in both men and women in the Europe. In 2002, alimentary cancer (oesophagus, stomach, intestines) made up 26% of the annual incident cases of cancer amongst males in Europe, whereby about half of those were cancers of the colon and rectum (Eurostat 2002). Epidemiological evidence accumulating over the last decades indicates that besides a genetic disposition, diet plays a strong epigenetic role in the genesis of cancer. It is generally assumed that diet is causal for up to 80% of colorectal cancer (Bingham 2000). With the prospect of an approximated 50% rise in global cancer incidence over the first two decades of the 21st century, the World Health Organisation (WHO) has emphasized the need for an improvement in nutrition. Indeed there is increasing public health awareness with respect to nutrition. Today, living healthily is associated with less consumption of animal fats and red (processed) meat, moderate or no consumption of alcohol coupled with increased physical activity, and frequent intake of fruits, vegetables and whole grains (Bingham 1999; Johnson 2004). This idealogy partly stems from scientific epidemiological evidence supportive of an inverse correlation between the consumption of fruits and vegetables and the development cancer. Besides fibre and essential micro-nutrients like ascobate, folate, and tocopherols, the anti-carcinogenic properties of fruits and vegetables are generally thought to be rooted in the bioactivity of secondary plant components like flavonoids (Johnson 2004; Rice-Evans and Miller 1996; Rice-Evans 1995).

Along with the increased public health awareness, has also come a burgeoning and lucrative dietary supplement industry, which markets products based on polyphenols and other potentially healthy compounds, sometimes with questionable promises of better health and increased longevity. These claims are based on accumulating *in vitro* and *in vivo* evidence indicating that flavonoids and polyphenols in fruits and vegetables can hinder proliferation, induce apoptosis of cancerous cells (Kern et al. 2005; Kumar et al. 2007; Thangapazham et al. 2007), act as antioxidants (Justino et al. 2006; Rice-Evans 1995) and influence cell signalling pathways (Marko et al. 2004; Joseph et al. 2007; Granado-Serrano et al. 2007), all of which are potential mechanisms proposed for their anti-carcinogenic activity. However, not only is the vast variety of supplements worrisome, but also problematic, is their easy accessibilty (just a click away on the internet) and the amount that can potentially be consumed. Such supplements are usually offered in pharmaceutical form (tablets, capsules, powder,

concentrates) containing concentrations well beyond what is normally comsumable from the diet. For example, quercetin's recommended intake is about 1g daily. However, estimates portend a possible daily increase of upto 1000 fold of the daily intake of quercetin (Hertog et al. 1995). Mindful of the concept of dose coined from the words of swiss scientist Paracelsus "What is it that is not poison? All things are poison and nothing is without poison. The right dose differentiates a poison and a remedy." ("Alle Dinge sind Gift und nichts ist ohn' Gift; allein die Dosis macht, dass ein Ding kein Gift ist"), it is thus conceivable that such high concentrations may not only reverse the acclaimed positive effects of flavonoids and polyphenols but also have negative effects thereby representing a health risk. The fact that direct evidence of the beneficial effects of flavonoids and polyphenols remains wanting, if not entirely lacking, coupled with the afore-mentioned marketing trend demands for a thorough examination of the possible adverse effects that may arise from increased consumption of flavonoids and polyphenols.

The genesis and progression of cancer is usually accompanied by dysfunctional signalling of certain cell signalling pathways. Typical for colon carcinogenesis is the malfunctioning of the Wnt-signalling pathway, a pathway, which is crucial for the growth and development of normal colonocytes. The dysfunction of the Wnt-signalling pathway occurs in a manner that culminates in a proliferation stimulus of colonocytes, while differentiation is increasingly minimized. Hence, tumourigenesis is promoted. Interupting the proliferation stumuli by intervening in the actions of components of the Wnt-signalling pathway is one potential mechanism for the anti-carcinogenic action of flavonoids and polyphenols (Pahlke et al. 2006; Dashwood et al. 2002; Park et al. 2005). However, as previously hinted, the indulgence in the consumption of flavonoids and polyphenols based supplements could instead lead to a proliferation stimulus and provoke or promote carcinogenesis in normal cells or pre-cancerous cells respectively.

2 Theory

2.1 Colon, Wnt-signalling and Colorectal Cancer

2.1.1 Colon

The intestinal tract consists of the small intestine (duodenum, jejunum and ileum) and the large intestine (colon, rectum). A single layer of epithelium cells lines the surface of the small and large intestines. The epithelium of the small intestine is arranged in two functional and morphological distinct compartments: flask-shaped submucosal invaginations known as crypts of Lieberkühn, and finger-shaped luminal protrusions termed villi. Differentiated cells (enterocytes, enteroendocrine cells and goblet cells) occupy the villi (figure 1). A fourth differentiated type, the Paneth cell (Porter 2002; Reya and Clevers 2005), resides at the bottom of the crypts and secretes antimicrobial agents. The remainder of the crypts constitutes the stem/progenitor compartment (figure 1). While the cells of the crypts that form the proliferative unit are monoclonal, the differentiated cells of the villi originate from different crypts and are polyclonal.

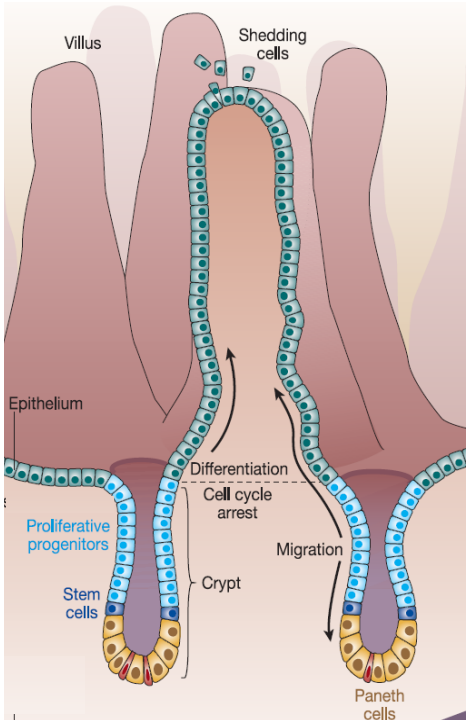

Figure 1: Architecture of the small intestine showing the putative stem cells (blue) directly placed above the paneth cells (yellow), which reside at the bottom of the crypt. Differentiated cells (green) consisting of enterocytes, goblet cells, and enteroendocrine cells populate the villi (Reya and Clevers 2005).

The colonic epithelium has larger crypts than the small intestines and there are no villi present. Instead the mucosa of the colon has a flat surface epithelium (figure 2). Proliferative stem and precursor cells occupy the bottom two-thirds of the crypts, whereas differentiated cells constitute the surface epithelium and top third of the crypts.

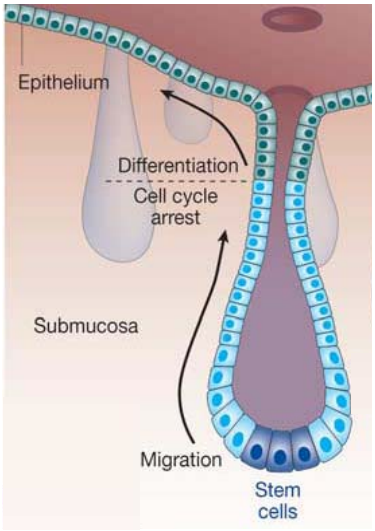

Figure 2: Tissue anatomy of the adult large intestine. Putative stem cells (dark blue) populate the bottom of the crypt. Proliferating progenitor cells (light blue) occupy two thirds of the crypt. Differentiated cells make up the rest one third and surface of the epithelium, which in contrast to the small intestine is a flat surface (Reya and Clevers 2005).

The life cycle of the cells in the small intestine starts from the multipotent stem cells located in the crypt, which divide and morph in to the fast dividing transit-amplifying cells (TA). The TA cells (progenitor cells), with a division rate of approx. 150 cells every 12h, expand into non-proliferating daughter cells, which accumulate in the medium third (figure 1) of the crypt to subsequently differentiate into the four cell lineages; enterocytes (90% of villus-associated cells) (Pinto and Clevers 2005), enteroendocrine cells (secrete hormones like serotonin) (Hocker and Wiedenmann 1998), paneth cells (secrete antibacterial peptides) (Porter 2002), and the goblet cells (mucous secreting) (Pinto and Clevers 2005). Differentiation of the cells is completed as the cells (enterocytes, goblet cells, enteroendocrine cells) migrate, upwards to the tip of the villi and in the case of the paneth cells, toward the base of the crypt, where they reside for about 20 days (Garabedian et al. 1997; Bry et al. 1994). The epithelium of the small intestine is renewed in man every 5 days (Wright and Irwin 1982). This corresponds to the time it takes for a differentiated cell to reach the tip of the villi where it dies and is exfoliated into the lumen (about 1400 dead cells on a daily basis) (Potten and Loeffler 1990). The canonical Wnt-signalling pathway controls the homoeostasis of the intestinal epithelium. In the next section, the crux of the pathway (which is most crucial for colon cancer initiation) is presented.

2.1.2 Wnt-signalling

The Wnt-signalling pathways encompass three different molecular pathways, namely; the Wnt/*β*-catenin pathway also referred to as canonical Wnt-pathway, the Wnt/Ca^{2+} pathway and lastly, the Wnt/JNK pathway. The last two pathways both make up the non-canonical Wnt-pathway (Janssens et al. 2006; Kuhl et al. 2000). Signal transduction via the Wnt-pathways is initiated when a Wnt ligand protein engages a cognate frizzled (Fz) trans-membrane receptor. Which of the three pathways is subsequently activated depends upon which Wnt ligand and Fz receptor is present and interacts. Twenty different Wnt ligands (Reya and Clevers 2005), classified in two functional groups, have been identified in mammals. The transforming group, also called the proto-oncogenic group or Wnt1 class, consists of Wnt1, -3A, -8, -8B and act via the Wnt-*β*-catenin pathway, whereas the Wnt proteins of the second group (Wnt5A class) e.g., Wnt4, -5A, and -11) stimulate transduction through the non-canonical pathways and act also to antagonize the canonical pathway (Du 1995; Kuhl 2002; Torres 1996.)

In the following section, only the Wnt/*β*-catenin pathway will be discussed in detail because of its immediate relevance to cancer.

2.1.2.1 Canonical Wnt-signalling Pathway in normal Intestine Cells

The canonical Wnt pathway regulates fundamental aspects of maintenance of intestinal and colonic cells. It is intricate in the regulation of processes like cell fate, proliferation, differentiation and apoptosis by controlling the intra-cellular levels of free cytoplasmic *β*-catenin (Cadigan and Nusse 1997; Malbon 2005).

At the bottom of the crypt, the Wnt proteins promote the proliferation of progenitor cells by accumulating *β*-catenin. The presence of an appropriate Wnt protein stimuli, causes the Fz receptors binding to the obligate low density lipoproteins receptor protein (LRP5/6) 5/6 co-receptors forming a trimeric complex (Tamai et al. 2000; Pinson et al. 2000). As a result dishevelled (Dvl) becomes phosphorylated. Phosphorylated Dvl associates with the

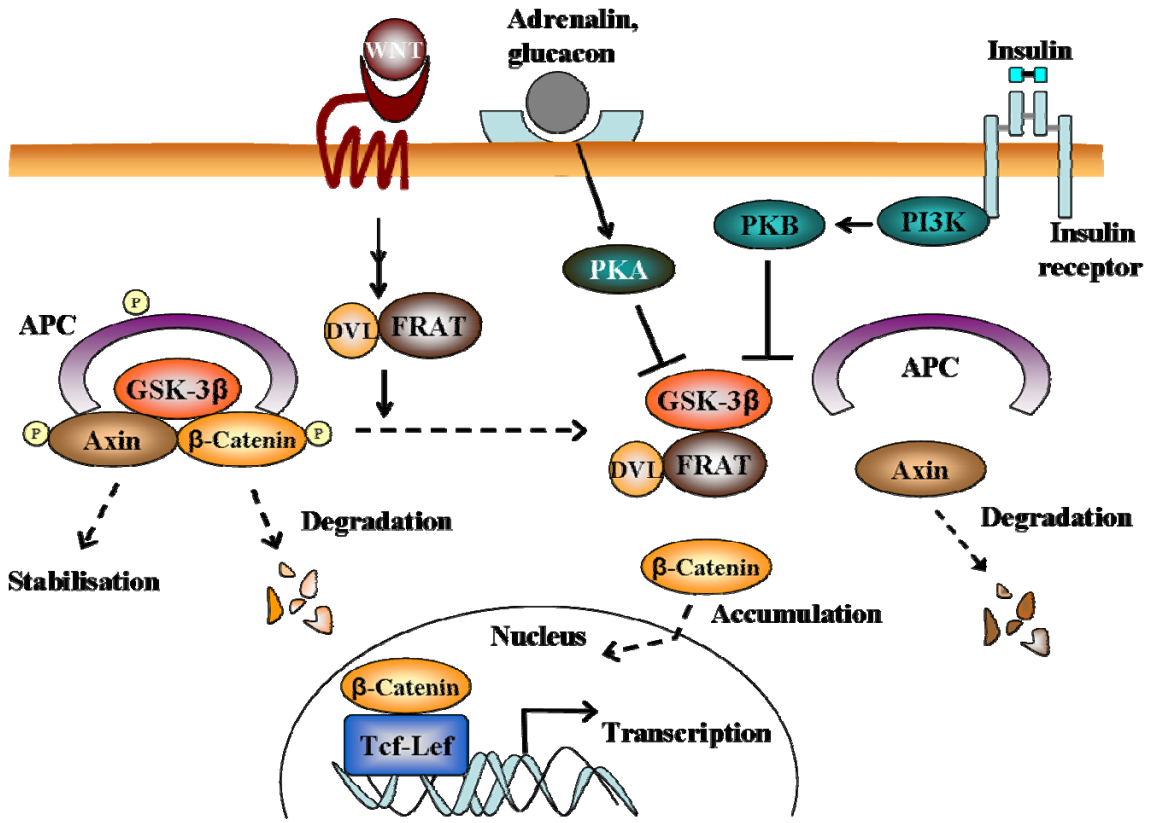

Figure 3: **The Wnt-signalling pathway. APC, adenomatous polyposis coli; Dvl, dishevelled; GSK-3, glycogen synthase kinase-3; PKA, protein kinase A; PKB, protein kinase B; PI3K, phosphatidylinositol 3-kinase; Tcf/Lef, T-cell factor-lymphoid enhancer factor.**

adenomatous polyposis coli (APC)/axin protein complex, where it acts in concert with Frat to interupt the phosphorylation of *β*-catenin by casein kinase I*α* (CK I*α*) and glycogen synthase kinase-3 (GSK-3) from (figure 3). The result is the dissociation of the APC complex and the subsequent breakdown of axin. Due to the failure of the phosphorylation of *β*-catenin, it escapes degradation because it is not recognized by *β*-transducin repeat containing protein (*β*-Trcp), a component of an E3 ubiquitin ligase complex that initiates the destruction of phosphorylated *β*-catenin. Consequentially, *β*-catenin accumulates in the cytoplasm from where it translocates in to the nucleus and engages T-cell factor-4 (TCF-4) DNA binding protein and co-activators, like CREB binding protein (CBP) and the chromatin-remodelling protein Brg-1 to induce the expression of pro-proliferation steering proteins like COX-1, c-myc, cyclin D1 and the tyrosine kinase guidance receptors ephrinB2 and ephrinB3 (Hecht A 2000; Hsu et al. 1998; van Noort and Clevers 2002).

Halfway up the crypt, Wnt protein actions in the progenitor cells are repressed so that free *β*-catenin is actively targeted for degradation. Various secreted factors, such as cerberus and frizzled-related proteins, bind to Wnt ligands and block their interaction with Fz. Dickkopf-1 (Dkk-1) secreted protein potently and specifically antagonizes canonical Wnt action by blocking access to the LRP5/6) co-receptors. Dkk-1 can induce LRP5/6 internalization and its subsequent removal from the plasma membrane, by cooperating with kremen 1/2 transmembrane proteins (Kawano and Kypta 2003). In the absence of Wnt signal stimulus, *β*-catenin is sequentially phosphorylated within the APC multi-protein complex composed of APC, axin, GSK-*3*, CK-I*α* and *β*-catenin (figure 3). Within the stabilized APC-axin complex, *β*-catenin phosphorylation is mediated by CK I*α* and GSK-3 in this order. The phosphorylation of *β*-catenin permits its recognition by *β*-Trcp, and subsequent proteasomal degradation. The intra-nuclear *β*-catenin levels are consequently reduced so that Tcf-*β*-catenin complex formation is held below the threshold required to stimulate Wnt-target gene expression. Concomitantly, proteins of the Groucho family interact and bind Tcf/lef transcriptional factors to repress the expression Wnt target genes. At this stage in the development/migration of the progenitor cells (Halfway up the crypt), differentiation of the cells into the various functional cell types commences (Hurlstone and Clevers 2002; Cavallo et al. 1998; Waltzer and Bienz 1999; Brantjes et al. 2001).

The Wnt signalling pathway is potentially influenced by crosstalk from other signalling pathways. Protein kinase A (PKA) of the cAMP signalling pathway and protein kinase B (PKB), of the insulin phosphatidylinositol-3-kinase pathway are able to phosphorylate GSK-3 (figure 3) and cause its inactivation (Du 1995; Jensen et al. 2007; Liu et al. 2006).

2.1.2.2 Canonical Wnt-signalling in Colorectal Cancer

There is strong evidence that dysregulation of Wnt-signalling is crucial for cell transformation in different human diseases including cancer. Germline or somatic mutations of genes encoding components of the Wnt-signalling pathway like APC or axin, or site specific substitutions in the N-terminus of *β*-catenin, are mutations which have been found to be prominent in some cancer types, including colorectal cancer (Liu et al. 2000; Fukushima 2001; Kim et al. 2003b; Ilyas et al. 1997; Smith et al. 1993). APC mutations (most of which

are truncation mutations) with approximately 85% occurrence, are the most frequent form of mutation in sporadic colorectal cancer (Waterman 2004). 10% of sporadic tumours, which do not harbor an APC aberration, have a mutation in the *β*-catenin gene (*CTNNB1*) (Smith et al. 1993). Over 70 *β*-catenin mutations have been reported in colorectal cancers, most of which are mis-sense mutations (Kim et al. 2003a). These mutations (APC, *β*-catenin, axin) preclude the degradation of *β*-catenin (described in chapter 2.1.2.1). The result is a shift in the homeostasis of *β*-catenin towards stabilization, leading to surge in cytoplasmic and nuclear levels of free *β*-catenin (Maruyama 2000; Hao 1997) and the constitutive expression of Wnt target genes. As a result, the termination of proliferation and the onset of differentiation of the progenitor cells into functional progeny is prevented (figure 4, right) a process, which normally occurs half-way up the crypt axis is prevented (figure 4, left).

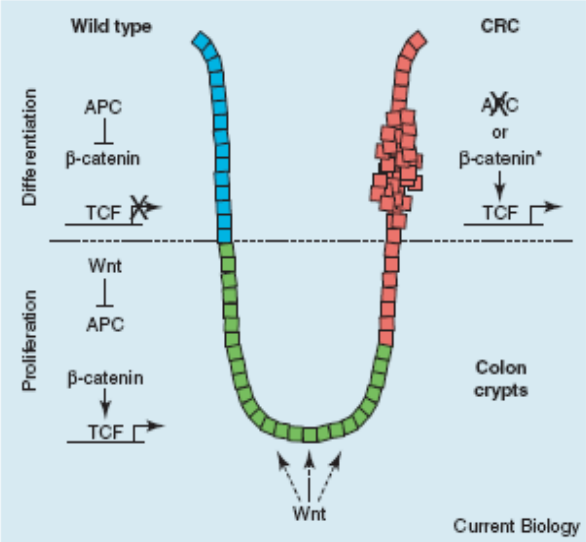

Figure 4: Schematic depiction of a colonic crypt, the left side is wild type and the right side shows the diseased condition. Left side: Wnt signal at the bottom of the crypt blocks *β*-catenin degradation, thereby activating target genes that maintain the cells in a proliferating state (green). Halfway up the crypts, *β*-catenin is downregulated and the progenitor crypt cells start to differentiate (blue). Right side: Mutations of APC and *β*-catenin causes the cells of the crypt to maintain their progenitor state and continuously proliferate (red) (R. Städeli 2006).

In today's proposed multi-step genetic model for colon carcinogenesis (figure 5) (Fearon and Vogelstein 1990; Vogelstein and Kinzler 1993), it is hypothesized that, the loss of heterozygosity at the APC loci (leading to inactivating mutations of both APC alleles) as well as mutations of *β*-catenin and axin are events that happen early in the adenoma-carcinoma sequence and are prerequisited to initiate transformation of normal epithelium cells into the aberrant crypts foci. Subsequent progression towards malignancy in colon carcinogenesis is accompanied by genomic instability (which leads to the formation of an early adenoma) and sequential mutations in K-ras (formation of an intermediate adenoma), SMAD4, (formation of the late adenoma), p53 (transition to carcinoma), as well as other unknown genes (figure 5). Several studies have led to the conclusion that tumour progression in the intestine is promoted

by the selection of specific genetic and epigenetic alterations that accumulate in strict order. Though mutation events are generally stochastic, the order in which they accumulate is non-random and certain mutations are needed to confer a selective advantage.

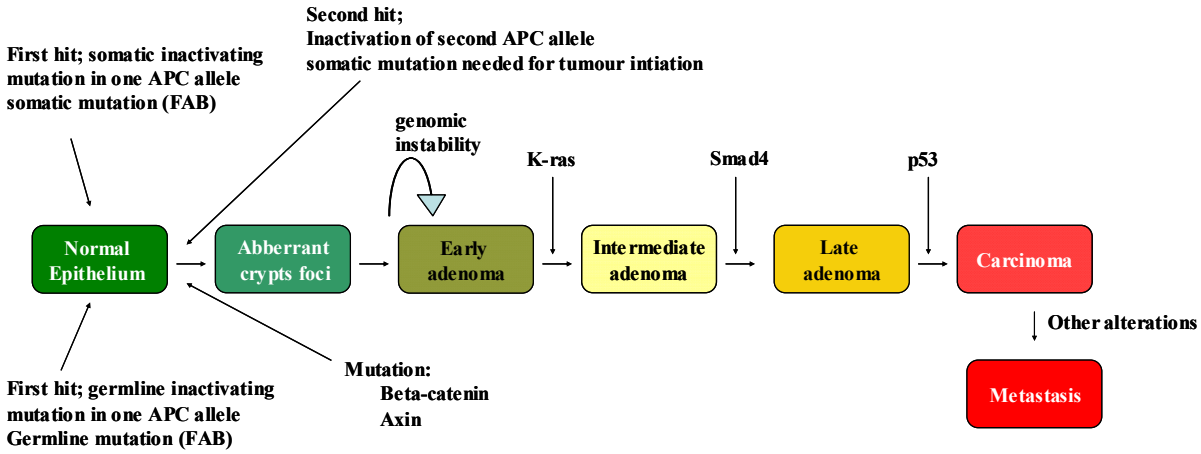

Figure 5: Genetic model of colorectal carcinogenesis adapted from (Fearon and Vogelstein 1990). FAP, familial adenomatous polyposis (Vogelstein and Kinzler 1993).

2.1.3 Key Components of the Wnt-signalling Pathway involved in Cancer

2.1.3.1 Adenomatous Polyposis Coli (APC)

The APC gene is located on chromosome 5q21 and encodes for a protein with a molecular weight of 310kDa. The APC protein (figure 5) comprises 2843 amino acids and encompasses numerous domains like conserved regions, such as the Armadillo repeats, and regions that interact with at least 10 protein partners, including axin, and *β*-catenin (Fodde et al. 2001). The N-terminus carries an oligomerisation domain followed by the Armadillo repeats. The arm repeats are highly conserved and can react with several proteins like ASEF (APC stimulated guanine nucleotide exchange factor), KAPS (Kinesin superfamily-associated protein 3A) and PPA2 (protein phosphatase 2). The central region of APC contains three 15-amino acid (aa) repeats and seven 20-aa repeats which extends into the C terminus. Both 15 and 20 aa repeats can bind *β*-catenin. Within the 20-aa repeat region, there are three SAMP motifs (Ser-Ala-Met-Pro), which mediate the binding of APC to axin.

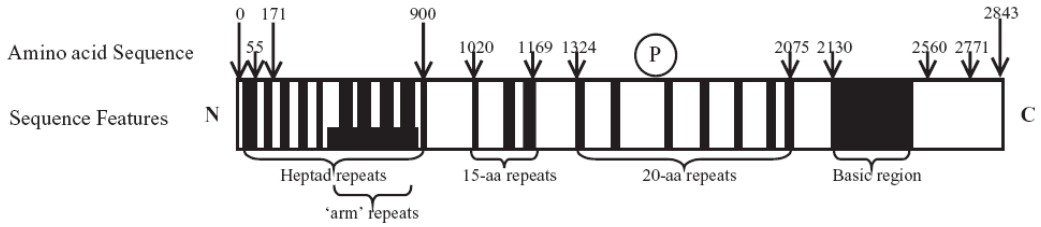

Figure 6: Structure of the APC gene, showing regions encoding binding sites for components of the Wnt pathway. aa, amino acid; SAMP, Ser-Ala-Met-Pro; P, phosphorylation site (Bright-Thomas and Harvest 2003)

The best-characterized function of APC is its role in the negative regulation of *β*-catenin in the Wnt-signalling pathway. APC is also involved in processes that regulate apoptosis, cell adhesion and migration, cell cycle and organisation of the cytoskeleton (Giles et al. 2003; Buda and Pignatelli 2002).

Mutations in the APC gene were initially identified as the basis for familial adenomatous polyposis coli (FAP), a heritable predisposition to colorectal cancer. Individuals with FAP

invariably develop hundreds to thousands of polyps in the colon at a very early age, which can grow in to cancer if they are not surgically removed (Bright-Thomas and Hargest 2003). Mutations in APC have also been identified in the majority of sporadic colorectal tumours where they appear early in the progression to cancer. Over 300 different APC germline mutations in FAP kindred have been identified whereby the most severe and common occur between codons 1055 and 1039 (Bright-Thomas and Hargest 2003). In sporadic cancer APC mutations are common between codons 1286 and 1513 (Bright-Thomas and Hargest 2003). These mutations result in a protein that is truncated at the C-terminus, eliminating five or more of the 20-aa repeats and the SAMP motifs necessary for *β*-catenin binding. As at least three of the 20-aa repeats are needed in order to downregulate *β*-catenin, these mutations ensure that *β*-catenin is able to accumulate and cause expression of proliferation stimulating genes. The 15 aa repeats, which are not required for the negative regulation of *β*-catenin are mostly retained in cancers.

2.1.3.2 Glycogen Synthase Kinase 3

Mammalian cells have three closely related forms of the serine/threonine kinase, GSK-3, namely, GSK-3*α* (51kDa), GSK-3*β* (47kDa), and the minor splice variant GSK-3*β*2, encoded by 2 separate genes that are located on chromosomes 19q13.2 and 3q13.3 respectively. The GSK-3 isoforms display 84% overall identity (98% within their catalytic domains) with the main difference being an extra glycine rich stretch (63 residues) in the N-terminal domain of GSK-3*α* (figure 7) (Woodgett and Cohen 1984; Woodgett 1990, 1991). The splicing variant of GSK-3*β* contains a 13-amino-acid insertion in the catalytic domain (Meijer et al. 2004).

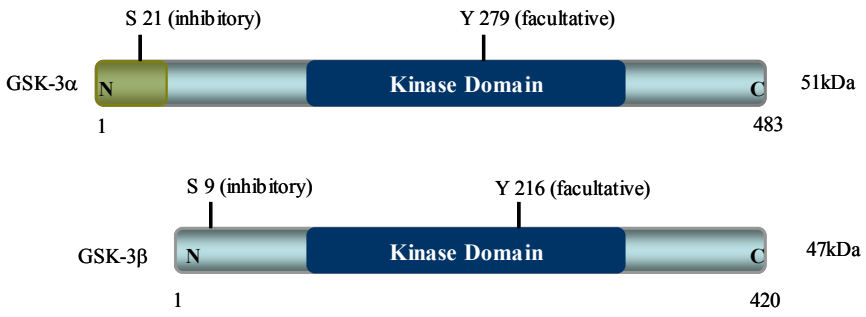

Figure 7: Scheme of the *α*- and *β*-isoforms of glycogen synthase kinase-3 indicating the serine inhibitory sites and tyrosine activating sites (Woodgett and Cohen 1984).

GSK-3 belongs to the superfamily of MAP-kinases (mitogen-activated protein) (Hanks and Hunter 1995). Like the other members of the MAP kinase family, GSK-3 has a small N-terminal lobe that consists mostly of β-sheets and a large C-terminal lobe, which is formed essentially of α-helices (Noble et al. 2004). The ATP-binding pocket is located between the two lobes. Arg96, Arg180 and Lys205 on the catalytic site form a pocket into which the phosphate group of a primed substrate binds (Lee and Kim 2007).

Under basal conditions, GSK-3 is active. The mechanisms by which GSK-3 activity is regulated in the cell include post translational reversible phosphorylation of GSK-3, binding to scaffold proteins, as well as the sub-cellular localization of GSK-3 and its substrates, (Lee and Kim 2007; Patel et al. 2004). The phosphorylation of GSK-3α on Ser21 and GSK-3β on Ser9 of the N-terminus leads to the inhibition of kinase activity. Upon phosphorylation, the N-terminus acts as a pseudo-substrate by folding back on itself and forming electrostatic interactions with the residues (Arg96, Arg180 and Lys205) of the catalytic site, thus occluding access of primed substrates to the catalytic site (Dajani et al. 2001; Bax et al. 2001; Frame et al. 2001). The inhibiting phosphorylation of the α-(Ser21), and β-(Ser9) isoforms of GSK-3 is mediated by several kinases including Akt (protein kinase B) of the insulin pathway, PKA of the cAMP-signalling pathway and PKC (Jensen et al. 2007; Liu et al. 2006; Du SJ 1995.; Liu et al. 2003; Wang et al. 2006). Conversely, tyrosine phosphorylation at the residue Y279 and Y216 in the activation loop of GSK-3α and GSK-3β respectively, enhances kinase activity. Whether the tyrosine phosphorylation is mediated by a kinase or is a result of autophosphorylation, still remains elusive (Cole et al. 2004).

Little is known about the isoform specific functions of GSK in the cell, however studies indicate that, despite their close structural similarities, they are not functionally redundant to each other (Lee and Kim 2007). GSK-3's function was initially associated with the regulation of glycogen synthase, the rate-determining enzyme for glycogen deposition (Frame and Cohen 2001). However, a plethora of GSK-3 substrates, about forty so far (Jope and Johnson 2004), have been identified, which now implicate GSK-3 in a broad range of cellular processes, including cell-division cycle, stem-cell renewal and differentiation, apoptosis, cell survival, transcription, neuronal functions, protein synthesis and even circadian rhythm (Meijer et al. 2004). With a few exceptions, like axin for example, GSK-3 generally requires 'primed' phosphorylation of its substrates by other kinases before it can phosphorylate them. GSK-3 will then phosphorylate the serine or threonine residue four amino acids N-terminal to

the primed residue. The minimal recognition motif for phosphorylation by GSK-3 is S/TXXX*S*/*T*(p), where "X" is any amino acid and "p" denotes the phosphorylated residue.

In view of the manifold substrates of GSK-3 and the wide variety of their cellular functions, GSK-3 has been implicated in a variety of human pathologies including cancer (Manoukian and Woodgett 2002; Hill and Hemmings 2002), type II diabetes, alzheimer's disease (Jope 1999; Kozlovsky et al. 2002), schizophrenia (Jope and Roh 2006; Li et al. 2007), and bi-polar mood disorder (Bhat et al. 2004). Its value as a target for type II diabetes and bi-polar disorder is widely discussed in the literature (Jope 1999; Patel et al. 2004). However, its therapeutic value is still shrouded in uncertainty over the Wnt-mimetic potential of GSK-3 antagonists, to promote other pathologies like tumorigenesis. GSK-3 inhibition stabilizes three cell-cycle regulators, namely cyclin D1, cyclin E and c-Myc, the overexpression of which is linked with tumorigenesis. Addressing this concern is necessary for each GSK-3 inhibitor. However, long term use of lithium chloride, a known inhibitor of GSK-3 used for the therapy of bi-polar mood disorder (Jope 1999) is not associated with increased cancer morbidity in patients (Cohen et al. 1998). Furthermore, lithium treatment does not significantly increase the number of tumors in a mutant adenomatous polyposis coli mouse model (Gould et al. 2003). Other examples of GSK-3 inhibitors are shown below in table 1.

Table 1: Pharmacological inhibitors of GSK-3 (Meijer et al. 2004).

Inhibitor	Class
Flavopyridol	Flavone
SB216763, SB415268	Arylindolemaleimide
CHIR98014, CT20026	Aminopyrimidine
Compound 8b	Triazole
Beryllium, Zinc, Lithium	Atom

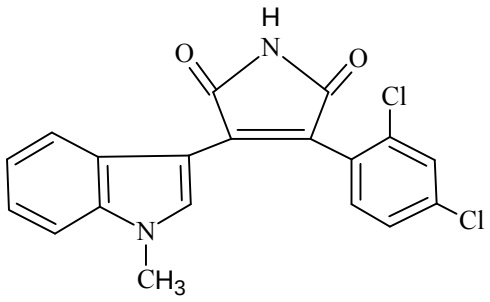

Figure 8: Structure of the GSK-3 specific inhibitor SB216763 (Meijer et al. 2004).

2.1.3.3 Beta Catenin

The *β*-catenin gene (*CTNNB1*) is located on chromosome 3p22 of the human genome and encodes a 92kDa large protein with 781 amino acids (aa). Beta-catenin is divided in to three structural domains: (figure 9) (Peifer et al. 1994).

- An N-terminal domain, which bears the phosphorylation and thus recognition sites for the *β*-catenin degradation machinery of the proteasome.
- A centrally placed 550 aa armadillo repeat domain (arm), with 12 armadillo repeats of 42 imperfect aa. The arm motifs harbor binding sites for APC, axin and E-cadherin.
- Lastly, a highly acidic 100 aa C-terminal domain imperative for the transcriptional co-activation of Tcf/Lef.

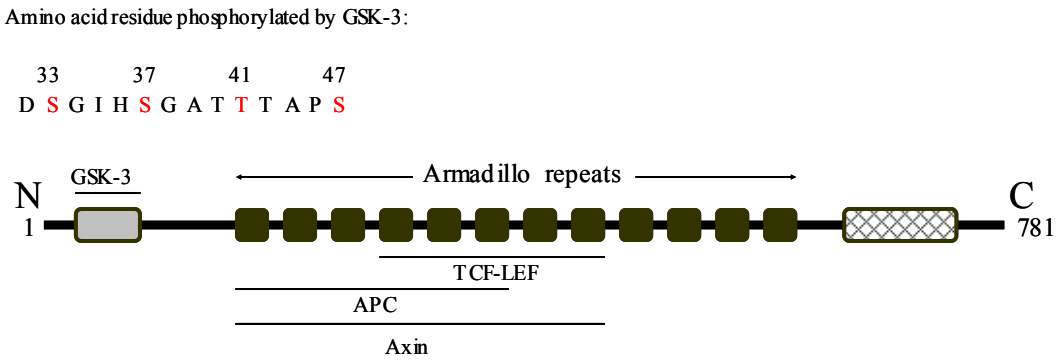

Figure 9: Scheme of the *β*-catenin protein showing the Wnt-relevant domains (Peifer et al. 1994).

Like APC, *β*-catenin belongs to the armadillo super-family of proteins, which all share as a common hallmark, a central domain with a minimum of 6 sets of repeated aa sequences called the arm motifs (Bright-Thomas and Hargest 2003). Like the other members of the armadillo family, *β*-catenin has been shown to typically combine structural functions such as cell contact and cytoskeletal-associated molecules with signalling functions. Indeed, *β*-catenin was initially discovered for its role in cell-adhesion (Kemler 1993). As a component of the adherens junctions, it binds directly to the cytoplasmic portion the transmembrane E-cadherin (Ca^{2+}-dependent homotypal adhesion molecules) and, by associating with *α*-catenin acts as an interfacing link between actin cytoskeleton and cell-cell junctions (Knudsen et al. 1995).

As described in chapter 2.2.1.1, *β*-catenin is the key mediator in the Wnt-signal pathway, where, upon stabilization in response to Wnt signals, it acts in conjunction with Tcf/Lef to promote the transcription of Wnt target genes. In normal unstimulated cells, i.e. in the absence of Wnt-signals, *β*-catenin levels are often low as a consequence of its destabilization in the Wnt signalling pathway. For the successful cytosolic destabilization of *β*-catenin, it has to be phosphorylated within the APC complex. This is accomplished by the serine (Ser)/threonine (Thr) kinases; CK-1*α* or CK-I*ε* and GSK-3 acting as a tag team, whereby CK-1 acts as the priming kinase for GSK-3. Only in the event of a previous phosphorylation of *β*-catenin by CK-1*α* or CK-I*ε* on the residue Ser45, can GSK-3 recognize and serially phosphorylate *β*-catenin on the residues Thr41, Ser37 and Ser 33 in this order. The phosphorylation of the last two residues, Ser37 and Ser 33 earmarks *β*-catenin for proteasomale degradation. Besides the GSK-3-regulated degradation of *β*-catenin, a second APC dependent, but Siah-1 regulated pathway for *β*-catenin degradation has been identified (Matsuzawa and Reed 2001). In addition, an APC independent pathway involving the retinoid X receptor (RXR) has also been implicated in the regulation of cellular *β*-catenin levels (Xiao et al. 2003).

2.1.3.4 T-Cell Factor-Lyphoid Enhancer Factor Transcription Factors (Tcf/Lef)

The mammalian Tcf/Lef family of transcriptional factors consists of four member proteins, TCF-1, TCF-3, TCF-4 and LEF-1 which each share a similar structure of four basic functional domains (figure 10) (Waterman 2004):

– An N-terminal *β*-catenin binding domain, a central transcription repression domain, a high mobility group (HMG) DNA binding domain and lastly, a C-terminal tail

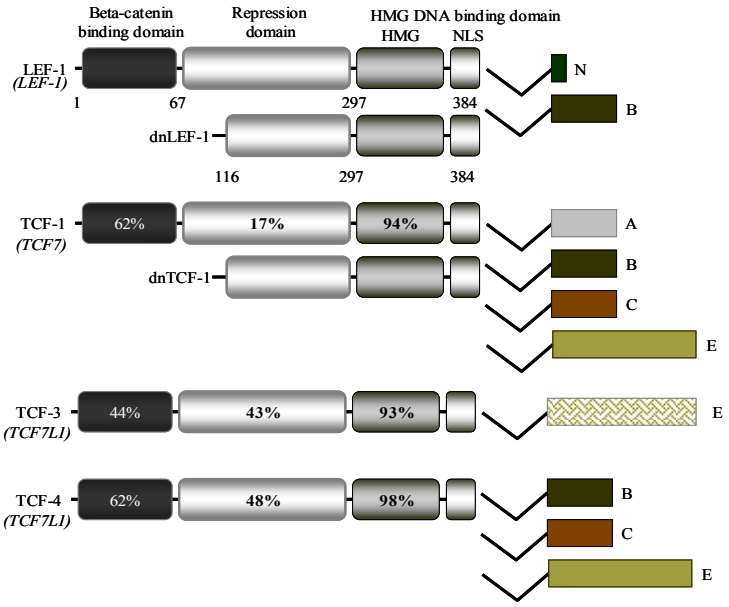

Figure 10: Structure and alignment of the isoform subtypes of the human T-cell factor/lymphoid enhancer factor (Tcf/Lef) family. Percent amino acid identity in select domains is shown relative to the amino acids sequence of LEF-1. Italicized names in parenthesis refer the official HUGO name of each of the genes. High mobility group: HMG, nuclear localization signal: NLS, dominant negative: dn (Waterman 2004).

The *β*-catenin binding domain (figure 10) is the second most highly conserved feature within the Tcf/Lef family. It binds *β*-catenin in a fashion that promotes interactions with the armadillo repeats of *β*-catenin (Waterman 2004). Independently, the Tcf/Lefs can bind DNA but lack the ability to activate target gene transcription because they have a weak transcription activation domain. This deficiency is remedied by binding *β*-catenin, which possesses a potent transcription activation domain but on its own cannot bind DNA. Together they complement one another to form a potent transcription regulatory complex. Flanking the *β*-catenin binding domain is a transcription repression domain (figure 10), which possesses a weak gene transcription suppressing activity and so recruits co-repressor proteins of the groucho family (Giese et al. 1995; Grosschedl et al. 1994). Sandwiched between the transcription repressor domain and the C-terminus is the highest conserved feature of the Tcf/Lefs, the DNA binding domain (figure 10) with a sequence identity between 93-99%. It contains an HMG-Box (high

mobility group) and a nuclear localization signal (Bustin and Reeves 1996). This domain has the function of recognizing, binding and bending (90°-130°) target DNA (consensus sequence YCTTTGWW), so as to maximize productive interactions between the DNA and the activating or repressing complex (Giese et al. 1992; Giese et al. 1991). The last notable feature of the Tcf/Lefs is the multiple C-termini generated from alternate splicing (figure 10). Alternate splicing increases the diversity of the Tcf/Lefs by producing C- termini of variable lengths, denoted with the letters A, B, C, E, and N (figure 10) (van de Wetering 1996; Hovanes et al. 2000; Duval et al. 2000). Although the definite function of each the alternative C-termini still remains at large, evidence points to the fact that the E tail could be involved the regulation of transcriptional activity (Hecht and Stemmler 2003; Atcha et al. 2003).

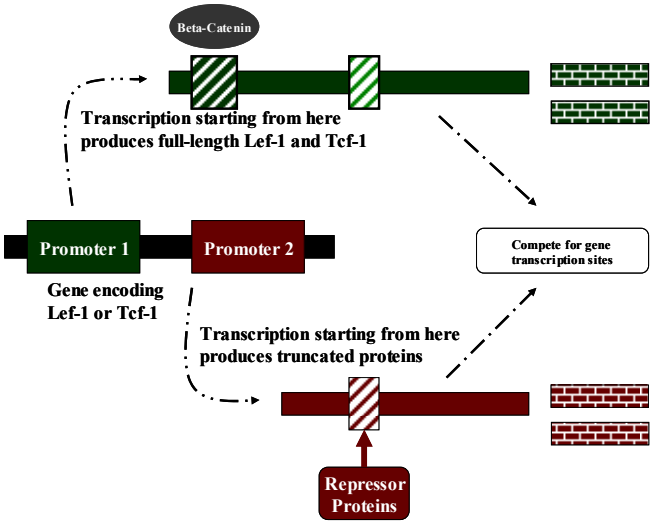

Figure 11: Different forms of Tcfs. Transcription starting at alternate promoters on Tcf genes can produce either full-length or truncated proteins. The full-length proteins tend to activate transcription of target genes, whereas truncated proteins will block transcription (Doucas et al. 2005).

Some of the Tcf/Lef family members, specifically, Tcf-1 and Lef-1 are expressed in two variations; as a full-length protein and in a shorter truncated form. This is possible because the genes that encode for Tcf-1 (*TCF-7*) and Lef-1 (*LEF-1*) each have 2 different promoters for transcription (figure 11) (Hovanes et al. 2001; Giese et al. 1991). Activation of the first promoter in each gene leads to the expression of the full-length protein while the second promoter, located in the second intron, favours the expression of the truncated protein. Truncated Tcf/Lef proteins lack the *β*-catenin binding domain and hence are incapable of transmitting Wnt signals. Since they can however still recruit the co-repressors of the groucho

family, they act in a dominant negative fashion, by competing for DNA regulatory sites with the full-length forms, and hence can suppress Wnt-signalling (Molenaar 1996 ; Hovanes et al. 2001).

Tcf/Lefs are normally expressed during embryogenesis (Oosterwegel et al. 1993), but in most tissues, they are down regulated once the tissues become terminally differentiated. However, in sites of continual cell growth and differentiation, some members of the family continue to be expressed (examples are listed in table 2). One site of continual Tcf/Lef expression is the crypts of the colon, where TCF-4 is expressed as the sole representative of the Tcf/Lef family. However, when colon cells turn cancerous, TCF-1 and LEF-1 are additionally expressed (Hovanes et al. 2001). While the expression pattern of TCF-1 i.e. the truncated form against full-length protein, in cancer is still unclear, TCF-4 and LEF-1 are expressed exclusively as full-length proteins (Hovanes et al. 2001). The physiological role of TCF-1 and LEF-1 in cancer development is still unknown, even though there is evidence that speaks for the fact that TCF-1 might rather function normally as a Wnt-linked tumour suppressor than a Wnt-linked tumour promoter. *In vivo* studies with *TCF-7* (encodes for TCF-1) deficient mice, which lacked of the TCF-1 protein showed that the absence of TCF-1 provoked the development of intestinal and mammary adenoma (Roose J 1999).

Table 2: Table listing the adult tissues of continual growth that express proteins of the Tcf/Lef family, the respectively expressed protein.

Tissue	Tcf/Lef Family Members	Literature
Intestinal mucosa	TCF-1, TCF-4	(Hovanes et al. 2001; Roose J 1999)
Colon	TCF-4	(Hovanes et al. 2001)
Thymus	LEF-1, TCF-1	(Reya et al. 2000)
Mammary epithelia	TCF-1, TCF-4	(Roose J 1999 ; Barker et al. 1999)
Bone marrow	LEF-1	(Reya et al. 2000)
Testes	LEF-1	(Porfiri et al. 1997)
Skin and dermal papillae at the base of the hair follicles	LEF-1, TCF-3	(Zhou et al. 1995; Merrill et al. 2001)

.

2.2 Glucose-Glycogen Homeostasis

2.2.1 Key regulatory Elements of the Glucose/Glycogen Homeostasis

2.2.1.1 Glycogen Synthase (EC 2.4.1.11)

As can be inferred from its name, glycogen synthase (GS, EC 2.4.1.11) is involved in the synthesis of glycogen. It catalyzes the rate limiting step in the formation of glycogen in the cell by linking a glucose molecule from uridine diphosphate (UDP)-glucose via an α-1,4-glycosidic bond to an already existing glycogen molecule. It belongs to the 3rd family of retaining glycosyltransferase (Campbell et al. 1997; Henrissat and Davies 2000). There are two isoforms in mammals encoded by separate genes. The first, muscle GS (MGS) is expressed predominantly in skeletal tissues and several other tissues (heart, fat, kidney, brain) and the second, liver GS (LGS), is expressed exclusively in the liver (Nuttall et al. 1994; Browner et al. 1989). Human LGS and MGS share an approximately 70% amino acid identity with the most divergence located on the N- and C-terminals. In comparison to the human MGS, which has 737 amino acids and weighs 85kDa, human LGS (80.9kDa) is with 703 amino acids, 34 amino acids shorter (Nuttall et al. 1994; Browner et al. 1989).

The N-terminal of GS has 2 phosphorylation sites, site 2 (ser7) and site 2a (ser10), whereby site 2 is phosphorylated *in vitro* by kinases like, the cyclic AMP-dependent protein kinase A (Huang and Krebs 1977), AMP-activated protein kinase (Carling and Hardie 1989), and phosphorylase kinase (Roach et al. 1978). Phosphorylation of site 2 is prerequisite for the subsequent phosphorylation of site 2a by casein kinase 1 (Flotow and Roach 1989; Flotow et al. 1990), which reduces GS activity *in vitro*. However, *in vivo*, the relevance of this phosphorylation site still remains to be substantiated.

The C-terminal of GS contains 7 phosphorylation sites in MGS (figure 12) and 5 sites in LGS, which lacks the C-terminal sites 1a (ser697) and 1b (ser710). *In vivo*, the phosphorylation of sites 3a (ser640) and 3b (ser644) (figure 12) is most influential on GS activity (Wang and Roach 1993). The phosphorylation of these sites, which is mediated by GSK-3, occurs likewise the phosphorylation of the N-terminal sites (2 and 2a) in a hierarchal fashion,

whereby CK-2 acts as the priming kinase for GSK-3. CK-2 phosphorylated site 5 (ser 656) creating a recognition site for GSK-3, which then phosphorylates site 4 (ser652), 3c (ser648), 3b and 3a in this order (figure 12) (Poulter et al. 1988; Wang and Roach 1993). An unknown kinase has been identified *in vitro* that in addition to GSK-3 targets site 3a (Poulter et al. 1988).

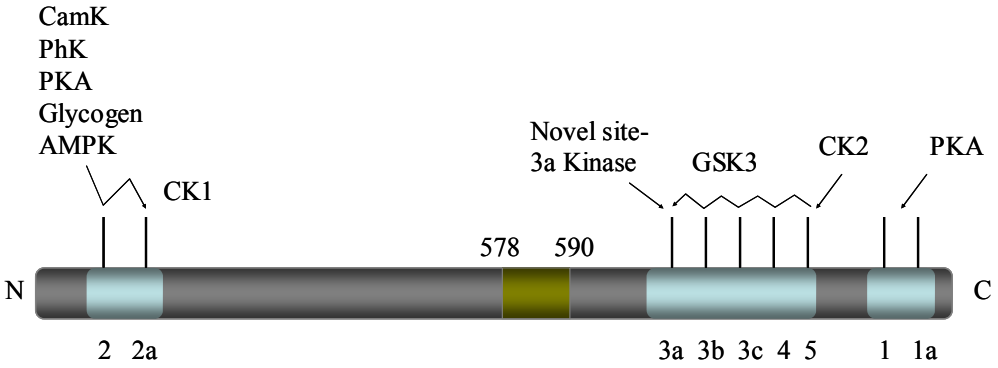

Figure 12: Schematic of the rabbit muscle glycogen synthase showing the nine serine residues, whose phosphorylation regulates the activity of glycogen synthase. All nine serine residues are conserved in the human MGS. AMPK, AMP-activated protein kinase; CaMK, calmodulin dependent protein kinase; CK 1 and 2, casein kinase 1 and 2; Phk, phosphorylase kinase; PKA, protein kinase A.

Active control of GS activity is mediated by allosteric ligands (Piras et al. 1968), kinase-mediated reversible phosphorylation (Roach 1990), which inactivates the enzyme, and also by feedback inhibition by glycogen (Laurent et al. 2000; Danforth and Harvey 1964; Piras and Staneloni 1969) via an unknown mechanism.

GS can assume two conformational states *in vivo*: A GS*a*-conformation, in which the enzyme is unphosphorylated and more active, and a GS*b*-conformation assumed upon phosphorylation that renders GS lesser active. The switch from GS*b* to GS*a* i.e. the dephosphorylation and activation of GS, is mediated in response to insulin stimulation of muscle GS by type 1 protein phosphatases (PP-1) with a type 1 catalytic subunit (Ragolia and Begum 1998; Roach 2002). In cell models, the dephosphorylation of all phosphorylation sites depicted in figure 12 is needed for full activation of GS (Skurat et al. 2000).

As mentioned above, GS activity is also regulated by the actions of allosteric ligands. While physiological concentrations of ATP, ADP, AMP and Pi bring about an inhibition of GS

activity, glycogen-6-phosphate (G-6-P) causes an activation of GS activity by binding and prompting a conformational change of GS so that PP-1 has better access to the phosphorylation sites of GS. The region between amino acids 578-590 has been shown to confer sensitivity to activation by G-6-P (figure 12) (Roach 2002).

Mutations in both of the GS genes have been observed. Several mutations of *GYS2,* encoding the liver form*,* lead to a disorder called glycogen storage disease 0, which is characterized by hypoglycemia, low glycogen levels in the liver and low GS activity. Mutant alleles of *GYS1*, encoding the MGS, have also been detected. While some studies correlate this mutation with type II diabetes development, it is yet to be fully substantiated (Roach 2002). In some cancer types, GS is overexpressed.

2.2.1.2 Glycogen Phosphorylase (EC 2.4.1.1)

Glycogen phosphorylase (EC 2.4.1.1) is a member of the 35th family of glycosyltransferases. It plays a central role in the mobilization of carbohydrate reserves in man by acting in conjunction with the debranching enzyme (EC 3.2.1.68) to degrade glycogen. During degradation, GP stalls four residues from an α-1, 6-branchpoint, from where the branching enzyme takes over. GP exists as a homodimer containing two identical subunits of molecular mass 97,500 (Hudson et al. 1993; Newgard et al. 1989). Three isoforms of GP, encoded by separate genes, exist in mammals. The brain GP (BGP) is the predominant isoenzyme in adult brain and most fetal tissues, whereas adult liver and muscle tissues are known to express primarily, the liver (LGP) and muscle isoforms (MGP), respectively (Hudson et al. 1993; Newgard et al. 1989). BGP is made up of 862 amino acids (AA), and shares more sequence similarity with MGP (841) than with LGP (841).

Like GS, GP activity is regulated by reversible phosphorylation and allosteric interactions. The phosphorylation of GP is mediated by GP-kinase, which in turn is activated in response to glucagon by the cAMP-dependent protein kinase or as a result of increased cellular Ca^{2+} levels (muscle contraction). Dephosphorylation is mediated in response to insulin by PP-1. Depending on the interaction with intracellular allosteric ligands or the state of phosphorylation, each of the GP isozymes can assume two interchangeable forms; an active GPa form and an inactive GPb form, which in turn can assume two interchangeable

conformations; an active relaxed conformation (R-conformer) and an inactive tensed conformation (T-conformer) (figure 13). In resting muscle cells, the lesser active form, GPb, becomes phosphorylated on ser14 and is converted to a more active GPa. Intracellular ligands, such as AMP and glycogen activate MGP by promoting formation of the active R conformer, while glucose, G-6-P purines and purine nucleosides stabilize the inactive T-conformer of MGP (figure 13). The liver isoform has generally similar properties as MGP. However it exhibits differential regulatory properties especially with regard to its response to allosteric ligands. For example, LGP experiences a significantly lesser activation by AMP than MGP. Moreover, it is insensitive to inhibition by G-6-P and ATP (Newgard et al. 1989).

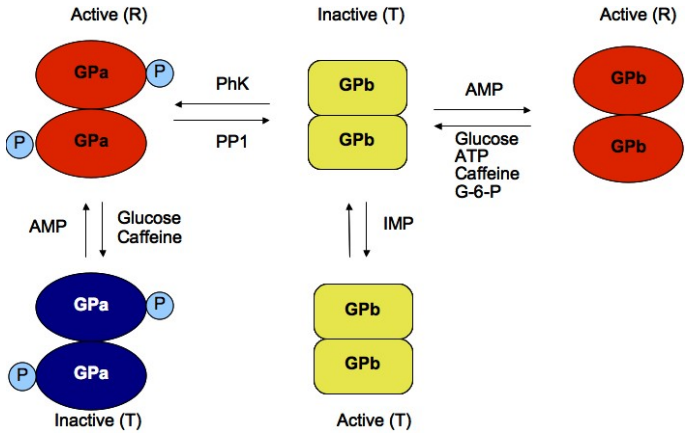

Figure 13: Regulation of muscle glycogen phosphorylase by phosphorylation and allosteric ligands. AMP, adenosine monophosphate; ATP, adenosine triphosphate; G-6-P, glucose-6-phosphate; GPa, glycogen phosphorylase a; GPb, glycogen phosphorylase b; IMP, inosine monophosphate; P, phosphate functional group; PhK, phosphorylase kinase; PP-1, protein phosphatase-1; R, relaxed; T, tensed.

Each GP isozyme fulfills different physiological requirements even though all forms catalyze the phosphorolysis of glycogen. While the muscle enzyme provides metabolic fuel for muscular contraction, the liver form plays a central role in the maintenance of blood glucose homeostasis, and the brain type is associated primarily with the provision of an emergency glucose supply during periods of anoxia or hypoglycemia.

Hyperglycemia is a hallmark of diabetes. Since LGP catalyzes the breakdown of glycogen stores and thus contributes to increase glucose levels of the bloodstream, GP is a potential pharmacological target for therapy of type 2 diabetes. However, due to the high similarities in the regulatory sites of the GP isoforms, isotype specific inhibitors are hard to synthesize.

Since MGP activity is crucial for normal skeletal functioning, fatigue may be a plausible side effect and so pose a major development hurdle for such a therapeutic strategy. Examples of GP-inihibitors include CP-91149 and CP-316819 (Lerin et al. 2004), which both principally bind the less active GP*b* on the glucose inhibitory site, so preventing the conformational change to the the more active GP*a* form.

2.2.2 Regulation of Glucose/Glycogen Homeostasis

Blood glucose homeostasis is determined by the factors that are rate limiting for glycogen anabolism and catabolism. Three set of events potentally determine the regulation of glycogen anabolism in skeletal muscle, adipose tissue and liver cells. First, the rate of glucose transportation in these cells, second, the subsequent phosphorylation of glucose by hexose kinase in muscle tissue and glucokinase in the liver, and lastly the activation state of glycogen synthase (Roach 2002). The activity of glycogen phosphorylase on the other hand is considered rate determining for the breakdown of glycogen, hence for the release of glucose molecules and rise in plasma glucose levels (Roach 2002).

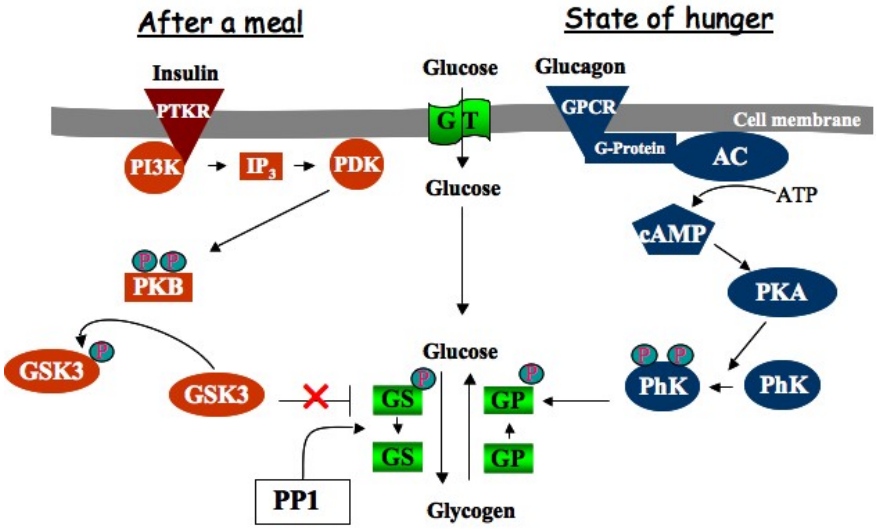

Figure 14: Schematic of the signalling pathways involved in the metabolism of glycogen. IP3, 3, 4, 5 phosphatidyl inositol-3-phosphate;

In mammals, after a meal, elevated plasma insulin, induced by high blood glucose levels, stimulates the transport of glucose into the cell by the glucose transporter proteins (figure 14) (GLUT4 in muscle and adipose tissue and SGLT2 in the liver) (Scheepers et al. 2004; Bornemann et al. 1992; Handberg et al. 1992). Simultaneously, insulin initiates the relay of a signal via the phosphatidylinositol-3-kinase (PI3-kinase) signalling pathway (Petersen et al. 2001; Vanhaesebroeck and Alessi 2000) resulting in the activation of protein kinase B (PKB), the deactivation of GSK-3 and eventually the dephosphorylation and activation of GS (figure 14). This results in reduced plasma glucose levels and the synthesis and accumulation of glycogen. However, not all of insulin dependent control of GS is explainable by the regulation

of GSK-3, considering that the key regulatory sites of GS (site 3a and 3b) (figure 12) are not solely phosphorylated by GSK-3 (Poulter et al. 1988; Skurat and Roach 1996; DePaoli-Roach et al. 1983). Moreover, insulin stimulus causes the dephosphorylation of both amino and carboxy termini of GS (Parker et al. 1983; DePaoli-Roach et al. 1983), including sites not phosphorylated by GSK-3. In the liver, glucose rather than insulin plays a superior role in the acute stimulation of glycogen synthesis. Insulin is involved more in the control of gene expression (O'Brien and Granner 1996). The acute rise in blood glucose correlates with increased glucose in hepatocytes and the allosteric activation of GS. Meanwhile, GP activity is simultaneously shut down by the allosterical actions of glucose and increased dephosphorylation by PP-1 (Roach 2002; Ragolia and Begum 1998)

In periods of hunger (figure 14), the GP-mediated breakdown of glycogen stores to glucose-1-phosphate is the primary response of the liver in order to maintain blood glucose levels at concentrations between 800-1200mg/l (van de Werve and Jeanrenaud 1987; Stalmans 1976), before gluconeogenesis can set in if hunger periods prolong into fasting. Glucagon is secreted into the bloodstream as a response to falling blood glucose levels where it gains ascendancy over insulin. In the liver, glucagon binds to a G-protein coupled receptor (GPCR) and initiates the cAMP signalling pathway leading to increased cytosolic cAMP levels and the subsequent activation of protein kinase A (PKA) (figure 14). Active PKA phosphorylates and activates GP-kinase, which in turn phosphoryates and activates GP (Hayes and Mayer 1981). GP then catalyzes the breakdown of glycogen. While relaying the signal that leads to the activation of GP, PKA also concurrently phosphorylates and inactivates GS. Altogether, decreased liver glucose levels cause the reversal of the glucose-mediated activation of GS hence precluding glycogen synthesis. In addition to glucagon, adrenaline can elicit similar effects through cAMP or Ca^{2+} signals but this is of higher relevance in muscles (Roach 2002).

2.3 Flavonoids and Polyphenols

Polyphenols constitute secondary metabolic products that arise biosynthetically from phenylalanine via two main pathways in plants: the shikimic pathway and the acetate pathway (Heller 1986). Flavonoids are the most abundant sub-class of polyphenols with over 5000 different structures identified. They all share a common nucleus (figure 15) consisting of a benzene ring A, condensed with a member ring C to which a phenyl benzene ring is connected at position 2. Flavonoids can be further divided into 6 sub-classes on account of the variations in the heterocyclic C-ring. Ring C may be a heterocyclic pyran, which yields flavanols (catechins) and anthocyanidins, or pyrone, which yields flavonols, flavones, isoflavones and flavanones (Kuhnau 1976). The patterns of substitution on the flavan nucleus include hydrogenation, hydroxylation, malonylation, methylation, and sulfation (Harborne 1986). Flavonoids occur richly in seeds, olive oil, fruits, tea, herbs, and wine where they provide much of the flavour and colour that accompany these products (Middleton et al. 2000). While most flavonoids occur naturally attached to sugar moieties (glycosides) such as glucose, rhamnose, galactose, arabinose, and thus tend to be water-soluble, a small fraction do not carry any sugar group and are termed aglygones.

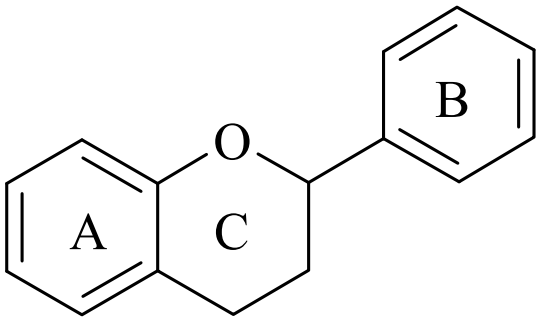

Figure 15: Flavan nucleus commonly shared by all flavonoids

2.3.1 Structure, Occurrence in Food and Intake

Information on the daily consumption of flavonoids in food is incomplete and often contradictory in the literature. This is because there still are some unresolved issues as far as overcoming the challenges that come with the task of determining intake is concerned. First,

there is the fact that flavonoid content can vary over wide ranges in the same food. For example, cherry tomatoes contain six times more quercetin per gram fresh weight than do normal tomatoes (Duthie and Crozier 2000). Flavonoid content is determined, not only by natural factors like climate, season, degree of ripeness, and plant genetics, but also by artificial factors such as variations in food preparation, food processing and storage conditions. A study by Ross et al. showed significant differences in the flavonoid content in nine commercial brands of grapefruit juice (Ross et al. 2000). Another difficulty with respect to determining flavonoid intake resides in the fact that there is a lack of agreement on an appropriate method to analyze polyphenols contents in general. Lastly, there is also the aspect of cultural and individual feeding habits that have to be considered.

Quercetin and EGCG ((-) Epigallocatechine-3-gallate) are the two central flavonoids relevant for the studies presented in this work. In the following subsection, mainly the flavonoid sub-classes, flavonols and catechins, to which these two substances belong respectively, are introduced. Also discussed will be the adsoption, metabolism and dietary relevance of flavonoids in cancer prevention.

2.3.1.1 Flavonols

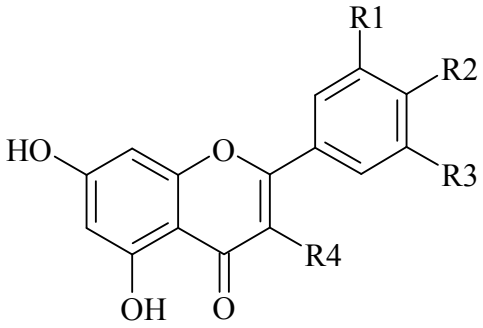

	R1	R2	R3	R4
Quercetin	OH	OH	H	OH
Kaempferol	H	OH	H	OH
Myricetin	OH	OH	OH	OH

Figure 16: Structure of the most prevalent flavonols in the human diet.

Flavonols are the most ubiquitously spread member of the flavonoid family in the plant kingdom, hence in food of plant origin. They belong to the group of 4-*oxo*-flavonoids, which carry a carbonyl group on position 4 of the C-ring (figure 16). Flavonols occur in food usually as O-glycosides, preferably on C-3 position and, less frequently on the C-7 position. D-glucose is the most usual sugar residue (Kuhnau 1976).

Prominent representatives of flavonols in the diet include quercetin, myricetin and kaempferol (figure 16) with quercetin being the most abundant. Major dietary sources for flavonols include beverages like tea (10-25mg/l) and red wine, onions, broccoli, kale, and fruits like cherries and apples. There exists little information on the daily intake amounts for flavonols. Three independent reseach groups estimated the daily intake to be 23mg/day (flavonols and flavones), 28 mg/day (flavonols, flavanones and flavones) and 115mg/day (flavonols and flavones), in the Netherlands, Denmark and the USA respectively (Leth 1998 ; Hertog et al. 1993; Kuhnau 1976). However, Hollman et al. (1997) advanced that the results by Kuhnau might be inflated because of the relatively unreliable methods of analysis back in the 1970s. Van der Woude et al. (2003) stated that the concentration of free quercetin can reach up to 100µM in the intestinal lumen after ingestion of a quercetin supplement (250–500 mg) (van der Woude et al. 2003).

2.3.1.2 Flavan-3-ols (Catechins)

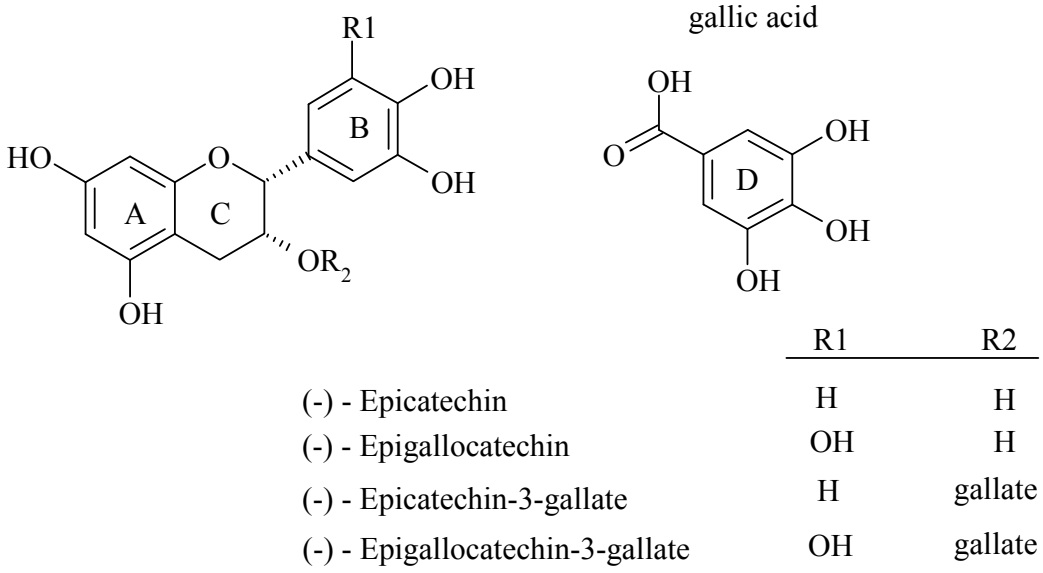

	R1	R2
(-) - Epicatechin	H	H
(-) - Epigallocatechin	OH	H
(-) - Epicatechin-3-gallate	H	gallate
(-) - Epigallocatechin-3-gallate	OH	gallate

Figure 17: Structure of the prominent members of the catechin class of flavonoids in tea

Major dietary sources of catechins include tea (*Camellia sinensis*), apples, grapes (red wine), and cacao (chocolate) (Ross and Kasum 2002). Catechins of tea are mostly galloylated on position 3, whereas flavan-3-ols in chocolate and grapes are (-)-epicatechin and (+)-catechin. Grapes (seeds) also contain condensed flavanols (4-11 units) called proanthocyananidins. Due to varying processing techniques, grape juice has lesser catechins than red wine because the wine making process extracts some flavonoids from seeds and the skin of grapes as well

(Yang et al. 2006). The total daily intake of catechins is rated between 200-800mg for tea drinkers (1-4 cups of green tea) (Yang et al. 2006).

Flavan-3-ols are by virtue of the vicinal dihydroxy or trihydroxy structures liable to air oxidization under alkaline and neutral pH (Yang et al. 2006). EGCG for example can autooxidize to generate a superoxide anion, H_2O_2, and dimers (figure 18) such as theasinensins. This reactions occur also during cell culturing, probably catalyzed by trace metals like Ca^{2+} and Fe^{3+}(Yang et al. 2006).

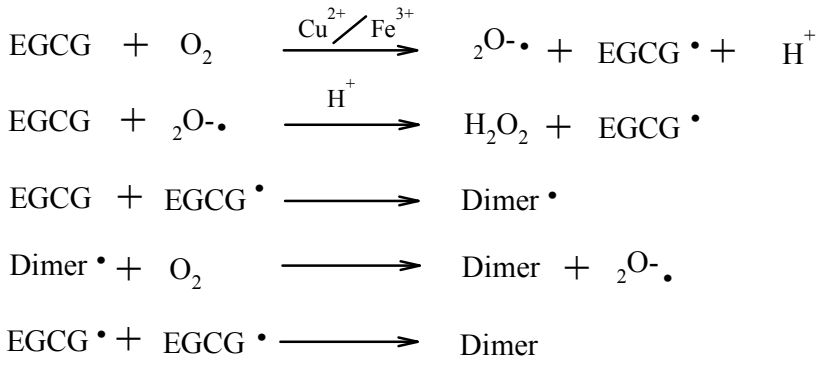

Figure 18: Proposed mechanism for the autooxidation of EGCG under neutral or slightly alkaline pH (Yang et al. 2006).

2.3.2 Resorption and Bioavailability

Although many answers have been provided over the years, the issue as to how flavonoids get past the gastrointestinal tract (GIT) into systemic circulation is still not totally understood. Kuhnau J initially postulated in the 1970s that flavonoids in glycosidized form (the form in which they mostly occur in foods) are not absorbed because the sugar moeities, which otherwise, render them water-soluble, hinder passive diffusion in the small intestine. He argued that, for these flavonoids to be absorbed, they have to be present as aglycones i.e. their sugar moeities needed to be cleaved. And since the human gut lacked the necessary enzymes, glycosides should pass the small intestines unchanged to be hydrolized by the microflora of the colon where absorption is minimal (Kuhnau 1976). In recent years however, there is rising evidence of a hydrolysis of glycosidized flavonoids as high up in the GIT as the oral cavity (Walle 2003). In the mammalian small intestine two enzymes are involved in the hydrolysis of glycosides: Lactase phloridzin hydrolase (LPH), located in the brushborder membrane and

the broad-specific *β*-glucosidase (BS*β*G), located within enterocytes, which may hydrolize glycosides should they gain assess into the cells (Day et al. 2003; Ioku et al. 1998). Indeed there is evidence, that some glycosides can intactly be absorbed via the actions of apical transporter proteins of the small intestines. The sodium dependent glucose transporter SGLT1 has, for example, been shown to transport quercetin glycosides across the brushborder membrane (Walgren et al. 2000; Wolffram et al. 2002; Gee et al. 1998). In another study, the tea catechin epicatechin gallate (ECG) was shown to be a substrate of the monocarboxylate transporter (MCT). Apically located multidrug-resistant associated proteins (MRP2) have been shown to also transport some flavonoid glycosides, however they act in opposition to SGLT 1 by ejecting the glycosides out of the enterocytes back to the luminal tract (Walgren et al. 2000; Vaidyanathan and Walle 2003), which is probably one factor that contributes to the low systemic concentrations generally seen for flavonoids in *in vivo* studies. ECG's bioavailabilty determined in rats lay between 1-3% for the doses of 12.5-50mg/kg (Takizawa et al. 2003). Bioavailability studies have shown that the concentrations of intact flavonoids in human plasma rarely exceed 1μM when the quantities of polyphenols ingested do not exceed those commonly ingested with the diet (Scalbert and Williamson 2000). Another factor that influences flavonoid absorption and bioavailability is the food source (food matrix). The recovery rate for quercetin for example, has been reported to be two fold higher from onions than from black tea (de Vries 1998).

2.3.3 Biotransformation and Excretion

After ingestion, metabolism of flavonoids occurs at the level of the brushborder membrane, the colon and beyond, in the circulatory system (liver), where flavonoids and polyphenols are subjected to hydrolysis and mostly conjugative metabolism leading to their glucuronidation, methylation, and sulfatation. The sequence and extent of metabolism depends on: the substrate specificity of the enzyme, which in turn determines the reactivity and position of the conjugation, the availability of conjugation enzymes and cofactors and lastly the concentration of the polyphenol.

2.3.3.1 Hydrolysis

Following ingestion, flavonoid metabolism starts in the oral cavity with the hydrolysis of glycosides and release of the aglycone (Walle 2003). As described in the previous chapter, the enzymes, LPH and BSβG also catalyse the hydrolysis of flavonoid glycosides in the small intestine. Five percent of Europeans and 90% of Africans and Asians have LPH deficiency in adulthood (Scalbert and Williamson 2000). For this set of people, the microflora of the colon is assumed to be the main source of glycoside hydrolysis. Phase I metabolism of flavonoids by cytochrom-P450 (CYP450) is also thought to occur. Experiments using rat and human liver microsomes have been used to show that CYP450 isoforms can catalylze the hydrolysis and demethylation of polyphenols. However, these findings are as yet unsubstantiated in intact cells or *in vivo* (Walle 2003). If CYP450 mediated hydrolysis occurs in the intestine, the isoforms CYP1A2 and CYP3A4 should predominantly be involved, given that they are the active isoforms in the small intestines (Breinholt et al. 2002).

2.3.3.2 Glucuronidation

UDP glucuronosyltransferase (UDPGT) catalyzes the conjugation of flavonoids and polyphenols to glucuronic acid, which increases water solubility and renal excretion. UDPGT is situated in the endoplasmic reticulum and exists as a large family of related enzymes. Glucuronidation of polyphenols is predominantly by the UGT1A family, which occurs in intestine, liver and kidney. Of all tissues, the liver has the greatest capacity for glucuronidation (Strassburg 1999; Mojarrabi 1998; Strassburg 1998). UDPGT isoforms demonstrate regioselectivity in the glucuronidation of flavonoids. In the case study of luteonin and quercetin, Boersma et al. (2002) showed that preferentially glucuronidated were positions 7-, 3-, 3'-, or 4'-hydroxyl moiety. They concluded that regioselectivity is dependent on the model flavonoid of interest and also on the isoenzyme of UDPGT involved, since glucuronidation of luteolin and quercetin did not following the same pattern, (Boersma 2002)

2.3.3.3 O-Methylation

Catechol-O-methyltransferase (COMT, EC 2.1.1.6), that otherwise plays a crucial role in the metabolism of dopamine, catalyzes the transfer of a methyl group to polyphenols from S-adenosylmethionine (SAM). COMT is expressed in a wide range of tissues. Which hydroxyl group is methylated by COMT is determined by specificity of the polyphenol (Scalbert and

Williamson 2000). A genetic polymorphism in the COMT gene in humans, leads to the expression of gene products with a three to fourfold difference in enzyme activity (Tiihonen et al. 1999).

2.3.3.4 Sulfatation

Phenol sulfotransferases (P-PST, SULT; EC 2.8.2.1) are a small group of cytosolic enzymes that are widely distributed. The isoform, SULT1A3, is highly expressed in the colon and has a high activity on catechol groups found in flavonoids and polyphenols, whereas SULT1A3 is predominant in the liver (Scalbert and Williamson 2000). Generally, sulfotransferases utilize 3'-phosphoadenosine 5'-phosphosulfate (PAPS) as sulfate donor for the sulfatation reactions. Some sulfotransferases are inhibited by polyphenols (Burchell and Coughtrie 1997).

Other phase II metabolism enzymes like *N*-Acetyl transferase which catalyzes the acetylation of amines, glutathione transferases, and epoxide hydrolases generally are thought to play a minor role in flavonoid and polyphenol metabolism (Scalbert and Williamson 2000).

2.3.3.5 Contribution of the Intestinal Microflora

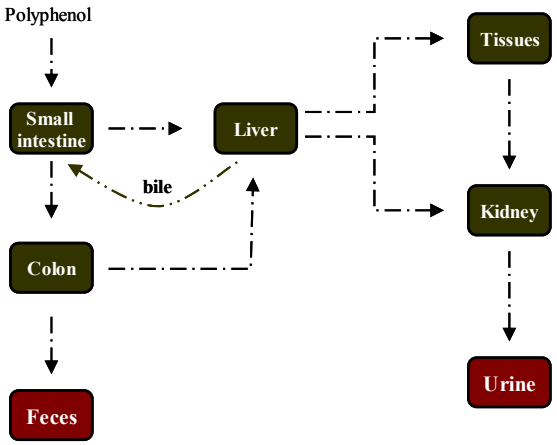

Figure 19: Possible routes for polyphenols in humans proposed by Scalbert and Williamson, 2000

An estimate 10^{13} bacteria of 400 different species colonize the human GIT, whereby 10^{1} reside in the stomach in comparison to 10^{8} and 10^{12} in the small and large intestines respectively. Over 99% of the bacteria are strict anaerobes with a small fraction being facultatively anaerobic. The microbiota of the GIT contribute to digestion by fermenting dietary compounds that are refractory to absorption and enzymatic breakdown in the stomach

and upper bowel. Their actions lead to the formation of short-chain fatty acids, acetate, propionate, butyrate, and of gases like carbon dioxide, methane and hydrogen (Blaut et al. 2003). When polyphenols are absorbed, some enter the enterohepatic circulation. This means, after absorption in the small intestine or colon; they are reintroduced into these organs in bile secretions as conjugated metabolites after passage and metabolism in the liver. Some of these metabolites are again absorbed and some pass on to reach the colon (figure 19).

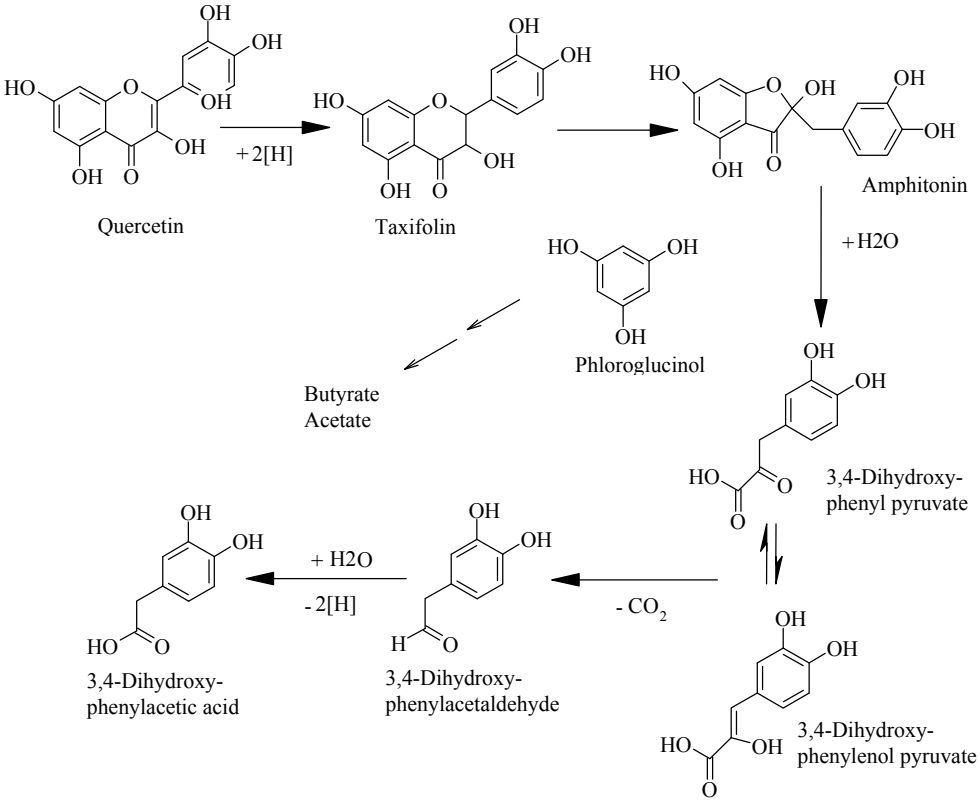

Figure 20: Degradation of quercetin by bacteria *Eubacterium ramulus* of the gut microflora (Scalbert and Williamson 2000).

Also reaching the colon are dietary polyphenols that escape absorption in the upper gastrointestinal tract. In the colon, they are broken down by the hydrolytic and catalytic activity of the microbiota. For example, quercetin, its 3-glycoside and rutin, have been shown to be broken down by *Eubacterium ramulus* and *Enterococcus casseliflavus*, whereby the latter only hydrolyzes the glycosidic bond whereas the former, not only mediates a cleavage of the glycosidic bond but also splits open the flavonoid ring converting quercetin to 3, 4-dihydroxy-phenylacetic acid and pholoroglucinol. Taxifolin and amphitonin are intermediate products in the breakdown of quercetin (figure 20). By-products of the reaction include carbon dioxide, butyrate and acetate. Generally, *E. ramulus* is thought to degrade flavonoids

devoid of the 3 hydroxyl group in the C-ring (flavones and flavanones) to the corresponding phenylpropionic acid, while flavonoids with a 3 hydroxyl group (flavonols and flavanols) are converted to the corresponding phenylacetic acid (Blaut et al. 2003).

2.3.4 Flavonoids, Nutrition and Colorectal Cancer

There is an increased incidence of (colorectal) cancer in developed nations compared to developing nations. The World Health Organisation (WHO), estimates that the rate of incidence of colorectal cancer in males in developing countries is one quarter the average rate in developed countries (Ferlay 2001; Doll and Peto 1981; Parkin et al. 2005). For example the age-standardised rate of incidence of colorectal cancer among males in Bangladesh is about 1 case per 100,000, compared to approximately 50 per 100,000 in Australia and New Zealand, and 60 per 100,000 in some Eastern European countries (Ferlay 2001).

Inferred from epidemiological studies (case-control and prospective), as well as by examining and comparing associations between dietary patterns and cancer rates in different populations around the world, the differences in consumed diet and in life style have been advanced as possible explanations for the demographic disparity in colorectal cancer and some other cancer types. It is generally assumed that diet is causal, in one way or the other, for up to 80% of colorectal cancer (Bingham 2000). However, the mechanisms underlying the epidemiological relationship between diet and cancer remains unclear (Johnson 2004).

The frequent consumption of red and processed meat, and a diet rich in animal fats and poor in micronutrients, which in effect is reflective of the western style diet, are generally viewed in combination with other factors like low energy expenditure, and obesity (Carroll 1998), as high risk factors for getting colorectal cancer. In one prospective study for example, the risk for consumers of processed red meat over non-consumers to get colorectal cancer was estimated at approximately 51% (Giovannucci 1994). The potential formation of known mutagens like heterocyclic amines and polycyclic aromatic hydrocarbons during high temperature cooking of red meat (Gooderham et al. 1997; Kazerouni et al. 2001), and also, the possible micro flora-dependent colonic conversion of nitrites (cured meat) to carcinogenic N-*nitroso* compounds (NOC) are being proposed as possible mechanism for the increased carcinogenic risk of red (processed) meat (Bingham 1999). In addition, high iron levels in the colon may increase the formation of mutagenic free radicals (Lund et al. 2001; Lund et al.

1999). On the other hand, the consumption of a diet rich in micronutrients i.e. a diet complemeted with fruits and vegetables as well as whole grains and tea for example, has been proposed to potentially inhibit the genesis of colorectal cancer in particular and cancer as a whole. It is thought that the non-nutritive bioactive components, flavonoids and polyphenols present in fruits, vegetables and tea are responsible for the inverse association seen between consumption of fruit, vegetables and tea with cancer.

Several mechanisms, based on *in vitro* and *in vivo* studies, have been suggested as to how flavonoids might act as anticarcinogens. These include: inhibition of protein kinases, induction of phase II enzyme activity, acting as antioxidants, inhibition of cyclooxygenase activity, modulating β-catenin signalling, inhibiting cell proliferation and inducing apoptosis (Johnson 2004). Flavonoids reportedly can inhibit cell proliferation in cancerous cell lines of colonic origin. Studying the effect of flavonoids on cell proliferation and apoptosis in the human colonic cell line (HT29), Daskiewicz et al. (2005) suggested the contribution of a positive apoptotic response to the observed flavonoid-dependent growth inhibition of HT29 cells. Generally, flavones and flavonols have been shown to possess greater antiproliferative activity than chalcones and flavanones (Daskiewicz et al. 2005). *In vivo* (rodents), quercetin and its glycosides, (3-O-glycoside and 3-O-rutinoside) have been demonstrated to suppress crypt cell mitosis and inhibit abberant crypt foci formation at diet relevant concentrations (Gee et al. 2002; Depeint et al. 2002). Also, tea which contains high levels of flavanols, especially EGCG, has been shown to have chemopreventive properties in mouse models of colorectal cancer. Orner and coworkers showed that tea at diet relevant concentrations, inhibited heterocyclic amine-initiated colonic aberrant crypt formation in rats, and reduced tumour incidence in $APC^{min/+}$ mice (Orner et al. 2002; Orner et al. 2003). The chemopreventive potential of tea is ascribed to the down regulation of β-catenin expression in the intestines by catechins. Ju et al. (2005) reported of an EGCG-induced reduction in the formation of intestinal tumour (37%-47%) in the $APC^{min/+}$ mouse model (Ju et al. 2005). In addition, the fermentation of flavonoids (see chapter 2.3.3.5) in the large intestine may generate short chain fatty acids such as butyrate (figure 20), which have potential anticarcinogenic properties by promoting differentiation, inducing apoptosis and/or inhibiting the production of secondary bile acids by reducing luminal pH (Hague et al. 1995; Nagengast et al. 1995).

3 Objectives and Problem Formulation

The World Health Organisation has prognosed a 50% rise in cancer incidences by 2020. Scientific data has been published supporting the epigenetic role of diet in the development of cancer. These factors coupled with public appreciation that getting cancer often commensurates a death sentence have fueled the race in the identification of the food components that might promote/prevent cancer. This led to the discovery and emergence of flavonoids and polyphenols as bioactive compounds with anti-carcinogenic potential.

This dissertation was performed within the scope of the project entitled "Impact of flavonoids/polyphenols on transporters and enzymes involved in glucose/glycogen homeostasis in different cells types and in humans". The project was supported by the "Deutsche Forschungsgemeinsschaft (DFG)" and was performed as part of the "Flavonet" network called "Plant flavonoids and polyphenols: Toward a better understanding of the molecular mechanisms of action relevant towards benefit/risk evaluation". The main goal of the network was to establish an objective scientific foundation that permits an improved judgemental assessment of the risks and benefits of human flavonoid and polyphenol consumption.

As an integral part of the glucose/ glycogen homeostasis, GSK-3 influences the glucose to glycogen flux by regulating the activity of glycogen synthase (GS). In this light, GSK-3 is a potential pharmacological target for diabetes therapy. GSK-3 also plays a pivotal role within the Wnt signalling pathway where it acts as part of the machinery regulating cellular β-catenin activity (Jope and Johnson 2004). In the event of the inactivation of GSK-3, β-catenin accumulates in the cell and is translocated in to the nucleus where by associating with other transcription factors (Tcf/Lef), it promotes the expression of proliferation stimulating genes. For cancerous cells or pre-malignant cells, such an event constitutes a proliferation stimulus that leads to increased growth and thus, increased tumourigenesis or carcinogenesis. Hence, while the inhibition of GSK-3, might lead to the abatement of blood glucose concentrations, it might concomitantly pose the risk of increased tumour growth formation by activation of β-catenin in the Wnt-signalling pathway. In view of the fact that high intake of flavonoid-based supplements might dramatically increase the load of flavonoids and because such high concentrations might inhibit GSK-3 kinase activity, the potential adverse effects of flavonoids

might outweigh the beneficial effects. The effects of flavonoids on GSK-3 in colon carcinoma cells was hence determined in order to provide more insight into the molecular-level understanding of mechanisms involved in the flavonoid-dependent modulation of the Wnt-signalling pathway.

To elucidate the impact of flavonoids on GSK-3 in HT29 cells, GSK-3 activity, expression and mRNA level was determined. SB216763, a specific GSK-3 inhibitor was employed as the positive control. Since the influence on GSK-3 activity should directly influence *β*-catenin cellular levels, potential modulating effects of flavonoids on cellular and nuclear *β*-catenin levels as well as the state of phosphorylation of *β*-catenin was determined. Also, the flavonoid-dependent modulation of mRNA transcripts for *β*-catenin was determined. Methodically, western blot analysis and quantitative TaqMan RT-PCR were employed to the end of achieving these goals.

To determine if the modulation of GSK-3 by the flavonoids and polyphenols culminates in a proliferation stimulus, a dual luciferase reporter gene assay tailored to the experimental question was validated and optimized in the immortalized human embryonal kidney cells, HEK293 (DMSZ) as well as the colon carcinoma cell lines HT29 and HCT116. The experimental plasmid of choice was TOP*flash* from Upstate Biotechnology. FOP*flash* was employed for negative control experiments.

Besides its *β*-catenin regulating role in the Wnt signalling pathway, GSK-3 also influences glycogen metabolism indirectly by regulating GS activity. *In vivo* experiments have shown that some flavonoids and polyphenols are potentially anti-diabetic, mimicking the hormonal effects of insulin, i.e. causing a reduction of level blood sugar levels. One possible mechanism of action may be via inactivation of GSK-3 and thus activating glycogen synthase (GS) and hence speeding up the flux of glucose to glycogen and uptake of glucose in the cells. To therefore determine if possible flavonoid-dependent modulations of GSK-3 in HT29 cells commensurately influence glycogen metabolism, time-course effects of flavonoids on GS activity in HT29 cells were investigated using the method described by Thomas et al. (1968). Another possible mechanism for the anti-diabetic properties of flavonoids may be via inhibition of glycogen phosphorylase (GP), responsible for the catalytic breakdown of glycogen to phosphorylated glucose. EGCG, for example, has been shown to potently inhibit the activity of isolated glycogen phosphorylase, the rate limiting enzyme in the breakdown of

glycogen (Jakobs et al. 2006). Using methods described by Layzer et al. (1967) and Kaiser et al. (2001), the GP activity in HT29 cells was determined. In addition the flavonoid-dependent modulation of GS and GP expression levels and mRNA transcripts was determined in HT29 cells using western blot analysis and quantitative TaqMan RT-PCR. Finally, as an overall parameter summing the effects of flavonoids on GS and GP, the glycogen content in HT29 cells was determined using a modification of the assay (Anthron assay) described by Pflüger et al. (1905). Since the liver is the principal organ responsible for regulating acute changes in the blood sugar level, a second cell line, derived from the liver, namely the hepatoma cell line HepG2 was employed to determine the time and concentration related effects of flavonoids on mRNA transcripts of GP and GS.

4 Results and Discussion

4.1 Optimization and Validation of TOP*flash* Luciferase Reporter Gene Assay

One goal of this thesis was to optimize and validate a dual luciferase reporter gene assay in human embyonal kidney cells (HEK293 cells) and human colon carcinoma cells (HCT116 cells). This kind of the luciferase reporter gene assay combines the differential biochemistries of two luciferase proteins; a firefly (*Photinus pyralis*)-derived luciferase protein and a sea pansy (*Renilla reniformis*)-derived luciferase protein. The aim was to establish an assay with the possibility of normalizing transfection efficiency, which is capable of detecting potential flavonoid-dependent stimulations of the *β*-catenin/Tcf/Lef-mediated transcription of Wnt target genes.

The TOP*flash* TCF plasmid from Upstate Biotechnology, which contains 2 sets of 3 copies of the Tcf binding site located upstream of a thymidin kinase (TK) promoter was the experimental plasmid of choice. Upon occupation of the Tcf binding sites by a *β*-catenin/Tcf complex, the TK promoter initiates the expression of a downstream to the TK promoter located open reading frame for the firefly luciferase protein (figure 21). FOP*flash*, which carries mutated Tcf binding sites was used a negative control. For normalization of the firefly luciferase expression, a second plasmid; pRL-TK-*Renilla* vector that constitutively expresses low levels of the *renilla* luciferase protein was also employed.

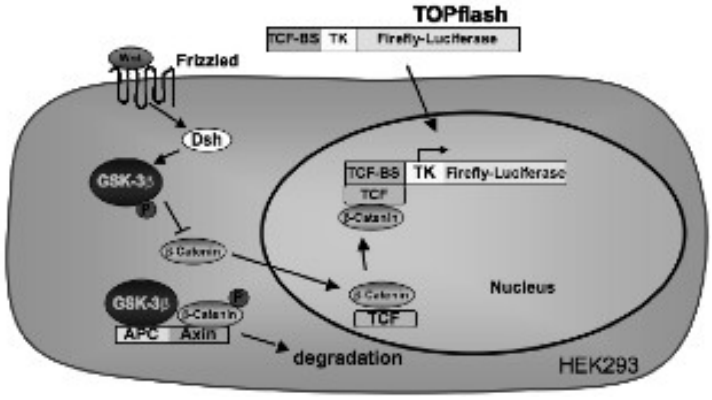

Figure 21: Schematic of the luciferase reporter gene assay with TOP*flash*

4.1.1 Optimization of the dual luciferase reporter gene assay in HEK293 cells (24 well plate format)

Log Phase Growth

The transfection of cells is most efficient when the cells are in the log phase of growth represented by a cell confluency between 60-70%, thus seeding experiments with HEK293 cells in 24 well dishes were performed using varying starting populations between 10,000 - 40,000 cells per well. The starting cell number of 40,000 cells per well, grown for 48h yielded the required cell confluency between 60-70%. Claudia Handrich performed the optimization of the starting cell population in the course of her Diploma thesis (Handrich 2004)

Ratio of Transfection reagent to DNA concentration

Next the optimal transfection reagent (FuGENE 6) to DNA concentration was determined with the optimal starting cell population of 40,000 HEK293 cells per well (24 well plate). In accordance with the recommendations of the producer's protocols (Promega-(7/01)), TOP*flash* and pRL-TK-*renilla* vector were transiently co-tranfected at a weight ratio of 10:1. At a starting plasmid concentration of 300ng TOP*flash* and 30ng pRL-TK-*renilla* vector, transfection experiments were performed in HEK293 cells at FuGENE 6 to DNA ratios of 3:1, 3:2 and 6:1 (w/v). The cells were harvested 24h post transfection and the luciferase activity determined with the dual luciferase assay kit from promega. The FuGENE 6 to DNA ratio 3:1 (FuGENE 6: DNA) evinced the highest transfection efficiency 24h post transfection as evidenced in the highest relative luciferase activity (figure 22).

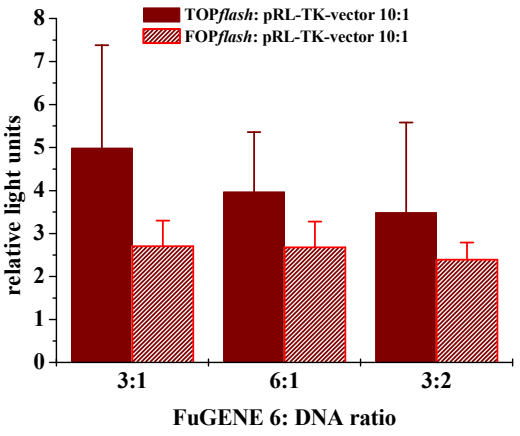

Figure 22: Determination of the optimal transfection efficiency in HEK293 cells with FuGENE6 at the FuGENE 6 to DNA ratios of 3:1, 3:2, 6:1. The cells were transfected with 300ng TOP*flash*/FOP*flash* and 30ng. Transfection efficiencies were determined 24h post transfection and expressed as the mean ± SD of the ratio of firefly luciferase activity to *renilla* luciferase activity of three independently performed experiments

Optimal Plasmid Concentration for TOP*flash* and FOP*flash*

Using the optimal FuGENE 6 to DNA ratio of 3:1, HEK293 cells were transiently transfected with increasing amounts of plasmid DNA (110ng and 550ng) (TOP*flash*: pRL-TK vector; 10:1) to determine the DNA concentration leading to a maximum luciferase expression. The increase in transfected DNA amount led to a linear increase in luciferase activity of both TOP*flash* and FOP*flash* transfected cells (figure 23). A plot of the data of luciferase activity against DNA concentration produced 2 curves for TOP*flash* and FOP*flash* divergent from the DNA concentration of 110ng (figure 23). The rate of increase of luciferase activity in TOP*flash* transfected cells was higher than that in FOP*flash* transfected cells as evidenced by the steeper nature of the TOP*flash* curve. Viewing the data, the DNA concentration of 440ng/well was thus selected for further tranfection reactions, because at this concentration, a maximal difference between TOP*flash* and FOP*flash* expression is evident.

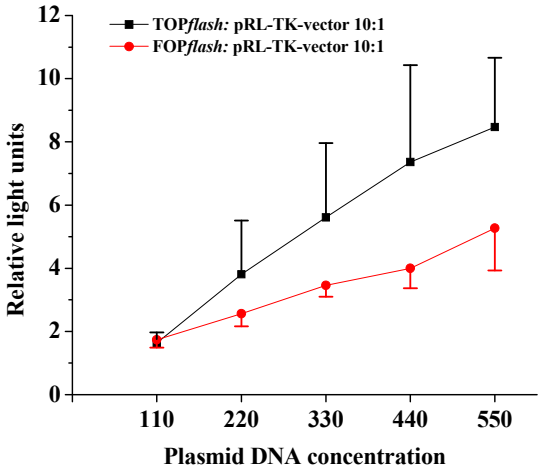

Figure 23: Transient transfection of HEK293 cells with TOP*flash* and FOP*flash* DNA using FuGENE 6 at the FuGENE 6 to plasmid DNA ratio of 3:1 with increasing concentrations of plasmid DNA. Transfection efficiencies are expressed normalized to *renilla* luciferase activity and are plotted as mean ± SD of three independently performed experiments.

Optimal Plasmid Concentration for pRL-TK-*renilla*

To determine the optimal pRL-TK-*renilla* plasmid concentration, transient transfection experiments were performed using the pRL-TK-*renilla* vector at varying concentrations between 40ng and 60ng DNA with increasing intervals of 5ng DNA. The TOP*flash*/FOP*flash*

plasmid concentration was kept constant at 400ng. The increase in pRL-TK-vector amount led to a drop of the transfection efficiencies for TOP*flash* and FOP*flash* from 45ng pRL-TK-*renilla* plasmid concentration (figure 24). The comparison of the relative luciferase activities at 40ng and 45ng pRL-TK plasmid concentrations showed an insubstantial change in activity, hence, for cost-effective reasons, 40ng pRL-TK plasmid/ well was employed for subsequent experiments.

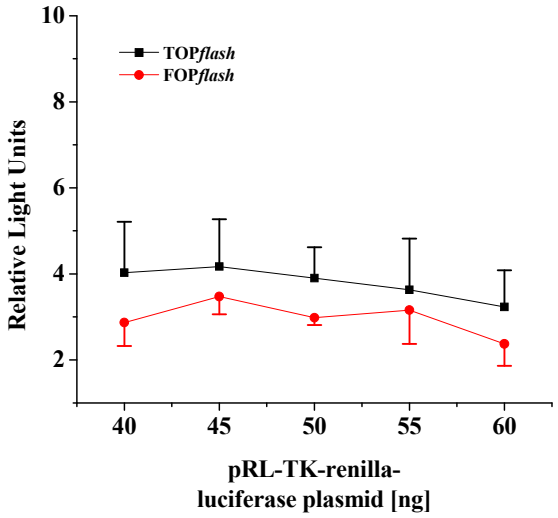

Figure 24: Determination of the optimal pRL-TK-vector DNA concentration. TOP*flash* and FOP*flash* transiently transfected into HEK293 cells at increasing pRL-TK-vector quantities (FuGENE 6 to plasmid DNA ratio of 3:1). Transfection efficiencies for TOP*flash*/FOP*flash* are expressed normalized to *renilla* luciferase activity plotted as mean ± SD of three independently performed experiments.

With the objective in mind to establish a reporter gene assay sensitive enough to detect increasing intracellular *β*-catenin levels, HEK293 cells were transiently co-transfected with pFLAG-CMV5a-Δ45-*β*-Catenin encoding a constitutively active mutant of *β*-catenin to determine if luciferase activity will be increased. pFLAG-CMV5a-Δ45-*β*-catenin carries the cDNA sequence a *β*-catenin protein mutated at Ser45. This mutation prevents the degradation of *β*-catenin so that an accumulation in HEK293 cells is expected. Theoritically, an increase in cellular *β*-catenin should lead to increased engagement of the Tcf binding sites on TOP*flash* and FOP*flash* by the *β*-catenin/Tcf complex. While for TOP*flash*-transfected cells, an increase in luciferase activity is expected, no change should be registered in FOP*flash*-

transfected cells owing to the mutated Tcf binding sites in FOP*flash*. To establish if the reporter gene assay is sensitive enough to capture increases in *β*-catenin levels, HEK293 cells were sequentially co-transfected with pFLAG-CMV5a-Δ45-*β*-Cateninbetween 5ng and 30ng per well at a TOP*flash*/FOP*flash* concentration of 400ng per well. The normalization plasmid, pRL-TK *renilla*, was also co-transfected at a concentration of 40ng per well. Luciferase activity was analysed 24h post transfection.

The serial increase of pFLAG-CMV5a-Δ45-*β*-catenin led to a dose dependent increase in luciferase activity of TOP*flash*-transfected cells that climaxed at 30ng with an approximately 80 fold increase (figure 25). As expected, no change in luciferase activity was registered in FOP*flash*-transfected cells. These results are in accordance with the findings of Ishitani et al. (1999) who reported a 25 fold increase of luciferase actvity when HEK293 cells were co-transfected with TOP*flash* and *β*-catenin that lacked the entire N-terminal region. No increase in luciferase activity was also detected when FOP*flash* was co-transfected with *β*-catenin (Ishitani 1999). In view of the stimulated increase of luciferase activity by the transient tranfection of pFLAG-CMV5a-Δ45-*β*-catenin, the reporter gene assay was thus considered validated.

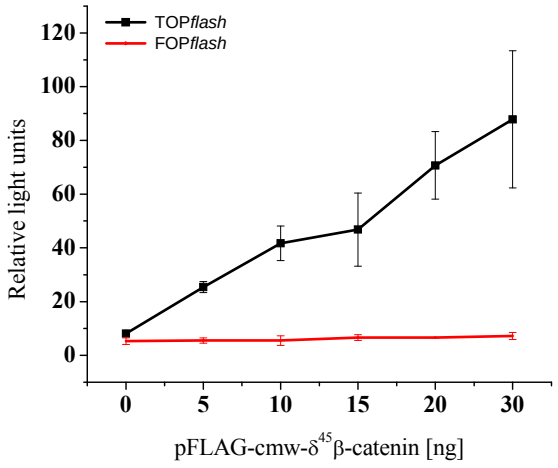

Figure 25: Transient co-transfection of HEK293 cells with TOP*flash*/FOP*flash* (400ng) and pFLAG-CMV5a-Δ45-*β*-catenin at the FuGENE 6: plasmid DNA ratio of 3:1. 40ng pRL-TK-vector was also co-tranfected as the normalization plasmid. TOP*flash* n=4; FOP*flash* n = 2

4.1.2 Optimization of Transfection Efficiency for Reporter Gene Assay in HEK293 cells (10cm Petri dish format)

Transfection optimization experiments were then performed only when cell confluency was between 60-70%. To obtain the optimal seeding cell number, seeding experiments were performed in 10cm (55cm^2) tissue culture dishes with varying amounts (500,000, 750,000 and 1.0 x 10^6) of HEK293 cells for 48 and 72h. 500,000 or 1.5 x 10^6 HEK293 cells grown for 72h and 48h respectively yielded cell confluencies between 60-70%. HEK293 cells were hence seeded in 10cm Petri dishes (55cm^2) at a density of 500,000 cells per dish and subsequently grown for 72 hours. Transfection was performed at varying FuGENE 6 volumes and a constant plasmid DNA concentration of 5µg. (FuGENE 6: DNA; 3:1, 6:1, 9:1).

A **B**

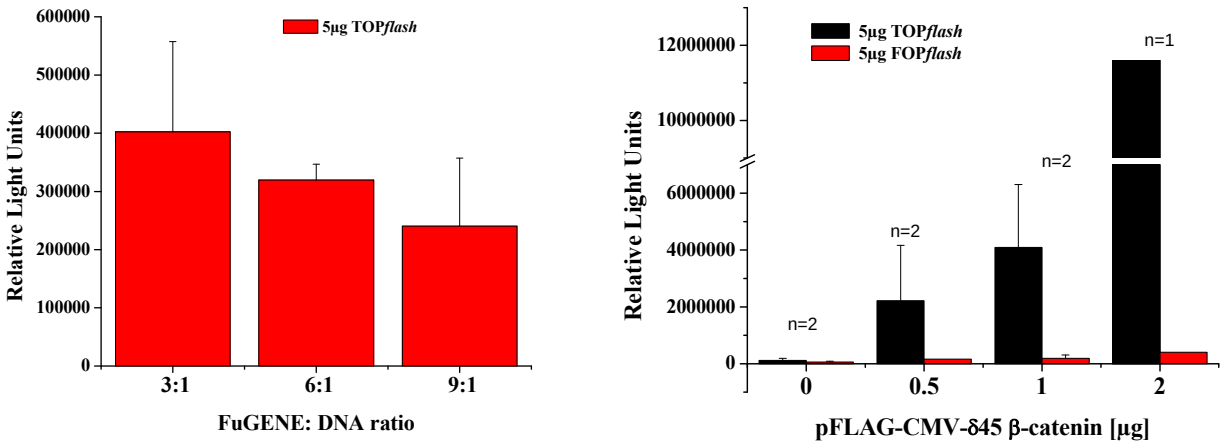

Figure 26: Determination of (A) the optimal FuGENE 6 to plasmid DNA ratio (TOP*flash*/FOP*flash* = 5µg) and (B) the optimal pFLAG-CMV5a-Δ45-*β*-catenin for co-transfection experiments with TOP*flash*/FOP*flash*.

Similar to the transfection experiments performed in 24 well plates, the transfection of HEK293 cells in 10cm plates at the FuGENE 6/DNA ratio of 3:1 produced the highest transfection efficiency when 5µg plasmid DNA was employed (figure 26A). When pFLAG-CMV5a-Δ45-*β*-catenin was serially co-transfected with 5µg TOP*flash* at the optimal FuGENE 6/DNA ratio of 3:1, luciferase activity was increased in a concentration dependent

manner (figure 26B). All tested concentrations of pFLAG-CMV5a-Δ45-*β*-catenin substantially increased luciferase activity. 1µg pFLAG-CMV5a-Δ45-*β*-catenin, which caused an approximately 400 fold surge in luciferase activity was arbitrarily selected for further incubation experiments.

4.1.3 Optimization of Transfection Efficiency for Reporter Gene Assay in HT29 cells and HCT116 cells (10cm Petri dish format)

Aim of the reporter gene assay was to establish an assay in a human colon carcinoma cell line, preferentially in HT29 cells since most experiments on the impact of flavonoids performed within the work group were carried out with HT29 cells.

All attempts to transiently tranfect HT29 cells with TOP*flash* or FOP*flash* remained unsuccessful. As many as 4 different transfection reagents namely; Fugene 6 from ROCHE, Gene jammer from Qiagen as well as Effectene and Superfect from Strategene were tested but none yielded successful results.

Transfection optimization experiments in HCT116 cells were performed when the cells had attained a confluency between 60-70%. This was attained when HCT116 cells (0.3×10^6 cells) were seeded in a 10cm Petri dish ($55cm^2$) and grown for 72h. Transfection optimization experiments were then performed using FuGENE 6 at the following FuGENE 6 to DNA combinations: 3:1, 6:1 and 9:1 whereby different DNA concentrations between 1-5µg per dish were employed. 24h after incubation the cells were lysed in cell culture lysis buffer (Promega) and the luciferase activity determined. The combination 9:1 (FuGENE 6: DNA) produced the highest transfection efficiency in HCT116 cells (figure 27) at all plasmid concentrations tested. Luciferase activities were normalized to protein concentration and are represented in figure 27 as luciferase activity per mg protein since initial experiments with pRL-TK-*renilla* in HEK293 cells showed that renilla expression was influenced by the test compounds. For subsequent incubation experiments, HCT116 cells were transfected at a FuGENE 6 to plasmid DNA ration of 9:1 using 5µg plamid DNA since this concentration yielded the highest transfection efficiency.

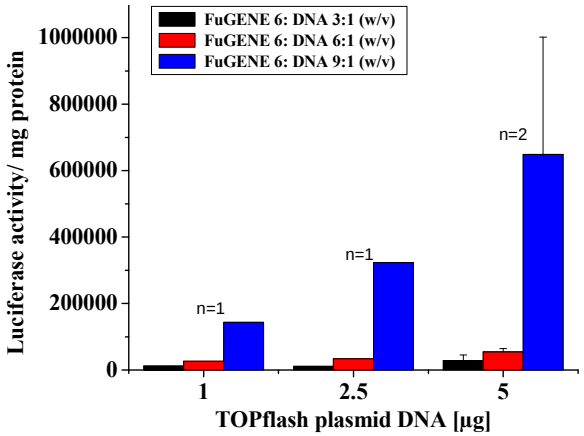

Figure 27 Determination of the optimal FuGENE 6 to plasmid DNA ratio for transient transfection of HCT116 cells with TOP*flash* at different concentrations.

4.1.4 Discussion of Optimization of the Tcf/Lef Reporter gene Assay

Washing steps with PBS in experiments with HEK293 cells were always accompanied with a tremendous loss of cells since HEK293 cells easily detach due to their semi-adherent nature. The consequence was an uneven distribution of cells in the wells leading to fluctuations in the transfection efficiencies from well to well and hence reduced experimental consistency. To circumvent this problem, the reporter gene assay in the 24 well format was modified. First the cells were seeded in a 10cm Petri dish. After attaining the needed confluency they were transiently transfected and allowed to acclimitize and stabilize for 24h. Thereafter the cells were treated with typsin/EDTA (10s) to promote efficient separation during counting. The cells were plated anew, this time in 12 well dishes (HEK293 cells: 200,000 cells per well, HCT116 cells: 150,000 cells per well) and grown for 24h before being subjected to incubation experiments. Because HEK293 cells were washed away during medium replacement, incubation occurred without removal of medium by adding a 2 fold concentrated dilution of the test substance to the well. Replatting the cells after transfection guaranteed higher and same transfection efficiencies in each well per experiment thus improving reproducibility and data consistency. This approach also reduced the number of handling steps and was time-effective since less time was spent per well during transfection. This experimental sequence was also employed for tranfection experiments with HCT116 cells with the difference that the

experimental steps were interjected with washing steps as HCT116 cell grow adherent and do not wash away easily.

Some flavonoids such as quercetin are known to bind to serum proteins contained in the culturing medium and thus influence their cellular bioavailabilty (Kitson 2004). A possible remedy for this problem would be to perform incubation experiments in a serum free medium. However incubation under serum-free conditions for long periods was not applicable for HEK293 cells, since they could not survive in serum free medium. Serum starvation of HEK293 cells led to increased cell detachment and death observable by visual and microscopic inspection of the cell culture. This phenomenom was also evidenced in a reduced luciferase activity in tranfection experiments with HEK293 cells (5µg TOP*flash* and 0.5µg pRL-TK-*renilla*) cultivated in a serum void medium versus a serum-containing medium (10%, 20%). The relative luciferase activity of serum-starved cells was reduced by 50% compared to cells grown in 10% and 20% FCS for 19h (figure 28). For this reason, reporter gene assays with HEK293 cells were carried out in serum containing medium (10% fetal calf serum). For cost-effective reasons 10% FCS was chosen over 20% FCS since both concentrations had similar effects on luciferase activity (figure 28). Data on HCT116 cells indicated that, in contrast to HEK293 cells, HCT116 cells are still viable after long periods of serum starvation. Incubation with flavonoids was hence performed in medium void of serum.

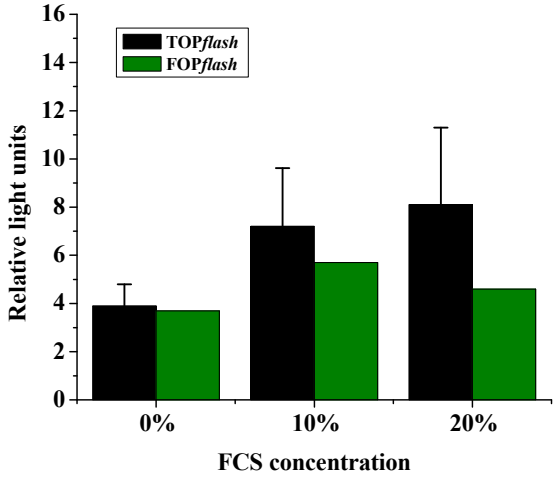

Figure 28: Effect of serum on the transfection efficiency in HEK293 cells measured 19h post transfection (with 5µg TOP*flash*/FOP*flash*). The results are expressed as mean ± SD of the relative luciferase activity (Firefly: *Renilla*) (TOP*flash* n>3, FOP*flash* n=1)

As described in the previous chapter pRL-TK-*renilla*-vector was employed for normalization in the dual luciferase reporter gene assay. In order to function as an efficient normalization tool, the expression of *renilla* luciferase protein, which occurs constitutively, must be indifferent to stimulus by the test compounds. However, early data from orienting incubation experiments with transiently transfected HEK293 cells could not unambiguously dismiss the contingency of a modulation of *renilla* luciferase expression by the test substances. As an alternative method of normalization, the luciferase activity was normalized to protein levels of the cells. This constituted a deviation from the initially intended dual luciferase reporter gene assay. To compare these two methods of normalization, HEK293 cells transfected with 10µg TOP*flash* and 1µg pRL-TK-*renilla* were incubated with two compounds; LiCl and SB216763 known to inhibit GSK-3 kinase activity *in vitro* (Rao et al. 2005; Rochat et al. 2004). Theoretically the inhibition of GSK-3 should provoke increased *β*-catenin levels in HEK293 cells and hence increase luciferase activity. In figure 29 the shaded bars represent results normalized to *renilla* expression and the red coloured bars represent data normalized to protein concentration. Normalization to protein indicated an about 3 fold increase of luciferase activity by 10mM LiCl, which is in line with literature observations (Rao et al. 2005). On the other hand normalization to *renilla* suggests no inhibition of GSK-3 by LiCl. It was hence conjectured that the differences in the effects produced by LiCl might derive from fluctuation in *renilla* expression. Both methods of normalization resulted in similar results for SB16763 at both tested concentrations suggesting no effect on *renilla* expression. 10µM SB216763 caused an approximately 14 fold increase of luciferase activity compared to a circa

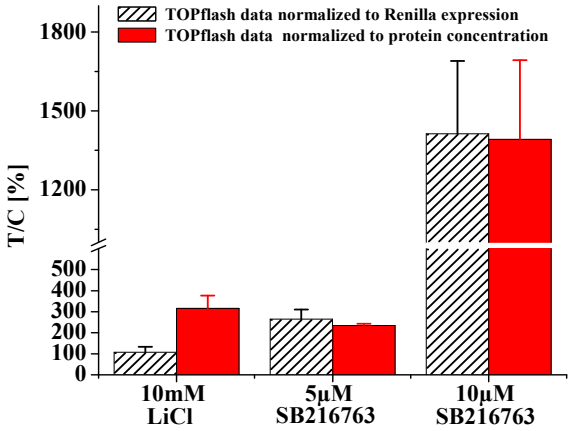

Figure 29: Effect of LiCl and SB216763 on the transcriptional activity of Tcf/Lef diven luciferase activity in HEK293 cells after 19h incubation. The results are represented as test over control (control = HEK293 cells treated with DMSO (1%)) of the mean ± SD of at least three independent experiments

3 fold increase at 5µM (figure 29). 10µM SB216763 was therefore employed for subsequent experiments as a positive control for GSK-3 inhibition since SB216763 seemed to potently inhibit GSK-3 at this concentration, a result consistent with literature descriptions of SB216763 as a potent inhibitor of GSK-3 (Meijer et al. 2004). These results also led to the choosing of the protein normalization method over the *renilla* method as the principal method of normalization for reporter gene assay results.

In summary, it has been shown that the optimized firefly reporter gene assay is a suitable model for measuring the inducing effects of substances on the *β*-catenin/Tcf/Lef transcriptional activity in HEK293 cells and HCT 116 cells. To verify the functionality and hence validate the luciferase reporter gene assay, potent inhibitors of GSK-3, (LiCl, SB216763) were employed. These inhibitors successfully increased the *β*-catenin dependent induction of Tcf/Lef drive luciferase activity in HEK293 cells. In addition, the transient co-transfection of HEK293 cells with a mutated form of *β*-catenin, strongly increased luciferase activity (figure 25). Table 3 summarizes the conditions optimized for the reporter gene assays in HEK293 and HCT116 cells

Table 3: Parameters for the firefly reporter gene assay in HEK293 cells and HCT116 cells

	HEK293 cells	HCT116 cells
Seeding amount/ 10cm dish	500,000 cells	300,000 cells
Growth incubation after seeding in 10cm dish	72h	72h
Transfetion	5µg TOP*flash*/FOP*flash* alone or with 1µg pFLAG-CMV5a-Δ45-*β*-Catenin	5µg TOP*flash*/FOP*flash*
Acclimitization length	24h	24h
Seeding amount/12 well plate	200,000 cells	150,000 cells
Growth incubation after seeding in 12 well dish	24h	24h
Incubation	24h (in serum containing medium)	24h (in serum free medium)
Normaliszation of results	Protein content	Protein content

.

4.2 Modulation of the Wnt-signalling Pathway by Flavonoids

4.2.1 Effects on the *β*-Catenin/Tcf/Lef Mediated Transcriptional Activity

The *β*-catenin/Tcf/Lef mediated transcriptional activity is measured as a cumulative parameter that sums up the effects of the tested flavonoid on the upstream elements of the Wnt-signalling cascade. Free *β*-catenin in the cytosol is transduced in to the nucleus where it associates with the transcription factors of the Tcf/Lef family. To investigate whether the effects flavonoids on the level of cellular and, in particular, on nuclear *β*-catenin would prompt a transcriptional response mediated by the *β*-catenin/Tcf/Lef transcriptional complex, the optimized luciferase reporter gene assay was employed. The expression of the luciferase reporter gene after transient transfection of the reporter plasmid TOP*flash* represents the expression of a Tcf/Lef driven gene.

Both HEK293 cells and HCT116 cells were incubated with the polyphenols of interest (quercetin, (-) epigallo catechin gallate (EGCG), epicatechin, pholretin, phloridzin, and the extract (AE02) of a consumer relevant apple juice) for 24h after transient transfection with the experimental plasmid. While HEK293 cells were transfected either with TOP*flash* only (HEK293-TOP cells) (chapter 6.3.5.3) or with TOP*flash* in combination with pFLAG-CMV5a-Δ45-*β*-catenin (HEK293-TOP-CAT cells) (chapter 6.3.6.3), HCT116 cells were transfected with only TOP*flash*. FOP*flash* transfected cells (chapter 6.3.5.3) were used as a negative transfection control to determine leakages of luciferase expression. The maleimide SB-216763, a GSK-3*β* specific inhibitor served as the positive control substance. The results are presented in percentage as test over control (T/C (%)) with the control being cells treated with the solvent DMSO (100%).

4.2.1.1 Effect of Flavonoids on *β*-catenin/Tcf/Lef driven transcriptional Activity in HEK 293 Cells

In HEK293 cells transfected with TOP*flash* (5µg) only, 10µM of the positive control compound (SB216763) potently increased luciferase activity up to 21 fold above that of the

DMSO solvent control cells (figure 30A) after 24h. In comparison to the positive control, the flavonol quercetin also increased luciferase activity, albeit moderately. The effect was nevertheless significant at 50µM (figure 30A), thus indicating a possible induction of the *β*-catenin/Tcf/Lef-driven gene transcription. The green tea catechin EGCG did not affect *β*-catenin/Tcf/Lef-communicated luciferase expression up to 50µM (figure 30B).

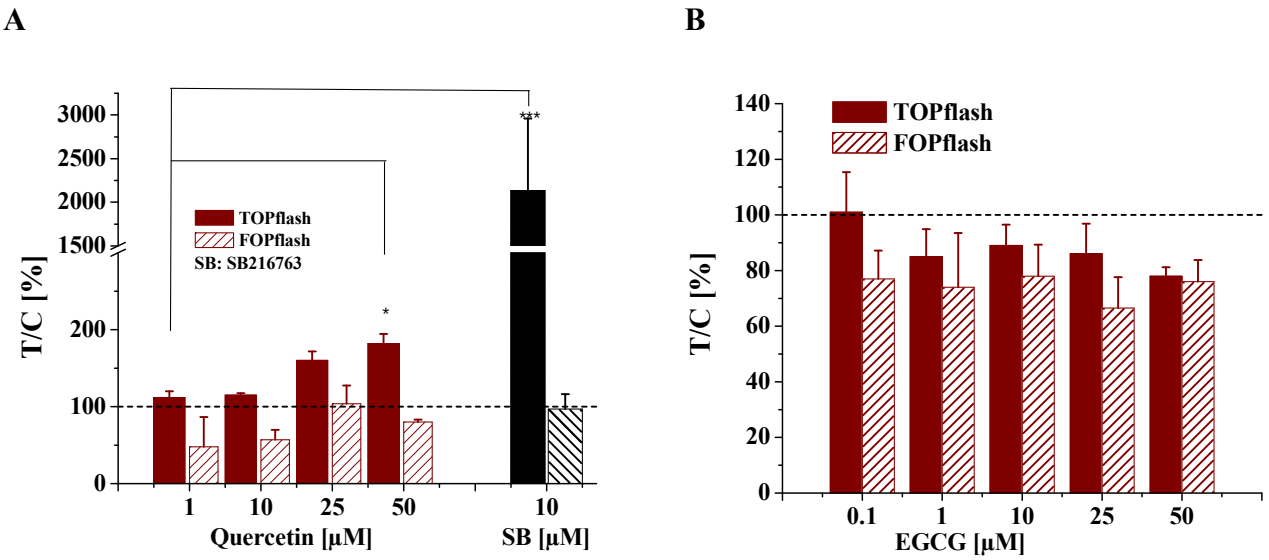

Figure 30: Impact of flavonoids on the Tcf/Lef mediated transcriptional activity in HEK 293 cells (TOP*flash* (5µg)) measured as luciferase activity after 24h incubation with (A) quercetin and (B) EGCG. The results are presented as test over control of the mean ± SD of at least three independent experiments. Significance calcultations were performed with the student's t-test (* = $p < 0.05$; *** = $p < 0.001$). SB, SB216763.

In comparison to the singly tested flavonoids, the effect of a polyphenol-rich extract of a consumer-relevant apple juice blend AE02 on the *β*-catenin/Tcf driven transcriptional activity was investigated (Schaefer et al. 2006). The juice of AE02 was prepared from a mixture of table apples (20%) and cider apple types harvested in the year 2002, which included, Topaz (25%), Bohnapfel (17.5%), Winterrambour (22.5%), and Bittenfelder (15%). The polyphenol fraction of the juice was seperated as described in Schaefer et al. (2005) and about 50% of the polyphenol composition was identified as listed in table 4

Table 4: Polyphenolic composition of the apple juice extract AE02 (Schaefer et al. 2006) (1g/l) Total polyphenolic amount; 576.4 mg

Compound	[mg]
Procyanidin B1	7.0
Procyanidin B2	15.1
Epicatechin	19.2
Phloretinglycoside 1	24.7
Phloretinglycoside 2	9.0
Phloretinxyloglucoside	138.9
Phloridzin	27.9
Chlorogenic acid	181.5
3-Coumaroyl-quinic acid	9.5
Caffeic acid	4.8
4-Coumaroyl-quinic acid	77.3
5-Coumaroyl-quinic acid	10.4
Quercetin-3-rutinoside	2.6
Quercetin-3-galactoside	0.8
Quercetin-3-glucoside	1.4
Quercetin-3-rhamnoside	4.1

AE02 had no effect on the luciferase activity in HEK293 cells transfected with TOP*flash*, after 24h incubation at concentrations between 100µg/ml and 500µg/ml AE02, suggesting no influence on the *β*-catenin/Tcf driven transcriptional activity (figure 31A), hence no proliferation stimulus.

Incubation of HEK293 (transiently transfected with TOP*flash* only) with the aglycones phloretin (10µM, 50µM), and phloridzin (10µM, 50µM), whose glycosides richly occur in AE02 extract (table 4) yielded no change in luciferase activity compared to DMSO treated cells (figure 31B). Epicatechin (50µM, 100µM), another polyphenol represented in the AE02 had no effect on the luciferase activity (figure 31B).

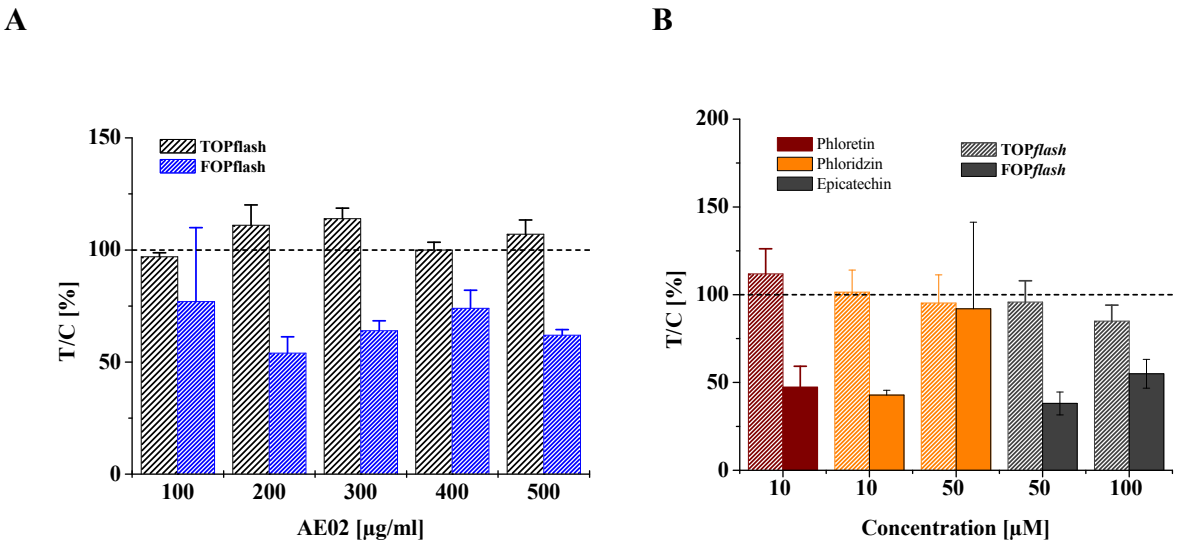

Figure 31: Effect on the Tcf/Lef mediated transcriptional activity in HEK 293 cells (TOP*flash* (5µg)) measured as luciferase activity after 24h incubation with (A) apple juice extract AE02 and (B) phloretin, phoridzin and epicatechin. The results are represented as test over control of the mean ± SD of at least three independent experiments.

Most tumours of colonic origin are hallmarked by an elevated cellular *β*-catenin level (Bright-Thomas and Hargest 2003). To emulate the situation in colon tumour cells, *β*-catenin (1µg), mutated at Ser45 was transiently co-transfected with TOP*flash* (5µg) into HEK293 cells. This mutation precludes the phosphorylation and hence the degradation of *β*-catenin so that *β*-catenin accumulates in the cell.

When in addition to TOP*flash* HEK293 cells were co-transfected with mutated *β*-catenin (HEK293-TOP-CAT), The GSK-3 inhibitor (10µM) SB216763 caused an approximately 1.4 fold increase in luciferase activity (figure 32A). Quercetin concentration-dependently increased luciferase activity in HEK293-TOP-CAT cells overexpressing mutated *β*-catenin after 24h of incubation. The induction of luciferase activity was significant from 25µM and attaining an approximately 2 fold increase at 50µM compared to solvent control (figure 32A). EGCG affected HEK293-TOP-CAT cells similarly as HEK293-TOP inducing no change in luciferase activity up to 50µM EGCG following a 24h (figure 32B).

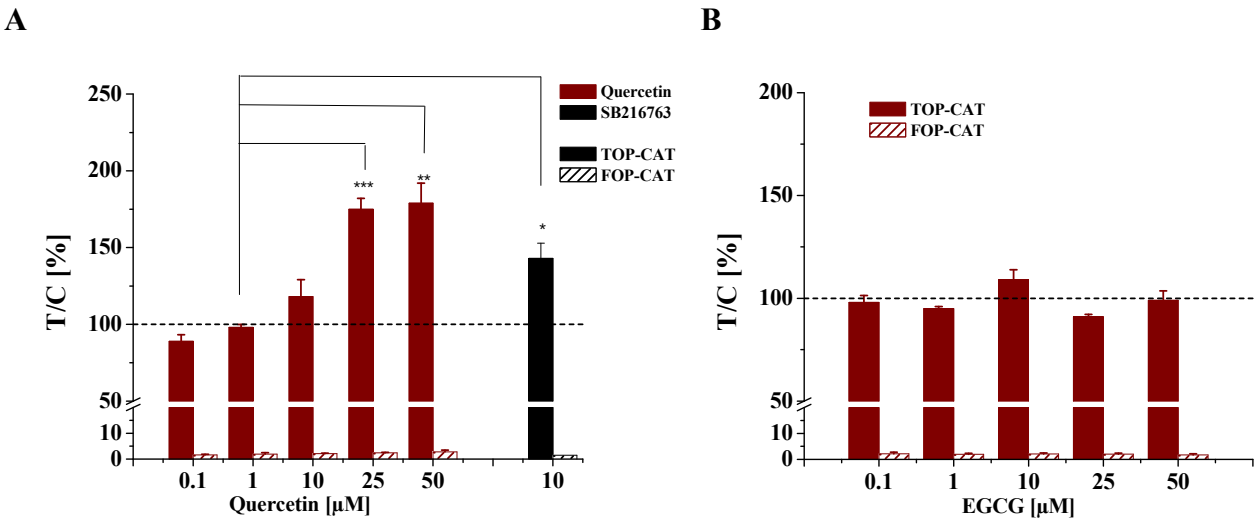

Figure 32: Impact of (A) quercetin and (B) EGCG on the *β*-catenin/Tcf/Lef driven luciferase expression in HEK393 cells after 24h incubation. The cells were co-transfected with TOP*flash* (5µg) and pFLAG-CMV5a-Δ45-*β*-catenin (1µg). The results are presented as test over control of the mean ± SD of at least three independent experiments. Significance calcultations were performed with the student's t-test (* = $p < 0.05$; ** = $p < 0.01$; *** = $p < 0.001$).

4.2.1.2 Effect of Flavonoids on *β*-catenin/Tcf driven transcriptional Activity in HCT116 Cells

The serum free incubation of HCT116 cells, known to possess one mutated allele for (Ser45) *β*-catenin, with quercetin (1µM, 10µM, 25µM) lead to a concentration dependent stimulation of luciferase expression, significant from 10µM (approximately 2 fold increase). SB216763 at a concentration of 10µM caused a marginal but significant increase in luciferase activity after 24h while EGCG, phloretin and epicatechin caused no substantial change of the luciferase activity in HCT116 cells after 24h of serum free incubation (figure 33B).

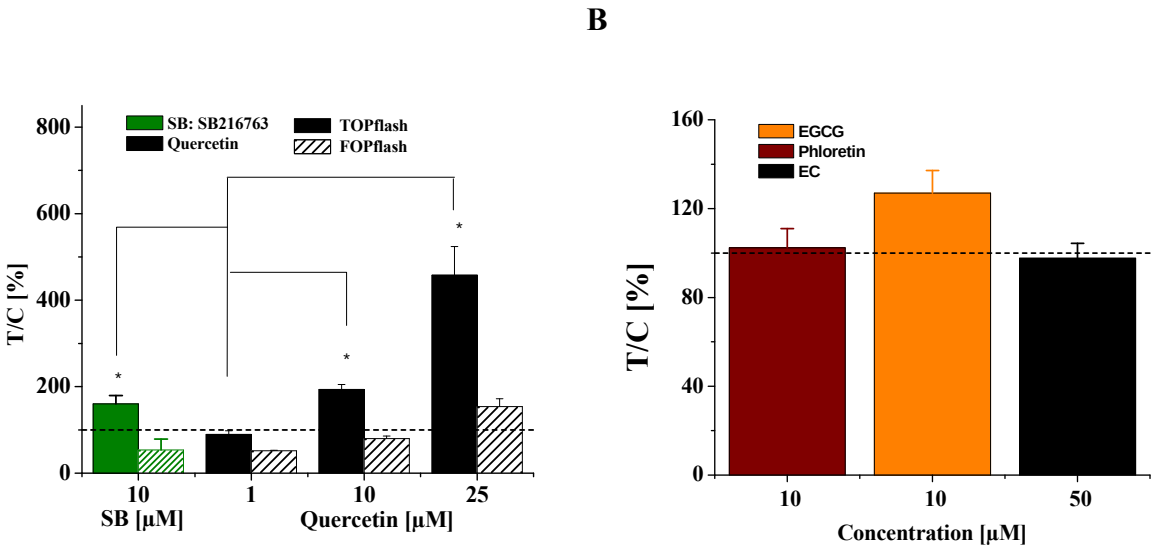

Figure 33: Effect on the Tcf/Lef mediated transcriptional activity in HCT116 cells (TOP*flash* (5µg)) measured as luciferase activity after 24h incubation with (A) quercetin and (B) phloretin, phoridzin and epicatechin. SB16763 served as a positive control for the induction of luciferase expression. The results are presented as test over control of the mean ± SD of two or more experiments.

In summary, it has been shown that quercetin might influence the *β*-catenin/Tcf/Lef driven transcriptional activity. Quercetin concentration-dependently upregulated luciferase expression in HEK293 cells reaching a significant increase of 182 ± 12.4% of control at 50µM (figure 30A). However compared to the positive control, SB216763, with over 2000% induction of luciferase activity, quercetin is a weak inducer of luciferase activity at 50µM (figure 30A). When mutated *β*-catenin (Ser45) was co-expressed in emulation of the situation in some colon cancer cells, quercetin still significantly increased luciferase expression in HEK293 cells, this time at a lower concentration (25µM quercetin) (figure 32A) in comparison to cells expressing only the Tcf/Lef binding sites. In the human colon carcinoma cell line HCT116, which is heterozygous for *β*-catenin and hence overexpresses *β*-catenin mutated at Ser45, quercetin also caused concentration-dependent increases of luciferase activity significant at even as low as 10µM. At 25µM quercetin, luciferase activity in HCT116 cells was increased upto about 5 fold compared to the solvent control (figure 33A). These results show that quercetin was a more potent inducer of Tcf/Lef driven luciferase

activity in HCT116 cells than in HEK293 cells co-expressing mutated *β*-catenin. Taken together, the results suggest that quercetin might act via the Wnt signalling pathway, modulating *β*-catenin/Tcf/Lef dependent gene expression probably causing a stronger proliferation stimulus in tumour cells. Indeed this hypothesis borrows support from the findings of van der Woude et al. (2003) who reported a cell type- and concentration-dependent biphasic influence of querectin on the growth of tumour cells. The growth of HCT116 cells was promoted by quercetin up to the concentration of 30µM, beyond which, cell growth became inhibited (van der Woude et al. 2003). Van der Woude and colleagues further posited in a follow-up paper that the proliferative effects of quercetin might be mediated via the estrogen receptor (ER) (van der Woude et al. 2005). Cumulatively, the results of this thesis suggest that in addition to the ER pathway, the Wnt pathway may also be involved in mediating quercetin's dependent proliferation stimulus.

The apple juice extract AE02 had no effect on the *β*-catenin-dependent transcriptional activiy in HEK293 cells up to a concentration of 500µg/ml suggesting that AE02 does not cause a stabilization of *β*-catenin. Indeed, experiments with AE02, performed in HT29 cells by Dr. Melanie Kern during her PhD fellowship, indicated that AE02 did not influence cellular *β*-catenin levels up to 250µg/ml. In contrast AE02 at 500µg/ml significantly reduced the cellular and phosphorylated levels of *β*-catenin after a 24h challenge (Kern et al. 2006). It is interesting that quercetin, when tested as an aglycone caused a dose dependent increase of luciferase acivity in HEK293 cells and HCT116 cells, yet within AE02, no effect on luciferase activity was registered. Apparently, quercetin at the concentration present in AE02 did not affect *β*-catenin homoestasis. Furthermore quercetin has been detected in AE02 mainly as glycosides. Identified in AE02 are the rhamnoside, glucoside, rutinoside, and galactoside of quercetin with a total concentration of 9µM (table 4.4-1). Given that, these quercetin glycosides have been shown in several test systems to be either inactive or at most bioactively less potent than the quercetin aglycone (Shen et al. 2003; Veeriah et al. 2006; Kern et al. 2005), it is hence conceivable that these quercetin glycosides are too low to increase the mediating potential of AE02.

The other characteristic compounds of AE02, phloretin, phloridzin and epicatechin did not influence luciferase expression, neither in HEK293 cells nor in HCT116 cells. The tea catechin, EGCG also had no effect on luciferase activity, hence on Tcf/Lef driven transcriptional activity neither in HEK293 cells nor HCT116 cells.

The GSK-3 inhibitor, SB216763, at 10μM, significantly induced luciferase activity in the cell models tested (figures 30A/32A&33A) indicating an induction of Tcf/lef driven transcriptional activity. In HEK293 cells, with a high expression of the Tcf binding sites, owing to the transfection of TOP*flash* (HEK293-TOP cells), SB216763 had the highest impact causing a significant near 22 fold increase of luciferase activity (figure 30A). However, when HEK293 cells and HCT116 cells expressing high levels of mutated *β*-catenin in addition to Tcf-binding sites were incubated with SB216763, the potent induction of luciferase activity observed in HEK293-TOP cells became much less potent, with a 12-14 fold reduction, yet to levels still significantly higher than the solvent control (figures 32A&33A). The lesser potency of SB216763 in HEK293-TOP-CAT cells and HCT116 cells than in HEK293-TOP cells may result from an exhaustion of the Tcf/Lef transcriptional factors by the overexpression of *β*-catenin so that luciferase activity plateaus leaving little room for further increase. Cumulatively, these results lend support to the thesis that SB216763 can inihibit GSK-3 kinase activity within the APC complex and that such inhibition might lead to the accumulation of *β*-catenin in the cell with the result that the Tcf-transcriptional activity is augmented constituting a proliferation stimulus.

4.2.2 Effects on Glycogen Synthase Kinase 3

The results obtained from the Tcf/Lef reporter gene assay identified quercetin, the most abundant flavonoid in the human diet as an inducer of Tcf/Lef driven luciferase activity, suggesting potential induction of proliferation stimulating genes. Thus the impact of quercetin on GSK-3*α* and GSK-3*β* upstream of the *β*-catenin-dependent gene transcription were investigated by western blot analysis in order to elucidate its mechanism of action. Because of its lack of influence on the Tcf/Lef transcription combined with its lack of influence of isolated GSK-3 (kinase assay) (schreiner 2004), the most abundant tea catechin EGCG was included in the studies as a negative control substance. SB216763 was employed at a concentration of 10µM as a control for GSK-3 inhibition. HT29 cells were incubated with the respective flavonoid for 24h under serum-free conditions.

4.2.2.1 Activity and Expression of GSK-3*α*/*β*

The phosphorylation of residues Ser21 or Ser9 of GSK-3*α* or GSK-3*β* respectively potentiates the inhibition of the respective enzyme activity. Hence, the phosphorylation status of GSK-3 was determined, using antiphospho-GSK-3*α/β* (Cell Signaling) by Western blot analysis as a barometer for flavonoid-dependent inhibition of GSK-3 in human colon cancer cells. The overall expression of GSK-3 was also determined using anti-GSK-3*α/β* antibodies (Santa Cruz).

Intracellular levels of phosphorylated GSK-3*α* (figure 34A/C) and phosphorylated GSK-3*β* (figure 34B/C) in HT29 cells were indifferent to treatment with up to 75µM quercetin (figure indicative of an insubstantial inhibition of GSK-3*α* and GSK-3*β* enzyme activity by quercetin. However, quercetin caused a marginal, yet significant reduction in the protein level of GSK-3*α*, which was not concentration dependent. At a concentration of 75µM quercetin GSK-3*α* protein levels experienced a remission to control levels (figure 34A/C).

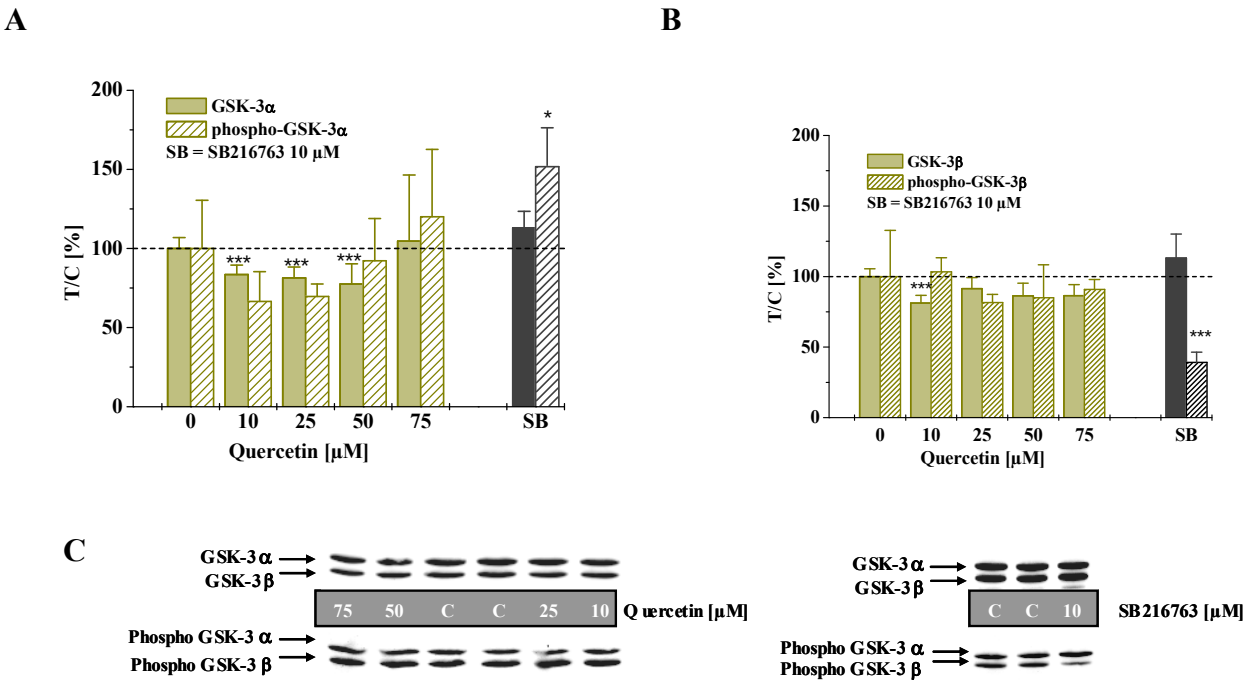

Figure 34: Western blot analysis of (A) GSK-3*α* and (B) GSK-3*β* in HT29 cells after 24h treatment with quercetin. SB216763 (SB) was employed as a control for the inhibition of GSK-3 activity. The data are presented as test over control (%) with the control being cells treated with 1% DMSO. The data are the mean ± SD of at least 3 independent experiments with similar outcome with (C) showing a respective representative Western blot with C as control (solvent-treated cells). The significances indicated are calculated compared to the solvent control using student's *t*-test (* = $p < 0.001$).**

In contrast to quercetin, the treatment of HT29 cells with EGCG for 24h resulted in the increase of GSK-3*α/β* (figure 35C) phosphorylation, which is indication of decreased enzyme activity of GSK-3*α* and GSK-3*β* (figure 35A/B). Phosphorylated GSK-3*α* levels increased significantly at a concentration of 0.5µM EGCG and peaked at 25µM EGCG (figure 35A). EGCG increased the levels of phosphorylated GSK-3*β* significantly from the concentration 0.5µM of EGCG (figure 35B), although less pronounced than for the GSK-3*α*. isoform. Concomitantly, the protein level of total GSK-3*α* and -*β* was not affected by treatment of HT29 cells with EGCG (figure 35A/B).

Interestingly, incubation of HT29 cells with the potent GSK-3 inhibitor, SB216763 had different outcomes on the phosphorylation of the two GSK-3 isoforms (figure 35A/B).

Whereas the intracellular level of phosphorylated GSK-3*α* in HT29 cells was significantly enhanced (up to 174 ± 27%) by SB216763 (10µM) (figure 35A/C) indicating inhibition of the enzyme activity, the amount of phosphorylated GSK-3*β* in HT29 cells was notably diminished by about 60%, suggesting the presence of active GSK-3*β* enzyme (figure 35B/C). The protein levels of both GSK-3 isoenzymes were marginally yet significantly increased by this compound (figure 35A/B/C).

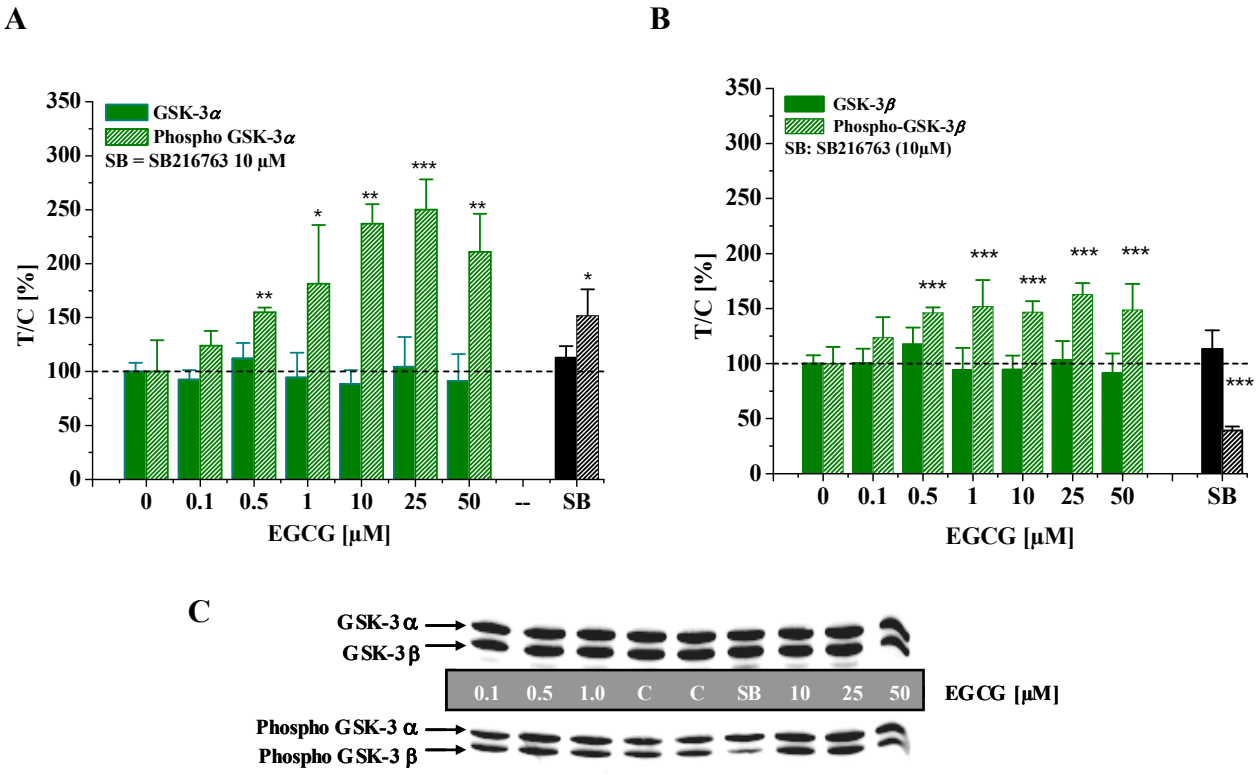

Figure 35: Western blot analysis of (A) GSK-3*α* and (B) GSK-3*β* in HT29 cells after 24 h treatment with EGCG. SB216763 was included in the tests as a control for the inhibition of GSK-3 activity. The data are presented as test over control (%) with the control being cells treated with 1 % DMSO. The data are the mean ± SD of at least 3 independent experiments with similar outcome, with (C) showing a respective representative Western blot (C=control (solvent-treated cells)). The significances indicated are calculated compared to the solvent control using student's t-test (* = p < 0.001).**

In summary, EGCG was identified as a potent inhibitor of both the *α*- and *β*-isoform of GSK-3 in the colon cancer cell line HT29. Sequential treatment with concentration of EGCG up to 50µM for 24h resulted in a significant increase of phosphorylation of GSK-3*α* and GSK-3*β* at Ser21 and Ser9 respectively, consistent with inactivation of the kinase (figure 35A/B/C). The inhibition of GSK-3*α*/*β* raises the question of the mode of action of EGCG. GSK-3*α*/*β* protein levels were not affected by EGCG up to 50µM (figure 35A/B/C) dismissing the possible upregulation of enzyme activity due to increased protein expression. In contrast to the potent inhibition of GSK-3 in HT29 cells, isolated GSK-3*α*/*β* has been shown to be indifferent to treatment with up to 100µM EGCG (Schreiner 2004). Although EGCG is readily taken up by HT29 cells with a predominant localization in the cytosol (Lambert et al. 2006; Hong et al. 2002), these results collectively suggest that the inhibition of GSK-3*α* and GSK-3*β* may primarily be based, on the interference of EGCG with other signalling cascades that target GSK-3 rather than on a direct targeting of the enzyme. Protein kinase A (PKA) of the cAMP pathway or protein kinase B (PKB) of the insulin/PI3 kinase cascade or Protein kinase C (PKC) all of which have been shown *in vitro* to target the Ser21 and Ser9 phosporylation sites of the *α*- and *β*-isoforms of GSK (Fang et al. 2000; Cross et al. 1995), are potential candidates involved in the communication of EGCG's inhibition of the GSK-3 isoenzymes. In accordance with this argument are the findings Lorenz and co-workers showing in endothelial cells that EGCG stimulates the activity of PKB and PKA at the same concentrations range employed in this work (1-50µM) (Lorenz et al. 2004).

Recently, it has been shown that dependent on cell type and cell culture conditions the autooxidation of EGCG can generate substantial amounts of H_2O_2 (figure 18) (Yang et al. 2006). Thus it is argued that the cellular effects attributed to EGCG might be totally or at least in part owed to the generated H_2O_2 (Dashwood et al. 2002). Hydrogen peroxide (100µM and 500µM) has however been reported to activate GSK-3*β* in HEK293 and in other cell lines (Shin et al. 2006). In contrast to the reported effect of H_2O_2, EGCG effectively inhibited GSK-3*α* and GSK-3*β* in HT29 cells (figure 35A/B/C). Furthermore, Dashwood et al. (2002) reported that upto 20µM H_2O_2 did not influence Tcf/Lef transcriptional activity in HEK293 cells. Finally, even at 0.5µM EGCG (figure 35A/B/C), a concentration far below the reported concentrations of EGCG that usually generate substantial amounts of H_2O_2, GSK-3*β* phosphorylation (Ser9) indicative of the inhibition of enzyme activity was already significantly increased (Dashwood et al. 2002). Cumulatively, these facts permit the

conclusion that H_2O_2 production by EGCG is likely of no substantial relevance for the biological effects observed in this work on key elements of the Wnt pathway.

Quercetin, employed at concentrations up to 75µM did not influence the phosphorylation status of either isoform of GSK-3 (figure 34A/B/C) indicating no influence on enzyme activity. Although the protein levels of both isoforms were marginally reduced, no consequences for the enzyme phosphorylation were evident. The lack of concentration dependency, coupled with the limited nature of the effects on protein expression levels argues for a non-specific mechanism, rather than a specific targeting of the respective enzyme in the cell. As a plausible explanation might be quercetin's postulated influence on protein synthesis. Quercetin has been shown to repress protein synthesis by activating eIF2alpha kinases (Ito et al. 1999). Conclusively, these results suggest that no inhibition of GSK-3 is expected from treatment of HT29 cells with quercetin.

Interestingly, SB216763 (10µM) had opposing outcomes on the phosphorylation of the two GSK-3 isoforms (figure 35A/B/C) in HT29 cells. The intracellular level of phosphorylated GSK-3*α* was significantly enhanced (up to 174 ± 27% of control) (figure 35A/C) indicating effective inhibition of the enzyme activity. On the other hand, the amount of phosphorylated GSK-3*β* was notably diminished, suggesting the presence of active GSK-3*β* enzyme (figure 35B/C). However, SB216763 is highly cell permeable (Meijer et al. 2004) and has been shown to indiscriminately bind to and block the active ATP binding sites of both GSK-3 isoforms (Coghlan et al. 2000; Meijer et al. 2004), thus inhibiting kinase activity. It is therefore unlikely that in HT29 cells GSK-3*β* will be active. The decreased phosphorylation might most probably be due to a concurrent inactivation of a kinase by SB216763 that targets GSK-3*β* at Ser9. The protein levels of both GSK-3 isoenzymes were marginally yet not significantly increased by this compound (figure 35A/B/C). This probably might be due to increased protein synthesis of the cells to compensate for the inhibition of GSK-3 activity.

4.2.3 Effect on *β*-Catenin

The impact of quercetin and EGCG on the activity and expression of GSK-3*α*/*β* raised the question whether the homeostatsis of *β*-catenin in HT29 cells is equally influenced by these flavonoids. Western blot experiments using polyclonal antibodies against total *β*-catenin (92kDA) and *β*-catenin phosphorylated at Ser33, Ser37 and Thr41 (92kDA) was performed in that respect. The incubation of the cells occurred in serum-free medium for 24h and the GSK-3 inhibitor SB216763 (10µM) was included in the experiments as a positive control.

4.2.3.1 Phosphorylation and Protein Level of cellular *β*-Catenin

Quercetin did not significantly affect the level of phosphorylated *β*-catenin at concentrations ranging from 10µM to 75µM quercetin (figure 36A/B). Total *β*-catenin level in HT29 cells remained unaffected as well (figure 36A/B).

As depicted in figure 36C, treatment of HT29 cells with the GSK-3 inhibitor SB216763 (10µM) for 24h yielded a strong reduction in the immuno-reactivity of anti-phospho-*β*-catenin (figure 36B) indicating that SB216763 potently reduced phosphorylated *β*-catenin (figure 36A). In line with this result, total *β*-catenin levels rose appreciably (figure 36A), as indicated by the increase in immuno-reactivity of the anti-*β*-catenin antibody (figure 36B). These results are supportive of the result that SB216763 effectively inhibits GSK-3 in the APC complex.

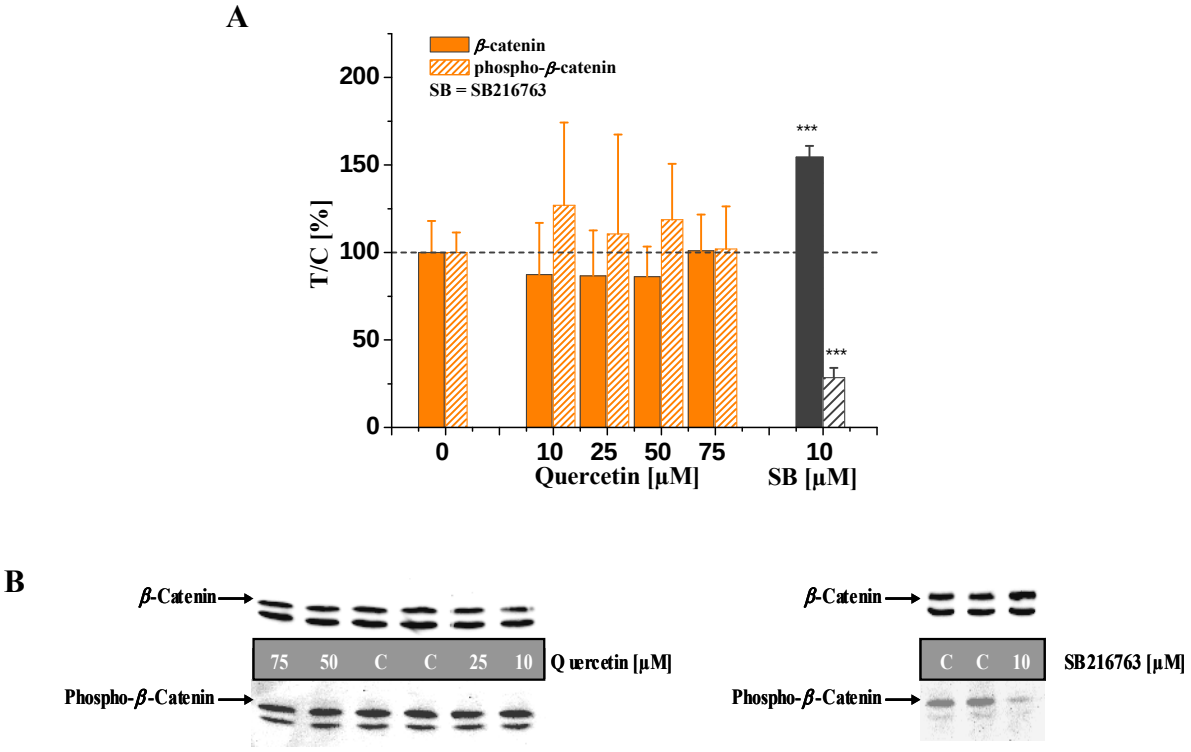

Figure 36: Effect of quercetin on phosphorylated and total *β*-catenin in HT29 cells with (A) showing a chart representation of the results after treatement for 24 h and (B) showing respective western blots for quercetin and SB216763. The results, plotted as test over control (T/C (%)), are presented as the mean ± SD of at least 3 independent experiments with similar outcome. Cells treated with 1% DMSO were employed as control while a GSK-3 selective inhibitor SB216763 served as the positive control. The significances indicated are calculated compared to the solvent control using student's t-test (* $p < 0.001$).**

EGCG effectively diminished the immno-reactivity of anti-phospho-*β*-catenin in a concentration dependent manner from 10µM with an IC_{50} value of 24 ± 7 µM, which is indicative of a reduction in the amount of phosphorylated *β*-catenin in HT29 cells (figure 37A/B). EGCG also caused a concentration dependent reduction in the amount of total *β*-catenin (figure 37A/B). The observed effect of EGCG on phosphorylated and total *β*-catenin in HT29 cells stands at variance with what would be expected, considering that with the inhibition of GSK-3 activity, non-phosphorylated *β*-catenin should escape proteasomal degradation and accumulate in the cell as was seen with SB216763 (figure 37A/B).

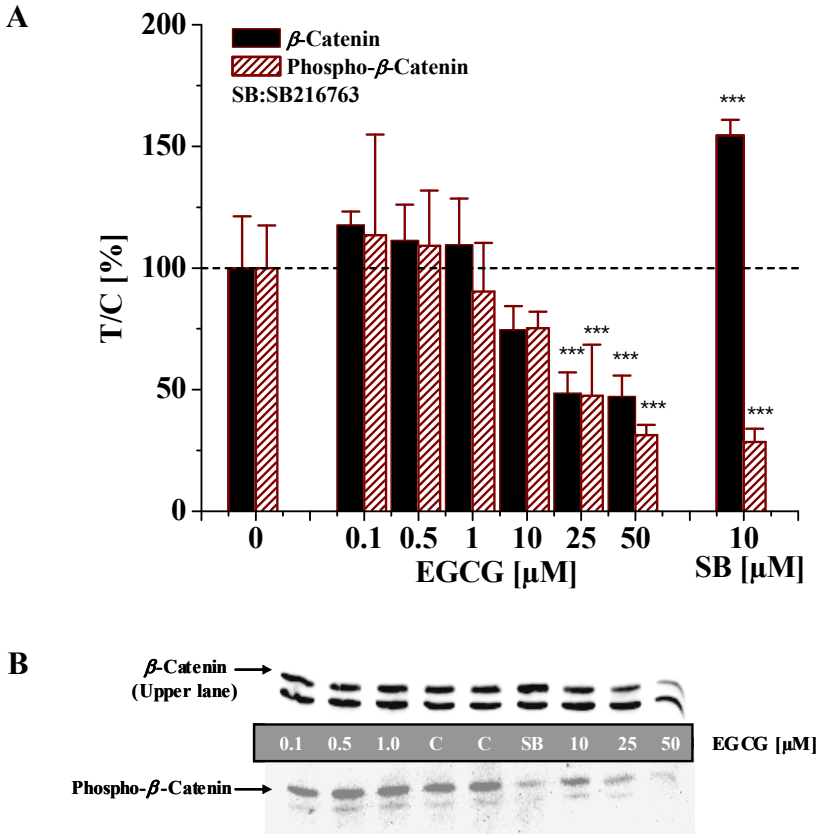

Figure 37: Effect of EGCG on phosphorylated and total *β*-catenin in HT29 cells with (A) showing a chart representation of the results after treatement for 24 h and (B) showing respective western blots for quercetin and SB216763. The results, plotted as test over control (T/C (%)), are presented as the mean ± SD of at least 3 independent experiments with similar outcome. Cells treated with 1% DMSO were employed as control while a GSK-3 selective inhibitor SB216763 served as the positive control. The significances indicated are calculated compared to the solvent control using student's t-test (* $p < 0.001$).**

4.2.3.2 Effect on the nuclear Level of *β*-Catenin

In view of the fact that intra-nuclear *β*-catenin levels crucially contribute to the Tcf/Lef-dependent transcriptional response (Hurlstone and Clevers 2002; van Noort and Clevers 2002) and that EGCG markedly diminished total *β*-catenin levels while quercetin did not; it was of interest to study whether the nuclear *β*-catenin levels were similarly influenced in response to treatment with quercetin and EGCG. For this purpose, the nuclear fraction of HT29 cells was isolated after a serum free incubation with these flavonoids for 24h. The *β*-catenin levels were detected by Western blot analysis using polyclonal antibodies against *β*-catenin.

Quercetin caused no significant impact on nuclear *β*-catenin level in HT29 cells (figure 38A/B). In contrast, EGCG diminished nuclear *β*-catenin an effect significant (50% T/C) at the concentration of 50µM (figure 38A/B), suggesting a suppression of Tcf/Lef driven gene transcription. The GSK-3 inhibitor SB216763 used as a positive control caused a strong increase of *β*-catenin in HT29 nuclei (figure 38A/B), in line with the effect of SB216763 on total *β*-catenin levels (figure 37A/B).

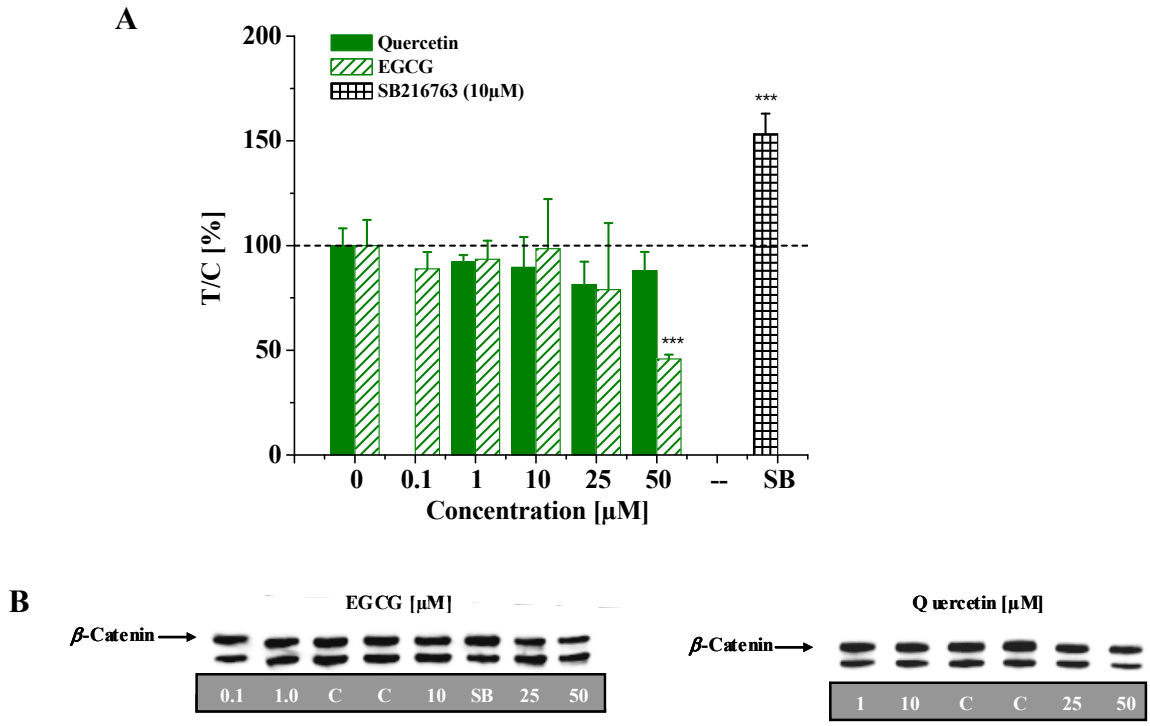

Figure 38: Effect of quercetin, EGCG and SB216763 on nuclear *β*-catenin in HT29 with (A) depicting a chart representation and (B) showing an exemplary picture representation after treatment for 24h. The GSK-3 selective inhibitor SB216763 served as positive control. The data are plotted as test over control (%) with the control being cells treated with 1% DMSO. The data are the mean ± SD of at least three independent experiments. The significances indicated are calculated in relation to the solvent control using student's t-test (* = p < 0.001).**

4.2.3.3 Effect on the *β*-catenin mRNA Transcript Level

The effect of EGCG on phosphorylated and total *β*-catenin (chapter 4.2.3.1) stands at variance with what was expected, considering the inhibitory properties of EGCG on GSK-3. Furthermore the reduction in phosphorylated *β*-catenin (figure 37A/B) did not provoke the

anticipated accumulation of total and nuclear *β*-catenin in the cell. Rather, the reduced phosphorylation of *β*-catenin was concomitantly accompanied by a reduction of total *β*-catenin (figure 37A/B). This raised the question whether the reduced *β*-catenin level might result from a reduction in the expression of *β*-catenin. Therefore transcripts of *β*-catenin were quantified after 24h incubations of HT29 cells with EGCG under serum-free conditions using a pre-developed assay reagent (Hs99999168_m1) for *β*-catenin (Applied Biosystems). The transcript level of the endogenous control gene *β*-Actin was determined for normalization.

EGCG appreciably suppressed the levels *β*-catenin transcripts in HT29 cells in a concentration-dependent manner (figure 39) after 24h incubation. An initial marginal decrease of *β*-catenin transcripts was observed at a concentration as low as 0.1µM, with a marked decrease (40%) at 25 µM. The positive control compound SB216763, did not influence *β*-catenin mRNA levels (figure 39).

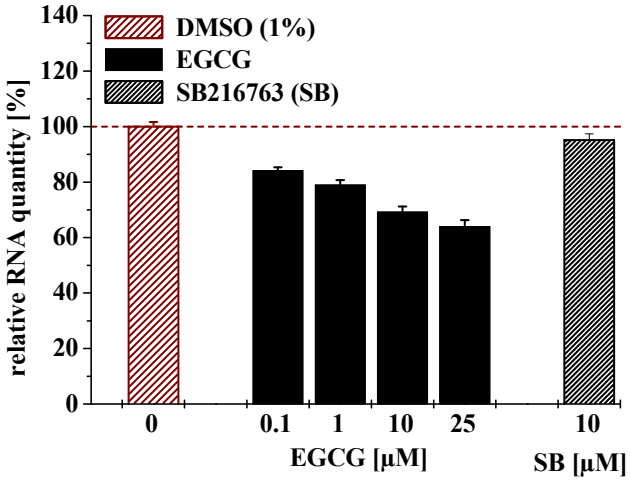

Figure 39: Effect of EGCG and SB216763 on *β*-catenin transcripts in HT29 cells. mRNA content was observed after a 24h serum free incubation. *β*-Catenin expression is normalized to *β*-actin expression and presented in percentage relative to the solvent control. The data are plotted as relative quantity ± delta Ct SD of triplicate experiments performed independently. The significances are calculated in relation to the solvent control using student's t-test (* P< 0.05: **< 0.01).

Incubation (serum free) of HT29 cells with quercetin for 24h caused a concentration dependent decrease in the level of *β*-catenin transcripts, which was maximal at 80µM quercetin with a reduction of about 23% (figure 40).

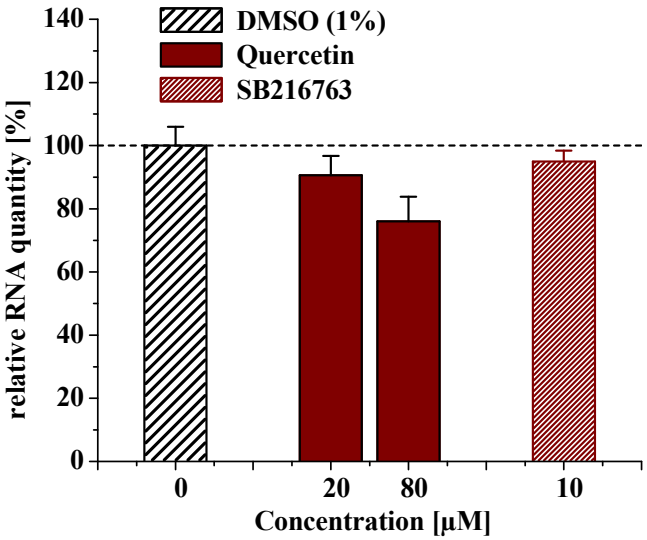

Figure 40: Effect of quercetin and SB216763 on *β*-catenin transcripts in HT29 cells. mRNA content was observed after a 24h serum free incubation. *β*-Catenin expression is normalized to *β*-actin expression and presented in percentage relative to the solvent control. The data are plotted as relative quantity ± delta Ct SD of triplicate experiments performed independently. The significances are calculated in relation to the solvent control using student's t-test (* P< 0.05: **< 0.01).

In summary, EGCG has been shown to effectively modulate cellular *β*-catenin levels in HT29 cells. Consistent with the inhibition of GSK*α*/*β*, sequential treatment of HT29 cells with EGCG for 24h led to a concentration-dependent decrease in phosphorylated *β*-catenin (figure 37). Phosphorylation of *β*-catenin within the APC complex of the Wnt signalling cascade by casein kinase-I and GSK-3 triggers its ubiquitination and eventual proteasomal degradation. A decrease in the phosphorylation of *β*-catenin should entail its stabilization as shown for the GSK-3 inhibitor SB216763 (figure 37). However, a concomitant drop significant os *β*-catenin from 25µM was registered when HT29 cells were treated with EGCG for 24h (figure 37A/B). The reduction of total *β*-catenin in the cells was also accompanied by a distinct reduction in nuclear *β*-catenin levels at 50µM EGCG (figure 38A/B). Analysis of the *β*-catenin transcript levels in HT29 cells after 24h incubation revealed a concentration dependent decrease of about 40% of *β*-catenin mRNA levels at 25µM EGCG, indicating that the drop in total *β*-catenin levels might result from downregulation of *β*-catenin expression. In accordance with

the results on *β*-catenin homeostasis, EGCG had no stimulating effect on the Tcf/Lef driven transcriptional activity in HEK293 cells and HCT116 cells as measured using a reporter gene assay fine-tuned to capture only stimulating effects. Collectively, these results suggest that EGCG influences the expression of Wnt-dependent target genes by suppressing *β*-catenin expression. In support of this notion are results of two groups, who reported an EGCG-dependent reduction of *β*-catenin expression and a reduction in the expression of cyclin D1 and COX-2, genes targeted by Wnt signals (Dashwood et al. 2002; Huh et al. 2004). The results hence lend more support to the already existing data on the cancer preventive potential of EGCG, suggesting that suppression of Wnt-dependent proliferation stimulus is one mechanism through which EGCG may exert at least part of its anticancer effect (Orner et al. 2002; Dashwood et al. 2002; Huh et al. 2004; Li et al. 2002). In tune with this, EGCG has been shown to inhibit growth of HT29 cells with IC_{50} values of 147 ± 18µM after 24h under serum deprived conditions and 40 ± 6µM after 72h in the presence of serum in the incubation medium (Pahlke et al. 2006).

In contrast, treatment of HT29 cells with up 75µM of the flavonol quercetin for 24h did not change the levels of phosphorylated *β*-catenin (figure 36A/B). Consistent with this result, total *β*-catenin and nuclear *β*-catenin levels in HT29 cells were not affected by quercetin (figures 36A/B & 38A/B). Accordingly, mRNA levels of *β*-catenin were not significantly influenced after 24h (figure 40). These results are in line with the results on GSK-3 activity, which was not influenced by quercetin as indicated by western blot analysis (figure 34A/B/C). Moreover, the results suggest that *β*-catenin/TCF/LEF-dependent gene transcription will not be stimulated by quercetin. In contrast though, quercetin marginally but significantly induced Tcf/Lef transcriptional activity in HEK293 cells and HCT116 cells suggestive of an inactive GSK-3 causing increased *β*-catenin levels. Theoritically, the stimulation of cell proliferation is a corollary of an increased *β*-catenin/Tcf transcriptionl activity. Hence, the question was raised whether the induced Tcf/Lef transcriptional activity by quercetin might be of any relevance to the proliferation of HT29 cells. At conditions similar to those used in this work, quercetin has been shown to rather concentration-dependently inhibit than stimulate growth of HT29 cells with IC_{50}values of 124 ± 8µM in serum free medium for 24h and 52 ± 11µM in serum containing medium for 72h (Pahlke et al. 2006). Noteworthy are also the findings of van der Woude et al. (2003) who reported a quercetin-dependent growth hormesis for HT29 cells. Up to 80µM quercetin, growth of HT29 cells was subtly stimulated, while beyond

80µM, growth was significantly inhibited. However, in contrast to this work, van der Woude and co workers modified their asssays by including 1µM ascorbic acids to stabilize quercetin, which may account for the initial proliferation stimulus.

Of note, in the human adenocarcinoma cell line SW480, a reduction in nuclear *β*-catenin at unchanged cytosolic *β*-catenin levels by quercetin has been reported (Park et al. 2005). Such differential effects on *β*-catenin levels might indeed be a reflection of different cellular context and experimental conditions, leading to differential responses. Incubation with quercetin starting 3h after transfection was reported to result in an effective decrease of Tcf/Lef-mediated reporter gene expression (Park et al. 2005). In the presented work, cells were allowed a 48h recovery and acclimatization phase after transfection prior to the incubation with the test compound. Under these experimental conditions, quercetin was found to be a weak inducer of Tcf/Lef-mediated gene transcription, an effect, which however, did not translate in cell growth stimulus of HT29 cells.

SB216763, applied at the concentration of 10µM, notably triggered a reduction of phospho-*β*-catenin concentrations in HT29 cells after treatment for 24h (figure 37A/B). Concomitantly total and nuclear *β*-catenin levels were appreciably increased (figures 37A/B & 38A/B). Beta-catenin transcript levels were indifferent to treatment with SB216763 suggesting that the obtained increase in total *β*-catenin levels is directly and solely related to the inhibition of GSK-3 within the APC complex. Consistent with increased cellular *β*-catenin levels, SB216763 significantly increased the Tcf/Lef- dependent transcriptional activity in HEK293 cells by approximately 21 fold compared to the sovent control (figure 30A). In conclusion, the GSK-3 inhibitor, SB216763 was shown to mimic Wnt proteins stimulation of Wnt-signalling as seen in the increased cellular *β*-catenin levels. This conclusion is consistent with literature, where SB216763 has been shown to induce mRNA expression of the Wnt target genes COX-2 and clycin D1 (Ma et al. 2005; Thiel et al. 2006).

4.3 Modulation of the Glucose-Glycogen Homeostasis

4.3.1 Impact on Glycogen Synthase

In addition to its role in the Wnt signalling pathway, GSK-3 is also an intergral part of the glycogen metabolism. GSK-3 regulates the activity of glycogen synthase (GS) by phosporylating the serin residues Ser653, Ser649, Ser645, and Ser641 thus being able to indirectly manipulate glycogen stores in the cell.

In chapter 4.2.2.1, it was shown that the activity of GSK-3 was suppressed by EGCG after a 24h serum free incubation of HT29 cells. To elucidate the physiological consequence of EGCG's inhibition of GSK-3 on GS, GS activity was determined in a cell homogenate after analogous treatment of the cells. Additionally the phosphorylation status (Ser641) of GS and, the expression (protein level and mRNA) were also determined by western blot and quantitative PCR after 24h treatment with EGCG (25µM).

4.3.1.1 Effects on the Activity of Glycogen Synthase

To determine the effect of EGCG on GS activity, HT29 cells were incubated in serum free medium for 0.5h, 1h, 3h, 6h, 12h, and 24h. GS activity was determined in the cell homogenate as the rate of incorporation of a tritium labelled glucose moiety from [^{3}H]-uridin diphosphate glucose [^{3}H- UDPG] into glycogen in the presence and absence of glucose-6-phosphate, an allosteric activator of GS. EGCG was employed at the concentration of 25µM because at this concentration, EGCG had the highest inhibitory effect on GSK-3. SB216763, a specific inhibitor for GSK-3 was employed as a positive control for the induction of GS activity.

At all time points between 0.5h and 24h, GS activity was substantially and significantly increased in response to treatment of HT29 cells with SB216763. The effect was not time dependent reaching a maximum after 6h with a roughly 2 fold increase in GS activity compared with control cells (DMSO (1%)) (figure 41). After 12h of incubation, although still significant, GS activity experienced a decline of about 75% to 150 ± 22 % which remained at the same level till 24h after incubation.

In comparison, GS activity in EGCG-treated cells remained largely unchanged up to 24h post incubation with 25µM EGCG. At 1h and 12h post incubation, GS activity was minutely decreased by EGCG, which lacked any significance. The lack of activation of GS by EGCG is surprising, considering that EGCG potently inhibited both isoforms of GSK-3 in HT29 cells under similar experimental conditions.

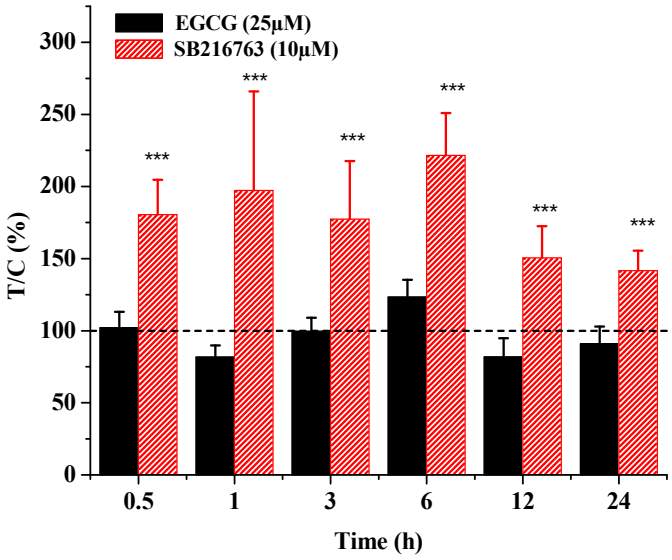

Figure 41: Effecr of EGCG and SB216763 on glycogen synthase activity in HT29 cells measured in a GS assay. GS activity is given as the expression of the rate of integration of a tritium labelled glucose molecule in glycogen by GS measured in the presence and absence glucose-6-phosphate (G-P-6). The data are plotted as test over control (%) with the control being cells treated with 1% DMSO. The data representation is of the mean ± SD of at least three independent experiments. The significances were calculated relative to the solvent control using student's t-test (* = p < 0.001).**

4.3.1.2 Effects on the Protein Level and Phosphorylation of Glycogen Synthase

To underpin the results obtained for GS-activity in the GS assay, Western blot analysis of phosphorylated GS was employed as an indirect measure for GS activity.The modulation of GS phosphorylation on Ser641 and of total GS protein level in HT29 cells was determined using polyclonal anti-phospho GS (Ser 641) and anti GS respectively fromCell Signaling after a serum free incubation for 15min, 30min and 24h with EGCG (25µM) and SB216763. The

serin residue 641 of GS is phosphorylated by GSK-3 and its phosphorylation is most crucial for the inhibition of GS activity.

Incubation of HT29 cells with SB216763 induced a strong and significant decrease in the phosphorylation of GS at Ser641 (figure 42/B). As early as 15 minutes post incubation, dephosphorylation of GS in HT29 cells was already well over 60%. The effect remained sustained for as long as 24h post incubation (figure 42A/B). Contrary to SB216763, Ser641 phosphorylation of GS in HT29 cells remained unchanged after treatment with EGCG for 15min, 30min and 24h (figure 42A/B).

A

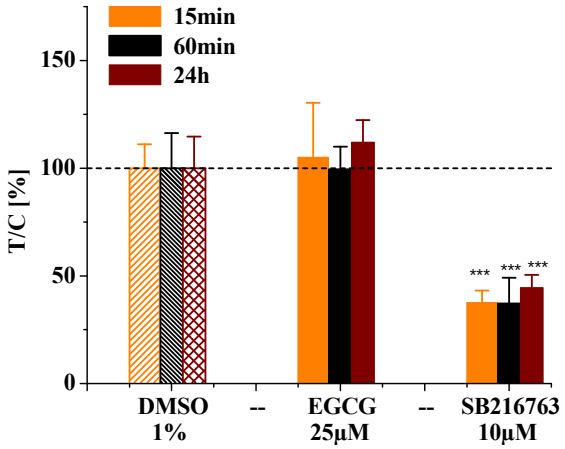

B

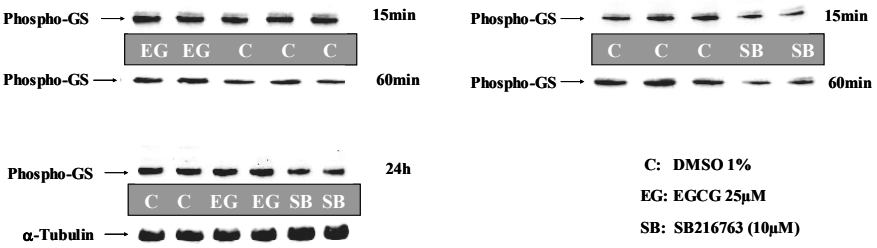

Figure 42 Effect of EGCG and SB216763 on the Ser 641 phosphorylation of glycogen synthase with (A) showing a chart representation and (B) showing an exemplary picture representation after a 24h challenge. The GSK-3 selective inhibitor SB216763 served as positive control. The data are plotted as test over control (%) with control being cells treated with 1% DMSO. The data are the mean ± SD of at least three independent experiments. Statistical significance was accepted at $p < 0.001$ (***) using student's t-test. Alpha- tubulin was determined as a loading control.

Alongside the phosphorylation status at Ser641, the cellular GS protein level was also analyzed by Western blot. Incubation of HT29 cells for 24h with SB216763 (10µM) caused a strong and significant increase of total GS protein levels by about 3 fold compared to the solvent control (figure 43A/B). EGCG caused a significant increase of total GS levels at 25µM, however the increase was minor compared to that caused by SB216763 (figure 43A/B).

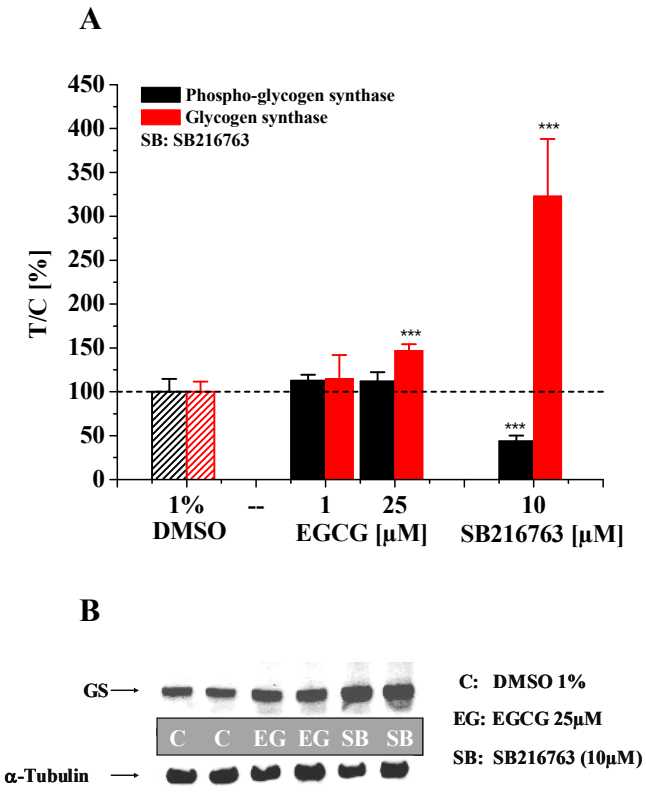

Figure 43 Effect of EGCG and SB216763 on total glycogen synthase in HT29 cells with (A) showing a chart representation and (B) showing an exemplary picture representation after a 24h challenge. The GSK-3 selective inhibitor SB216763 served as positive control. The data are the mean ± SD of at least three independent experiments. Statistical significance was accepted at p < 0.001 (***) using Student's t-test. Alpha-tubulin was determined as the loading control.

4.3.1.3 Effect on the mRNA Levels of Glycogen Synthase

The question whether the almost 4 fold increase in GS protein level in HT29 cells after the incubation with SB216763 is caused by increased GS transcripts was addressed using qualitative real time PCR. The effect of flavonoids on GS transcription was also studied in HepG2 cells. Cells were incubated for 6h with EGCG (1µM, 10µM), quercetin (20µM,

80µM) and for 24 h with EGCG (1µM, 10µM, 25µM), quercetin (20µM, 80µM) and SB216763 (10µM) under serum-free conditions prior to extraction of total RNA. Total mRNA was reverse transcribed with the cDNA Archive High Capacity Kit from Applied Biosystems after which the cDNA was amplified in a RT-PCR step using TaqMan MGB probes and gene specific primers and random hexamers. Beta-actin was co-amplified as endogenous control for normalization. Effects on both isoforms of glycogen synthase (GS), muscle glycogen synthase (MGS) and liver glycogen synthase (LGS) were investigated.

4.3.1.3.1 HT-29 cells

After 6h of incubation, EGCG fostered a concentration dependent decrease of the transcript levels of MGS and LGS (figure 44A). This effect was however abolished for LGS when incubations periods were prolongated to 24h (figure 44B). While mRNA levels of LGS responded indifferently to the 24h treatment with EGCG (figure), EGCG caused a slight reduction of mRNA levels of MGS. The effect, which was not concentration-dependent, remained at the same level between 1µM till 25µM EGCG, reaching a minimum of 77 ± 6 % at 1µM EGCG compared to DMSO (1%) treated control cells.

A **B**

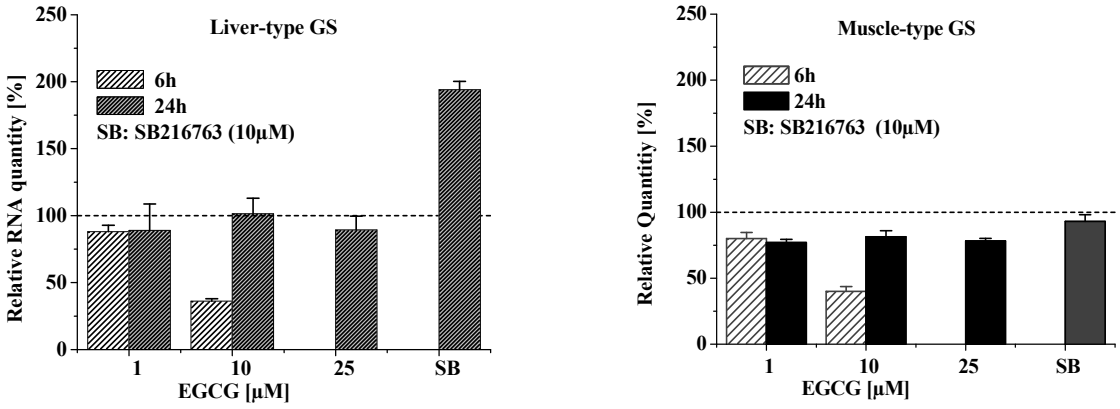

Figure 44: Effect of EGCG and SB216763 on the transcript level of (A) LGS and (B) MGS in HT29 cells after treatment for 6h and 24h. Glycogen synthase expression is normalized to *β*-actin expression and presented in percentage relative to the solvent control. The data is plotted as relative quantity ± delta Ct SD of triplicate experiments performed independently.

The GSK-3 inhibitor SB216763, applied at a concentration of 10µM did not influence cellular levels of MGS in HT29 cells after 24h incuabtion (figure 44B). On the other hand, LSG transcripts experienced a near 2 fold increase compared to the solvent control (figure 44A).

Quercetin increased LGS levels in HT29 cells after 6h incubation by about 1.5 fold at 80µM (figure 45). After 24h, the LGS transcript status was not affected by quercetin (figure 45). In contrast, quercetin prompted a concentration dependent decrease of MGS transcript levels in HT29 cells after 6h (figure 45) attaining a minimum of about 40%. While MGS transcript levels at 20µM recuperated to the levels of DMSO treated cells after 24h, 80µM quercetin still caused an approximately 15% reduction in MGS RNA levels (figure 45).

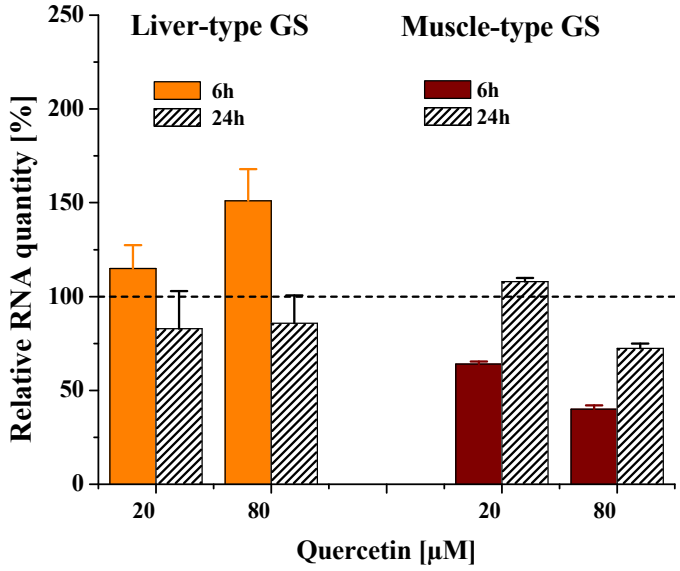

Figure 45: Effect of quercetin on the transcript level of LGS and MGS in HT29 cells after incubation for 6h and 24h. Glycogen synthase expression is normalized to *β*-actin expression and presented in percentage relative to the solvent control. The data is plotted as relative quantity ± delta Ct SD of triplicate experiments of similar outcome performed independently.

4.3.1.3.2 HepG2 cells

Short-term (6h) incubations of HepG2 cells with EGCG (1µM, 10µM) hardly influenced mRNA levels of MGS (figure 46A). Merely at 1µM EGCG after 24h was there an increase in MGS levels of about 20% compared to the solvent control (figure 46A). No substantial effect

on LGS mRNA levels was determined for EGCG after 6h. However, after 24h, EGCG decreased LGS levels by about 50% of the DMSO control (figure 46A).

Quercetin did not substantially affect MGS transcript levels in HT29 cells after 6h and 24h of incubation (figure 46B). LGS RNA levels remained largely unchanged after 6h. After 24h, 20µM quercetin appreciably reduced LGS mRNA transcription reaching 26.5 ± 15% of the DMSO control. At the higher concentration of 80µM quercetin LGS transcript levels increased by about 3 fold compared to the DMSO solvent control (figure 46B).

A **B**

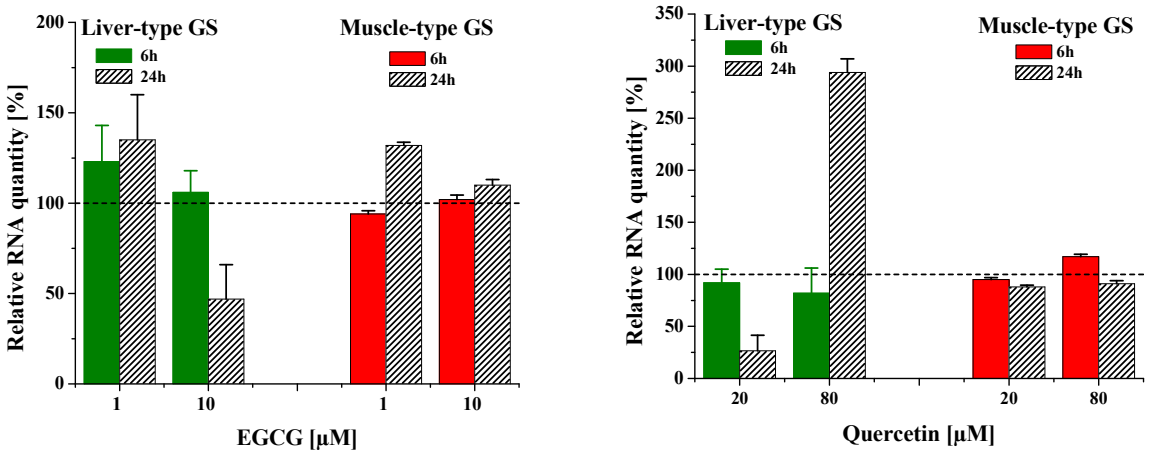

Figure 46: Effect of (A) EGCG and (B) quercetin on the transcript levels of LGS and MGS in HepG2 cells after treatment for 6h and 24h. Glycogen synthase expression is normalized to *β*-actin expression and presented in percentage relative to the solvent control. The data is plotted as relative quantity ± delta Ct SD of triplicate experiments of similar outcome performed independently.

In summary, the inhibition of GSK-3 kinase activity observed in HT29 cells after the 24h incubation with EGCG was on a whole without consequence for GS activity. Little to no change on the activity of GS was observed as determined by western blot and GS-assay, following the time-dependent incubation of HT29 cells with 25µM EGCG, a concentration that was most potent in inactivating both isoforms of GSK-3. Although the total GS protein level was significantly increased, it however had no influence on GS activity after 24h

incubation. The lack of activation of GS by EGCG is insofar surprising as EGCG (25µM) potently inhibited both isoforms of GSK-3 in HT29 cells. The stimulation of GS activity by SB216763 (10µM) dismisses the possibility of this result arising due as an assay artefact. The phosphorylation-dependent inactivation of GS is known to depend, not exclusively on the GSK-3-mediated phosphorylation of sites 4 (Ser653), 3c (Ser649), 3b (Ser645) and 3a (Ser 641) (Poulter et al. 1988), but also, on the phosphorylation of sites 2 (Ser7) and 2a (Ser10) on the N terminus of GS. Phosphorylation of the N- terminal sites, which also is kinase-mediated (AMPK, PKA), additionally potentiates the inactivation of GS (Carling and Hardie 1989). It has indeed been shown that EGCG can induce AMPK (Hwang et al. 2005; Hwang et al. 2007; Moon et al. 2007), which targets site 2 (Carling and Hardie 1989). It is thus conceivable that, the AMPK-dependent inactivating effect on site 2 might be acting in opposition, thus compensating for the activating effect on site 3a by GSK-3 so that the overall GS activity experiences little change. Furthermore, PKA which also is known to target site 2 of GS is activated by EGCG (Lorenz et al. 2004). Lastly, site 3a of GS can also be phosphorylated in addition to GSK-3 by a yet unidentified kinase (Roach 1990, 2002; DePaoli-Roach et al. 1983; Skurat et al. 2000), which may be activated by EGCG thus compensating for GSK-3 dependent reduction of phosphorylation of Ser641 on GS.

Alongside the phosphorylation status, the total protein level of GS was also determined in HT29 cells. EGCG caused a concentration dependent increase in the GS protein level (figure 43A/B); which, even though significant at 25µM, evidently influenced neither GS activity (figure 41) nor GS phosphorylation after 24h incubation (figure 42A/B). Short-term incubation (6h) of HT29 cells with 10µM EGCG appreciably diminished the mRNA levels of both GS isoforms (figure 44A/B). 24h treatment of HT29 cells had no effect on LGS mRNA levels while mRNA for MGS was slightly reduced by an average 20% of the control (figure 44B). The effect however remained at the same level from 1µM to 25µM. Generally, the GS transcript levels were on the average higher after 24h than after 6h, suggestive of cellular compensation through enhanced biosynthesis, which might explain the increased GS-protein levels detected by western blot (figure 43A/B). Quercetin had opposite effects on LGS and MGS transcription after 6h of incubation. While MGS transcript levels were reduced in HT29 cells, LGS mRNA levels were concomitantly increased. After 24h both MGS and LGS transcription was stabilized in HT29 cells, restoring transcript levels to near control levels (figure 45).

In HepG2 cells, MGS transcript levels were slightly increased after 24h by 1µM EGCG. LGS mRNA levels responded indifferently to EGCG after 6h of incubation, however after 24h, LGS were strongly reduced (figure 46A). 20µM and 80µM quercetin provoked opposite responses with respect to LGS transcription. While at the lower concentration of 20µM LGS mRNA expression was appreciably reduced, reaching 26.5 ± 15% of control, at the higher concentration 80µM quercetin (figure 46B) increased LGS transcript levels by about 3 folds compared to the DMSO control.

In accordance with the effects on GSK-3 activity, the GSK-3 inhibitor SB216762 (10µM) caused a sustained and significant activation of GS activity between 30min and 24h (figure 41). In reflection of the increased GS activity, SB216763 appreciably diminished the phosphorylation of GS on Ser641 (figure 42A/B). As early as 15 minutes post incubation, dephosphorylation of GS in HT29 cells was already well over 60%. The effect was sustained for as long as 24h post incubation (figure 42A/B). Quantitive PCR results indicate a near 2 fold increase of LGS transcripts after 24h incubation with SB216763 while MGS transcript levels proved unresponsive to SB216763 (figure 44A/B). The increase of LGS mRNA levels was accompanied by a concomitant increase in total GS protein levels of about 3 fold as determined by western blot (figure 43A/B). It thus would seem probable that the SB216763-mediated increase of the LGS transcript levels translates into increased expression of GS protein. Taken together, the results on GSK-3 and GS argue for rather an indirect interference of SB216763 on GS activity via inhibition of GSK-3 than via allosteric action on GS. In addition the results suggest that the apparent increase in GS activity caused by SB216763 in HT29 cells, most likely, is a product of an initial increased dephosphorylation of GS observed as early as 15min post incubation that later (with increasing incubation duration upto 24h) is buttressed by increasing GS protein expression.

4.3.2 Impact on Glycogen Phosphorylase

4.3.2.1 Expression Profile of Glycogen Phosphorylase in HT29 Cells and HepG2 cells

To identify the glycogen phosphorylase isoforms expressed in HT29 cells and HepG2 cells, total RNA isolated from the cells was reverse transcribed using gene specific primers for muscle, liver and brain isoforms of glycogen phosphorylase and the titan one tube PCR kit from Qiagen. cDNA was resolved in a 1.3% agarose gel at 80V. DNA fragments were visualized by staining with ethidium bromide. *β*-Actin was co-detected as endogenous control. These results were obtained by Bülent Soyalan, in course of his "Forschungspraktikum".

The results of the agarose gel electrophoresis show that both cell lines; HT29 cells and HepG2 cells express glycogen phosphorylase transcripts for the liver- and brain isotypes (figure 47). In accordance with literature data, BGP, a potential marker for colon carcinogenesis represented the most highly expressed isoform in both cell lines, evidenced in the comparably high band intensity with respect to *β*-actin (Tashima et al. 2000). In both cell lines weak signals for muscle-type GP transcripts were detected by RT-PCR (figure 47). The allocation of the DNA bands to the respective isozyme (BGP: 677 bp, MGP: 534 bp und LGP: 445 bp) was performed by comparison with literature values.

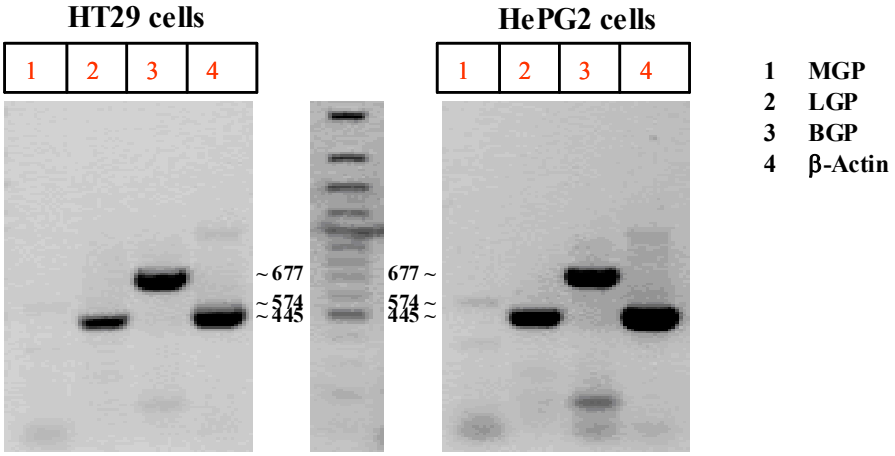

Figure 47: Agarose gel images showing the glycogen phosphorylase isoforms expressed in HT29 cell and HepG2 cells. The DNA samples were resolved in 1.3% agarose and visualized by staining with eithidium bromide.

4.3.2.2 Effects on the Activity of Glycogen Phosphorylase

To determine the effect of EGCG and SB216763 on the activity of GP in HT29 cells, the cells were incubated time-dependently (0.5h, 1h, 3h, 6h, 12h, and 24h) in serum free medium with EGCG (25µM) and SB216763 (10µM). GP activity was subsequently measured in cell homogenate using a method that combines the GP-catalyzed breakdown of glycogen with the reduction of $NADP^+$ (oxidized nicotinamide adenine di-nucleotide phosphate) to $NADPH_2$ so that the process can be monitored photometrically at 340nm.

Neither EGCG (25µM) nor and SB216763 (10µM) caused a substantial change in the activity of GP in HT29 (figure 48)

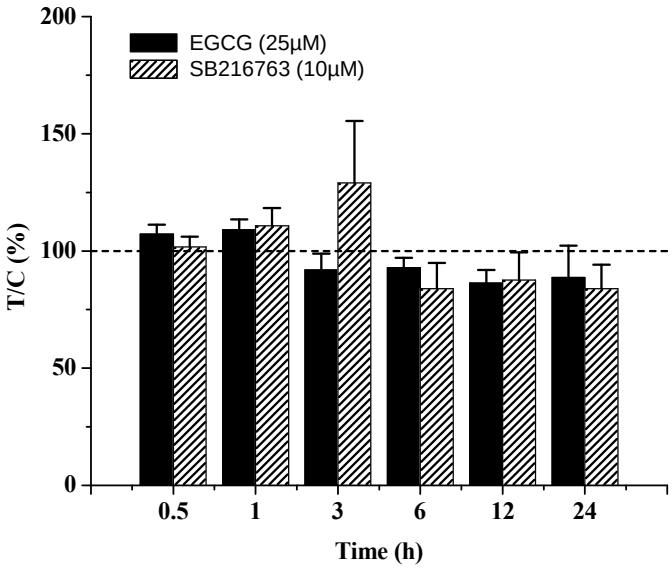

Figure 48: Time-dependent effect of EGCG and SB216763 on the activity of glycogen phosphorylase in HT29 cells. The data are plotted as test over control (%) with the control being cells treated with 1% DMSO. The data representation is of the mean ± SD of at least three independent experiments.

4.3.2.3 Effects on the cellular protein level of Glycogen Phosphorylase

The impact of EGCG on the GP protein level in HT29 cells was determined by western blot using anti-GP (Santa Cruz) that co-determines brain type- and muscle type-GP. The cells were incubated serum free with EGCG (1µM, 25µM) for 24h.

EGCG had no significant effect on GP protein level in HT29 cells after 24h at the concentrations of 1µM and 25µM EGCG (figure 49A/B). Incubation with SB216763 resulted too in no of change cellular GP levels (figure 49/B).

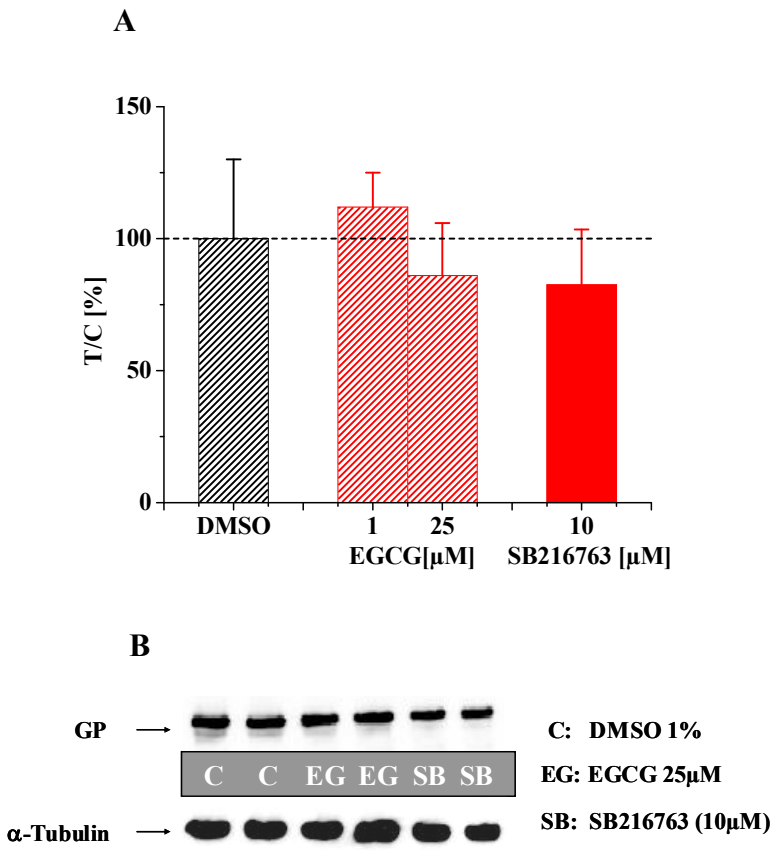

Figure 49 **Effect of EGCG and SB216763 on the expression of glycogen phosphorylase in HT29 cells with (A) showing a chart representation and (B) showing an exemplary Western blot picture after a 24h long incubation. The data are plotted as test over control (%) with control being cells treated with 1% DMSO. The data are the mean ± SD of at least three independent experiments.**

4.3.2.4 Effects on the Transcript Level of the GP-Isoenzymes

The effect of EGCG on the mRNA level of BGP, LGP and MGP was investigated in HT29 cells and HepG2 cells using TaqMan RT-PCR. The cells were incubated in serum free medium for 6h and 24h. Total RNA was isolated, reverse transcribed in the presence of random hexamers and amplified with gene specific primers. The mRNA level of the house keeping gene, *β*-actin was determined and used for normalization.

4.3.2.4.1 HT-29 cells

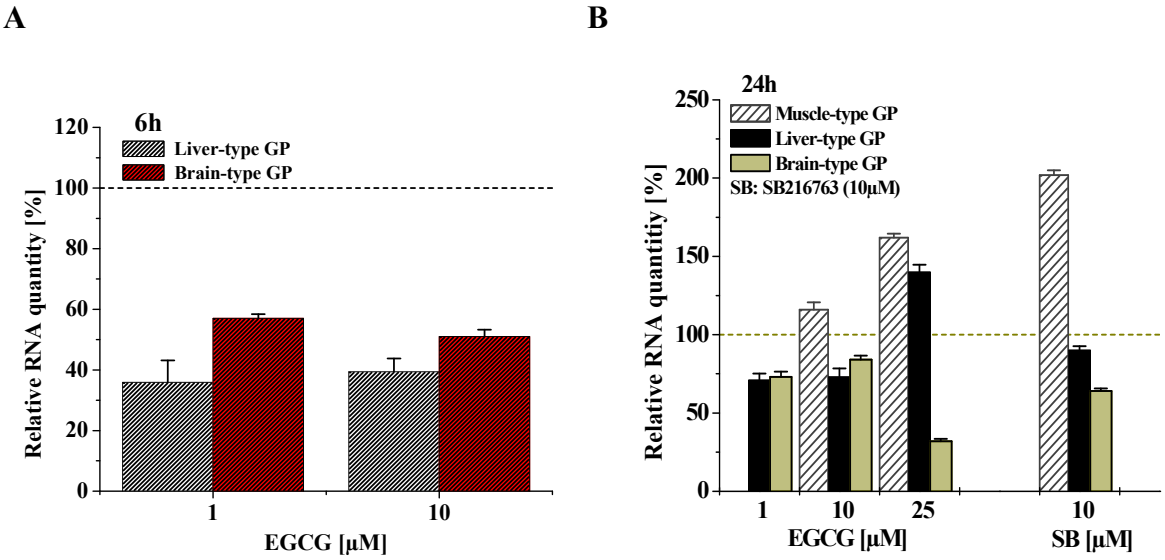

Figure 50: Effect of EGCG and SB216763 on the transcript level of GP in HT29 cells after (A) 6h and (B) 24h. Glycogen synthase expression is normalized to *β*-actin expression and presented in percentage relative to the solvent control. The data is plotted as relative quantity ± delta Ct SD of triplicate experiments performed independently. Statistical significance was accepted when p < 0.05 (*) using student's t-test.

EGCG (1µM, 10µM) effectively downregulated LGP and BGP transcripts in HT29 cells after 6h reaching maximal reductions of roughly 40% and 60% respectively compare to the solvent control (figure 50A). Although the reduction of LGP transcript levels remained till 24h after incubation at 1µM and 10µM, the effect however became less prominent compared to 6h, probably due to counter-regulatory processes in the cell (figure 50B). At 25µM, EGCG increased the mRNA levels of both MGP and LGP while the level of BGP, which quantitatively is the most predominant isoform in HT29 cells was appreciably reduced by

about 70% compared to DMSO (1%)-treated cells (figure 50B). Although BGP transcripts were strongly diminished at 25µM EGCG, this seemingly did not translate into reduction of the GP protein levels as determined by western blot (figure 49A/B). One could then argue that the increased expression of MGP compensated for the reduced level of BGP expression hence little change in (BGP and MGP) protein level was observed.

The GSK-3 inhibitor, SB216763 increased MGP transcripts in HT29 cells by about 2 fold after 24h. BGP transcript levels were appreciably reduced by SB216763 after 24h reaching about 65% (figure 50B). LGP mRNA levels were not influenced by 10 µM SB216763 after 24h (figure 50B).

The incubation of HT29 cells with 20µM and 80µM quercetin triggered a concentration-dependent reduction of BGP mRNA after 6h and 24h respectively reaching a minimum of 66 ± 3.1% after 6h and 40 ± 2.6% after 24h compared to the solvent control (figure 51). LGP transcript levels decreased by about 40% after 6h incubation with 20µM and 80µM quercetin (figure 51). The reductions were maintained up till 24h after incubation (figure 51).

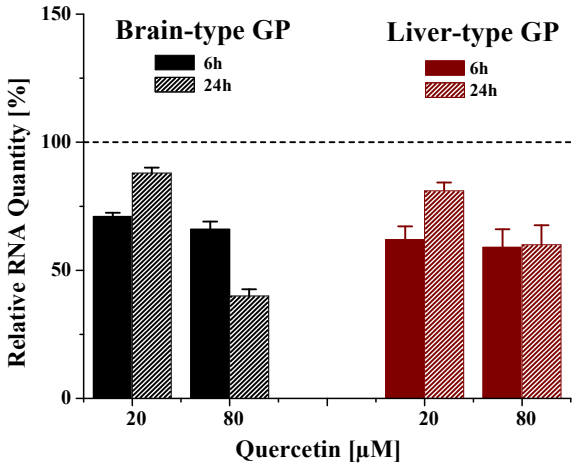

Figure 51: Effect of quercetin on the transcript level of BGP and LGP in HT29 cells after incubation for 6h and 24h. Glycogen synthase expression is normalized to *β*-actin expression and presented in percentage relative to the solvent control. The data is plotted as relative quantity ± delta Ct SD of triplicate experiments performed independently.

4.3.2.4.2 HepG2 Cells

EGCG (1µM, 10µM) caused a concentration-dependent reduction of BGP transcript levels in HepG2 cells, attaining a minimum of about 73% compared to DMSO (1%) treated cells (figure 52A). After 24h, EGCG did not interfere with the BGP RNA levels in HepG2 cells (figure 52A). LGP transcript levels were also diminished in a concentration dependent fashion by EGCG after 6h reaching a minimum order of magnitude of about 70% of the control at 10µM, which persisted for up to 24h post incubation (figure 52A).

Quercetin (20µM, 80µM) also reduced BGP transcript levels dose-dependently in HepG2 cells after 6h of incubation (figure 52B). The decrease was highest at 80µM quercetin with about 25% reduction. After 24h, BGP transcript levels in HepG2 cells were slightly increased by about 1.5 fold. LGP transcript levels dropped in a concentration dependent manner at both time points (6h and 24h) reaching a maximal reduction of about 33% of the control after 24h.

A **B**

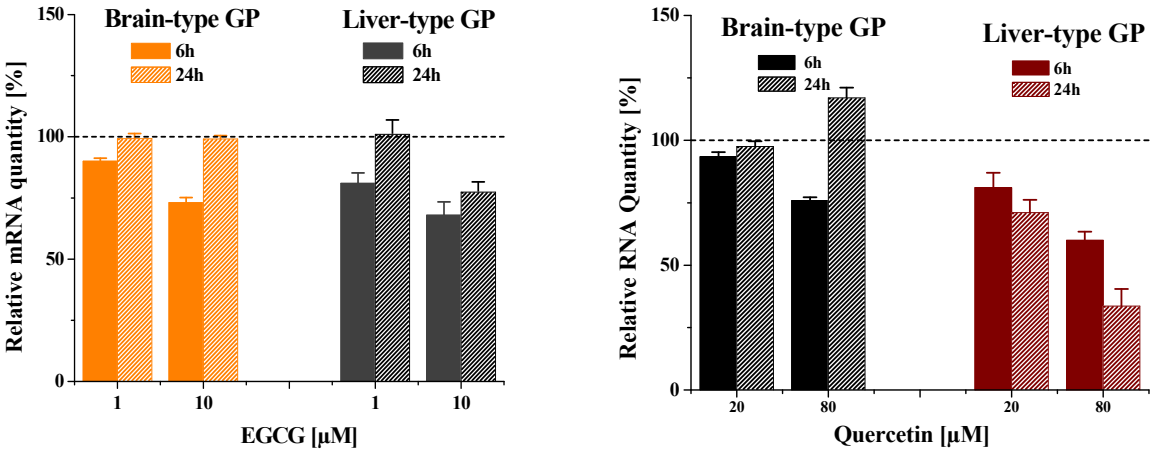

Figure 52: Effect of EGCG and quercetin on the BGP and LGP transcript levels in HepG2 cells after incubation for 6h and 24h. Glycogen synthase expression is normalized to *β*-actin expression and presented in percentage relative to the solvent control of three independent experiments.

In summary, the qualitative PCR analysis of total RNA from HT29 cells and HepG2 cells, indicated that both cell lines express all three forms of glycogen phosporylase LGP, MGP and BGP (figure 47). As can be inferred from their names, the brain-type GP is predominantly expressed in brain tissue while the liver and muscle types are principally expressed in liver and muscle tissue respectively. However, in both cancer cells lines, HT29 and HepG2 of colonic and liver origin respectively, BGP, was the predominantly expressed isoform (figure 47) although it normally should be absent in these tissues. In line with this result are data indicating that BGP expression is highly increased in many cancer types (Shimada et al. 2002; Barbosa and Castro 2002; Shimada et al. 2001; Tashima et al. 2000; Shimada et al. 1999), giving room for conjecture that BGP might be turned on in cancerous tissues to meet increased energy needs of the cells. Qualitative PCR results indicated that LGP was the second most abundant GP isoform in HT29 cells and HepG2 cells, followed by MGP. Signals for MGP were very weak in both cell lines. In support of the results of qualitative PCR, data gathered during quantitative analysis indicated a predominant transcription of BGP, followed by LGP and MGP in HT29 cells. While BGP on the average had strong fluorescence signals already after 18 PCR cycles, signals for LGP and MGP were detected after a Ct of 23 and 32 respectively.

Treatment of the colon carcinoma cell line HT29 with 1µM and 10µM EGCG for 6h substantially reduced LGP mRNA levels, which apparently were not fully recovered after 24h (figure 50A). 25µM EGCG caused a distinct reduction of BGP levels after 24h, while MGP and LGP transcript levels were increased (figure 50B). It is hence conceivable that MGP and LGP expression might have been upregulated in compensation of the reduction in BGP levels to maintain the energy homeostasis of the cells. In support of this assumption, no change of protein level (BGP and MGP) was detected in HT29 cells after a 24h treatment with 25µM EGCG (figure 49A/B). Concomitantly, 25µM EGCG also did not influence GP activity (figure 48). Contribution of LGP protein modulation to the total protein could not be ascertained since the GP-antibody used during Western blot can only cross-detect BGP and MGP but not LGP.

SB216763 (10µM) did not influence LGP transcription after 24h. However, while BGP transcription was distinctly downregulated by about 25%, MGP levels became upregulated by about 2 fold (figure 50B) suggesting a compensation process of the cells. Consistently, no

change in GP protein levels (BGP and MGP) was observed in Western blot analysis (figure 49A/B). GP activity too was not influenced to EGCG at a concentration of 25µM (figure 48).

In HepG2 cells, EGCG (1µM, 10µM) concentration-dependently reduced BGP levels after 6h (figure 52A). However, BGP transcript levels recuperated after 24h (figure 52A). LGP transcript levels were also decreased in a concentration-dependent manner after 6h (figure 52A). In summary, transcript levels of both BGP and LGP isoforms after treatment with EGCG were generally higher after 24h than after 6h, suggesting a correction by biosynthetic control mechanisms.

Quercetin distinctly diminished LGP transcript levels in both cell lines 6h and 24h after incubation suggesting a reduction in the expression of LGP in both cells lines (figure 51 & figure 52B). While BGP levels in HT29 cells were reduced after 6h and 24h (figure 51), in HepG2 cells only 80µM quercetin affected BGP transcription. After 6h BGP, transcript levels dropped by about 25%, whereas after 24h, they experienced a slight increase (figure 52B) suggesting over-correction by biosynthetic control mechanisms in HepG2 cells.

4.3.3 Effects on the Glycogen Levels

To investigate whether a modulatory effect on GS and/or GP in HT29 cells has an impact on the glycogen deposition, cellular glycogen content was determined. HT29 cells were incubated with 25µM EGCG and 10µM SB216763 for 0.5h, 1h, 3h, 6h, 12h and 24h after which they were subjected to alkali hydrolysis. Glygogen was then precipitated with ethyl alcohol and sodium sulfate, and quantified spectrophotometrically at 620nm in the Anthron assay by means of linear interpolation and a standard curve.

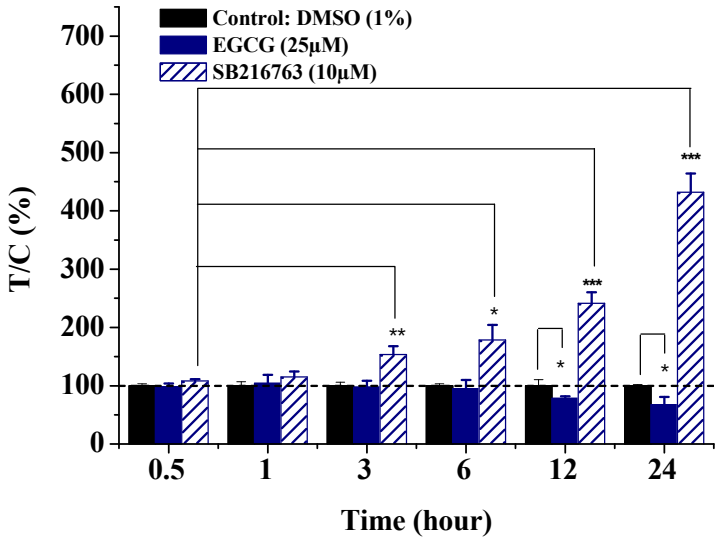

Figure 53: Time-dependent effecr of EGCG and SB216763 on the glycogen content in HT29 cells Data are presented as mean ± SD of at least three independent experiments. Statistical significance was accepted when *p < 0.05* = *; *p < 0.01*= **; *p < 0.001*= *.**

The incubation of HT29 cells with the GSK-3 inhibitor SB216763 caused a time-dependent increase of glycogen, which peaked after 24h with a plus of 432 ± 32% compared to DMSO-treated cells (figure 53). The rise in glycogen was significant as from 3h post incubation. In contrast, incubation of HT29 cell with 25µM EGCG for up to 6h caused no change in cellular glycogen levels (figure 53). However, after 12h incubation with EGCG, glycogen levels in HT29 cells significantly declined by 20%. The decrease in glycogen after 24h was even more prominent, reaching about 30% compared to the DMSO control (figure 53).

The cellular glycogen content was determined as a parameter that sums up the effects on the upstream (to glycogen) located GS and GP proteins. Incubated in time sequential fashion between 30min and 24h, 25µM EGCG had no effect up to 6h post incubation on the deposition of glycogen in HT29 cells (figure 53). After 12h and 24h cellular glycogen content was subtly but significantly reduced (figure 53). This is rather surprising, considering that neither GS nor GP activities were influenced by EGCG. Hence an indirect interference of EGCG on the glycogen catabolic machinery in HT29 cells might be involved causing the drop in glycogen. The debranching enzyme, which functions in concert with GP to breakdown glycogen, may be a possible candidate through whom EGCG might accelerate glycogen breakdown in HT29 cells.

Antidiabetic potential of EGCG has been shown *in vivo* in diabetic rat models (Anton et al. 2007; Koyama et al. 2004; Waltner-Law et al. 2002; Wolfram et al. 2006). Regulation of the expression of key enzymes involved in gluconeogenesis have been shown to be possible targets for the repression of hepatic glucose formation in these models (Anton et al. 2007; Koyama et al. 2004; Waltner-Law et al. 2002; Wolfram et al. 2006). The results of this work suggest that in HT29 cells, regulation of GS and GP of the glycogen anabolic and glycogen catabolic pathways respectively, may not contribute to the anti-diabetic potential reported for EGCG *in vivo*.

In contrast, SB216763 progressively increased glycogen content over a period of 24h in HT29 cells, reaching a maximum of fold of control (figure 4.3-13). The increased cellular glycogen levels correlate with the increased and sustained activity of GS activity over the entire incubation period of 24h (figure 41). In accordance, GP activity was not affected by SB216763, indicating that the deposition of the glycogen stores in HT29 cells was an additive process, resulting mainly from the stimulation of GS activity via GSK-3 inhibition. In summary, the results on glycogen deposition show that SB216763 is a potent inducer of GS synthase activity in HT-29 cells. This conclusion is supported by the data of Coghlan and co workers who reported a potent inhibition of GSK-3 also accompanied by accumulation of glycogen in liver cells (Coghlan et al. 2000).

4.4 Final Discussion

The phosphorylation of GSK-3 on Ser21 and Ser9, consistent with inhibition of GSK-3α and GSK-3β (Grimes and Jope 2001) was determined by western blot as an indicator for GSK-3 activity. The level of phosphorylated GSK-3α and -β in HT29 cells was not substantially influenced by quercetin (figure 34A/B/C), indicating that the inhibition of GSK-3α and GSK-3β activity remained largely unaffected. GSK-3 protein levels were subtly but appreciably diminished for both proteins, however, the effect was not concentration-dependent which speaks for some non-specific mechanisms, rather than a specific interference of quercetin with the respective target enzyme. Taken together, quercetin is not expected to cause substantial inhibition of GSK-3α and -β in HT29 cells. In accordance with the lack of activation of both GSK-3isoforms, quercetin also did not appreciably alter cellular levels of β-catenin and phosphorylated β-catenin in HT29 cells after 24h treatment (figure 36A/B), indicating that quercetin possesses no β-catenin stabilizing potential in HT29 cells. Consistently, β-catenin mRNA (figure 39) remained unaffected up to a concentration of 50µM quercetin. Also, nuclear β-catenin levels were unaltered by quercetin (figure 38A/B) permitting the assumption that β-catenin/Tcf/Lef-dependent gene transcription will not be influenced by quercetin. However, in the relevant reporter gene assay models in HEK293 cells and HCT116 cells, incubation with quercetin (10-50µM) enhanced Tcf/Lef-driven reporter gene expression (figures 30A, 32A, 33A), suggesting rather a proliferative stimulus for these cells. This does give room for speculation if the differential effects observed may be reconciled with inherent differences of the various cell-types and/or variations in experimental conditions used. In this light quercetin has been shown in SW480 cells to cause a reduction in nuclear β-catenin at unchanged cytosolic β-catenin levels, resulting in an effective decrease of Tcf/Lef-mediated reporter gene expression (Park et al. 2005). In principle, up-or downregulation of the Tcf/Lef-mediated gene expression is expected to either up-or downregulate proliferation respectively. The above mentioned discrepancy in the effects of quercetin on Tcf/Lef transcriptional activity in the various cells types thus raises the question whether the signals commensurately translate in stimulation of growth for the respective cells. Indeed, in line with the increased β-catenin/Tcf/Lef transcriptional activity in HCT116 cells (figure 33A), these cells have been shown to experience a slight but significant proliferation phase within the same concentration range tested in this work (1-25µM) (van der Woude et al. 2005). On the other hand, at experimental conditions similar to those employed in this work for HT29 cells, Pahlke et al.

(2006) reported no stimulatory effect of quercetin on the growth of HT29 cells. In contrast, quercetin was found to rather inhibit the growth of HT29 cells in a concentration dependent manner (Pahlke et al. 2006). In view of quercetin's negligibly small effect on total *β*-catenin, and nuclear *β*-catenin in particular, it can be inferred that Wnt-dependent modulation of growth is not a mechanism through which quercetin exacts growth inhibition of HT29 cells.

In contrast to quercetin, the green tea catechin EGCG was identified as a potent inhibitor of GSK-3*α*- and GSK-3*β* activity in HT29 human colon carcinoma cells, measured (Western blot) as increased phosphorylation of Ser21 and Ser9 respectively. Even at low micromolar concentrations EGCG inhibited the activity of GSK-3*α* and GSK-3*β* in HT29 cells after 24h (figure 35A/B/C) independent of altered protein expression (figure 35A/B/C). However, EGCG has been shown to have no effect on isolated GSK-3*β* up to 100 µM (Schreiner 2004). Therefore it is thus plausible, that although EGCG has been shown to be readily taken up by HT29 cells and to be predominantly localized in the cytosol (Hong et al. 2002), the EGCG-induced cellular inhibition of GSK-3 activity is mediated indirectly, probably via influencing intervening cellular signalling cascades upstream of GSK-3 rather than via a direct targeting of the enzyme. PKA of the cAMP pathway and PKB of the insulin/PI3 kinase cascade, both of which have been shown *in vitro* to target the Ser21 and Ser9 phosporylation sites of the GSK-3 isoforms are activated by EGCG within the same concentration range employed in this work (1-50µM) (Lorenz et al. 2004). EGCG has been shown to generate substantial amounts of H_2O_2 under cell culturing condition which raises the question as to whether H_2O_2 may be in part or totally responsible for the effects observed for EGCG (Hong et al. 2002; Dashwood et al. 2002). However, hydrogen peroxide itself (100µM and 500µM) has been reported to activate rather than inhibit GSK-3*β* in HEK293 and in other cell lines (Shin et al. 2006). Furthermore, GSK-3 activity was already diminished at 0.5µM EGCG (figure 35A/B), a concentration far below the reported concentrations of EGCG known to generate substantial amounts of H_2O_2 (Dashwood et al. 2002; Shin et al. 2006). Lastly, 25µM H_2O_2 has been shown to have no effect on Tcf/Lef transcriptional activity in HEK293 cells (Dashwood et al. 2002). Thus, it is not likely that H_2O_2 production by EGCG is of substantial relevance for the inhibition of GSK-3 in HT29 cells. In accordance with the inhibition of the activity of GSK-3*α* and -3*β*, incubation of HT29 cells with EGCG resulted in a concentration-dependent decrease of phosphorylated *β*-catenin (figure 37A/B). Surprisingly, the decrease of *β*-catenin phosphorylation was not associated with a stabilization of intracellular *β*-catenin as evidenced

by the reduced total and nuclear *β*-catenin protein levels detected by Western blot (figures 37-A/B & 38A/B). The decrease of the cellular *β*-catenin level, inspite reduced phosphorylation might result from the suppression of *β*-catenin expression, indicated by the decrease of *β*-catenin mRNA (figure 39). Thus, the interfering effect of EGCG with *β*-catenin homeostasis might primarily be governed by its effect on *β*-catenin expression. In accordance with the reduced *β*-catenin levels, EGCG did not induce Tcf/Lef-mediated gene expression in the reporter gene assay (figures 30B, 32B, 33B). The employed reporter gene system was designed and optimized to detect stimulating effects on Tcf/Lef-dependent gene expression which explains why no reduction of Tcf/Lef transcriptional activity could be detected. However in line with the reduced *β*-catenin levels noticed in HT29 cells, Dashwood et al reported a significant reduction of Tcf/Lef transcriptional activity in HEK293 cells (Dashwood et al. 2002). In support of the results observed with the reporter gene assay, EGCG has also been shown to inhibit the growth of HT29 cells in a SRB assay (Pahlke et al. 2006). Collectively, the results obtained with EGCG permit the conclusion that EGCG may induce growth inhibition of HT29 cells via the Wnt pathway by downregulating *β*-catenin neogenesis, which is one mechanism probably responsible for the cancer preventive properties of EGCG.

Besides its involvement in the Wnt-signalling pathway, the serine/threonine kinase GSK-3 is also involved in the regulation of the glucose/glycogen homeostasis by regulating glycogen synthase activity. To elucidate the consequence of the inhibition of GSK-3 on the glycogen homeostasis in HT29 cells, the cells were incubated for 24h with EGCG at the concentration which had the highest impact on GSK-3 inhibition (25µM). However, EGCG surprisingly had no effect on GS activity as measured in a GS-assay (figure 41). In accordance with this finding, EGCG also did not influence the phosphorylation at Ser641 of GS as determined by Western blot analysis (figure 42A/B). Total protein levels were slightly but significantly increased (figure 43A/B) apparently with no effect on GS activity. Quantitative PCR results, indicated that the increased GS protein levels might be a corollary of an increased expression of the liver isoform of GS, as evidenced by high LGS transcript levels (figure 44). Evidently the inhibition of GSK-3 activity by EGCG after 24h incubation was on a whole without relevance for GS activity in HT29 cells. A reason for the discrepancy may be interfering effects from/ or with other signalling pathways which converge on GS. EGCG has been shown to activate PKA and AMPK, both of which are known to target GS. It is thus

conceivable that these kinases might be acting in opposition thus compensating the stimulating effects mediated by the inhibition of GSK-3. In accordance with the lack of stimulation of GS by EGCG, cellular glycogen was not increased in HT29 cells in a 24h incubation time frame. On the contrary, from 12h post incubation, glycogen deposits were diminished (figure52) suggesting an activation of glycogen phosphorylase, the rate limiting enzyme, catalyzing the breakdown of glycogen. However, EGCG (25µM) did not influence GP activity (24h) (figure 48) thus leading to the assumption that EGCG affects the glycogen breakdown machinery by another mechanism. The debranching enzyme, which functions in concert with GP to breakdown glycogen, may be a possible candidate through whom EGCG might accelerate glycogen breakdown in HT29 cells. In line with the lack of change of GP activity, total GP proteins levels (MGP and BGP) were unaltered as determined by Western blot analysis. Analysis of the effects of EGCG on the expression the mRNA of the GP isoforms (BGP, MGP) indicated that at 25µM EGCG, BGP levels were diminished while MGP levels were increased. It is conceivable that due to corrections by biosynthetic control mechanisms, the decrease in BGP expression was compensated for by increasing the expression of MGP, thus leading to no net change in GP protein levels. The antidiabetic potential of EGCG has been shown *in vivo* in diabetic rat models. Regulation of the expression of key enzymes involved in gluconeogenesis have been shown to be possible mechanisms for the repression of hepatic glucose formation in these models (Anton et al. 2007; Koyama et al. 2004; Waltner-Law et al. 2002; Wolfram et al. 2006). The results of this work suggest that regulation of GS and GP of the glycogen anabolic and glycogen catabolic pathways respectively, does not contribute to the anti-diabetic potential for EGCG in HT29 cells.

5 Summary of Results

Many beneficial health effects have been ascribed to flavonoids and the group of polyphenols as a whole. However, rather few studies have addressed the possible adverse health effects of flavonoids. The Wnt pathway represents one of the major signalling cascades which have been implicated in the development of colon cancer. Glycogen synthase kinase (GSK-3) is a key element of the Wnt-signalling pathway where it regulates cellular *β*-catenin levels. Inhibition of GSK-3 leads to the stabilization of cellular *β*-catenin which can then translocate into the nucleus and initiate processes that eventually lead to the stimulation of cell growth. The aim of this work was to identify flavonoids with a potential to induce a Wnt-dependent proliferation stimulus in human colon carcinoma cells. A flavonoid dependent growth stimulus may pose a potential health risk, considering that such stimulus might lead to increased tumourigenesis of cancer precursor cells.

To screen for substances with a potential to induce Wnt-dependent cell growth, a relevant reporter gene assay was established, optimized and fine-tuned to determine only stimulating effects on the *β*-catenin/Tcf/Lef transcriptional activity in HEK293 cells and HCT116 cells. Quercetin emerged as a potential inducer of cell growth because it increased the Tcf/Lef transcriptional activity in HEK293 cells and HCT1116 cells. Moreover, quercetin has been shown to potently inhibit isolated GSK-3 activity (kinase assay) (Kern et al 2006). (-) Epigallocatechin-gallate (EGCG) on the other hand had no influence on Tcf/Lef transcriptional activity (reporter gene assay) and did not inhibit isolated GSK-3 activity (kinase assay) (Schreiner 2004). EGCG was hence included in the experiments as a negative control substance. The GSK-3 inhibitor, ”SB216763” significantly increased Tcf/TLef transcriptional activity (about 21 folds). It was employed as a positive control for activation of Wnt signalling.

The effect of quercetin on the expression and activity of GSK-3*α*/*β* and *β*-catenin, both key elements of the Wnt signalling pathway was investigated by Western blot in the human colon carcinoma cell line HT29. Quercetin had no effect on the activity of GSK-3*α* and -3*β* in HT29 cells, measured as phosphorylation at Ser21 and Ser9, respectively. Consistently, quercetin did not substantially affect *β*-catenin homeostasis suggesting that it might not induce a mitogenic stimulus in HT29 cells. Conversely quercetin stimulated the Tcf/Lef mediated

transcriptional activity in HEK293 cells and HCT116 cells. Incubation of HT29 cells with EGCG caused a potent inhibition of GSK-3α and -3β activity at unaltered total protein levels. Concomitantly, the amount of phosphorylated β-catenin was diminished in a concentration-dependent manner. However, the overall amount of β-catenin was also decreased to a similar extent. Quantification of β-catenin transcripts in HT29 cells by RT-PCR indicated a reduction in β-catenin transcripts by EGCG, suggesting that the decrease in overall β-catenin levels might originate from a downregulation of β-catenin neogenesis. As expected, the GSK-3 inhibitor, SB216763 reduced GSK-3 activity in HT29 cells leading to increased in total β-catenin levels and the induced Tcf/Lef driven transcriptional activity in HEK293 cells as well as in HCT116 cells. In conclusion the results suggest that neither quercetin nor EGCG at the concentrations tested in the work mediate a proliferative stimuli in HT29 cells by interfering with key elements of the Wnt pathway. On the contrary, EGCG is rather expected to mediate anti-proliferative effects due its reduction of celular β-catenin.

Besides being actively involved in the Wnt- signalling pathway, GSK-3 also influences the cellular glucose/glycogen homeostasis by phosphorylating and inactivating glycogen synthase (GS). In view of the inhibition of GSK-3 activity by EGCG in HT29 cells it raised the question whether this effect was of any significance for the glucose/glycogen homeostasis. Apparently, EGCG's inhibition of both GSK-3 isoforms did not translate into the stimulation of glycogen synthase in HT29 cells since GS activity was not influence by EGCG when applied at 25µM, the concentration which had the most impact on GSK-3 activity. In accordance, the phosphorylation of Ser641 on GS was not affected as determined by Western blot analysis. GS protein levels were significantly increased by about 50% (T/C), however with no consequence on GS activity. Quantitative Real-time PCR data, indicated that increased LGS transcription may contribute to the increased GS protein level in HT-29 cells after the incubation with EGCG. In accordance with the lack of stimulation of GS by EGCG, glycogen was not deposited in HT29 cells. On the contrary, after prolonged incubation (12h - 24h) with EGCG, glycogen deposits were instead diminished. A rather surprising result considering that the activity of glycogen phosphorylase (GP), which is the rate limiting enzyme catalyzing the breakdown of glycogen was also not influenced in HT29 cells by EGCG (25µM), upto 24h post incubation. Total GP protein levels also remained unchanged after the 24h exposure of HT29 cells to EGCG. Quantitative Real-time PCR analysis

indicated a reduction of BGP transcript levels in HT29 cells accompanied by increased mRNA levels of MGP and LGP. It is conceivable that due to correction by biosynthetic control mechanisms, the decrease in BGP (brain-type-GP) expression is compensated by increasing the expressions of MGP (Muscle-type-GP) and LGP (Liver-type-GP). In line with GSK-3 inhibition, the GSK-3 inhibitor, SB216763 (10μM) mediated an early (15min) conspicuous activation of GS in HT29 cells, which was mantained upto 24h. Consistently GS phosphorylation on Ser641 was significantly diminished as determined by Western blot analysis. Total GS protein level were significantly increased, presumably by the upregulation of LGS as evidenced by increased LGS transcripts. In accordance with the activation of GS, glycogen deposits were progressively increased in HT29 cells. GP activity was not influenced by SB216763. Collectively the results indicate that EGCG's influence on GSK-3 has no consequence for the glucose/glycogen homeostasis and hence does not contribute to the anti-diabetic property of EGCG in HT29 cells.

5.1 Zusammenfassung

Im Allgemeinen werden Flavonoiden gesundheitsfördernde Eigenschaften zugeschrieben. Wenig ist jedoch über gesundheitlich nachteilige Effekte von Flavonoiden bekannt. Der Wnt-Signalweg zählt u. a. zu den Signalwegen, die eine wesentliche Rolle in der Kolonkanzerogenese spielen. Ein Schlüsselelement dieses Signalweges stellt die Glykogensynthasekinase 3 (GSK-3) dar, die den zellulären ß-Cateninspiegel reguliert. Kommt es zu einer Hemmung von GSK-3, reichert sich *β*-Catenin im Zytosol an und wird in den Zellkern transloziert. Im Zellkern fördert *β*-Catenin die Stimulierung proliferationsassoziierter Gene und somit das Zellwachstum. Das Ziel dieser Arbeit lag in der Identifizierung von Flavonoiden, die einen Wnt-abhängigen Proliferationsstimulus in humanen Kolonkarzinomzellen induzieren können.

Im Rahmen dieser Dissertation wurden die Effekte des Flavonols Quercetin, das in zahlreichen Früchten und Gemüsen vorkommt und des Grünteecatechins (-)-Epigallocatechin-3-gallat (EGCG) auf die Aktivität der GSK-3 in der humanen Kolonkarzinomzelllinie HT29 mittels Western Blot Analyse untersucht. Quercetin ist bereits als potenter Inhibitor der isolierten GSK-3ß bekannt (Kern et al., 2006), während EGCG keinen Einfluss auf die isolierte GSK-3ß Aktivität hat (Schreiner 2004). Der GSK-3 spezifische Hemmstoff

SB216763 wurde als Positivkontrolle der Aktivitätshemmung eingesetzt. Als Maß für die Hemmung der Enzymaktivität wurde der Phosphorylierungsstatus von GSK-3*α*/*β* bestimmt, da durch Phosphorylierung an Ser21 und Ser9 die GSK-3*α* bzw.-3*β* Aktivität unterdrückt wird.

Nach 24-stündiger, serumfreier Zellinkubation zeigte sich, dass Quercetin keinen signifikanten Einfluss auf den Phoshorylierungsstatus und damit auf die Aktivität der GSK-3*α* und 3*β* hat. In Übereinstimmung mit dem Ergebnis auf die GSK-3*α*/*β* beeinflusst Quercetin die *β*-Cateninhomeostase nicht. Dies lässt den Schluss zu, dass Quercetin keinen mitogenen Wachstumsstimulus in HT29 Zellen induziert. Im Gegensatz dazu erhöht Quercetin die Tcf/Lef vermittelte Transkriptionsaktivität in HEK293 Zellen und HCT116 Zellen.

Die Behandlung von HT29 Zellen mit dem Grünteecatechin EGCG führt im Vergleich zum Quercetin zu einer Zunahme der GSK-3*α*/*β* Phosphorylierung und somit zu einer signifikanten Hemmung der GSK-3*α*/*β* im mikromolaren Konzentrationsbereich. Die Expression von GSK-3*α*/*β* wurde durch EGCG nicht beeinflusst Einher mit der Hemmung der GSK-3 geht eine konzentrationsabhängige und signifikante Abnahme von phosphoryliertem *β*-Catenin bei gleichzeitiger Abnahme von Gesamt-*β*-Catenin in HT29 Zellen. Mittels quantitativer real-time PCR konnte zusätzlich gezeigt werden, dass die EGCG bedingte Abnahme an Gesamt-*β*-Catenin vermutlich auf eine Reduktion der Transkription von *β*-Catenin und folglich auf dessen Neogenese zurückzuführen ist. In Übereinstimmung mit der Abnahme von Gesamt-*β*-Catenin wird die Tcf/Lef vermittelte Transkriptionsaktivität im Reportergenassay nicht induziert. Erwartungsgemäß erwies sich SB216763 als potenter Hemmstoff der GSK-3 in intakten HT29 Zellen. Damit einher geht die signifikante Abnahme von phosphoryliertem *β*-Catenin. Gleichzeitig nimmt der Gehalt an Gesamt-*β*-Catenin zu. Die Ergebnisse dieser Arbeiten legen nahe, dass Quercetin und EGCG in humanen Kolonkarzinomzellen keinen Wachstumsstimulus über den Wnt-Signalweg induzieren und aufgrund der Abnahme des *β*-Cateninspiegels eher antiproliferative Effekte von EGCG zu erwarten sind. Neben der Schlüsselrolle im Wnt-Signalweg ist die GSK-3 in der Lage, die Glykogensynthase (GS) zu phosphorylieren und nimmt dadurch Einfluss auf die Glukose-/Glykogehomeostase. Im Hinblick auf die potente Hemmung der GSK-3 durch EGCG stellte sich die Frage, ob diese Hemmung auch mit einer Modulation der Glukose-/Glykogenhomeostase einhergeht. Die Effekte von EGCG auf die Aktivität, Expression und Transkription der Schlüsselenzyme der Glukose- /Glykogenhomeostase, GS und

Glykogenphosphorylase (GP), wurden deshalb in HT29 Zellen untersucht. Zusätzlich wurde der Einfluss auf den Glykogenspiegel in HT29 Zellen bestimmt. EGCG wurde in einer Konzentration von 25µM eingesetzt, da bei dieser Konzentration die Aktivität der GSK-3 am stärksten gehemmt werden konnte. SB216763 diente als Positivkontrolle der Stimulierung der GS Aktivität. Eine Hemmung der GSK-3 durch EGCG führte zu keiner Stimulierung der GS Aktivität. In Einklang mit diesem Befund zeigen die Ergebnisse der Western Blot Analyse, dass die Phosphorylierungsstelle Ser641 der GS durch EGCG nicht beeinflusst wird. Der Gesamt-GS-Spiegel wird leicht aber signifikant erhöht, jedoch mit keiner Auswirkung auf die GS Aktivität. Mittels quantitativer real-time PCR konnte gezeigt werden, dass der Anstieg des Gesamt-GS-Spiegels womöglich auf eine gesteigerte Transkription und Expression von Leber GS zurückzuführen ist. Übereinstimmend mit der fehlenden Hemmung von GS durch EGCG kommt es zu keiner Glykogenakkumulation in HT29 Zellen. Allerdings konnte eine Abnahme des Glykogenspiegels beobachtet werden. Dies ist insoweit überraschend, da EGCG (25 µM) keinen Einfluss auf die GP Aktivität, das geschwindigkeitsbestimmende Enzym des Glykogenabbaus, gezeigt hat. Die Western Blot Analyse bestätigt, dass der Gesamt-GP-Spiegel nach 24 h unverändert bleibt. Mittels quantitativer real-time PCR Analyse konnte gezeigt werden, dass die Transkripte für BGP (Gehirn GP) reduziert werden, während die Transkripte für LGP (Leber GP) nach 24 h ansteigen. Es ist also denkbar, dass die Expression von LGP gesteigert wird, um die Abnahme von BGP zu kompensieren. In Einklang mit der potenten GSK-3 Hemmung durch SB216763 (10µM) wird auch die GS Aktivität in HT29 Zellen stimuliert. Dem entsprechend zeigen die Western Blot Daten, dass die Phosphorylierung von GS an Ser641 durch SB216763 signifikant reduziert wird. Damit einher geht die Zunahme des Glykogenspiegels in HT29 Zellen. Zusätzlich bewirkt SB216763 nach 24h eine signifikante Erhöhung des Gesamt-GS-Spiegels. Die quantitative real-time PCR zeigt, dass der Anstieg des Gesamt-GS-Spiegels vermutlich auf die erhöhte Transkription und Expression von LGS zurückzuführen ist. Sowohl die Aktivität der GP als auch die Expression werden nicht durch den Hemmstoff SB216763 beeinflusst. Die Ergebnisse deuten somit darauf hin, dass die EGCG bedingte Modulation der GSK-3 keinen Einfluss auf die Glukose-/Glykogenhomeostase in HT29 Zellen nimmt und somit nicht zum antidiabetischen Potential von EGCG in HT29 Zellen beiträgt.

6 Materials and Methods

6.1 Cell Culture

Cell culture embodies the practices implemented in order to achieve and maintain an atmosphere most conducive for the vital growth of cells. The factors that negatively influence mammalian cell vitality include: maintaining a confluent population in the culture flask, maintaining high concentrations of cellular metabolic wastes in the growth medium, no contamination of cell cultures with bacteria and/or fungus and lastly, a deviation from optimal growth conditions (37°C, 5% CO_2 and 95% air moisture). When growing, cells go through the 3 growth phases depending on their type, plating density, media ingredient and antecedent handling:

- An opening quiescent lag phase
- A log phase when growth is exponential and the metabolic activity is at its highest
- Finally, a stationary phase where the cell number is constant.

6.1.1 Cell Lines

6.1.1.1 HEK-293 Cell Line

HEK-293 cells also known plainly as 293, are fibroblastoid semi-adherent cells that grow as a monolayer with a doubling time of 20-24h. They were established in 1977 from a human primary embryonal kidney using the adenovirus type 5. They are rated “risk category 1” by the German Central Commission for Biological Safety (DSMZ).

HEK-293 cells were grown in Dubelscco‘s Modified Eagle Medium (with 4500 mg/l Glucose, and pyridoxin HCl, without Natrium-Pyruvat) containing 1% (v/v) penicillin/streptomycin (10,000 units/10,000µg per ml), 10% (v/v) heat-inactivated fetal calf serum (FCS) in a humidified incubator.

6.1.1.2 HT29 Cell Line

HT29 cells are epithelial-like adherent cells that grow as monolayer in large colonies with a doubling time of 40-60h. They were first established in 1964, originally from a primary colonic tumour of a 44-year old Caucasian female. They form a well-differentiated adenocarcinoma consistent with colony primary grade I and possess a hyper-triploid karyotype with a 17.5% polyploidy (DSMZ). HT29 cells have been described to have a mutation in the APC gene and an intact *β*-catenin gene (*CTNNB1)* (Ilyas et al. 1997).

HT29 cells were cultured in Dubelscco's Modified Eagle Medium (with 4500 mg/l Glucose, and pyridoxin HCl, without Natrium-Pyruvat) containing 1% (v/v) penicillin/streptomycin (10,000 units/10,000µg per ml), 10% (v/v) heat-inactivated FCS in a humidified incubator.

6.1.1.3 HCT-116 Cells

HCT116 cells are colon carcinoma cells with a diploid karyotype (DSMZ, Braunschweig). In contrast to HT29 cells, HCT-116 cells have an intact APC gene. The *β*-catenin gene, *CTNNB1* has a three base deletion mutation of heterozygous nature corresponding to codon 45 in Exon 3, which causes an in frame deletion of the *β*-catenin protein (Ilyas et al. 1997). The cells were a gift from Prof Dr. Bibby of the Tom Connors Cancer Reseach centre, University of Bradford.

HCT116 cells were cultured in RPMI 1640 medium containing L-glutamin, 1% (v/v) penicillin/streptomycin (10,000 units/10,000µg per ml), 10% (v/v) heat-inactivated FCS and 1% (v/v) sodium pyruvate in a humidified incubator.

6.1.1.4 HepG2 cells

HepG2 cells are human hepatoma cancer cells which were established from the tumour of a 15 year old Argentinian harboring a hyperploid kayrotype (DMSZ). They are adherent cells which grow in a monolayer.

HepG2cells were cultured in RPMI 1640 medium containing L-glutamin, 1% (v/v) penicillin/streptomycin (10,000 units/10,000µg per ml), 10% (v/v) heat-inactivated FCS and 1% (v/v) sodium pyruvate in a humidified incubator.

6.1.2 Changing Cell Medium

The medium in which cells are cultured has a dual function. Primarily, it acts as a conduit through which cells are provided with nutrients vital for cell growth, and secondly, it functions as the collector for excreted cellular wastes. Increasing accumulation of cellular metabolic excrements leads to an increasing acidity of the growth medium, which can be monitored by the gradual change in the colour (from red to yellow) of the phenol red indicator contained in the growth medium. This rising acidity of the medium plus the increasing dearth of nutrients, if sustained, will negatively influence cell growth and vitality.

To change the growth medium, old medium is removed and the cells are rinsed once with 10ml PBS (37°C) to wash out dead cells. Subsequently, 40ml of pre-warmed (37°C) adequate growth medium is added and the flask (175cm^2) is placed in the humidified incubator (37°C, 5% CO_2, 95% moisture).

6.1.3 Subculture of Cells

Many adherent cell lines, tumour or otherwise artificially transformed cell lines, grow optimally as monolayer in cell culture flasks. On attaining a confluent population, some cell lines transcend to multilayer growth by adding multiple layers over first, in which case the cells growth is suppressed (contact inhibition) and the cells experience a change in metabolism. To maintain monolayer cell growth, the cells were passaged when they had reached a semi-confluent population.

The growth medium is aspirated and the cells are rinsed with 10ml PBS to remove dead cells and residual growth medium (would inactivate Trypsin/EDTA and hinder cell detachment). 2.5ml pre-warmed (37°C) Trypsin/EDTA is added and the culture is placed in a humidified incubator (HT29: 3min, HEK-293: 10s, HCT-116: 1min). The culture flask is gently clapped to detach the cells. 8ml pre-warmed (37°C) serum-supplemented medium is added (inhibits the lysing activity of Trypsin/EDTA) and the cells are re-suspended by pipetting up and down. 0.5-1ml of the cell suspension is transferred to an unused culture flask (175cm^2). 40ml adequate pre-warmed serum and antibiotic supplemented medium is added, and the cells are incubated under normal growth conditions (37°C, 5% CO_2).

Phosphate Buffered Saline (PBS), 10x	**NaCl**	**1.71M**
	Na_2HPO_4	**0.10M**
	KCl	**34mM**
	KH2PO4	**8mM**
		Dissolved with 1l re-distilled water. Set to pH 7.4. Diluted to 1x and sterilized by autoclaving before use.
Trypsin/EDTA	**Trypsin (3.6U/mg)**	**500mg**
	EDTA	**250mg**
	10x PBS	**100ml**
		Stirred overnight at 4°C. Set to pH 7-7.4 and filled to 1l mark with re-distilled water. Filtered (0.22µm) sterilely and aliquoted (5ml) before use. Stored at -20°C.

6.1.4 Counting Cells

To enumerate cells, a standard Neubauer double grid ruling counting chamber was employed (figure 54). Shortly before the cells are passaged, the counting chamber is prepared as follows: the cover glass and the external supports of the counting chamber are breath-moistened. The cover glass is then gently slid onto the counting chamber. The formation of Newton rings between the external support and the cover glass indicates correct positioning of the cover glass. Equal volumes of cell suspension (preparation see chapter 6.1.3) and the cell dye Trypanblue are mixed homogeneously in a 1.5ml test tube. To load the counting chamber, the pipette is held at an oblique angle and its tip placed at the juncture between cover glass and counting chamber. As a result of the capillary effect, the liquid is drawn in between the cover glass and the chamber. Counting is performed in the squares denoted 1, 2, 3 and 4 (figure 54) under a light microscope. Living cells appear illuminated because of their ability to actively eliminate the dye (trypan blue) while dead cells lacking this ability appear blue. Only the living cells are counted. The mean value for all four counting nets is multiplied by the dilution factor 2 and 10000 to obtain the amount of cells/ml of the cell suspension (Lindl 2000).

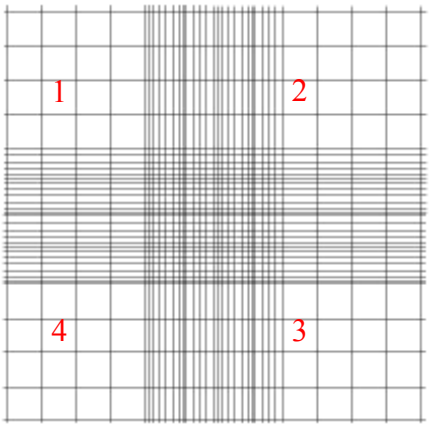

Figure 54: Neubauer improved cell counting chamber [modified] (Lindl 1987).

6.1.5 Storage of Cells

For the storage of cells 3ml (30%, v/v) DMSO-solution is added to 7ml (70%, v/v) FCS-solution, mixed thoroughly and dispensed into 20 sterile cryotubes at 500µl for each tube. 1ml of the cell suspension is then added to each tube thereby diluting DMSO, which functions as an anti-freeze to 10% (v/v). The tubes are capped and stored at –80°C in a freezer (Lindl 1987)

6.1.6 Re-culturing Cells

During cell culture, it is of utmost importance to be mindful because some cell lines, while in culture, change their physiological properties with increasing passage number. It is therefore necessary to replace old cells from stocks to maintain reproducible results. Cells were replaced after attaining a passage number of 30 (Lindl 1987).

The frozen cell suspension is thawed quickly in a water bath at 37°C. The cell suspension is taken up straightaway in 10ml medium (10% FCS, v/v) and centrifuged at R.T and 200g for 4 min. The supernatant is discarded and the cell pellet re-suspended in 5ml FCS (20%, v/v) supplemented medium. Finally, the entire cell suspension is transferred to a small tissue culture flask (25cm^2) and incubated at 37°C, 5% CO_2 and 95% humidity (Lindl 1987). Upon achieving high confluency, the cells are passaged into a medium culture flask (80cm^2) and

thereafter into a large culture flask (175 cm^2). Cells were maintained for at least 2 week in culture before attaining experimental competence.

6.1.7 Testing for Mycoplasma Contamination

Mycoplasma, also called pleuropneumonia-like organisms is defined as any of a genus (family Mycoplasmataceae) of pleomorphic gram-negative and chiefly non-motile bacteria of mostly parasitic nature. They vary in form and size, ranging from 0.22µm to 2µm. Contamination of cultures with mycoplasma is durable and brings about metabolic alterations in the infected cells. This calls for frequent testing and in positive cases urgent removal of the mycoplasma (Lindl 1987).

To test for mycoplasma infection, the cells are plated on a glass slide and allowed 24h for regeneration and growth. Thereafter, the growth medium is washed off the slide with cold methanol (-20°C) and the slide placed in methanol (-20°C) for at least 15min to affix the cells. Subsequently, the cells are stained with DAPI/SR101 solution (4'-6-diamidino-2-phenylindol-di-hydrochloride/sulforhodamine 101) and scrutinized under a fluorescence microscope. Nucleic acid appears blue (DAPI) and plasma-proteins appear red (SR101). Scattered small bluish dots seen over the red regions of the plasma are a positive sign for mycoplasma infection (Lindl 1987).

DAPI/SR 101-Solution (Partec)	**Tris-Cl, pH 7.6**	**0.2M**
	4´, 6-Diamidino-2 phenylindoldihydrochloride	**8µM**
	Sulforhodamine	**50µM**
	NaCl	**0.2mM**

6.1.8 Seeding Cells

6.1.8.1 Seeding HT29 Cells for Western Blot, Glycogen Synthase Assay, Glycogen Phosphorylase Assay and Glycogen Assay

2.5 x 10^6 cells are seeded per Petri dish (175cm^2) in a volume of 20ml Dulbecco's Modified Eagle Medium DMEM (4500 mg/ml glucose, L-glutamine, without sodium pyruvate, Invitrogen GmbH)) supplemented with FCS (10%, v/v) and penicillin/Streptomycin (1%, v/v). They are grown for 72h in a humidified incubator at 5% CO_2 and 37°C. Thereafter, the old medium is replaced with medium whose FCS content is 1% (v/v). After a further 24h of growth, the cells are incubated in a serum free environment with the compound(s) of interest.

6.1.8.2 Seeding HT29 Cells for Gene Expression Analysis with TaqMan® RT-PCR

1.2 x 10^6 cells are seeded per Petri dish (55cm^2) in a volume of 10ml Dulbecco's Modified Eagle Medium DMEM (4500mg/ml glucose, L-glutamine, without sodium pyruvate, Invitrogen GmbH)) supplemented with FCS (10%, v/v) and penicillin/Streptomycin (1%, v/v). They are grown for 48 hours in a humidified incubator at 5% CO_2 and 37°C after which the old medium is replaced with medium whose FCS content is 1% (v/v). After a further 24h of growth, the cells are incubated in a serum free environment with the compound(s) of interest.

6.1.8.3 Seeding HEK-293 Cells and HCT-116 cells for Tcf/Lef Reporter Gene Assay

0.5 x 10^6 cells per Petri dish (55cm^2) are seeded in a volume of 10ml Dulbecco's Modified Eagle Medium DMEM (4500mg/ml glucose, L-glutamine, without sodium pyruvate) that is supplemented with FCS (10%, v/v) and penicillin/Streptomycin (1%, v/v). They are grown for 72h in a humidified incubator at 5% CO_2 and 37°C before being transfected with the plasmid(s) of interest (chapter 6.3.7).

6.1.9 Incubating Cells

6.1.9.1 Incubation of HT29 Cells

By virtue of their labile nature in aqueous solution, the candidate compound(s) (flavonoids), once weighed, are dissolved appropriately in DMSO and diluted in serum free DMEM medium (so that DMSO has and end concentration of 1% (v/v)), moments prior to application. Before the application of the diluted compound, the cells are rinsed two consecutive times with sterile 10ml and 5ml 1x PBS to removes all traces of FCS containing DMEM medium. For all experiments, a solvent control plate (DMSO 1%, v/v) is always included.

6.1.10 Harvesting cells and Preparation of Protein Extracts

6.1.10.1 Lysis of Cells for Luciferase Assay

At the end of the incubation period the medium is removed and the cells are rinsed with 1ml 1x ice cold PBS. Since HEK-293 cells easily detach from the surface of the Petri dish due to their semi-adherent nature, the washing step is performed, with extreme care taken to avoid high loss of cells. After the washing step, 500µl of 1x cell culture lysis reagent (Promega) is added per well and the cells incubated for 15min at room temperature under mild shaking. After lysis, cell debris is separated from the lysate by centrifugation for 2min at 4°C and 1000rpm (Eppendorf 5804R). The debris free lysate is employed in a luciferase assay. The protein concentration of the lysate is determined for normalization purposes (chapter 6.2.1).

Cell Culture Lysis Reagent, 1x (Promega)	**Tris-phosphate (pH 7.8)**	**25mM**
	DTT	**2mM**
	1,2-diaminocyclohexane-N,N,N´,N´-tetraacetic acid	**2mM**
	Glycerol	**10%**
	Triton® X-100	**1%**
		CCLB is delivered as a 5x concentrate. Before use, it is diluted to 1x with distilled water

6.1.10.2 Lysis of HT29 Cells and Extraction of Total Protein

Harvesting cells and the preparation of the cell lysate is performed entirely on ice (4°C).

- The lysis buffer is prepared freshly prior to use. The medium is decanted and the cells rinsed twice with 10ml of ice-cold 1x PBS respectively. The cells are scraped in 500µl lysis buffer, and then transferred to an ice-cooled 2ml glass homogenizer. With 40 strokes of the tight pistill, the cells are disrupted and homogenized. Cell debris is separated by centrifugation at 20,000g and 4°C for 15min. The supernatant is transferred to a pre-cooled 1.5ml reaction tube. The protein concentration of the supernatant is determined using the Bradford assay as described in chapter 6.2.1.

Lysis Buffer	**Tris-Cl**	**25mM**
	EDTA	**3mM**
	EGTA	**3mM**
	Sucrose	**0.27M**
	NaF	**50mM**
	***β*-Glycerophosphate**	**10mM**
	Sodium Pyrophosphate	**5mM**
	Igepal-CA-630 or Triton X 100	**1% (v/v)**
	Na_3VO_4	**2mM**
	Complete Enzyme Coctail (Protase inhibitor mix)	**2% (v/v)**
	2-Mercaptoethanol	**0.1% (v/v)**
Complete Enzyme Coctail (Roche)	**1 Tablet**	**Dissolved in 2ml re-distilled water**

6.1.10.3 Lysis of HT29 Cells and Extraction of Nuclear Proteins

The entire process is carried out on ice (4°C)

- The medium is decanted and the cells washed twice with 10ml ice-cold of 1x PBS respectively. The cells are diligently scraped in 1ml ice-cold PBS. The cell suspension is transferred to a pre-cooled 1.5 reaction tube and pelleted by centrifugation at 15,000g and 4°C for 5min. The supernatant is discarded.

The pellet is treated with 200µl buffer A and incubated on ice for 20min, after which the test tube are centrifugated for 5min at 15,000g and 4°C. The supernatant is discarded and the pelleted nuclei are re-suspended in 200µl buffer B. The pellet is incubated in buffer B for 20min on ice. The nuclear extract (supernatant) is obtained by centrifugation at 20,000g and 4°C for 5min. The protein content of the nuclear extract is determined with the bradford assay (chapter 6.2.1).

Buffer A	**HEPES-KOH, pH 7.9**	**10mM**
	MgCl2	**1.5mM**
	KCl	**10mM**
	Following components are added freshly	
	DTT	**0.5mM**
	PMSF	**0.2mM**
	Igepal CA-630	**0.5% (v/v)**
	Complete Enzyme Coctail (Protease inhibitor mix)	**2% (v/v)**
Buffer B	**HEPES-KOH,pH 7.9**	**20mM**
	MgCl2	**1.5mM**
	NaCl	**0.42mM**
	EDTA	**0.2mM**
	Glycerol	**25% (v/v)**
	Following components are added freshly	
	DTT	**0.5mM**
	PMSF	**0.2mM**
	Complete Enzyme Coctail (Protease inhibitor mix)	**2% (v/v)**

6.2 Biochemical Methods

6.2.1 Determining Protein Concentration with the Bradford Assay

The protein concentration of samples was determined using a photometric method developed by Bradford (Bradford, 1976). This method is based on the strong binding affinity of the dye, coomassie brilliant blue G-250 (figure 55) to proteins. The dye interacts electro-statically in acidic medium with the amino and carboxyl groups of proteins to form strong non-covalent bonds. The protein/coomassie bond causes a shift of the absorption maximum in the absorption spectrum of the dye from λ = 465nm (red) to λ = 595nm (blue). The colour response is non-linear over a wide range of protein concentrations. A standard curve is therefore required.

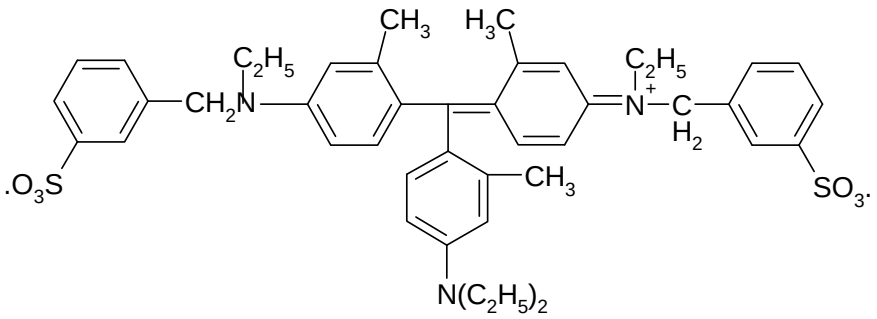

Figure 55: Structure of the coomassie brilliant blue G250

Procedure

- A sequential standard row from 0.1-1.0mg/ml protein (Table 6.2-1) is prepared with bovine serum albumin (BSA, 2mg/ml, Pierce). If required, the samples are diluted with re-distilled water. 10µl of (diluted) probe is pipetted into a 1.5ml reaction tube. 10µl of each standard is pipetted into separate 1.5ml eppendorf tubes. 1ml of Bradford solution is added to each tube. 200µl of each probe and standard is pipetted in triplicates into a 96 well dish. The 96 well plate is measured at λ = 595nm in a microplate reader.

Table 5: Diluting bovine serum albumin to create a standard row for the determination of protein concentration

Final [mg/ml]	BSA [2mg/ml]	Distilled water
0.1	10µl	190µl
0.2	20µl	180µl
0.4	40µl	160µl
0.5	50µl	150µl
0.6	60µl	140µl
0.8	80µl	120µl
1.0	100µl	100µl

Bradford Reagent:	**Coomassie-Blue G250**	**0.10g**
	Ethanol	**50ml**
	Ortho-phosphorous acid	**100ml**
		Filled with re-distilled water to 1l. Stored in the dark (RT) for a minimum of one month before use. Filtered before use.

6.2.2 Analysis of Glycogen Phosphorylase Activity in HT29 Cells

HT29 Cells were seeded and treated with the compound(s) of interest as described in chapters 6.1.8.1 and 6.1.9.1 respectively. After incubation of the cells, a whole cell lysate of the cells was prepared as described in chapter 6.1.10.2 and the glycogen phosphorylase activity was determined in a glycogen phosphorylase assay.

6.2.2.1 Glycogen Phosphorylase Assay

The method employed for the characterization of the glycogen phosphorylase (GP) activity is a modification of the method described by (Layzer et al. 1967) and (Kaiser et al. 2001). It couples a GP catalysed enzymatic reaction with other enzymatic reactions that have $NADP^+$ (oxidized nicotinamide adenine di-nucleotide phosphate) as a co-substrate, whereby $NADP^+$ is reduced to $NADPH_2$. The reduction of $NADP^+$ to $NADPH_2$ causes a shift in its absorption maximum from λ = 260nm to λ = 340nm in the UV spectrum. This shift in the absorption maxima makes it possible to optically follow the course of the reaction. The activity of GP is determined by measuring the absorbance at λ = 340nm over 9min. The slope of the curve is an expression of GP activity.

The enzyme processes involved in glycogen phosphorylase assay is tiered in 3 stages.

- Glycogen phosphorylase (GP) cleaves an α-D-glucose molecule from glycogen to form α-D-glucose-1-phosphate

(n) Glycogen + Pi → (n-1) Glycogen + *α*-D-glucose-1-phosphate

- Phosphoglucomutase (PGM) transforms α-D-Glucose-1-phosphate to α-D-glucose-6-phosphate.

***α*-D-glucose-1-phosphate → *α*-D-glucose-6-phosphate**

- Glucose-6-dehydrogenase (DH) dehydrogenates α-D-glucose-6-phosphate is to 6-phosphogluconate while $NADP^+$ is reduced to $NADPH_2$.

***α*-D-glucose-6-phosphate + *β*-NADP+ → 6-phosphogluconate + *β*-$NADPH_2$**

Procedure

- A master mix is prepared on ice in a 50ml Polypropylene (PP)-tube by mixing the assay components chronologically as shown in table 4. The samples are vortexed briefly but thoroughly and 50µl lysate of each sample prepared as described in chapter 6.1.10.2 is pipetted into a 1.5ml semi-micro cuvette (12.5x12.5x45mm). For the blank, 50µl of the cell lysis buffer is employed. 900µl of the master mix is dispensed in each semi-micro cuvette. The cuvettes are loaded on the sample chamber in the photometer and temperated for 2min to 25°C. 50µl (20mg/ml) of glycogen solution is added into each cuvette as a reaction starter. The enzyme reaction is measured photometrically over a period of 9min (Cary 1 Bio UV-Visible Spectrophotometer, Varian)

Table 6: Preparation of the GP master mix. To allow for incidental fluid losses that occur during pipetting, an n = 4+1 is prepared for 4 samples. DH: Glucose-6-dehydrogenase, $NADP^+$: oxidized nicotinamide adenine di-nucleotide phosphate, PGM: phosphoglucomutase

Reagent	[Stock]	Blank	n = 1	n = 4+1
Assay Buffer	-	780	780	3900
$NADP^+$	20mM	50	50	250
DH	0.5U/10µl	30	30	150
PGM	0.8U/10µl	40	40	200

To capture the effects on the constitutionally lesser active form of glycogen phosphorylase, GPb, it is activated post isolation, with the allosteric GPb activator, AMP at a concentration of 200nM (table 5). GP activity is normalized against protein concentration and expressed as percentage change relative to the DMSO control sample which is set at 100%.

Table 7: Pipetting chronology for the preparation of the master mix used for the glycogen phosphorylase assay with the addition of AMP as a GPb allosteric activator.

Reagent	[Stock]	Blank	n = 1	n = 4+1
Assay Buffer	-	780	780	3900
$NADP^+$	20mM	50	50	250
AMP	200mM	50	50	250
DH	0.5U/10µl	30	30	150
PGM	0.8U/10µl	40	40	200

Assay Buffer (AB)	**20mM Na_2HPO_4**	**2.84g**
	2.0mM $MgSO_4$	**0.24g**
		Dissolved in 1l re-distilled water. pH adjusted to 7.2 with H_2SO_4. Stored at 4°C.
Nicotinamide Adenine di-Nucleotide		
Phosphate (NADP+) (Sigma)	**20mM**	**76.56mg**
		Dissolved in 5ml AB. Stored at -20°C.
Glucose-6-Dehydrogenase (Sigma)		**0.5U/10µl re-distilled water. Stored at 4°C.**
Phophoglucomutase (Sigma)		**0.8U/10µl AB. Stored at 4°C**
Glycogen (Sigma)	**20mg/ml**	**100mg**
		Dissolved in 5ml AB. Stored at 4°C
AMP (Sigma)	**200 mM**	**14 mg**
		Dissolved in 10ml AB. Stored at 4°C

6.2.3 Analysis of the Glycogen Synthase Activity in HT29 Cells

After incubation of the HT-29 cells, a whole cell lysate of the cells was prepared as described in chapter 6.1.10.2 and the glycogen synthase activity was determined in a glycogen synthase assay.

6.2.3.1 Glycogen Synthase Assay

The sequential phosphorylation of glycogen synthase by glycogen synthase kinase 3 (GSK-3) on the serin residues 652, 648, 644, 640 renders the enzyme inactive. However, the allosteric effector of glycogen synthase, glucose-6-phosphate (G-6-P) is capable of restoring full activity to the phosphorylated enzyme. The glycogen synthase (GS) activity can hence be determined by measuring the rate of incorporation of a tritium labelled glucose moiety of [^{3}H]-uridin diphosphate glucose [^{3}H- UDPG] (figure 56) into glycogen in the absence and presence G-6-P. The ratio of the two activities i.e. activity without G-6-P to activity with G-6-P is employed as an index of the state of activation of glycogen synthase (Thomas et al. 1968).

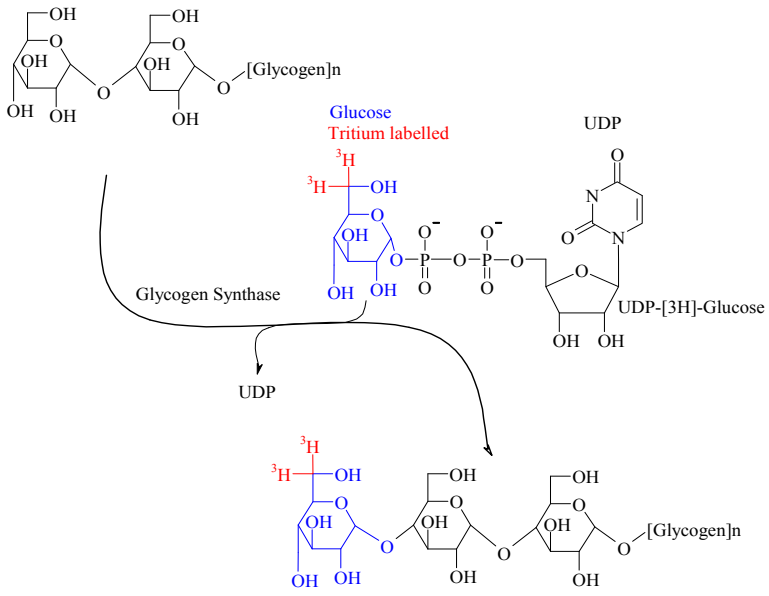

Figure 56: Scheme showing the basic reaction of the glycogen synthase assay where tritium labelled glucose is incorporated into an existing glycogen chain by active glycogen synthase.

Procedure

- The assay reaction buffers A and B are prepared on ice. Two master mixes (A and B) are prepared by adding the appropriate volume of UDP-[6-^{3}H]-Glucose solution (10µl of a 100µCi UDP-[6-^{3}H]-Glucose solution) to assay buffers A and B and vortexing briefly. 45µl lysate of sample (prepared as described in chapter 6.1.10.2) is introduced into each of 2 pre-cooled 1.5ml reaction tubes previously labelled as 1A and 1B. In order to detect the background activity, a blank using 45µl of cell lysis buffer is employed. 55µl of master mix A are pippeted in the caps of the reaction tubes 1A and 55µl master mix B in 1B. The reaction tubes are capped and the assay buffers spun down in a centrifuge. The reaction is started by incubating the reaction tubes at 37°C for 30min. Every 10min, the contents of the reaction tubes are homogenized by tipping the tubes. After 30min, the reaction tubes are placed on ice and incubated for 3 min to stop the reaction. The reaction tubes are vortexed and the content of each tube is pipetted in triplicates onto previously cut and numerated whatmann® cellulose sheets (1.2x1.2cm) at a volume of 28µl per cellulose sheet. The cellulose sheets are air dried for 5min then washed 3x consecutively, the first two times for 5min and lastly for 10min in 66% (v/v) ethanol. The cellulose sheets are again washed, this time in aceton for 5min and subsequently air-dried. The cellulose sheets are introduced into scincillation tubes, which were previously filled with 4.5ml scincillation coctail. The tubes are capped, shaken vigorously and measured in a β-counter for 2min (LS 1701, Beckman)

Calculation of the Index of the Glycogen Synthase Activity

$$\textbf{Index} = \frac{\textbf{Counts per minute (cpm) of reaction without glucose-6- phosphate}}{\textbf{Counts per minute (cpm) of reaction with glucose-6- phosphate}}$$

The index for the solvent control sample is arbitrarily set as 100%. The rest of the samples are expressed as percentage change with respect to the solvent control sample.

Tris-Cl/EDTA	**200mM Tris-Cl, pH 7.5 [Roth]**	**33.3ml**
	100mM EDTA, pH 7.5 [Roth]	**6.7ml**
	Water	**35ml**
		Stored at 4°C
1, 4-Dithiothreitol [Roth]	**20mM DTT**	**Diluted 1M stock solution 1:50 in re-distilled water i.e. 1ml stock + 49ml re-distilled water.**
UDP-[6-^{3}H-Glucose] (Amersham)	**100µCi UDP-[6-3H]-Glucose**	**Diluted 1mCi stock solution 1:10 in re-distilled water i.e. 10µl activity +90µl re-distilled water**
Assay Buffer A (1ml)	**Tris-Cl/EDTA**	**750.0µl (67mM Tris-Cl/6.7mM EDTA)**
	DTT	**250.0µl (5mM)**
	89 mM UDP-Glucose	**54.3mg**
	Glycogen	**13.0mg**
		Mixed by vortexing until no clumps are visible
Assay Buffer B (1ml)	**Tris-Cl/EDTA**	**750.0µl (67mM/6.7mM)**
	DTT	**250.0µl (5mM)**
	UDP-Glucose	**54.3mg (89mM)**
	Glucose-6-phosphate	**6.8mg (20mM)**
	Glycogen	**13.0mg**
		Mixed by vortexing until no clumps are visible
Master Mix A	**Assay Buffer A**	**45.0µl**
	UDP-[6-3H]-Glucose solution (100µCi)	**10.0µl (10µCi end concentration)**
Master Mix B	**Assay Buffer B**	**45.0µl**
	UDP-[6-3H]-Glucose solution (100µCi)	**10.0µl (10µCi end concentration)**

6.2.4 Analysis of Glycogen Content in HT29 Cells

HT29 cells were seeded and treated with the compound(s) of interest as described in chapters 6.1.8.1 and 6.1.9.1 respectively. Incubation of the cells is terminated as described below.

6.2.4.1 Harvesting cells and Isolation of Glycogen

- The medium is discarded and cells are rinsed with ice cold 1x PBS. The cells are scraped in 400µl 30% (g/v) potassium hydroxide and transferred to a 2ml reaction tube. To ensure complete lysis of the cells, the tube is capped and heated at 95°C for 15min, after which the tubes are cooled on ice. 200µl sodium sulfate and 1.2ml 66% (v/v) ethyl alcohol are added to precipitate glycogen. The sample is stored over night at 4°C. On the following morning, the precipitated glycogen is pelleted by centrifuging at 20,000g and 4°C for 30min. The pelleted glycogen is rinsed with 2ml 66% (v/v) ethyl alcohol and subjected to another centrifugal step for 30min at similar conditions. The supernatant is discarded. Residual traces of ethanol are removed with a filter paper and the pellet air-dried. The dry pellet is employed in the anthron assay.

6.2.4.2 Anthron Assay

Glycogen was determined using a simplified modification of the method described by (Pfluger 1905). Glycogen is released from the cells by means of alkali lysis and precipitated with sodium sulfate and ethyl alcohol. The alkali stable but acidic-labile α-glycosylic bonds of glycogen are subsequently hydrolized to open chain glucose molecules by heat treatment in concentrated sulfuric acid. The high temperature together with the acidic medium provokes the formation of the furane compound (hydroxymethyl-furfural, HMF) through a mechanism marked by tautomerism, ring formation and triple dehydration of glucose (figure 57 and 58).

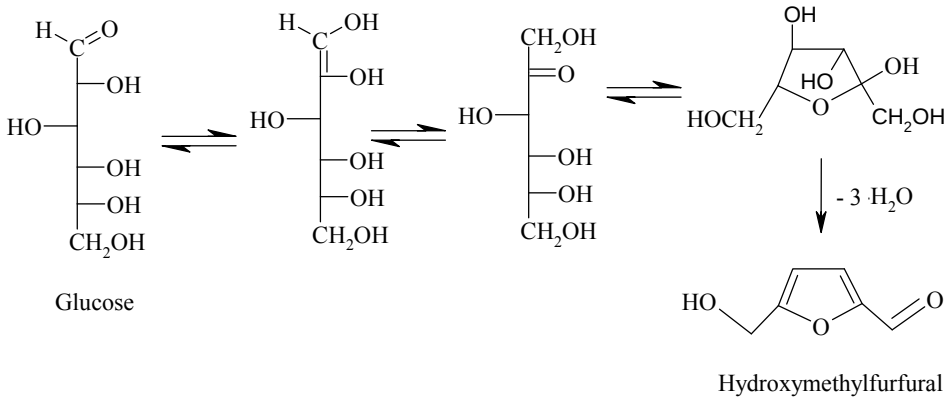

Figure 57: Mechanism of the formation of hydroxymethylfurfural (HMF) from glucose under acidic conditions and high temperatures.

In the ensuing step, HMF reacts with anthron in a colorimetric assay to a green complex, which has an absorption maximum of 620nm. With the aid of a standard curve, the glycogen content in each sample is quantifiable by means of linear interpolation.

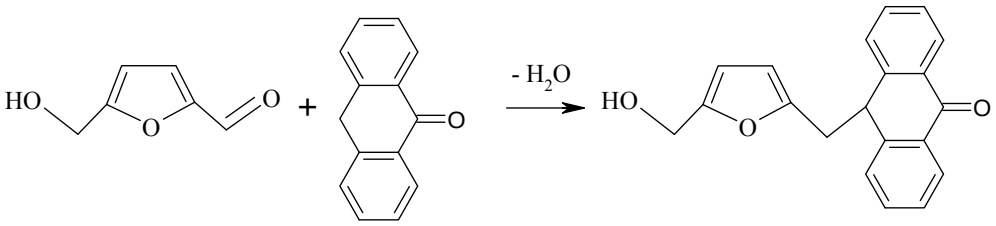

Figure 58: Reaction of HMF and anthron to a green complex with a maximum absorption at 620nm.

Procedure

- The dry glycogen pellet (chapter 6.2.4.1) is taken up in 1ml anthron II solution, vortexed until the pellet comes off the wall of the tube and heated at 95°C under vigorous agitation for 15min (Eppendorf Thermomixer 5436, Heinz). Simultaneous to the sample set up, a sequential 10 points glycogen standard row is prepared in bi-distilled water as indicated in table 6 and diluted with 720µl anthron I solution. The standard row is heated likewise the samples at 95°C under vigorous agitation for 15min (Eppendorf Thermomixer 5436, Heinz). The tubes are cooled to 4°C on ice, the samples appropriately diluted and their absorptions measured photometrically in a cuvette at 620nm. Each sample is measured twice. The glycogen

concentration in the sample is established by means of linear interpolation from the generated standard curve. Anthron II solution is employed as blank.

Table 8: Preparation of the glycogen standard row (1ml)

Desired Glycogen Concentration [µg/ml]	Required Volume of a 0.1mg/ml Stock Glycogen Solution [µl]	Re-distilled Water [µl]	Anthron I Solution [µl]
2	20	260	720
4	40	240	720
6	60	220	720
8	80	200	720
10	100	180	720
12	120	160	720
14	140	140	720
16	160	120	720
18	180	100	720
20	200	80	720

Anthron Solution I, 10ml	**Anthron [Sigma]**	**210µg (0.21%) [Sigma]**
	Concentrated H_2SO_4	**10ml**
		Always prepared freshly
Anthron Solution II, 10ml	**Anthron [Sigma]**	**150µg (0.15%)**
	Aqueous H_2SO_4	**10ml (H_2O : H_2SO_4, 1 : 2.5)**
		Always prepared freshly

6.2.5 SDS-PAGE (Sodium Dodecyl Sulfate Polyacrylamide Gel Electrophoresis)

6.2.5.1 Denature of Proteins

The sample is prepared in a sample buffer, which contains amongst others, sodium dodecyl sulfate (SDS) and 2-mercaptoethanol. SDS is an anionic detergent that binds to proteins and in the course of doing so disrupts their quaternary, tertiary and to a certain extent their secondary structures. Together with 2-mercaptoethanol it accounts for the cleavage of inter- and intra-chain disulphide bonds. As a result, the proteins are enveloped uniformly in a coating of SDS. This bestows a net negative charge upon the proteins. The motility of the proteins is now determined solely by their relative molecular weight, which now possesses a relationship of simple linearity with their electrophoretic mobility.

Procedure

- The protein concentration in each sample is ascertained by means of the bradford assay (chapter 6.2.1) and diluted to 2mg/ml with re-distilled water. A volume of 10µl of the diluted sample containing 20µg protein is mixed with 2µl sample buffer and heated at 95°C for 15min (Eppendorf Thermomixer 5436, Heinz). The sample is loaded on the gel immediately after protein denature.

SDS Sample Buffer, 6x	**0.5M Tris-Cl, pH 6.8 [Roth]**	**50ml**
	Glycerol [Merck]	**40ml**
	SDS [Roth]	**1.24g**
	Bromophenol blue [Sigma]	**0.16g**
	2-Mercaptoethanol [Roth]	**5% (v/v)**
		2-Mercaptoethanol is added freshly before use

6.2.5.2 Discontinuous Zone Electrophoresis

Discontinuous zone electrophoresis, also known as disc-electrophoresis for short, is the standard technique mostly employed nowadays for the analysis of proteins. This technique

derives its name from the fact that the polyacrylamide gel used in the methodology is made up of 2 dissimilar parts:

- The first moiety to concentrate the sample called, the stacking gel, which is buffered by Tris-Cl at pH 6.8, and whose characteristical low acrylamide/bis-acrylamide concentration ensures a high porosity of the gel.
- The second moiety to separate the sample, called the resolving gel, which is also Tris-Cl-buffered (pH 8.8), but is characterized by smaller pores due to a higher acrylamide composition.

Additionally, discontinuous zone electrophoresis is distinguishably marked by its use of different types of charge carriers: firstly, there are the chloride ions that are prevalent in both sample and gel and, secondly, the glycine ions, which are profuse in the electrophoresis buffer. During electrophoresis, the chloride ions in the gel migrate with high mobility toward the anode thus quickly creating an anion gradient between the cathode end and the anode end of the gel. The glycine ions on the other hand, moving from the running buffer into the stacking gel take up a zwitterionic configuration due to the almost neutral pH of 6.8 in the stacking gel, migrate slowly as a consequence and play a subordinate role in current transfer. The SDS coated protein molecules, which have a lower charge to mass ratio than chloride ions but a greater mass to charge ratio than glycine zwitterions, align themselves as current carriers between the fast chloride ions and the lagging slower glycine zwitterions, so that another anionic gradient builds up toward the cathode. This leads to the formation of tight successive stacks of proteins between the leading chloride ions and lagging glycine ions at the boundary of the stacking and separating gels. When the sample front enters the separating gel, which has a higher pH (pH 8.8) than the stacking gel, the glycine ions become fully dissociated and migrate faster. They overtake the proteins so that the proteins are forced to act as charge carriers behind the glycinate and chloride ions. The SDS-coated protein molecules, whose migration is now restricted by the sieving effect of the separating gel slow down and become separated according to size, whereby smaller proteins are less restrained and thus migrate faster than larger proteins (Pingoud 2002).

Casting Discontinuous Polyacrylamide Gels

The SDS-PAGE was carried out using a vertical flatbed apparatus (figure 59), Mini-PROTEAN II Electrophoresis cell from BIO-RAD using slab gels

- The glass plates and spacers needed for casting of the gels are thoroughly cleaned with 70% (v/v) ethanol to rid them of grease that will disturb gel polymerization.
- After assembling of the glass plates and spacers (0.1cm thickness) on the casting stand to form a cassette (figure 59), the components for the separating monomer gel are mixed chronologically as depicted in table 13 and introduced into the cassette to a height of 5cm (~ 3.5ml).

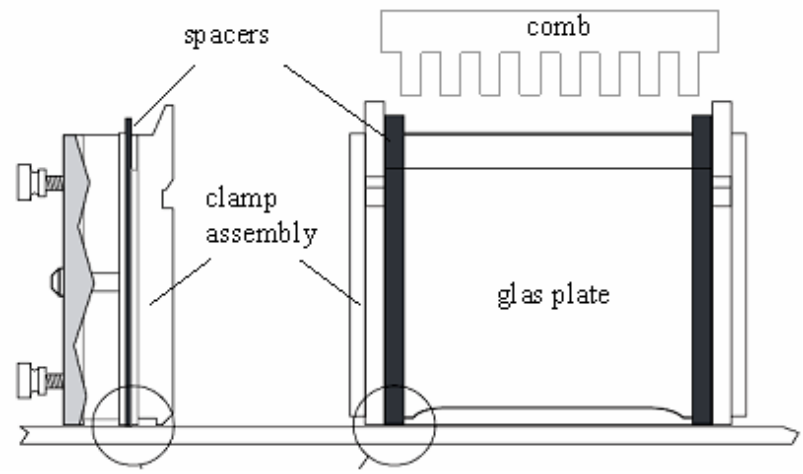

Figure 59: Sketch of the vertical flatbed apparatus Mini-PROTEAN® II from BIO-RAD displaying A: the frontal and sideways view of the clamp assembly mounted with the glass plates and spacer forming a cassette.

- The gel is overlayed with water-saturated n-butanol, which serves to exclude oxygen that impedes polymerization and to flatten the top surface of the gel. Upon completion of the polymerization (45-60min), the overlay solution is rinsed with distilled water and the area above the separating gel dried with filter paper.

- A comb is placed between the sandwiched plates (figure 59).
- The reagents for the stacking gel are combined as shown on table 14 and the monomer solution loaded. When polymerization is completed, the comb is removed and the residual water is aspirated from the gel pockets.
- Alongside with the sample (12µl, ≅ 20µg protein per pocket), is also loaded in both outermost wells, 15µl of the tracking dye (table 15, SeeBlue® Plus2, Invitrogen) to enable the monitoring of the electrophoresis. Both upper and lower electrophoresis chambers are filled with running buffer (1x) and the gel ran for 120min, initially at a constant voltage of 100V then eventually at 120V when the sample front reaches the separating gel.

Table 9: Preparation of separating gels for SDS-PAGE. The rotiphorese solution [Roth] contains acrylamide (AA) and N, N' methylene bis-acrylamide in a ratio of 37.5:1. The acrylamide concentration determines the length of the polyacrylamide chain. Bis-acrylamide determines the degree of cross-linking. N, N, N', N' tetra-methylendiamine (TEMED) [Roth] acts as a catalyst for the reaction. Ammonium persulphate (APS) [Roth] is a radical starter and initiates the polymerisation reaction.

Component	Seperating gel	
	10% AA	12% AA
Re-distilled water	2.05ml	1.72ml
Tris-Cl (1.5M), pH 8.8, [Roth]	1.23ml	1.23ml
Rotiphorese (37.5:1)-solution [Roth]	1.65ml	1.97ml
10% SDS solution [Roth]	49.2µl	49.2µl
10% APS solution [Roth]	24.6µl	24.6µl
TEMED [Roth]	2.46µl	2.46µl
∑	5.0ml	5.0ml

Table 10: Preparation of the stacking gel with an acryl amide content of 4% for SDS-PAGE.

Component	Stacking gel 4% AA
Re-distilled water	1.20ml
Tris-Cl (0.5M), pH 6.8 [Roth]	500ml
Rotiphorese (37.5:1)-solution [Roth]	250µl
10% SDS solution [Roth]	20µl
10% APS solution [Roth]	20µl
TEMED [Roth]	2µl

Table 11: Apparent molecular weights of the protein bands in SeeBlue® Plus2 Pre-Stained Standard (Invitrogen) in a Tris-Glycine buffer system

Myosin	250kDa
Phosphorylase	148kDa
BSA	98kDa
Glutamic Dehydrogenase	64kDa
Alcohol Dehydrogenase	50kDa
Carbonic Anhydrase	36kDa
Myoglobin Red	22kDa
Lysosome	16kDa
Aprotinin	6kDa
Insulin, B Chain	4kDa

Running Buffer, 10x	**250mM Tris-Cl [Roth]**	**60.6g**
	2M Glycin [Roth]	**300g**
	1% (w/v) SDS [Roth]	**20g**
		Dissolved in 2l re-distilled water. Set to pH 8.3 with HCl.

6.2.5.3 Western Blot

To further characterize proteins which have been separated by SDS-PAGE (chapter 6.3.4) often requires their extraction from the electrophoresis gel onto a nitrocellulose membrane. "Semi-dry blotting" was employed for protein transfer (figure 60). The gel is placed on a sheet of nitrocellulose membrane. Both gel and membrane are sandwiched between two pairs of whatmann filter paper (figure 10). Prior to use, the whatmann filter paper and nitrocellulose membrane are soaked in 1x blotting buffer for 30min. The sandwiched gel is clamped between the horizontal electrodes of the blotter so that the membrane lies contiguous to the anode and the gel bordering the cathode. Before blotting is commensed, air bubbles caught in the filter papers, which will impede current transfer, are released using a roller pin. The blot is run for 90min at a current of 50mA per gel. (Blotter (SEMI-PHOR™ Blotter, Hoefer Scientific Instruments, San- Francisco).

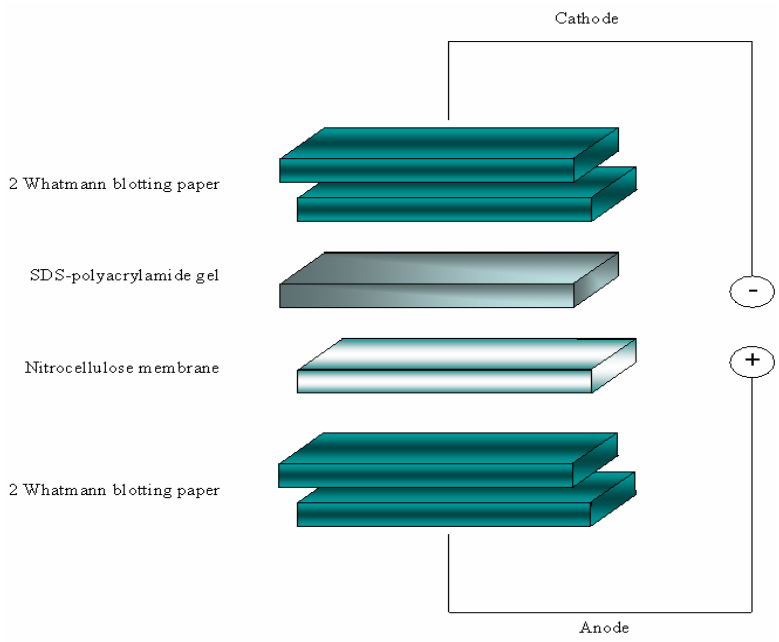

Figure 60: Schematic representation of a "semi-dry western blot"

Blotting Buffer, 2x		**96mM Tris-Cl [Roth]**	**23.3g**
		78mM Glycin [Roth]	**11.7g**
		0.074% (w/v) SDS [Roth]	**1.48g**
		40% (v/v) Methanol [Merck]	**800ml**
			Dissolved in 2l with re-distilled water

6.2.5.4 Blocking the non-specific Protein Binding Sites on the Membrane

Nitrocellulose membranes can bind protein indiscriminately with a binding capacity between 100-200µg/cm^2. To prevent the non-specific binding of antibodies on the nitrocellulose membrane, unoccupied hydrophobic binding sites on the membrane are blocked by incubating the membrane in blocking buffer containing non-fat dried milk for 1h at room temperature with gentle agitation.

Tris Buffered Saline (TBS) (20x)	**2.6M NaCl**	**303.9g**
	0.4M Tris-Cl	**96.9g**
		Dissolved in 2l re-distilled water. Set to pH 7.6 with HCl
TBS/0.1%Tween-20 (1x)	**TBS (1x)**	**100ml (20xTBS)**
	Tween-20 (0.1%) [Sigma]	**2ml**
		Diluted in 2l re-distilled water. Store at RT
Blocking Buffer	**(1x) TBS / (0.1%) Tween 20**	**100 ml**
	5% (w/v) Non-Fat Dried Milk	**5g**

6.2.5.5 Immunological Detection

- After blocking the nitrocellulose membrane, it is washed 3 times consecutively for 5min respectively in wash buffer.
- The membrane is incubated with the primary antibody (diluted in (1x) TBS-(0.1%) Tween 20) overnight at 4°C with gentle agitation. (The primary antibody binds specifically to the protein of interest).
- The membrane is again washed 3 times consecutively for 5 min respectively in washing buffer.
- The membrane is incubated with the secondary antibody (1:2000) for 1h at room temperature with gentle agitation. The secondary antibody is coupled with HRP (horse raddish peroxidase), an enzyme that catalyzes the chemiluminescent reaction between luminol and peroxide (figure 61) thus making it possible to visualize of the proteins.

- The membrane is washed 3 times consecutively for 5min each in washing buffer.
- The membrane is incubated with 10ml LumiGLO® reagent (Cell Signaling Technology) with gentle agitation for 1min at room temperature.
- The detection of chemiluminescence is carried out on the Lumi-Imager™ (Boehringer Mannheim)

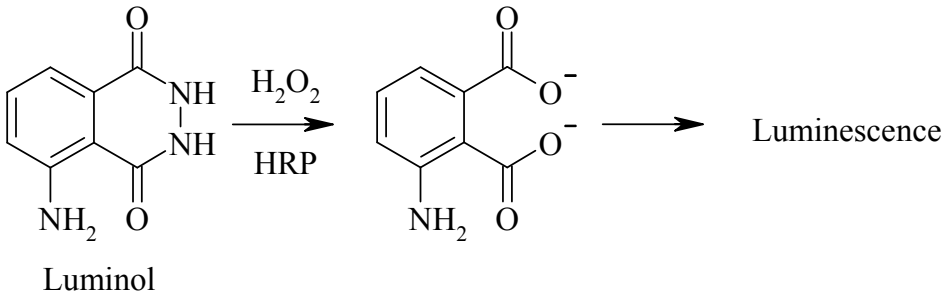

Luminol

Figure 61: Chemiluminescent reaction between luminol and H_2O_2 catalysed by horse raddish peroxidase

Washing Buffer	**TBS (1x)**	**250ml (20x TBS)**
	Tween-20 (0.3%)	**15ml**
		Diluted in 5l-distilled water. Stored at RT
LumiGLO™ Detection Solution	**20x Luminol**	**0.5ml**
(Cell Signaling Technology)	**20x Peroxide**	**0.5ml**
	Water	**9ml**
Primary Antibody Dilution	**(1x) TBS-(0.1%)-Tween 20**	**10ml**
	Bovine Serum Albumin (Pierce)	**0.5g**

Secondary Antibodies: HRP-coupled „Anti-mouse"-IgG (Santa Cruz) and HRP-coupled „Anti-rabbit"-IgG (Cell Signaling Technology) were diluted in blocking buffer.

6.2.6 Semi-quantitative Analysis of Protein Phosphorylation and Protein Expression in HT29 Cells using Western Blot Analysis

To determine the flavonoid-dependent modulation of phosphorylated and total protein levels for the proteins listed in table 12, 2.0 x 10^6 HT29 cells seeded per Petri dish (175cm^2) were cultivated under the conditions described in chapter 6.1.8.1 and incubated in serum free medium with the compound(s) of interest (chapter 6.1.9.1).

Table 12: Table of the characterized proteins, showing their molecular weights and the acrylamide concentration in the separating gel used for SDS-PAGE.

Protein	Apparent Molecular Weight [kDa]	Acrylamide Gel
GSK-3*β*	47	12%
GSK-3*α*	51	12%
Glycogen synthase	85	10%
β-Catenin	92	10%
Glycogen phosphorylase	97	10%

6.2.6.1 Detection of Total GSK-*3α/β*, Glycogen Synthase, Glycogen Phosphorylase and *β*-Catenin

To capture the modulations in the protein level of GSK-3-*α/β*, glycogen synthase, glycogen phosphorylase and *β*-catenin, after the treatment of HT29 cells with the compound(s) of interest (SB216763, EGCG, quercetin) a protein fraction of incubated HT29 cells (chapter 6.1.9.1) is isolated as described in chapter 6.1.10.2. 10µl (20µg) of the whole protein extract is heat-treated (95°C) for 15min with 2µl 6x SDS sample buffer (chapter 6.3.4.1). The proteins are separated by SDS-PAGE (chapter 6.3.4.2), which precedes their transfer onto a nitrocellulose membrane (chapter 6.3.4.3, (50mA per membrane for 90min)) and blocking of the nitrocellulose membrane (1h, RT, chapter 6.3.4.4). The nitrocellulose membrane is subsequently incubated, first, with the specific primary antibody (overnight at 4°C), and then with the appropriate secondary antibody (1h, RT (table 13)). To visualize the protein bands on the membrane, it is incubated in LumiGLO™ (Cell Signaling Technology) for 1min and

luminescence measured in the LumiImager (Boehringer Mannheim). The protein bands are analysed with the Lumianalyst 3.0 software (Boehringer Mannheim). The results are expressed as percentage change with respect to the DMSO-solvent control (T/C (%))

Table 13: Table showing the used antibodies, their concentrations, and the duration of the exposure of the nitrocellulose membranes during detection. The secondary antibodies were employed at the dilution of 1:2000 in blocking buffer.

Primary Antibody	Dilution	Source	Secondary Antibody	Exposure Time
Anti-GSK-*3α/β*-IgG2$_a$ (0011-A) (Santa Cruz)	1:2000	Mouse monoclonal	HRP-anti-Mouse IgG (Santa Cruz)	30s
Anti-*β*-Catenin (Cell Signaling)	1:1000	Rabbit Polyclonal	HRP-anti-Rabbit IgG (Cell Signaling)	5min
Anti-*β*-Catenin-IgG$_1$ (E-5) (Santa Cruz)	1:2000	Mouse Monoclonal	HRP-anti-Mouse IgG (Santa Cruz)	30s
Anti-GS (Cell Signaling)	1:2000	Rabbit Polyclonal	HRP-anti-Rabbit IgG (Cell Signaling)	5min
Anti-GP-IgG$_1$ (9F5) (Santa Cruz)	1:2000	Mouse Monoclonal	HRP-anti-Mouse IgG (Santa Cruz)	30s

6.2.6.2 Detection of Nuclear GSK-3 and *β*-Catenin

Nuclear proteins are extracted as described in chapter 6.1.10.3. 10µl (20µg total protein) of nuclear lysate is subjected to heat treatment (95°C) for 15min in the presence of SDS-buffer (2µl 6x SDS sample buffer (chapter 6.3.4.1). The proteins are subsequently separated by SDS-PAGE (chapter 6.3.4.2) and transferred onto a nitrocellulose membrane (50mA per membrane for 90min) chapter 6.3.4.3). After an initial blocking incubation in non-fat dry milk (1h, RT chapter 6.3.4.4)), the nitrocellulose membrane is consecutively incubated, first, with the specific primary antibody (overnight at 4°C), then with the appropriate secondary antibody (1h, RT, table 13). The nitrocellulose membrane is then incubated in LumiGLO™ (1min, Cell Signaling Technology) and luminescence is measured in the LumiImager (Boehringer Mannheim). The protein bands are analysed with the Lumianalyst 3.0 software

(Boehringer Mannheim). The results are expressed as percentage change with respect to the DMSO-solvent control (T/C (%))

6.2.6.3 Detection of the Phosphorylated GSK-3*β*, Glycogen Synthase and *β*-Catenin

To determine the phosphorylation state of GSK-3-*α*/*β* (Ser21/Ser9), glycogen synthase (Ser 641), and *β*-catenin (Thr41/Ser37/Ser33) in HT29 cells in response to the intervention with the compound(s) of interest, a cellular extract of the incubated HT29 cells (chapter 6.1.8.1) is prepared as described in chapter 6.1.10.2. 10µl (20µg total protein) of the whole protein extract is heat-treated (95°C) for 15min with 2µl 6x SDS sample buffer (chapter 6.3.4.1). The proteins are separated by SDS-PAGE (chapter 6.3.4.2), transferred onto a nitrocellulose membrane (chapter 6.3.4.3, (50mA per membrane for 90min)) and the nitrocellulose membrane blocked for 1h at RT (chapter 6.3.4.4). The nitrocellulose membrane is subsequently incubated, firstly, with the specific primary antibody (overnight at 4°C, table 1), then with the appropriate secondary antibody (1h, RT, table 14). To visualize the protein bands on the membrane, it is incubated in LumiGLO™ (Cell Signaling Technology) for 1min and luminescence measured in the LumiImager (Boehringer Mannheim). The protein bands are analysed with the Lumianalyst 3.0 software (Boehringer Mannheim). The results are expressed as percentage change with respect to the DMSO-solvent control (T/C (%)).

Table 14: Table showing the primary antibodies used to detect phosphorylated proteins, the concentrations at application dilution factors and the duration of exposure of the nitrocellulose membranes in the LumiImager.

Primary Antibody	Dilution	Source	Secondary Antibody	Exposure time
Anti phospho-GSK-3*α*/*β* (ser21/9) (Cell Signaling)	1:1000	Rabbit Polyclonal	HRP-anti-Rabbit IgG (Cell Signaling)	10min
Anti.phospho-*β*-catenin (ser33/37/Thr41) (Cell Signaling)	1:1000	Rabbit Polyclonal	HRP-anti-Rabbit IgG (Cell Signaling)	10min
Phospho-glycogen synthase (ser641) (Cell Signaling)	1:1000	Rabbit Polyclonal	HRP-anti-Rabbit IgG (Cell Signaling)	10min

6.3 Molecular Biological Methods

6.3.1 Isolation of Total RNA

Total RNA was isolated with the RNeasy Mini Kit from Qiagen. This method takes advantage of the highly selective binding property of silica-gel membranes to RNA. The silica-gel membrane can bind up to 100µg RNA, of a size of 200 nucleotides and longer. It provides thus an enrichment of mRNA since most RNA < 200 bases such as tRNA and 5S RNA, that make up 15-20% of total RNA are selectively excluded.

To avoid contamination with RNases and unwanted nucleic acids, the following precursions are taken, gloves were worn, the working utensils (pipettes, working bench) were cleaned with RNase away, and moreover sterile filter tips were used for pipetting.

Harvesting Cells

- The medium is aspirated and the cells are washed with 10ml ice-cold PBS. PBS is removed and 600µl Buffer RLT containing 1% (v/v) *β*-Mercaptoethanol (10µl in 1ml buffer RLT) is added to the cell-culture dish. Buffer RLT contains highly denaturing guanidine isothiocyanate, which immediately inactivates RNases to ensure isolation of intact RNA.
- The cells are scraped and the cell lysate collected with a sterile disposable cell scrapers. The cell lysate is transferred to a sterile 1.5ml microcentrifuge tube.

RNA-Isolation

- In order to shear genomic DNA and reduce the viscosity of the cell lysate, it is passed 5x through a sterile 20-gauge needle (0.9mm diameter) fitted onto an RNase-free syringe.
- 600µl 70% (v/v) ethanol is added to the lysate and mixed by pipetting up and down. Ethanol provides appropriate binding conditions for RNA to bind to the silica-gel membrane and causes the precipation of proteins.

- The RNeasy® mini column is fitted in a 2ml collection tube. 600µl of the sample, along with any precipitate that may have been formed is loaded on the Rneasy® mini column where the total RNA binds to the silica gel membrane. The column is centrifuged (13.000rpm for 15s, centrifuge 5415, Eppendorf) and the flow-through is decanted. The centrifugal process repeated with the remaining 600µl of the sample.
- To wash away contaminants, the RNeasy column is washed once with Buffer RW1 and twice with Buffer RPE.
    - 700µl Buffer RW1 (13.000rpm for 15s, centrifuge 5415, Eppendorf).
    - The RNeasy column is transferred into a new 2ml collection tube.
    - 500µl RPE Buffer (13.000rpm for 15s, centrifuge 5415, Eppendorf).
    - The flow through is discarded.
    - 500µl RPE Buffer (13.000rpm for 2min, centrifuge 5415, Eppendorf).
- The column is transferred to a sterile 1.5ml reaction tube and centrifuged at 14,000rpm for 1min (centrifuge 5415, Eppendorf) in order to remove residual RPE Buffer and dry the column. Buffer RPE contains ethanol, which would interfere with elution of RNA if not entire removed. Also residual ethanols might reduce the efficiency of reverse transcription. The dried column is transferred to a sterile 1.5ml reaction tube.
- Total RNA is eluted with 60µl (2x 30µl) RNase-free water (14,000rpm for 60s). The eluted total RNA solution is apportioned in 30µl aliquots (sterile micro-centrifuge tubes) and stored at -80°C.

6.3.2 Qualitative Gene Expression Analysis of the Iso-forms of Glycogen Phosphorylase (GP) in HT29 Cells

To identify the isoforms of glycogen phosphorylase that are expressed in HT29 cells, 1.2 x 10^6 cells are plated (55cm^2) and incubated at normal growth conditions (37°C, 5% CO_2) for 48h. Total RNA was extracted (chapter 6.3.1) and subjected to RT-PCR with the Titan One Step RT-PCR kit from ROCHE. The sequences for the human GP-isoform specific primers were synthsized by MWG Biotechnology. Beta-actin was co-amplified and detected as the endogenous control.

6.3.2.1 One Step RT-PCR with the Titan One-Tube Kit

The Titan One Step PCR assay is designed to perform the processes of reverse transcription and cDNA amplification in a single reaction set-up. The AMV-RT (avian myeloblastosis virus reverse transcriptase) is responsible for the synthesis of the first strand DNA from mRNA, while two DNA-polymerases, Taq DNA polymerase and Tgo DNA polymerase perform the amplification of DNA in concert with one another.

Brain GP forward primer:	**5´-GCT CAA CGG GGC CCT CAC CAT CGG C-3´**	
	Concentration in 1ml	**43pmol/µl**
	Volume needed for 100pmol/µl	**430µl (DEPC-H2O)**
	MW	**7589g/mol**
	Tm	**72.8°C**
	GC-percentage	**72%**
Brain GP, reverse primer:	**5´-ACT AGG AGC ACT TCT AGC ACA TTC C-3´**	
	Concentration in 1ml	**50pmol/µl**
	Volume needed for 100pmol/µl	**500µl (DEPC-H2O)**
	MW	**7586g/mol**
	Tm	**63°C**
	GC-percentage	**48%**

Muscle GP, forward primer:	**5´-GCT CAA CGG GGC TCT GAC CAT TGG C -3**	
	Concentration in 1ml	**38pmol/µl**
	Volume needed for 100pmol/µl	**380µl (DEPC-H2O)**
	MW	**7659g/mol**
	Tm	**69.5°C**
	GC-percentage	**64%**
Muscle GP, reverse primer:	**5´-TGG CCC AAG AGA GTG TGA CAG ACT C -3´**	
	Concentration in 1ml	**34pmol/µl**
	Volume needed for 100pmol/µl	**340µl (DEPC-H2O)**
	MW	**7716g/mol**
	Tm	**66.3°C**
	GC-percentage	**56%**
Liver GP, forward primer	**5´-GAG GCA CTT CCA GAG CTG AAG CTG G -3´**	
	Concentration in 1ml	**20pmol/µl**
	Volume needed for 100pmol/µl	**200µl (DEPC-H2O)**
	MW	**7732g/mol**
	Tm	**67.9°C**
	GC-percentage	**60%**
Liver GP, reverse primer	**5´-TCC CTC CCC ATT CCC AGA GAT ACT C -3´**	
	Concentration in 1ml	**51pmol/µl**
	Volume needed for 100pmol/µl	**509µl (DEPC-H2O)**
	MW	**7458g/mol**
	Tm	**66.3°C**
	GC-percentage	**56%**
***β*-actin, forward primer**	**5´-CCC CAT TGA ACA CGG CAT TG -3´**	
	MW	**6062**
	Tm	**59,4 °C**
	GC-percentage	**55%**
***β*-actin, reverse primer**	**5´-GGA GTC CAT CAC AAT GCC AG -3´**	
	MW	**6111**
	Tm	**59.4 °C**
	GC-percentage	**55%**

Procedure

- Before beginning, all utensils are cleansed with RNase Away (Invitrogen). The components of the titan one tube kit are thawed, vortexed briefly and placed on ice.
- The components for master mix I (table 15) and master mix II (table 16) are pipetted together on ice into two separate RNase-free microfuge tubes. The components of master mix II are pippetted together the enzyme mix (table 16), which is added only moments prior to use. On ice, the forward and reverse primers are pipetted into a RNase-free microfuge reaction tube. The master mixes I and II are added to the microfuge reaction tube containing the primers. The tube is vortexed briefly and centrifuged to collect the contents at the bottom of the tube (table 17). The PCR run is performed using the program shown on table 20

To exclude artefacts from DNA targets, for example, genomic DNA residual of RNA preparations or contaminating DNA from previous PCR experiments, a no-template control reaction (table 18) and a no-reverse transcriptase control reaction (table 19) is always set up. After the RT-PCR assay, the PCR products are detected on agarose gel (1.2%) with ethidium bromide staining (chapter 6.3.6).

The RT-PCR experiments were carried out by Bülent Soyalan in the course of his "Forschungsarbeit" (Soyalan 2005)

Table 15: Master mix I (n=1)

DEPC-H_2O	11µl
DTT (100 mM)	2.5µl
dNTP (10 mM each)	1µl
RNase inhibitor	0.5µl
Template RNA (50ng/µl)	2µl
Σ	17µl

Table 16: Master mix II (n=1)

DEPC-H2O	14µl
RT-PCR Buffer (5x)	10µl
Enzyme mix	1µl
Σ	25µl

Table 17: Set up for a RT-PCR reaction of n=1

Table 18: Master mix I for no-template control

Upstream primer (5µM)	4µl
Downstream primer (5µM)	4µl
Master mix I	17µl
Master mix II	25µl
Σ	50µl

DEPC-H_2O	13µl
DTT (100mM)	2.5µl
dNTP (10mM each)	1µl
RNase Inhibitor	0.5µl
Σ	17µl

Table 19: Master Mix II for minus RT reaction (n=1)

DEPC-H_2O	15µl
RT-PCR Buffer (5x)	10µl
Σ	25µl

Table 20: Thermal cycling conditions for RT-PCR with the Titan one step PCR kit from Roche.

Reverse transcription			
Step	Temperature	Duration	
1	50°C	31min	
2	ENDE		
PCR			
Step	Temperature	Duration	
1	94°C	2min	
2	94°C	30s	Denature
3	67°C	1min	Annealing
4	68°C	3min	Elongation
5	Repeat steps 2-4 (9)		
6	94°C	30s	
7	67°C	1min	
8	68°C	3min	
9	68°C	5s + 5s/ Cycle	
10	Repeat steps 6-9 (25 times)		
11	68°C	7min	
12	4°C		
13	ENDE		

6.3.3 DNA Agarose Gel Electrophoresis

Agarose gel electrophoresis is the most prevalent method employed in molecular biology for the analysis and characterization of nucleic acids. It owes its popularity to a couple of factors namely, it's applicability as a high resolution method for a wide range of nucleic acid sizes (100bp - 10kbp), the reproducibility of results, and finally because it presents the possibility to obtain the products for preparative purposes. Separation of DNA takes place according to DNA size in the agarose gel connected to an electric field, whereby smaller DNA molecules by virtue of their size migrate through the pores of gel faster than larger molecules migrate (Brown 2002). The pore size and structure is determined by the concentration of agarose. High agarose concentrations yield small pores while low agarose concentrations give rise to large pores. Most commonly used are gels with agarose concentrations between 0.7-1% (w/v), however, gels with as low a concentration as 0.3% (w/v) agarose or as high as 2% (w/v) agarose can be employed depending on the size of the DNA fragments expected.

6.3.3.1 Casting Agarose Gel and Electrophoresis

The casting of agarose gels for the purpose of DNA characterisation was performed in a horizontal flat-bed apparatus.

- The casting tray is sealed off on both ends with tape and placed in the chamber on a flat surface. In a 250ml Schott bottle, 1.2g agarose powder and 100ml 1x TAE buffer (1.2% w/v) are heated while stirring until the solution boils and the agarose is melted completely. The contents of the bottle are cooled under a running tap to about 60°C. 5µl of a 10mg/ml concentrated solution of ethidium bromide (has final concentration of 0.5µg/ml) is added and the solution mixed thoroughly.

- The gel is poured carefully into the casting tray with a comb inserted on the cathode bordering side of the gel. Air bubbles trapped in the gel are quickly shifted to a corner. The gel is allowed to cool at room temperature. Upon cooling, the galactose and 3,6 anhydrogalactose chains of agarose is rearranged into helical structures, which bundle up into a three dimensional network (Pingoud 2002). When the gel has solidified, the comb is removed

and the chamber filled with 1x TAE buffer (Tris-acetate, EDTA) until the gel is slightly but entirely submerged.

- 20µl sample is mixed with 4µl (6x) loading dye solution (MBI Fermentas) and subsequently loaded on the agarose gel using a pipette. To facilitate the allocation of the DNA fragments after electrophoresis, 5µl of an appropriate DNA-marker (DNA-Marker-Mix und 1kb DNA-Marker, MBI Fermentas) is also loaded in a separate well.
- The apparatus is closed and the gel ran at 60-70V. Due to the net negative charge of DNA, owing to the negatively charged phosphate groups in the DNA backbone, DNA molecules migrate toward the anode upon application of current, whereby, small DNA molecules migrate faster than large molecules
- After electrophoresis, the DNA fragments are visualized as distinct bands within the gel on a UV-transillumator (Eagle Eye™ II, Stratagene®). This is made possible by ethidium bromide (added to the gel), which can bind double stranded DNA indiscriminately by intercalating between the base pairs. The bond with DNA provokes a sharp increase in the fluorescence of ethidium bromide upon excitation with UV light (excitation: λ=302nm), which otherwise fluoresces weakly when unbound. After excitation, ethidium bromide emits light of wavelength λ=510nm (Pingoud 2002).

Tris-Acetate-EDTA-Buffer (TAE) 50 x	**Tris-Cl**	**242.0g**
	Acetic acid	**51.1ml**
	0.5M EDTA-solution	**100.0ml**
		Filled to 1l with re-distilled water. Set to pH 8.0-8.3. Diluted to 1x before use. The 1x working solution is 40mM Tris-acetate/ 1mM EDTA. Stored at RT.

6.3.4 Plasmid Preparation

Prior to this thesis, the plasmids described in the following section were transformed, amplified and subsequently stored (–80 °C) as E. Coli glycerol stocks by Claudia Handrich during her diploma thesis (Diplom Arbeit, 2004). Before being employed for transfection reactions, the plasmids were isolated and their integrity ascertained as described in the following chapter.

6.3.4.1 TOP*flash* (Tcf Reporter Plasmid)

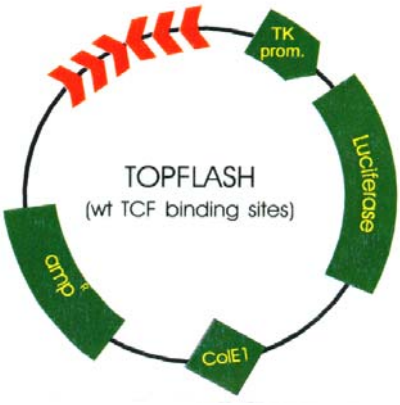

Location:

TCF-Binding site	404 - 492 bp
HSV-TK-promoter	528 - 688 bp
Luciferase-ORF	691 - 2343 bp

Figure 62: Vector map of the Tcf Reporter Plasmid TOP*flash* (Upstate Biotechnology, 2003)

TOP*flash* is a 5.5 kb construct made up of 6 copies of the wild type Tcf binding site arrayed in 2 two groups of 3 each, that lie back to back. The two groups lie in opposite orientation to one another (figure 62). The cluster of Tcf binding sites is flanked upstream by a sequence that encodes for the selective marker ampicillin and downstream by a Thymidin Kinase (TK) minimal promoter that drives the transcription of the open reading frame for the monomeric 61kDa luciferase enzyme (figure 62). A replication origin of the natural occurring E. coli plasmid, colicin E1 guarantees the expression and amplification of TOP*flash* in the E. coli (figure 62)

6.3.4.2 FOP*flash* (TCF Reporter Plasmid)

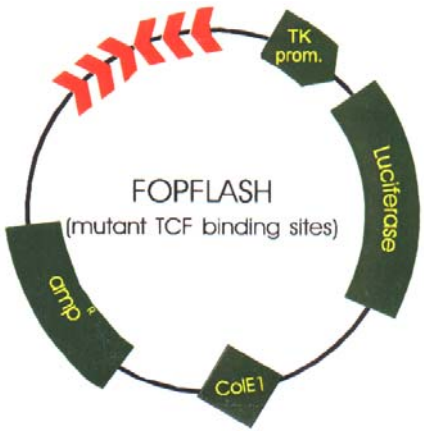

Location:

TCF-Binding site	396 - 480 bp
HSV-TK-promoter	518 - 678 bp
Luciferase-ORF	681 - 2333 bp

Figure 63: Vector map of the Tcf Reporter Plasmid FOP*flash* (Upstate Biotechnology, 2003)

FOP*flash* is used as a negative control to TOP*flash*. It has an identical molecular weight and is similarly constructed as TOP*flash* but possesses mutated copies of the Tcf binding sites (figure 63). Hence binding of *β*-catenin/Tcf/Lef is less efficient and luciferase expression is less.

6.3.4.3 pFLAG-CMV5a-Δ45-*β*-Catenin

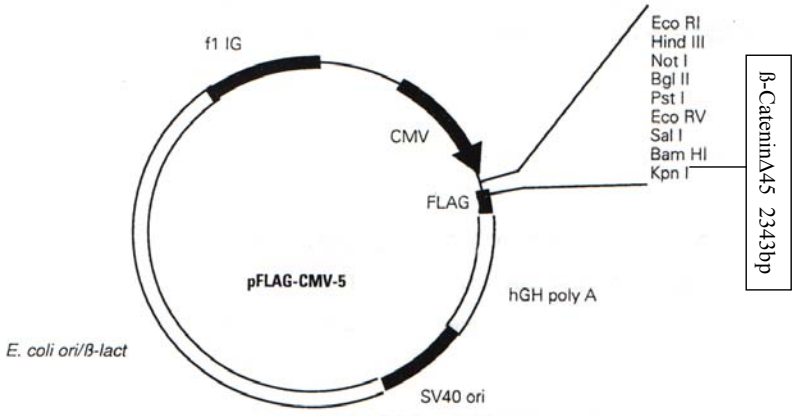

Figure 64: Circle map of pFLAG-CMV5a-Δ45-*β*-catenin plasmid (7011 bp) (Handrich 2004).

Beta catenin was isolated from HCT-116 cells and cloned into a pFLAG-CMV-5a vector (figure 64) by (Sigma, 03/1999). The pFLAG-CMV-5a vector in to which *β*-catenin cDNA was cloned is a component of the Mammalian Carboxy-terminal FLAG® Transient Expression Kit from Sigma and contains following elements; a CMV-promoter that drives the transcription of the FLAG fusion construct (419-909 bp), a multiple cloning site with 9

different restriction sites (912-974 bp), a FLAG Tag made up of 8 amino acids (N-AspTyrLysAspAspAspAspLys-C), which can be used to monitor protein expression using anti-FLAG antibodies (975-998 bp), origin of replications (ori) of SV40 (1652-2002 bp) and E.coli for replication in COS cells and E.coli respectively, and finally a *β*-lactamase coding gene segment (Amp^r) that confers ampicillin resistance to E.coli. The pFLAG-CMV5a-*β*-catenin plasmid is used to validate the reporter gene assay. As a result of the mutation on Ser 45, *β*-catenin escapes degradation and is expected to bind to initiate expression of luciferase when the plasmid is cotranfected with TOP*flash.*

6.3.4.4 pRL-TK Vector

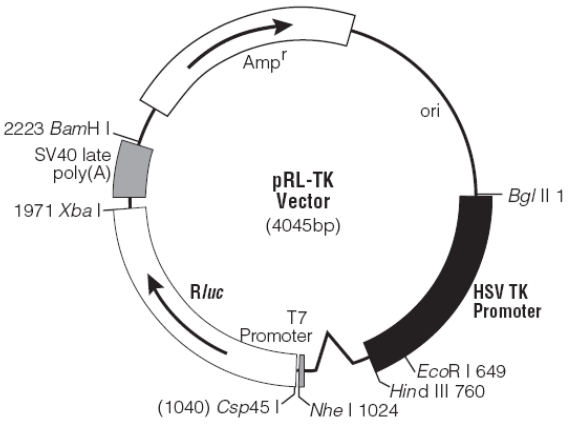

Lokation:

HSV-TK-Promoter 7 - 759 bp

T7 RNA polymerase-promotor (-17 bis +2) 1006 - 1024 bp

R*luc* Reporter gene 1034 - 1969 bp

SV40 Late Polyadenylation signal 2011 - 2212 bp

ß-Lactamase (Amp^r) coding region 2359 - 3219 bp

Figure 65: The pRL-TK vector map and sequence reference points. -^-, position of intron; R*luc*, cDNA encoding the *Renilla* luciferaseenzyme; Ampr, gene conferring ampicillin resistance in *E. coli*; ori, origin of plasmid replication in *E. coli*. Arrows within the *Rluc* and Amp^r gene indicate the direction of transcription (Promega-(7/01))

The pRL-TK vector (figure 65) is a 4 kb construct intended for use as an internal control reporter in a dual luciferase reporter gene assay. It contains the cDNA (R*luc)* encoding a *Renilla* luciferase originally cloned from the marine *Renilla reniformis.* R*luc* is located downstream a thymidin kinase promoter derived from the Herpes simplex virus that provides low to moderate levels of the monomeric *Renilla* luciferase (36kDa) expression. Situated between R*luc* and the open reading frame of a gene Amp^r encoding ampicillin resistance is an SV40 late poyladenylation signal. The origin of replication ori guarantees the replication of pRL-TK-vector in E.coli (Promega-(7/01)).

6.3.4.5 Plasmid Purification

Plasmids were isolated using anion exchange chromatography with the Qiagen Plasmid Maxi Kit that yields a maximum of 500µg plasmid. The procedure is based on the interaction between the negatively charged phosphate groups of the DNA backbone and the positively charged diethyl-aminoethanol (DEAE) groups of the resin (figure 66). At neutral pH and medium salt concentrations, DNA binds to the resin while impurities like RNA, proteins and carbonhydrates are washed out. At high salt concentrations, DNA is eluted because chloride anions compete with DNA-phosphate groups for the DEAE groups.

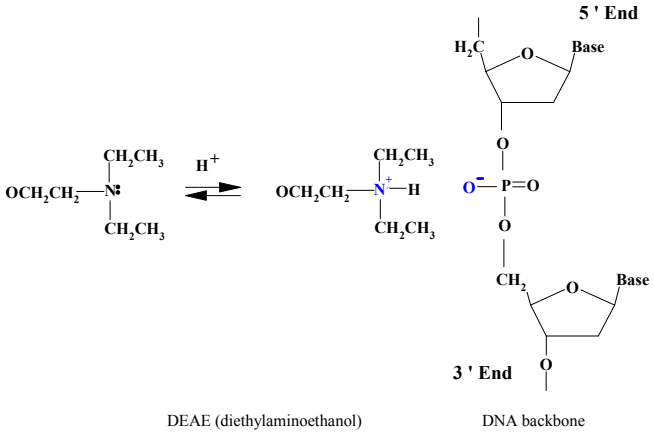

Figure 66: Interaction between negatively charged phosphates of the DNA backbone and positively charged DEAE groups on the surface of the resin (Qiagen 09/2000)

6.3.4.6 Incubation of the Starter Culture

A sterile pipette tip is used to inoculate frozen *Escherichia coli* cells habouring the appropriate vector (glycerin stock) into 5ml LB-medium that contains ampicillin (5µl of a 50mg/ml stock). The cells are incubated for 8h at 37°C with vigorous shaking (275rpm). The entire starter culture is pipetted into a 1l sterile Erlenmeyer flask and diluted with 250ml of ampicillin supplemented (250µl of a 50mg/ml stock).LB medium. The cells are then incubated for 16h at 37°C under vigorous shaking (275rpm)

LB Medium	**Tryptone**	**10g**
	Yeast Extract	**5g**
	NaCl	**10g**
		Dissolved in 1l re-distilled water. Set to pH 7.0. Sterilized by autoclaving.

6.3.4.7 Extraction of Plasmid DNA

Before the plasmid isolation is commensed, the centrifuge is pre-cooled to 4°C

- The E. coli cells are harvested by centrifugation at 6000g for 15min at 4°C. The supernatant is decanted and the centrifugation tube cleared of all traces of supernatant with a filter paper. The pellet is completely re-suspended in 10ml Buffer P1 by pippeting up and down until no cell clumps are visible. Buffer P1 contains RNase A, which digests RNA liberated in the following step (alkali lysis). The bacteria are lysed in 10ml NaOH-SDS lysis buffer (Buffer P2) for a maximum of 5min. SDS solubilizes the phospholipid and protein components of the cell membrane while NaOH denatures proteins. Prolonged lysis, i.e. above 5min, can irreversibly denature the plasmid and make it resistant to restriction enzyme digestion. The lysate is neutralized with 10ml of ice cold Buffer P3 (acidic potassium acetate) and incubated on ice for 20min. SDS inhibits the binding of DNA to the resin. So, to allow complete precipitation of SDS, the tube is capped and the contents gently and thoroughly mixed. A white fluffy precipitate containing cellular debris, denatured proteins, chromosomal DNA and potassium dodecyl sulphate is formed. The plasmid DNA is separated from the precipitate by centrifugation at 20,000g for 30min at 4°C. The plasmid containing supernatant is transferred to a new sterile centrifugation tube. The supernatant is centrifuged at 20,000g for 15min at 4°C. At this stage, the plasmid DNA re-natures, since the solution is now free of denaturing compounds. The Qiagen-tip 500 is equilibrated with 10ml Buffer QBT. The column is allowed to empty by gravity flow. (The equilibaration of the Qiagen-tip 500 is begun simultaneously to the previous step so that the column is ready by the end of the centrifugation). The equilibrated column is loaded with the plasmid containing supernatant and allowed to empty by gravity flow. At this step

plasmid DNA binds to the resin. The column is washed with 60ml Buffer QC (contains 1M NaCl, pH 7). While plasmid DNA remains bound to resin, contaminants like RNA and carbonhydrates are washed off. Plasmid DNA is eluted with 15ml Buffer QF (Elution Buffer, contains 1.25M NaCl, pH 8.5). The eluate is collected in a 30 ml centrifugation tube. To precipitate plasmid DNA, 10.5ml isopropanol (RT) is added. The contents of the centrifugation tube are mixed properly and centrifuged at 15,000g for 10min at 4°C. The supernatant is discarded and with a bold marker the position of the pellet marked on outside of the tube. The pellet is washed with 15ml 70% (v/v) ethanol (temperated to RT) and centrifuged at 15,000g for 10min at 4°C. The supernatant is decanted with care in order not to disrupt the pellet. The pellet is air-dried for approximately 10min. The plasmid DNA is dissolved in a suitable volume of water or 10mM Tris-Cl, pH 8.5 (200µl-300 µl) by rinsing the walls of the tube. Pipetting up and down for re-suspension is avoided because this would cause shearing of the DNA. Plasmid DNA yield and purity is determined using 260nm absorption and 260/280nm ratio on a UV-spectrophotometer (Nano Drop) respectively. Restriction mapping is used to ascertain the "quality" of DNA isolated (chapter 6.3.6.8). The plasmid solution is diluted to 500ng/µl and stored at -20°C.

6.3.4.8 Restriction Mapping of Plasmid DNA

Restriction mapping was used to determine the integrity of the isolated plasmid DNA. It entails specifying the location of a set of restriction sites on the plasmid DNA using restriction endonucleases. The resulting DNA fragments are separated by electrophoresis in an agarose gel and viualised under UV light. A comparative analysis of the results of single and double digestions forms the basis for the identification and verification of the "quality" of the DNA (Pingoud 2002).

6.3.4.8.1 Restriction Digestion

Restriction digestion is the cutting of DNA into fragments with restriction enzymes. Restriction enzymes recognize and cut duplex DNA at enzyme specific recognition sites, which have sequences of mostly palindromic nature. The resulting fragments can have one of

three different kinds of ends: 5' overhang, 3' overhang (sticky ends) and blunt end. The cleavage leaves a phosphate group at the 5' end and a hydroxyl group at the 3' end. The restriction enzymes employed for the characterization of plasmid DNA are shown on (table 21)

Table 21: Table of the restriction enzymes employed to characterize plasmid DNA.

Plasmide DNA	Linear Digestion	Double Digestion
TOP*flash*	*Bam*HI	*Bam*HI/*Not*I
FOP*flash*	*Bam*HI	*Sac*I/*Not*I
pFLAG-CMV5a-Δ45-*β*-Catenin	*Bam*HI	*Bam*HI/*Kpn*I
pRL-TK-*Renilla* Luciferase	*Bam*HI	*Bam*HI/*Eco*RI

Procedure

- Water, DNA-solution, restriction enzyme and respective buffers are mixed in a sterile DNase-free 1.5ml reaction tube at the volumes indicated in tables (22 to 25). The reaction tube is incubated for 90min in a water bath temperated at 37°C. After the incubation period, the reaction tube is placed on ice to stop the reaction. 20µl of the probe is then mixed with 4µl DNA loading dye (6x Mass Loading Dye Solution, MBI Fermentas), vortexed briefly and applied to agarose gel electrophoresis (chapter 6.3.3).

Table 22: Restriction digestion of TOP*flash*.

	Water (DEPC)	Buffer	Plasmid (0.5µg/µl)	Restriction Enzyme	Site	Size of Fragment
No Digestion	19.5µl	-	0.5µl	-	-	
Linearistion	16.5µl	2µl BamHI Buffer	0.5µl	1µl *Bam*HI	519bp	5500bp
Double Digestion	16.5µl	4µl Y^+/Tango Buffer	0.5µl	1µl *Bam*HI	519bp	1893
				1µl *Not*I	2412bp	3607

Table 23: Restriction digestion of FOP*flash*

	Water (DEPC)	Buffer	Plasmid (0.5µg/µl)	Restriction Enzyme	Cleaving Site	Size of Fragment
No Digestion	19.5µl	-	0.5µl	-	-	
Linearistion	16.5µl	2µl BamHI Buffer	0.5µl	1µl *Bam*HI	509bp	5500bp
Double Digestion	16.5µl	4µl Y^+/Tango Buffer	0.5µl	1µl *Sac*I	2402bp	889bp
				1µl *Not*I	3291bp	4611bp

Table 24: Restriction digestion of pRL-TK-*renilla* plasmid.

	Water (DEPC)	Buffer	Plasmid (0.5µg/µl)	Restriction Enzyme	Cleaving Site	Size of Fragment
No Digestion	19.5µl	-	0.5µl	-	-	
Linearistion	16.5µl	2µl BamHI Buffer	0.5µl	1µl *Bam*HI	2223bp	4045bp
Double Digestion	16.5µl	4µl Y^+/Tango Buffer	0.5µl	1µl *Eco*RI	649bp	1574bp
				1µl *Bam*HI	2223bp	2471bp

Table 25: Restriction digestion of pFLAG-CMV5a-Δ45-*β*-Catenin.

	Water (DEPC)	Buffer	Plasmid (0.5µg/µl)	Restriction Enzyme	Cleaving Site	Size of Fragment
No Digestion	19.5µl	-	0.5µl	-	-	
Linearistion	16.5µl	2µl BamHI Buffer	0.5µl	1µl *Bam*HI	963bp	7071bp
Double Digestion	16.5µl	4µl Y^+/Tango Buffer	0.5µl	1µl *Bam*I	963bp	1574bp
				1µl *Kpn*I	973bp	2471bp

6.3.5 Tcf/Lef Reporter Gene Assay

Reporter genes are molecular biological tools, which can be employed to study cellular processes like receptor function, protein-protein interactions, intracellular signal transduction, gene promoter regulation and the actions of certain transcription factors (Promega Notes, 1998). They are usually cloned into a plasmid, downstream of an "indicator sequence" specific to the experimental question. Introduced into an organism, their expression is independently driven by a separate promoter and is either constitutive or triggered by external intervention. Once expressed, they confer measurable and identifiable characteristics such as fluorescence and luminescence to the organism. Today's popular reporter genes include green fluorescent protein (GFP), luciferase (LUC), *β*-galactosidase (LacZ), *β*-glucuronidase (GUS) and chloramphenicol acetyl transferase (CAT) (Ziemienowicz 2001)

To investigate the influence of flavonoids/ polyphenols on the *β*-catenin-Tcf/Lef driven transcriptional activity in HEK-293 cells and HCT-116 cells, a mammalian cell-based reporter gene assay system from Upstate Biotechnology was employed in combination with the pFLAG-CMV5a-Δ45-*β*-catenin plasmid (chapter 6.3.6.3). The assay kit from Upstate Biotechnology consists of the two plasmids, TOP*flash* (chapter 6.3.6.1) and FOP*flash* (chapter 6.3.6.2), where TOP*flash* is the experimental plasmid and FOP*flash* the negative control.

6.3.5.1 Optimization of the dual luciferase assay reporter gene assay

Transfection of cells is most efficient when the cells are in the log-phase of growth. Therefore, to determine the starting cell number that will yield a 60-70% confluency at the time point of trasfection, HEK293 cells were seeded in 24 well dishes at varying starting populations between 10,000 cells per well and 40,000 cells per well. The optimization of the starting cell population was performed by Claudia Handrich in the course of her Diploma thesis (Handrich 2004).

6.3.5.1.1 Transfection with FuGENE 6 Transfection Reagent

Serum-and antibiotic free medium is pipetted in to a DNase free 1.5ml reaction tube and the appropriate amount of FuGENE 6 is added to the tube by pipetting directly into the medium without making contact with the plastic surfaces of the tube. Prior contact of FuGENE 6 with

plastic surfaces of the reaction tube negatively influences transfection efficiency. The tube is flicked to mix its contents and then incubated for 5min at room temperature. Plasmid DNA added accordingly, the tube is capped, vortexed briefly and incubated for 15min at room temperature. The FuGENE 6: plasmid DNA complex is added drop-wise to the cells and the Petri dish swirled to ensure an even distribution.

6.3.5.1.2 Transfection Optimization in 24 well plates

Table 26 shows the parameter used for the optimization experiments carried out in 24 well dishes. 40,000 HEK293 cells seeded per well and grown for 48h yielded the required cell confluency optimal for transfection experiments i.e. between 60-70%. Hence, this cell number was employed for transfection optimization experiments in 24 well plates.

Table 26: Optimization of the transfection efficiencies in HEK293 cells in 24 well dishes.

	TOP-/FOP*flash* [ng]	pRL-TK-vector [ng]	pFLAG-CMV5a-Δ45-*β*-catenin [ng]	FuGENE 6: DNA ratio
Optimization of the FuGENE 6: plasmid ratio	300	30	-	3:1, 3:2, 6:1
Optimization of the TOP*flash*/FOP*flash* concentration	100, 200, 300, 400, 500	10, 20, 30, 40, 50	-	3:1
Optimization pRL-TK-vector concentration	400	40, 45, 50, 55, 60	-	3:1
Optimization pFLAG-CMV5a-Δ45-*β*-catenin concentration	400	40	5, 10, 15, 20, 30	3:1

Lysis of the cells is performed in passive lysis buffer (Promega) at room temperature. The cells are lysed by adding 100µl of the passive lysis buffer per well and incubating the cells at room temparture on a shaker for 15min. Measurement of luciferase activity is performed immediately using the Stop and Glo buffers of the dual-luciferase™ reporter assay system (Promega), which enables the determination of both firefly and *renilla* luciferase activities in the same reaction. 10µl of the lysate is transferred in duplicates to a 96 well dish (Lumitrac

200 (Greiner-Bio-One) or fluoroNunc (Nunc)) and luciferase activity measured with the luminometers Sirius HT from MWG or Luminoskan RT from Labsystems at the parameters indicated on table 27 and 28 respectively. After data analysis, the firefly luciferase activity is normalized to the the *renilla* luciferase activity.

Table 27: Reading parameters on Sirius HT (MWG) for the dual luciferase assay

	Volume	Read	Interval	Sensitivity	Reading mode
Dispenser 1 Luciferase assay reagent II	50µl @ 300µl/sec	12s	1s	125	Kinetic
Dispenser II Stop and Glo Buffer	50µl @ 300µl/sec	12	1s		

Table 28: Reading parameters on Luminoskan from Labsystems for the dual luciferase assay

	Volume	Shake before read	Read	Interval
Luciferase assay reagent II	50µl	2s	10s	Continuous
Stop and Glo Buffer	50µl	2s	10	Continuous

Dual luciferase reporter Assay system (Promega)	**Luciferase assay buffer I**	**10ml**
	Luciferase assay substrate	**Lyophilized** **The kit components are frozen (dry ice) at delivery. Stored before reconstitution at -20°C and after reconstitution at -80°C. Before use, the assay buffer is thawed in the dark and temperated to RT. The lyophilized substrate is dissolved in entire 10 ml of assay buffer.**
	Stop & Glo Buffer	**10ml**
	Stop & Glo substrate	**200µl** **Stored before reconstitution at -20°C and after reconstitution at -80°C. Entire 200µl of substrate is added to buffer before use. Kept away from direct light.**

6.3.5.2 Optimization of the firefly luciferase assay in 10cm Petri dishes

To determine the optimal seeding cell number, seeding experiments were performed at varying starting cell populations for 48h and 72h. 500,000 HEK293 cells and 300,000 HCT116 cells incubated for 72h yielded a confluency of about 70%. Transfection optimization experiments were hence performed with this starting cell number. Table 29 and table 30 shows the parameter used for the optimization experiments carried out with HEK293 cells and HCT116 cells respectively.

Table 29: Optimization of the transfection efficiencies in HEK293 cells in 10cm Petri dishes.

	TOP*flash*/FOP*flash* [µg]	pFLAG-CMV5a-Δ45-*β*-catenin [µg]	FuGENE 6: DNA ratio
Optimization of the FuGENE 6: plasmid ratio	5	-	3:1, 6:1, 9:1
Optimization pFLAG-CMV5a-Δ45-*β*-catenin concentration	5	0.5, 1.0, 2.0	3:1

Table 30: Optimization of the transfection efficiencies in HCT116 cells in 10cm Petri dishes

	TOP*flash*/FOP*flash* [µg]	FuGENE 6: DNA ratio
Optimization of the FuGENE 6: plasmid ratio	1, 2.5, 5	3:1, 6:1, 9:1

24h post transfection, the cells are lysed in 500µl 1x cell culture lysis buffers and the luciferase activity measured (Sirius HT, MWG or Luminoskan RT, Labsystems).under the conditions depicted in tables 34 and 35.

6.3.5.3 Transfection of HEK-393 Cells and HCT-116 Cells with FuGENE 6 at the optimized experimental conditions

72h prior to transfection, 0.5 x 10^6 HEK-293 cells per 10cm Petri dish and 0.3 x 10^6 HCT-116 cells per 10cm Petri dish are plated in serum and antibiotics containing DMEM and RPMI medium respectively (37°C, 5% CO_2, (chapter 6.1.8.3)). Transfection was performed with

FuGENE 6 (Roche Applied Sciences), at a transfection reagent/plasmid DNA ratio of 3:1 (v/w) for HEK293 cells and 9:1 for HCT116 cells.

Tables 31 to 33 show the volumes for transfection reactions prepared with FuGENE 6 for the transfection of HEK293 cells and HCT116 cells with TOP*flash*/FOP*flash* and the co-transfection of HEK293 cells with TOP*flash*/FOP*flash* and pFLAG-CMV5a-Δ45-*β*-Catenin. Transfection was performed 72h after seeding.

Table 31: Transfection of HEK-293 cells with TOP*flash*/FOP*flash* at a FuGENE 6 reagent: DNA ratio of 3:1 (n = 1 Petri dish).

DMEM-medium (serum and antibiotic free)	475µl
FuGENE 6	15µl
TOP*flash*/FOP*flash* (500ng/µl)	10µl (5µg)
∑	500µl

Table 32: Co-transfection of TOP*flash* or FOP*flash* and pFLAG-CMV5a-Δ45-*β*-catenin into HEK-293 cells at a FuGENE 6 reagent: DNA ratio of 3:1 (n = 1 Petri dish).

DMEM-medium (serum and antibiotic free)	465µl
FuGENE 6	18µl
TOP*flash* or FOP*flash* (500ng/µl)	10µl (5µg)
pFLAG-CMV5a-Δ45-*β*-catenin (100ng/µl)	10µl (1µg)
∑	**500µl**

Table 33: Transfection of HCT116 cells with TOP*flash*/FOP*flash* at a FuGENE 6 reagent: DNA ratio of 9:1 (n = 1 Petri dish).

RPMI-medium (serum and antibiotic free)	475µl
FuGENE 6	45µl
TOP*flash*/FOP*flash* (500ng/µl)	10µl (5µg)
∑	500µl

24h post transfection, the Fugene 6 containing medium is aspirated. The cells are rinsed in 5ml 1x PBS. 1ml trypsin/EDTA is added and spread to cover cells by swirling the dish (max

10sec for HEK293 cells and 1min for HCT116 cells). The cells are resuspended in 10ml of appropriate medium and counted and reseeded in a 12 well dish, HEK-293 cells at a density of 0.2 x 10^6 cells per well and HCT-116 cells at 0.15 x 10^6 cells per well. The cells were incubated at normal culturing conditions (37°C, 5% CO_2) for 24h before treatment with the compound(s) of interest.

6.3.5.4 Incubation of HEK-293 Cells

The fact that HEK-293 cells are semi-adherent in nature makes them detach very easily from the surface of the culture dish. To prevent cell loss during incubation, the candidate compound was weighed, dissolved in DMSO and diluted with DMEM medium (FCS 10%, (v/v), 1%, (v/v) pen/strep) so that DMSO has a concentration of 2% and candidate compound 2 times more concentrated as the final concentration. 1ml of the 2 fold concentrated compound dilution is added drop-wise into the well containing 1ml of medium from re-seeding.

6.3.5.5 Incubation of HCT-116 Cells

The candidate compound is weighed, dissolved appropriately (DMSO), and diluted with RPMI medium (FCS 10%, (v/v), 1%, (v/v) pen/strep) so that DMSO has a final concentration of 1%. Old growth medium is aspirated and the wells rinsed once with pre-warmed (37°C) 1x PBS. 1 ml of the diluted compound solution is added to the well by pipetting on the wall.

6.3.5.6 Luciferase Assay

The luciferase assay is conducted using Promega's firefly luciferase assay system kit. To terminate the incubation of the cells with the candidate compound(s), the compound dilution is aspirated, and the wells of the cell culture dish are rinsed in quick succession with ice cold 1x PBS (1 ml). Diligence is required in handling HEK-293 cells because they detach easily from the surface of the dish. After rinsing, PBS is removed completely and the cells are incubated for 15min in 1x luciferase cell culture lysis buffer (500µl/well) (chapter 6.1.10.1). The cell lysate is transferred to 1.5 ml reaction tubes and centrifuged (2min, 1000rpm, 4°C, (Eppendorf 5804 R)) to separate cell debris. The supernatant is transferred in duplicates to a fluoroNunc 96 well dish (10µl/well) and the plate measured immediately in the luminometer. Two different luminometers, whose reading parameters are depicted in table 35 and table 35,

were employed for the measurement of luminescence (Sirius HT, MWG and Luminoskan RT, Labsystems). The luminometers automatically add 50µl of reconstituted luciferase assay reagent per well.

	Volume	Read	Interval	Sensitivity	Reading mode
Dispense/well	50µl @300µl/sec	12s	Every 1s	125	Kinetic

Table 34: Reading setting on Sirius HT (MWG) for the Luciferase assay

	Volume	Shake before read	Read	Interval
Dispense/well	50µl	2s	10s	Continuous

Table 35: Reading setting on Luminoskan from Labsystems for the Luciferase assay

Luciferase Assay Reagents (Promega)	**Luciferase assay buffer**	**10ml**
	Luciferase assay substrate	**Lyophilized**
		The kit components are frozen (dry ice) at delivery. Stored before reconstitution at -20°C and after reconstitution at -80°C. Before use, the assay buffer is thawed in the dark and temperated to RT. The lyophilized substrate is dissolved in entire 10 ml of assay buffer.

6.3.6 Reverse Transcription of Total RNA

Total RNA was reversed transcribed using the High Capacity cDNA Archive Kit from Applied Biosystems and the PTC 100™ programmable Thermal Controller from MJ Reasearch, Inc. The High Capacity cDNA Archive Kit contains a multiscribe reverse transcriptase and a recombinant moloney murine leukamia virus (rMoMuLV) reverse transcriptase, which allows for the reverse transcription of up to 10µg RNA.

All steps during the reverse transcription were carried out on ice. Prior to the reverse transcription, the RNA-concentration was determined using the Nano Drop® System from Agilent. The following description is exemplary for an n = 1, 10µg cDNA per 100µl volume.

- The components of the High Capacity cDNA Archive Kit are thawed. A volume (Xµl) of total RNA-solution containing a maximum of 10µg RNA is added to a RNase free PCR-tube. DEPC- treated water is pipetted in a PCR-tube (Volume of water = 71 µl – volume of RNA solution (µl)). A 2x RT-master mix is prepared by chronologically pipetting the kit components together as shown in table 36. To prepare the 2x RT-master mix for one sample, allowances have to be made for the incidental loss of solution that occurs during pipetting. E.g. for an n = 1 reaction, a master mix is prepared for (1 + 1) reactions. 29µl of the 2x RT-master mix is added to the PCR-tube to a total volume 100µl. The PCR-tube is closed, vortexed, briefly centrifuged, placed in a thermal cycler and the reaction started. The cycling conditions for the amplification are shown below in table 37.

Table 36: 2x RT-master mix for the reverse transcription of total RNA

Component	n = 1 +1
Reverse Transcription Buffer, 10x	20µl
dNTPs, 25x	8µl
random primers, 10x	20µl
Multiscibe™ Reverse Transcriptase, 50 U/µl	10µl
∑	**58µl**

Table 37: Thermal cycling conditions for the reverse transcription of total RNA (10µg) with the High Capacity cDNA Archive kit from Applied Biosystems

	Step 1	Step 2	Step 3
Temperature	25°C	37°C	4°C
Time	10min	120min	24h

To verify for genomic DNA contamination, a reaction containing no reverse transcriptase (Multicribe™) is also reverse transcribed. Also, a no template control, a reaction without RNA-template is carried out to verify the quality of the reverse transcription. After the reverse transcription, obtained cDNA solutions are stored at -20°C.

6.3.7 Quantitative Gene Expression Analysis of GSK-*3β*, GS, GP and *β*-Catenin using TaqMan® Real-time PCR

6.3.7.1 TaqMan® Real-time PCR

Real-time PCR represents a molecular biological technique of high sensitivity that enables, in contrast to conventional PCR, the amplification and detection of specific nucleic acids in real time. The PCR product are detected using either fluorescent dyes capable of binding double-stranded DNA e.g. SYBR Green I or fluorescently labelled sequence-specific probes e.g. TaqMan® probes, molecular beacons, FRET probes.

The TaqMan® real-time PCR makes use of TaqMan® MGB probes. These are sequence specific oligonucleotide that carry on the 5' base, a fluorophore e.g. 5- 6-carboxyfluorescein [5(6)-FAM], and on the 3' base, a quenching dye e.g. 5-(and 6)-carboxy-tetramethyl rhodamine [5(6)-TAMRA] or a minor groove binder (MGB) (figure 67) (P.E Applied Biosystems). MGBs increase the stability of the template-probe hybrid by binding snugly into the minor grooves of duplex DNA (P.E Applied Biosystems).

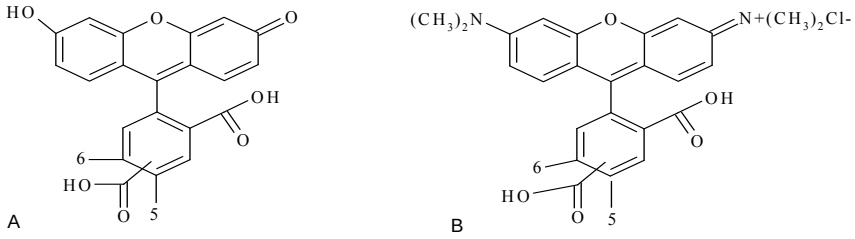

Figure 67: Structures of A: 5(6)-FAM and, B: 5(6)-TAMRA. FAM is excited at 494 nm and emits at 518 nm. TAMRA is excited at 560 nm and emits at 582 nm

At close proximity to one another, the quencher dye quenches the fluorescence of the reporter dye by means of fluorescence resonance energy transfer (FRET). However, during the PCR extension step, the probe - hybridized specifically to its target sequence that lies between the forward and reverse primer binding sites (figure 68) is cleaved by the 5'-3' exonuclease activity of Amplitaq® DNA polymerase. This leads to the separation of the fluorescent and the quencher dyes. FRET becomes interrupted (figure 68) making it possible for the reporter to fluoresce upon excitation with laser light of wavelength between 500-660nm. Since this

process recurs in every PCR cycle, the fluorescent signal increases progressively and does so proportionally to the amount of PCR product produced (Qiagen).

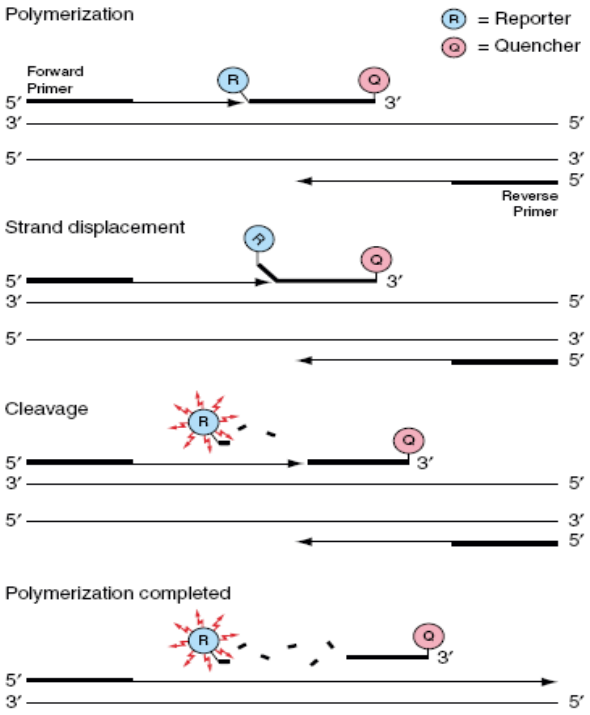

Figure 68: Schematic illustration of the chemistry of TaqMan real-time PCR. R: reporter dye, Q: quencher dye (Applied Biosystems).

6.3.7.2 TaqMan RT-PCR using Pre-developed Assay Reagents (PDAR) and Assays on Demand (AOD)

The ABI PRISM™ 7900 sequence detection system from Applied Biosystems was employed in combination with the TaqMan® RT-PCR method to study the effects of the compound(s) of interest on gene expression in HT29 cells. Listed in table 38 are the genes, whose expressions were investigated using assays from Applied Biosystems. Each assay contained a gene specific MGB-probe and a gene specific primer pair, 20 times more concentrated than the final concentration per reaction (of 250nM for the MGB-probe and 900nM for each primer). Due to the photosensitive character of the MGB-probe, exposure of the assays to daylight was avoided at all times.

Table 38: List of genes quantified using PDARs and AOD's from Applied Biosystems.

Gene	Assay ID	RefSeq	Reporter dye
Glycogen synthase (muscle type)	Hs00157863_m1	NM_002103.3	FAM
Glycogen synthase (liver type)	Hs00608677_m1	NM_021957.2	FAM
Glycogen phosphorylase (muscle type)	Hs00194493_m1	NM_005609.1	FAM
Glycogen phosphorylase (liver type)	Hs00161132_m1	NM_002863.3	FAM
Glycogen phosphorylase (brain type)	Hs00267875_m1	NM_002862.3	FAM
β-Catenin	Hs99999168_m1	NM_001904	FAM
β-Actin (endogenous control)			VIC (MGB)

Before amplification, total RNA is isolated (chapter 6.3.1) from the treated HT29 cells (chapter 6.1.9), reverse transcribed (chapter 6.3.9) and the obtained cDNA amplified in a TaqMan® RT-PCR assay as described below.

For each round of PCR, i.e. on each 96 well plate, a No Template Control, which is a reaction containing no cDNA, is performed and *β*-actin is always co-amplified as the endogenous control.

- The 20x target mix is thawed at 4°C and kept in the dark (refrigerator). It contains the sequence specific forward and reverse primers as well as the TaqMan® probe in already optimized concentrations. Simultaneously, the cDNA probes, generated by reverse transcription with the High Capacity Archive Kit from Applied Biosystems (chapter 6.3.9) are also thawed and kept on ice. 2µl cDNA-solution containing 200ng cDNA (stock: 100ng/µl) is pipetted into a sterile DNase-free PCR test tube. In a DNase-free 1.5 reaction tube, a master mix made up of DEPC-water, 20x target mix and 2x universal PCR master mix is prepared on ice. The universal master mix contains AmpliTaq GOLD® polymerase, AmpErase UNG, dNTPs, a passive reference dye and optimized buffer components. 98µl of the master mix is dispensed into a PCR tube containing cDNA. The tube is capped and vortexed briefly. The contents of each tube are loaded in triplicates at 25µl/well in a 96 well optical reaction plate. Each well contains a final cDNA template amount of 50ng. The 96 well plate is sealed with a ABI

PRISM™ optical adhesive cover. The plate is centrifuged for 5min at 800rpm and 4°C (Minifuge T, Hereaus). The plate is loaded in the sequencer (ABI PRISM™ 7900 Sequence Detection System) and the gene specific sequence amplified using the thermal cycling conditions indicated on table 40

Table 39: PCR reaction mix for routine analysis with a PDAR. The dye-labeled MGB-probe has a final concentration of 250nM and each primer has a final concentration of 900nM. The table is exemplary for 2 samples. To allow for pipetting solution loss, a master mix for n = 2.5 samples is prepared.

Components	Final concentration	n = 1	n = 2.5
cDNA 100µg/µl	50ng/ well	2µl	-
DEPC-H_2O	-	43µl	107.5µl
Target Mix, 20x	-	5µl	12.5µl
Universal Master Mix, 2x	-	50µl	125µl
Total		**100µl**	**245 µl**

The results are analysed with the help of the software SDS 2.1 (Applied Biosystems) using the relative quantification method with *β*-actin as the endogenous control and DMSO solvent sample as the sample control.

Table 40: Universal thermal cycling conditions for template amplification in the 7900 HT sequence detection system. UNG (AmpErase® uracil-N-glycosylase) contained in the Universal Master mix prevents cross over contamination of the samples by the hydrolysis of uracil-glycosidic dU containing single and double stranded DNA, thereby creating an alkali-sensitive apyrimidic site in the DNA (Longo et al. 1990).

Step	UNG incubation	AmpliTaq Gold activation	PCR Cycle (40 cycles)	
	HOLD	HOLD	Denature	Anneal/Extend
Temperature	50°C	95°C	95°C	60°C
Time	2min	10min	15s	1min

6.3.7.3 Gene Expression Assays designed with Primer Express™ Software

To study the gene expression profile of GSK-3*β* in HT29 cells after the incubation with the compound(s) of interest, a set of primers, and the TaqMan® (table 41) for the gene expression assay was designed with the Primer Express™ software version 2.0 (Applied Biosystems) and sent for synthesis to Applied Biosystems.

Table 41: Accession number, location and sequence of the set of primers and the TaqMan® probe designed and employed for GSK-3*β* expression analysis

GSK-3*β*	Assession number	Location	Exon boundary	Sequence
Forward Primer	L33801	852	-	AGGGAGCAAATCAGAGAAATGAA
Reverse primer	L33801	979	-	AGACGGCTACACAGTGCAATTG
TaqMan® probe	L33801	915	E8/E9, 929	CATCCTTGGACTAAGGTC

The assay components were stored upon delivery at -20°C. Each primer solution and the TaqMan® probe solution had a stock concentration of 10mM. The TaqMan® probe being photosensitive was always handled in the dark.

Procedure

The solutions containing the forward primer, the reverse primer and TaqMan® probe are thawed at 4°C in a dark environment (refrigerator). The reaction mix is pipetted successively into a sterile DNase-free PCR reaction tube as shown in table 42. The tube is capped and vortexed briefly. A volume of 25 µl of the reaction mixture is loaded in triplicates into a 96 well optical reaction plate. The plate is sealed with the ABI PRISM™ optical adhesive cover, then centrifuged for 5min at 800rpm and 4°C (Minifuge T, Hereaus) and detected in 7900 HT sequence detection system at the thermal cycling conditions shown in table 40. The results are analysed with the help of the software SDS 2.1 (Applied Biosystems) using the relative quantification method with *β*-actin as the endogenous control and DMSO solvent sample as sample control.

Table 42: PCR reaction mix for routine analysis of GSK-3*β*. The dye-labeled MGB-probe has a final concentration of 200nM and each primer has a final concentration of 900nM. The table is exemplary for 4 samples. To allow for pipetting solution loss, a master mix for n = 5 samples is prepared.

Components	Volume / Reaction	n = 4+1	Concentration/ Well
DEPC-H_2O	2µl	10µl	-
Forward primer (9mM)	2.5µl	12.5µl	900nM
Reverse primer (9mM)	2.5µl	12.5µl	900nM
DNA sample (100ng/µl)	0.5µl	2.5µl	50ng
TaqMan® probe (2mM)	2.5µl	12.5µl	200nM
Universal Master Mix, 2x	12.5µl	62.5µl	1x
∑	**25 µl**	**125µl**	

.

7 Bibliograpyh

Anton, S., L. Melville, and G. Rena. 2007. Epigallocatechin gallate (EGCG) mimics insulin action on the transcription factor FOXO1a and elicits cellular responses in the presence and absence of insulin. *Cell Signal* 19 (2):378-383.

Atcha, F. A., J. E. Munguia, T. W. Li, K. Hovanes, and M. L. Waterman. 2003. A new beta-catenin-dependent activation domain in T cell factor. *J Biol Chem* 278 (18):16169-16175.

Barbosa, A. J., and L. P. Castro. 2002. BGP expression in gastric epithelium and early gastric cancer. *Gastric Cancer* 5 (3):123-124.

Barker, N., G. Huls, V. Korinek, and H. Clevers. 1999. Restricted high level expression of Tcf-4 protein in intestinal and mammary gland epithelium. *Am J Pathol* 154 (1):29-35.

Bax, B., P. S. Carter, C. Lewis, A. R. Guy, A. Bridges, R. Tanner, G. Pettman, C. Mannix, A. A. Culbert, M. J. Brown, D. G. Smith, and A. D. Reith. 2001. The structure of phosphorylated GSK-3beta complexed with a peptide, FRATtide, that inhibits beta-catenin phosphorylation. *Structure* 9 (12):1143-1152.

Bhat, R. V., S. L. Budd Haeberlein, and J. Avila. 2004. Glycogen synthase kinase 3: a drug target for CNS therapies. *J Neurochem* 89 (6):1313-1317.

Bingham, S. A. 1999. High-meat diets and cancer risk. *Proc Nutr Soc* 58 (2):243-248.

———. 2000. Diet and colorectal cancer prevention. *Biochem. Soc. Trans.* 28:12–16.

Blaut, M., L. Schoefer, and A. Braune. 2003. Transformation of flavonoids by intestinal microorganisms. *Int J Vitam Nutr Res* 73 (2):79-87.

Boersma, M. G., van der Woude, H., Bogaards, J., Boeren, S., Vervoort, J., Cnubben, N. H., van Iersel, M. L., van Bladeren, P. J., Rietjens, I. . 2002. Regioselectivity of phase II metabolism of luteolin and quercetin by UDP-glucuronosyl transferases. *Chem Res Toxicol* 15:662-670.

Bornemann, A., T. Ploug, and H. Schmalbruch. 1992. Subcellular localization of GLUT4 in nonstimulated and insulin-stimulated soleus muscle of rat. *Diabetes* 41 (2):215-221.

Brantjes, H., J. Roose, M. van De Wetering, and H. Clevers. 2001. All Tcf HMG box transcription factors interact with Groucho-related co-repressors. *Nucleic Acids Res* 29 (7):1410-1419.

Breinholt, V. M., E. A. Offord, C. Brouwer, S. E. Nielsen, K. Brosen, and T. Friedberg. 2002. In vitro investigation of cytochrome P450-mediated metabolism of dietary flavonoids. *Food Chem Toxicol* 40 (5):609-616.

Bright-Thomas, R. M., and R. Hargest. 2003. APC, beta-Catenin and hTCF-4; an unholy trinity in the genesis of colorectal cancer. *Eur J Surg Oncol* 29 (2):107-117.

Brown, T. A. 2002. *Gentechnologie für Einsteiger.* . Third Edition, ed: Spektrum Akademischer Verlag GmbH Heidelberg Berlin.

Browner, M. F., K. Nakano, A. G. Bang, and R. J. Fletterick. 1989. Human muscle glycogen synthase cDNA sequence: a negatively charged protein with an asymmetric charge distribution. *Proc Natl Acad Sci U S A* 86 (5):1443-1447.

Bry, L., P. Falk, K. Huttner, A. Ouellette, T. Midtvedt, and J. I. Gordon. 1994. Paneth cell differentiation in the developing intestine of normal and transgenic mice. *Proc Natl Acad Sci U S A* 91 (22):10335-10339.

Buda, A., and M. Pignatelli. 2002. Genetics--cellular basis. *Br Med Bull* 64:45-58.

Burchell, B., and M. W. Coughtrie. 1997. Genetic and environmental factors associated with variation of human xenobiotic glucuronidation and sulfation. *Environ Health Perspect* 105 Suppl 4:739-747.

Bustin, M., and R. Reeves. 1996. High-mobility-group chromosomal proteins: architectural components that facilitate chromatin function. *Prog Nucleic Acid Res Mol Biol* 54:35-100.

Cadigan, K. M., and R. Nusse. 1997. Wnt signalling: a common theme in animal development. *Genes Dev* 11 (24):3286-3305.

Campbell, J. A., G. J. Davies, V. Bulone, and B. Henrissat. 1997. A classification of nucleotide-diphospho-sugar glycosyltransferases based on amino acid sequence similarities. *Biochem J* 326 (Pt 3):929-939.

Carling, D., and D. G. Hardie. 1989. The substrate and sequence specificity of the AMP-activated protein kinase. Phosphorylation of glycogen synthase and phosphorylase kinase. *Biochim Biophys Acta* 1012 (1):81-86.

Carroll, K. K. 1998. Obesity as a risk factor for certain types of cancer. *Lipids* 33 (11):1055-1059.

Cavallo, R. A., R. T. Cox, M. M. Moline, J. Roose, G. A. Polevoy, H. Clevers, M. Peifer, and A. Bejsovec. 1998. Drosophila Tcf and Groucho interact to repress Wingless signalling activity. *Nature* 395 (6702):604-608.

Coghlan, M. P., A. A. Culbert, D. A. Cross, S. L. Corcoran, J. W. Yates, N. J. Pearce, O. L. Rausch, G. J. Murphy, P. S. Carter, L. Roxbee Cox, D. Mills, M. J. Brown, D. Haigh, R. W. Ward, D. G. Smith, K. J. Murray, A. D. Reith, and J. C. Holder. 2000. Selective small molecule inhibitors of glycogen synthase kinase-3 modulate glycogen metabolism and gene transcription. *Chem Biol* 7 (10):793-803.

Cohen, Y., A. Chetrit, Y. Cohen, P. Sirota, and B. Modan. 1998. Cancer morbidity in psychiatric patients: influence of lithium carbonate treatment. *Med Oncol* 15 (1):32-36.

Cole, A., S. Frame, and P. Cohen. 2004. Further evidence that the tyrosine phosphorylation of glycogen synthase kinase-3 (GSK-3) in mammalian cells is an autophosphorylation event. *Biochem J* 377 (Pt 1):249-255.

Cross, D. A., D. R. Alessi, P. Cohen, M. Andjelkovich, and B. A. Hemmings. 1995. Inhibition of glycogen synthase kinase-3 by insulin mediated by protein kinase B. *Nature* 378 (6559):785-789.

Dajani, R., E. Fraser, S. M. Roe, N. Young, V. Good, T. C. Dale, and L. H. Pearl. 2001. Crystal structure of glycogen synthase kinase 3 beta: structural basis for phosphate-primed substrate specificity and autoinhibition. *Cell* 105 (6):721-732.

Danforth, W. H., and P. Harvey. 1964. Glycogen synthetase and control of glycogen synthesis in muscle. *Biochem Biophys Res Commun* 16 (5):466-471.

Dashwood, W. M., G. A. Orner, and R. H. Dashwood. 2002. Inhibition of beta-catenin/Tcf activity by white tea, green tea, and epigallocatechin-3-gallate (EGCG): minor contribution of H(2)O(2) at physiologically relevant EGCG concentrations. *Biochem Biophys Res Commun* 296 (3):584-588.

Daskiewicz, J. B., F. Depeint, L. Viornery, C. Bayet, G. Comte-Sarrazin, G. Comte, J. M. Gee, I. T. Johnson, K. Ndjoko, K. Hostettmann, and D. Barron. 2005. Effects of flavonoids on cell proliferation and caspase activation in a human colonic cell line HT29: an SAR study. *J Med Chem* 48 (8):2790-2804.

Day, A. J., J. M. Gee, M. S. DuPont, I. T. Johnson, and G. Williamson. 2003. Absorption of quercetin-3-glucoside and quercetin-4'-glucoside in the rat small intestine: the role of lactase phlorizin hydrolase and the sodium-dependent glucose transporter. *Biochem Pharmacol* 65 (7):1199-1206.

de Vries, J. H., Hollman P.C., Meyboom, S., Buysman, M.N., Zock, P.L.,van Staveren J.H. and Katan M.N. 1998. Plasma concentrations and urinary excretion of the antioxidant flavonols quercetin and kaempferol as biomarkers for dietary intake. *American Journal of Clinical Nutrition* Vol 68:60-65.

DePaoli-Roach, A. A., Z. Ahmad, M. Camici, J. C. Lawrence, Jr., and P. J. Roach. 1983. Multiple phosphorylation of rabbit skeletal muscle glycogen synthase. Evidence for interactions among phosphorylation sites and the resolution of electrophoretically distinct forms of the subunit. *J Biol Chem* 258 (17):10702-10709.

Depeint, F., J. M. Gee, G. Williamson, and I. T. Johnson. 2002. Evidence for consistent patterns between flavonoid structures and cellular activities. *Proc Nutr Soc* 61 (1):97-103.

Doll, R., and R. Peto. 1981. The causes of cancer: quantitative estimates of avoidable risks of cancer in the United States today. *J Natl Cancer Inst* 66 (6):1191-1308.

Doucas, H., G. Garcea, C. P. Neal, M. M. Manson, and D. P. Berry. 2005. Changes in the Wnt signalling pathway in gastrointestinal cancers and their prognostic significance. *Eur J Cancer* 41 (3):365-379.

Du SJ, P. S., Christian JL, McGrew LL, Moon RT. 1995. Identification of distinct classes and functional domains of Wnts through expression of wild-type and chimeric protein in Xenopus embryos. *Mol Cell Biol* 15:2625–2634

Du, S. J. P. S., Christian JL, McGrew LL, Moon RT. 1995. Identification of distinct classes and functional domains of Wnts through expression of wild-type and chimeric protein in Xenopus embryos. *Mol Cell Biol* 15:2625–2634

Duthie, G., and A. Crozier. 2000. Plant-derived phenolic antioxidants. *Curr Opin Clin Nutr Metab Care* 3 (6):447-451.

Duval, A., S. Rolland, E. Tubacher, H. Bui, G. Thomas, and R. Hamelin. 2000. The human T-cell transcription factor-4 gene: structure, extensive characterization of alternative splicings, and mutational analysis in colorectal cancer cell lines. *Cancer Res* 60 (14):3872-3879.

Eurostat. 2002. *Eurostat Yearbook 2002* Luxembourg,: Office for Official Publications of the European Communities.

Fang, X., S. X. Yu, Y. Lu, R. C. Bast, Jr., J. R. Woodgett, and G. B. Mills. 2000. Phosphorylation and inactivation of glycogen synthase kinase 3 by protein kinase A. *Proc Natl Acad Sci U S A* 97 (22):11960-11965.

Fearon, E. R., and B. Vogelstein. 1990. A genetic model for colorectal tumorigenesis. *Cell* 61 (5):759-767.

Ferlay, J. B. F., Pisani, P. Parkin, D.M. 2001. Cancer Incidence, Mortality and Prevalence Worldwide *GLOBOCAN 2000* 2002 (IARC Cancer Base no. 5).

Flotow, H., P. R. Graves, A. Q. Wang, C. J. Fiol, R. W. Roeske, and P. J. Roach. 1990. Phosphate groups as substrate determinants for casein kinase I action. *J Biol Chem* 265 (24):14264-14269.

Flotow, H., and P. J. Roach. 1989. Synergistic phosphorylation of rabbit muscle glycogen synthase by cyclic AMP-dependent protein kinase and casein kinase I. Implications for hormonal regulation of glycogen synthase. *J Biol Chem* 264 (16):9126-9128.

Fodde, R., J. Kuipers, C. Rosenberg, R. Smits, M. Kielman, C. Gaspar, J. H. van Es, C. Breukel, J. Wiegant, R. H. Giles, and H. Clevers. 2001. Mutations in the APC tumour suppressor gene cause chromosomal instability. *Nat Cell Biol* 3 (4):433-438.

Frame, S., and P. Cohen. 2001. GSK-3 takes centre stage more than 20 years after its discovery. *Biochem J* 359 (Pt 1):1-16.

Frame, S., P. Cohen, and R. M. Biondi. 2001. A common phosphate binding site explains the unique substrate specificity of GSK-3 and its inactivation by phosphorylation. *Mol Cell* 7 (6):1321-1327.

Fukushima, H. Y. H., Itoh F, et al. 2001. Frequent alterations of the beta-catenin and TCF-4 genes, but not of the APC gene, in colon cancers with high-frequency microsatellite instability. *J Exp Clin Cancer Res* 20(4) 553–559.

Garabedian, E. M., L. J. Roberts, M. S. McNevin, and J. I. Gordon. 1997. Examining the role of Paneth cells in the small intestine by lineage ablation in transgenic mice. *J Biol Chem* 272 (38):23729-23740.

Gee, J. M., M. S. DuPont, M. J. Rhodes, and I. T. Johnson. 1998. Quercetin glucosides interact with the intestinal glucose transport pathway. *Free Radic Biol Med* 25 (1):19-25.

Gee, J. M., H. Hara, and I. T. Johnson. 2002. Suppression of intestinal crypt cell proliferation and aberrant crypt foci by dietary quercetin in rats. *Nutr Cancer* 43 (2):193-201.

Giese, K., A. Amsterdam, and R. Grosschedl. 1991. DNA-binding properties of the HMG domain of the lymphoid-specific transcriptional regulator LEF-1. *Genes Dev* 5 (12B):2567-2578.

Giese, K., J. Cox, and R. Grosschedl. 1992. The HMG domain of lymphoid enhancer factor 1 bends DNA and facilitates assembly of functional nucleoprotein structures. *Cell* 69 (1):185-195.

Giese, K., C. Kingsley, J. R. Kirshner, and R. Grosschedl. 1995. Assembly and function of a TCR alpha enhancer complex is dependent on LEF-1-induced DNA bending and multiple protein-protein interactions. *Genes Dev* 9 (8):995-1008.

Giles, R. H., J. H. van Es, and H. Clevers. 2003. Caught up in a Wnt storm: Wnt signalling in cancer. *Biochim Biophys Acta* 1653 (1):1-24.

Giovannucci, E., Rimm, E.B., Stampfer, M.J., Colditz, G.A., Ascherio, A., Willett. W.C. . 1994. Intake of fat, meat, and fiber in relation to risk of colon cancer in men *Cancer Res* 54 (9):2390–2397.

Gooderham, N. J., S. Murray, A. M. Lynch, M. Yadollahi-Farsani, K. Zhao, K. Rich, A. R. Boobis, and D. S. Davies. 1997. Assessing human risk to heterocyclic amines. *Mutat Res* 376 (1-2):53-60.

Gould, T. D., N. A. Gray, and H. K. Manji. 2003. Effects of a glycogen synthase kinase-3 inhibitor, lithium, in adenomatous polyposis coli mutant mice. *Pharmacol Res* 48 (1):49-53.

Granado-Serrano, A. B., M. A. Martin, M. Izquierdo-Pulido, L. Goya, L. Bravo, and S. Ramos. 2007. Molecular mechanisms of (-)-epicatechin and chlorogenic acid on the regulation of the apoptotic and survival/proliferation pathways in a human hepatoma cell line. *J Agric Food Chem* 55 (5):2020-2027.

Grimes, C. A., and R. S. Jope. 2001. The multifaceted roles of glycogen synthase kinase 3beta in cellular signalling. *Prog Neurobiol* 65 (4):391-426.

Grosschedl, R., K. Giese, and J. Pagel. 1994. HMG domain proteins: architectural elements in the assembly of nucleoprotein structures. *Trends Genet* 10 (3):94-100.

Hague, A., D. J. Elder, D. J. Hicks, and C. Paraskeva. 1995. Apoptosis in colorectal tumour cells: induction by the short chain fatty acids butyrate, propionate and acetate and by the bile salt deoxycholate. *Int J Cancer* 60 (3):400-406.

Handberg, A., A. Vaag, H. Beck-Nielsen, and J. Vinten. 1992. Peripheral glucose uptake and skeletal muscle GLUT4 content in man: effect of insulin and free fatty acids. *Diabet Med* 9 (7):605-610.

Handrich, C. 2004. Untersuchungen zur ß-Catenin-Expression und ß-Catenin-vermittelten Gentranskription in humanen Zellen.

Hanks, S. K., and T. Hunter. 1995. Protein kinases 6. The eukaryotic protein kinase superfamily: kinase (catalytic) domain structure and classification. *Faseb J* 9 (8):576-596.

Hao, X. T. I., Ilyas M, et al. x. 1997. Reciprocity between membranous and nuclear expression of beta-catenin in colorectal tumours. . *Virchows Arch* 431 (3):167–172.

Harborne, J. B. 1986. Nature, distribution and function of plant flavonoids. *Prog Clin Biol Res* 213:15-24.

Hayes, J. S., and S. E. Mayer. 1981. Regulation of guinea pig heart phosphorylase kinase by cAMP, protein kinase, and calcium. *Am J Physiol* 240 (3):E340-349.

Hecht, A., and M. P. Stemmler. 2003. Identification of a promoter-specific transcriptional activation domain at the C terminus of the Wnt effector protein T-cell factor 4. *J Biol Chem* 278 (6):3776-3785.

Hecht A, V. K., Stemmler MP, van Roy F, Kemler R 2000. The p300/CBP acetyltransferases function as transcriptional coactivators of beta-catenin in vertebrates. . *Embo J* 19 1839–1850

Heller, W. 1986. Flavonoid biosynthesis, an overview. *Prog Clin Biol Res* 213:25-42.

Henrissat, B., and G. J. Davies. 2000. Glycoside hydrolases and glycosyltransferases. Families, modules, and implications for genomics. *Plant Physiol* 124 (4):1515-1519.

Hertog, M. G., P. C. Hollman, M. B. Katan, and D. Kromhout. 1993. Intake of potentially anticarcinogenic flavonoids and their determinants in adults in The Netherlands. *Nutr Cancer* 20 (1):21-29.

Hertog, M. G., D. Kromhout, C. Aravanis, H. Blackburn, R. Buzina, F. Fidanza, S. Giampaoli, A. Jansen, A. Menotti, S. Nedeljkovic, and et al. 1995. Flavonoid intake and long-term risk of coronary heart disease and cancer in the seven countries study. *Arch Intern Med* 155 (4):381-386.

Hill, M. M., and B. A. Hemmings. 2002. Inhibition of protein kinase B/Akt. implications for cancer therapy. *Pharmacol Ther* 93 (2-3):243-251.

Hocker, M., and B. Wiedenmann. 1998. Molecular mechanisms of enteroendocrine differentiation. *Ann N Y Acad Sci* 859:160-174.

Hong, J., H. Lu, X. Meng, J. H. Ryu, Y. Hara, and C. S. Yang. 2002. Stability, cellular uptake, biotransformation, and efflux of tea polyphenol (-)-epigallocatechin-3-gallate in HT-29 human colon adenocarcinoma cells. *Cancer Res* 62 (24):7241-7246.

Hovanes, K., T. W. Li, J. E. Munguia, T. Truong, T. Milovanovic, J. Lawrence Marsh, R. F. Holcombe, and M. L. Waterman. 2001. Beta-catenin-sensitive isoforms of lymphoid enhancer factor-1 are selectively expressed in colon cancer. *Nat Genet* 28 (1):53-57.

Hovanes, K., T. W. Li, and M. L. Waterman. 2000. The human LEF-1 gene contains a promoter preferentially active in lymphocytes and encodes multiple isoforms derived from alternative splicing. *Nucleic Acids Res* 28 (9):1994-2003.

Hsu, S. C., J. Galceran, and R. Grosschedl. 1998. Modulation of transcriptional regulation by LEF-1 in response to Wnt-1 signalling and association with beta-catenin. *Mol Cell Biol* 18 (8):4807-4818.

Huang, T. S., and E. G. Krebs. 1977. Amino acid sequence of a phosphorylation site in skeletal muscle glycogen synthetase. *Biochem Biophys Res Commun* 75 (3):643-650.

Hudson, J. W., G. B. Golding, and M. M. Crerar. 1993. Evolution of allosteric control in glycogen phosphorylase. *J Mol Biol* 234 (3):700-721.

Huh, S. W., S. M. Bae, Y. W. Kim, J. M. Lee, S. E. Namkoong, I. P. Lee, S. H. Kim, C. K. Kim, and W. S. Ahn. 2004. Anticancer effects of (-)-epigallocatechin-3-gallate on ovarian carcinoma cell lines. *Gynecol Oncol* 94 (3):760-768.

Hurlstone, A., and H. Clevers. 2002. T-cell factors: turn-ons and turn-offs. *Embo J* 21 (10):2303-2311.

Hwang, J. T., J. Ha, I. J. Park, S. K. Lee, H. W. Baik, Y. M. Kim, and O. J. Park. 2007. Apoptotic effect of EGCG in HT-29 colon cancer cells via AMPK signal pathway. *Cancer Lett* 247 (1):115-121.

Hwang, J. T., I. J. Park, J. I. Shin, Y. K. Lee, S. K. Lee, H. W. Baik, J. Ha, and O. J. Park. 2005. Genistein, EGCG, and capsaicin inhibit adipocyte differentiation process via activating AMP-activated protein kinase. *Biochem Biophys Res Commun* 338 (2):694-699.

Ilyas, M., I. P. Tomlinson, A. Rowan, M. Pignatelli, and W. F. Bodmer. 1997. Beta-catenin mutations in cell lines established from human colorectal cancers. *Proc Natl Acad Sci U S A* 94 (19):10330-10334.

Ioku, K., Y. Pongpiriyadacha, Y. Konishi, Y. Takei, N. Nakatani, and J. Terao. 1998. beta-Glucosidase activity in the rat small intestine toward quercetin monoglucosides. *Biosci Biotechnol Biochem* 62 (7):1428-1431.

Ishitani, T., Ninomiya-Tsuji, J., Nagai, S., Nishita, M., Meneghini, M., Barkers, N., Waterman, M., Bowerman, B., Clevers, H., Shibuya, H. and Matsumoto, K. . 1999. The TAK1-NLK-MAPK-related pathway antagonize signalling between ß-catenin and transcription factor TCF. *Nature* 399:798-802.

Ito, T., S. P. Warnken, and W. S. May. 1999. Protein synthesis inhibition by flavonoids: roles of eukaryotic initiation factor 2alpha kinases. *Biochem Biophys Res Commun* 265 (2):589-594.

Jakobs, S., D. Fridrich, S. Hofem, G. Pahlke, and G. Eisenbrand. 2006. Natural flavonoids are potent inhibitors of glycogen phosphorylase. *Mol Nutr Food Res* 50 (1):52-57.

Janssens, N., M. Janicot, and T. Perera. 2006. The Wnt-dependent signalling pathways as target in oncology drug discovery. *Invest New Drugs* 24 (4):263-280.

Jensen, J., E. O. Brennesvik, Y. C. Lai, and P. R. Shepherd. 2007. GSK-3beta regulation in skeletal muscles by adrenaline and insulin: evidence that PKA and PKB regulate different pools of GSK-3. *Cell Signal* 19 (1):204-210.

Johnson, I. T. 2004. New approaches to the role of diet in the prevention of cancers of the alimentary tract. *Mutat Res* 551 (1-2):9-28.

Jope, R. S. 1999. Anti-bipolar therapy: mechanism of action of lithium. *Mol Psychiatry* 4 (2):117-128.

Jope, R. S., and G. V. Johnson. 2004. The glamour and gloom of glycogen synthase kinase-3. *Trends Biochem Sci* 29 (2):95-102.

Jope, R. S., and M. S. Roh. 2006. Glycogen synthase kinase-3 (GSK-3) in psychiatric diseases and therapeutic interventions. *Curr Drug Targets* 7 (11):1421-1434.

Joseph, J. A., B. Shukitt-Hale, and F. C. Lau. 2007. Fruit polyphenols and their effects on neuronal signalling and behavior in senescence. *Ann N Y Acad Sci* 1100:470-485.

Ju, J., J. Hong, J. N. Zhou, Z. Pan, M. Bose, J. Liao, G. Y. Yang, Y. Y. Liu, Z. Hou, Y. Lin, J. Ma, W. J. Shih, A. M. Carothers, and C. S. Yang. 2005. Inhibition of intestinal tumorigenesis in Apcmin/+ mice by (-)-epigallocatechin-3-gallate, the major catechin in green tea. *Cancer Res* 65 (22):10623-10631.

Justino, G. C., C. F. Correia, L. Mira, R. M. Borges Dos Santos, J. A. Martinho Simoes, A. M. Silva, C. Santos, and B. Gigante. 2006. Antioxidant activity of a catechol derived from abietic acid. *J Agric Food Chem* 54 (2):342-348.

Kaiser, A., K. Nishi, F. A. Gorin, D. A. Walsh, E. M. Bradbury, and J. B. Schnier. 2001. The cyclin-dependent kinase (CDK) inhibitor flavopiridol inhibits glycogen phosphorylase. *Arch Biochem Biophys* 386 (2):179-187.

Kawano, Y., and R. Kypta. 2003. Secreted antagonists of the Wnt signalling pathway. *J Cell Sci* 116 (Pt 13):2627-2634.

Kazerouni, N., R. Sinha, C. H. Hsu, A. Greenberg, and N. Rothman. 2001. Analysis of 200 food items for benzo[a]pyrene and estimation of its intake in an epidemiologic study. *Food Chem Toxicol* 39 (5):423-436.

Kemler, R. 1993. From cadherins to catenins: cytoplasmic protein interactions and regulation of cell adhesion. *Trends Genet* 9 (9):317-321.

Kern, M., G. Pahlke, Y. Ngiewih, and D. Marko. 2006. Modulation of key elements of the Wnt pathway by apple polyphenols. *J Agric Food Chem* 54 (19):7041-7046.

Kern, M., Z. Tjaden, Y. Ngiewih, N. Puppel, F. Will, H. Dietrich, G. Pahlke, and D. Marko. 2005. Inhibitors of the epidermal growth factor receptor in apple juice extract. *Mol Nutr Food Res* 49 (4):317-328.

Kim, H. S., E. K. Hong, S. Y. Park, W. H. Kim, and H. S. Lee. 2003a. Expression of beta-catenin and E-cadherin in the adenoma-carcinoma sequence of the stomach. *Anticancer Res* 23 (3C):2863-2868.

Kim, I. J., H. C. Kang, J. H. Park, Y. Shin, J. L. Ku, S. B. Lim, S. Y. Park, S. Y. Jung, H. K. Kim, and J. G. Park. 2003b. Development and applications of a beta-catenin oligonucleotide microarray: beta-catenin mutations are dominantly found in the proximal colon cancers with microsatellite instability. *Clin Cancer Res* 9 (8):2920-2925.

Kitson, T. M. 2004. Spectrophotometric and kinetic studies on the binding of the bioflavonoid quercetin to bovine serum albumin. *Biosci Biotechnol Biochem* 68 (10):2165-2170.

Knudsen, K. A., A. P. Soler, K. R. Johnson, and M. J. Wheelock. 1995. Interaction of alpha-actinin with the cadherin/catenin cell-cell adhesion complex via alpha-catenin. *J Cell Biol* 130 (1):67-77.

Koyama, Y., K. Abe, Y. Sano, Y. Ishizaki, M. Njelekela, Y. Shoji, Y. Hara, and M. Isemura. 2004. Effects of green tea on gene expression of hepatic gluconeogenic enzymes in vivo. *Planta Med* 70 (11):1100-1102.

Kozlovsky, N., R. H. Belmaker, and G. Agam. 2002. GSK-3 and the neurodevelopmental hypothesis of schizophrenia. *Eur Neuropsychopharmacol* 12 (1):13-25.

Kuhl. 2002. Non canonical Wnt signalling in Xenopus: regulation of axis formation and gastrulation *Semin Cell Dev Biol* 13:324-249.

Kuhl, M., L. C. Sheldahl, M. Park, J. R. Miller, and R. T. Moon. 2000. The Wnt/Ca2+ pathway: a new vertebrate Wnt signalling pathway takes shape. *Trends Genet* 16 (7):279-283.

Kuhnau, J. 1976. The flavonoids. A class of semi-essential food components: their role in human nutrition. *World Rev Nutr Diet* 24:117-191.

Kumar, N., D. Shibata, J. Helm, D. Coppola, and M. Malafa. 2007. Green tea polyphenols in the prevention of colon cancer. *Front Biosci* 12:2309-2315.

Lambert, J. D., M. J. Lee, L. Diamond, J. Ju, J. Hong, M. Bose, H. L. Newmark, and C. S. Yang. 2006. Dose-dependent levels of epigallocatechin-3-gallate in human colon cancer cells and mouse plasma and tissues. *Drug Metab Dispos* 34 (1):8-11.

Laurent, D., R. S. Hundal, A. Dresner, T. B. Price, S. M. Vogel, K. F. Petersen, and G. I. Shulman. 2000. Mechanism of muscle glycogen autoregulation in humans. *Am J Physiol Endocrinol Metab* 278 (4):E663-668.

Layzer, R. B., L. P. Rowland, and H. M. Ranney. 1967. Muscle phosphofructokinase deficiency. *Arch Neurol* 17 (5):512-523.

Lee, J., and M. S. Kim. 2007. The role of GSK-3 in glucose homeostasis and the development of insulin resistance. *Diabetes Res Clin Pract*.

Lerin, C., E. Montell, T. Nolasco, M. Garcia-Rocha, J. J. Guinovart, and A. M. Gomez-Foix. 2004. Regulation of glycogen metabolism in cultured human muscles by the glycogen phosphorylase inhibitor CP-91149. *Biochem J* 378 (Pt 3):1073-1077.

Leth, T., Justesen, U. . 1998 Analysis of flavonoids in fruits, vegetables and beverages by HPCL-UV and LC-MS and estimation of the total daily flavonoid intake in Denmark. . *In Polyphenols in Food, ed. R Amado, H Andersson, S Bardocz, F Serra, Luxembourg: Off. Official Publications Eur. Commun.*: 39–40.

Li, X., K. M. Rosborough, A. B. Friedman, W. Zhu, and K. A. Roth. 2007. Regulation of mouse brain glycogen synthase kinase-3 by atypical antipsychotics. *Int J Neuropsychopharmacol* 10 (1):7-19.

Li, Z. G., Y. Shimada, F. Sato, M. Maeda, A. Itami, J. Kaganoi, I. Komoto, A. Kawabe, and M. Imamura. 2002. Inhibitory effects of epigallocatechin-3-gallate on N-nitrosomethylbenzylamine-induced esophageal tumorigenesis in F344 rats. *Int J Oncol* 21 (6):1275-1283.

Lindl, J. B. a. T. 1987. Zell- und Gewebekultur; Einführung in die Grundlagen sowie ausgewählte Methoden und Anwendungen. : Gustav Fischer Verlag Stuttgart New York.

Liu, F., Z. Liang, J. Shi, D. Yin, E. El-Akkad, I. Grundke-Iqbal, K. Iqbal, and C. X. Gong. 2006. PKA modulates GSK-3beta- and cdk5-catalyzed phosphorylation of tau in site- and kinase-specific manners. *FEBS Lett* 580 (26):6269-6274.

Liu, S. J., A. H. Zhang, H. L. Li, Q. Wang, H. M. Deng, W. J. Netzer, H. Xu, and J. Z. Wang. 2003. Overactivation of glycogen synthase kinase-3 by inhibition of phosphoinositol-3 kinase and protein kinase C leads to hyperphosphorylation of tau and impairment of spatial memory. *J Neurochem* 87 (6):1333-1344.

Liu, W., X. Dong, M. Mai, R. S. Seelan, K. Taniguchi, K. K. Krishnadath, K. C. Halling, J. M. Cunningham, L. A. Boardman, C. Qian, E. Christensen, S. S. Schmidt, P. C. Roche, D. I. Smith, and S. N. Thibodeau. 2000. Mutations in AXIN2 cause colorectal cancer with defective mismatch repair by activating beta-catenin/TCF signalling. *Nat Genet* 26 (2):146-147.

Longo, M. C., M. S. Berninger, and J. L. Hartley. 1990. Use of uracil DNA glycosylase to control carry-over contamination in polymerase chain reactions. *Gene* 93 (1):125-128.

Lorenz, M., S. Wessler, E. Follmann, W. Michaelis, T. Dusterhoft, G. Baumann, K. Stangl, and V. Stangl. 2004. A constituent of green tea, epigallocatechin-3-gallate, activates endothelial nitric oxide synthase by a phosphatidylinositol-3-OH-kinase-, cAMP-dependent protein kinase-, and Akt-dependent pathway and leads to endothelial-dependent vasorelaxation. *J Biol Chem* 279 (7):6190-6195.

Lund, E. K., S. J. Fairweather-Tait, S. G. Wharf, and I. T. Johnson. 2001. Chronic exposure to high levels of dietary iron fortification increases lipid peroxidation in the mucosa of the rat large intestine. *J Nutr* 131 (11):2928-2931.

Lund, E. K., S. G. Wharf, S. J. Fairweather-Tait, and I. T. Johnson. 1999. Oral ferrous sulfate supplements increase the free radical-generating capacity of feces from healthy volunteers. *Am J Clin Nutr* 69 (2):250-255.

Ma, Y., Q. Feng, D. Sekula, J. A. Diehl, S. J. Freemantle, and E. Dmitrovsky. 2005. Retinoid targeting of different D-type cyclins through distinct chemopreventive mechanisms. *Cancer Res* 65 (14):6476-6483.

Malbon, C. C. 2005. Beta-catenin, cancer, and G proteins: not just for frizzleds anymore. *Sci STKE* 2005 (292):pe35.

Manoukian, A. S., and J. R. Woodgett. 2002. Role of glycogen synthase kinase-3 in cancer: regulation by Wnts and other signalling pathways. *Adv Cancer Res* 84:203-229.

Marko, D., N. Puppel, Z. Tjaden, S. Jakobs, and G. Pahlke. 2004. The substitution pattern of anthocyanidins affects different cellular signalling cascades regulating cell proliferation. *Mol Nutr Food Res* 48 (4):318-325.

Maruyama, K. O. A., Akimoto S, et al. . 2000. Cytoplasmic beta catenin accumulation as a predictor of hematogenous metastasis in human colorectal cancer. *Oncology* 59 (4):302–309.

Matsuzawa, S. I., and J. C. Reed. 2001. Siah-1, SIP, and Ebi collaborate in a novel pathway for beta-catenin degradation linked to p53 responses. *Mol Cell* 7 (5):915-926.

Meijer, L., M. Flajolet, and P. Greengard. 2004. Pharmacological inhibitors of glycogen synthase kinase 3. *Trends Pharmacol Sci* 25 (9):471-480.

Merrill, B. J., U. Gat, R. DasGupta, and E. Fuchs. 2001. Tcf3 and Lef1 regulate lineage differentiation of multipotent stem cells in skin. *Genes Dev* 15 (13):1688-1705.

Middleton, E., Jr., C. Kandaswami, and T. C. Theoharides. 2000. The effects of plant flavonoids on mammalian cells: implications for inflammation, heart disease, and cancer. *Pharmacol Rev* 52 (4):673-751.

Mojarrabi, B. M., P. I. 1998. Characterization of two UDP glucuronosyltransferases that are predominantly expressed in human colon. *Biochem. Biophys. Res. Commun. 247: 704–709.* 247:704–709.

Molenaar, M., van de Wetering, M., Oosterwegel, M., Peterson-Maduro, J., Godsave, S., Korinek, V., Roose, J., Destree, O., Clevers, H. 1996 XTCF-3 transcription factor mediates b-catenin-induced axis formation in Xenopus embryos. . *Cell* 86:391–399.

Moon, H. S., H. G. Lee, Y. J. Choi, T. G. Kim, and C. S. Cho. 2007. Proposed mechanisms of (-)-epigallocatechin-3-gallate for anti-obesity. *Chem Biol Interact* 167 (2):85-98.

Nagengast, F. M., M. J. Grubben, and I. P. van Munster. 1995. Role of bile acids in colorectal carcinogenesis. *Eur J Cancer* 31A (7-8):1067-1070.

Newgard, C. B., P. K. Hwang, and R. J. Fletterick. 1989. The family of glycogen phosphorylases: structure and function. *Crit Rev Biochem Mol Biol* 24 (1):69-99.

Noble, M. E., J. A. Endicott, and L. N. Johnson. 2004. Protein kinase inhibitors: insights into drug design from structure. *Science* 303 (5665):1800-1805.

Nuttall, F. Q., M. C. Gannon, G. Bai, and E. Y. Lee. 1994. Primary structure of human liver glycogen synthase deduced by cDNA cloning. *Arch Biochem Biophys* 311 (2):443-449.

O'Brien, R. M., and D. K. Granner. 1996. Regulation of gene expression by insulin. *Physiol Rev* 76 (4):1109-1161.

Oosterwegel, M., M. van de Wetering, J. Timmerman, A. Kruisbeek, O. Destree, F. Meijlink, and H. Clevers. 1993. Differential expression of the HMG box factors TCF-1 and LEF-1 during murine embryogenesis. *Development* 118 (2):439-448.

Orner, G. A., W. M. Dashwood, C. A. Blum, G. D. Diaz, Q. Li, M. Al-Fageeh, N. Tebbutt, J. K. Heath, M. Ernst, and R. H. Dashwood. 2002. Response of Apc(min) and A33 (delta N beta-cat) mutant mice to treatment with tea, sulindac, and 2-amino-1-methyl-6-phenylimidazo[4,5-b]pyridine (PhIP). *Mutat Res* 506-507:121-127.

Orner, G. A., W. M. Dashwood, C. A. Blum, G. D. Diaz, Q. Li, and R. H. Dashwood. 2003. Suppression of tumorigenesis in the Apc(min) mouse: down-regulation of beta-catenin signalling by a combination of tea plus sulindac. *Carcinogenesis* 24 (2):263-267.

Pahlke, G., Y. Ngiewih, M. Kern, S. Jakobs, D. Marko, and G. Eisenbrand. 2006. Impact of quercetin and EGCG on key elements of the Wnt pathway in human colon carcinoma cells. *J Agric Food Chem* 54 (19):7075-7082.

Park, C. H., J. Y. Chang, E. R. Hahm, S. Park, H. K. Kim, and C. H. Yang. 2005. Quercetin, a potent inhibitor against beta-catenin/Tcf signalling in SW480 colon cancer cells. *Biochem Biophys Res Commun* 328 (1):227-234.

Parker, P. J., F. B. Caudwell, and P. Cohen. 1983. Glycogen synthase from rabbit skeletal muscle; effect of insulin on the state of phosphorylation of the seven phosphoserine residues in vivo. *Eur J Biochem* 130 (1):227-234.

Parkin, D. M., F. Bray, J. Ferlay, and P. Pisani. 2005. Global cancer statistics, 2002. *CA Cancer J Clin* 55 (2):74-108.

Patel, S., B. Doble, and J. R. Woodgett. 2004. Glycogen synthase kinase-3 in insulin and Wnt signalling: a double-edged sword? *Biochem Soc Trans* 32 (Pt 5):803-808.

Peifer, M., S. Berg, and A. B. Reynolds. 1994. A repeating amino acid motif shared by proteins with diverse cellular roles. *Cell* 76 (5):789-791.

Petersen, K. F., G. W. Cline, D. P. Gerard, I. Magnusson, D. L. Rothman, and G. I. Shulman. 2001. Contribution of net hepatic glycogen synthesis to disposal of an oral glucose load in humans. *Metabolism* 50 (5):598-601.

Pfluger. 1905. "Das Glykogen"

Pingoud, A., Urbanke, C., Hoggett, J., Jeltsch A. 2002. *Biochemical Methods: A Concise Guide for Students and Researchers*.

Pinson, K. I., J. Brennan, S. Monkley, B. J. Avery, and W. C. Skarnes. 2000. An LDL-receptor-related protein mediates Wnt signalling in mice. *Nature* 407 (6803):535-538.

Pinto, D., and H. Clevers. 2005. Wnt, stem cells and cancer in the intestine. *Biol Cell* 97 (3):185-196.

Piras, R., L. B. Rothman, and E. Cabib. 1968. Regulation of muscle glycogen synthetase by metabolites. Differential effects on the I and D forms. *Biochemistry* 7 (1):56-66.

Piras, R., and R. Staneloni. 1969. In vivo regulation of rat muscle glycogen synthetase activity. *Biochemistry* 8 (5):2153-2160.

Porfiri, E., B. Rubinfeld, I. Albert, K. Hovanes, M. Waterman, and P. Polakis. 1997. Induction of a beta-catenin-LEF-1 complex by wnt-1 and transforming mutants of beta-catenin. *Oncogene* 15 (23):2833-2839.

Porter, E. M., Bevins, C.L., Ghosh, D. and Ganz, T. . 2002. The multifaceted Paneth cell. . *Cell Mol. Life Sci.* 59 156–170.

Potten, C. S., and M. Loeffler. 1990. Stem cells: attributes, cycles, spirals, pitfalls and uncertainties. Lessons for and from the crypt. *Development* 110 (4):1001-1020.

Poulter, L., S. G. Ang, B. W. Gibson, D. H. Williams, C. F. Holmes, F. B. Caudwell, J. Pitcher, and P. Cohen. 1988. Analysis of the in vivo phosphorylation state of rabbit skeletal muscle glycogen synthase by fast-atom-bombardment mass spectrometry. *Eur J Biochem* 175 (3):497-510.

Promega-(7/01). pRL-TK-Vektor. Technical Bulletin No. 240

Qiagen. 09/2000. Plasmid purification handbook.

R. Städeli, R. H. a. K. B. 2006. Transcription under the Control of Nuclear Arm/beta-Catenin. *Current Biology 1* 6:R378–R385.

Ragolia, L., and N. Begum. 1998. Protein phosphatase-1 and insulin action. *Mol Cell Biochem* 182 (1-2):49-58.

Rao, A. S., N. Kremenevskaja, J. Resch, and G. Brabant. 2005. Lithium stimulates proliferation in cultured thyrocytes by activating Wnt/beta-catenin signalling. *Eur J Endocrinol* 153 (6):929-938.

Reya, T., and H. Clevers. 2005. Wnt signalling in stem cells and cancer. *Nature* 434 (7035):843-850.

Reya, T., M. O'Riordan, R. Okamura, E. Devaney, K. Willert, R. Nusse, and R. Grosschedl. 2000. Wnt signalling regulates B lymphocyte proliferation through a LEF-1 dependent mechanism. *Immunity* 13 (1):15-24.

Rice-Evans, C. 1995. Plant polyphenols: free radical scavengers or chain-breaking antioxidants? *Biochem Soc Symp* 61:103-116.

Rice-Evans, C. A., and N. J. Miller. 1996. Antioxidant activities of flavonoids as bioactive components of food. *Biochem Soc Trans* 24 (3):790-795.

Roach, P. J. 1990. Control of glycogen synthase by hierarchal protein phosphorylation. *Faseb J* 4 (12):2961-2968.

———. 2002. Glycogen and its metabolism. *Curr Mol Med* 2 (2):101-120.

Roach, P. J., A. A. DePaoli-Roach, and J. Larner. 1978. Ca2+-stimulated phosphorylation of muscle glycogen synthase by phosphorylase b kinase. *J Cyclic Nucleotide Res* 4 (4):245-257.

Rochat, A., A. Fernandez, M. Vandromme, J. P. Moles, T. Bouschet, G. Carnac, and N. J. Lamb. 2004. Insulin and wnt1 pathways cooperate to induce reserve cell activation in differentiation and myotube hypertrophy. *Mol Biol Cell* 15 (10):4544-4555.

Roose J, H. G., van Beest M, Moerer P, van der Horn K, Goldschmeding R, Logtenberg T, Clevers H. 1999 Synergy between tumor suppressor APC and the beta-catenin-Tcf4 target Tcf1. *Science* 285:1923–1926.

Ross, J. A., and C. M. Kasum. 2002. Dietary flavonoids: bioavailability, metabolic effects, and safety. *Annu Rev Nutr* 22:19-34.

Ross, S. A., D. S. Ziska, K. Zhao, and M. A. ElSohly. 2000. Variance of common flavonoids by brand of grapefruit juice. *Fitoterapia* 71 (2):154-161.

Scalbert, A., and G. Williamson. 2000. Dietary intake and bioavailability of polyphenols. *J Nutr* 130 (8S Suppl):2073S-2085S.

Schaefer, S., M. Baum, G. Eisenbrand, H. Dietrich, F. Will, and C. Janzowski. 2006. Polyphenolic apple juice extracts and their major constituents reduce oxidative damage in human colon cell lines. *Mol Nutr Food Res* 50 (1):24-33.

Scheepers, A., H. G. Joost, and A. Schurmann. 2004. The glucose transporter families SGLT and GLUT: molecular basis of normal and aberrant function. *JPEN J Parenter Enteral Nutr* 28 (5):364-371.

Schreiner, V. 2004. Diplom Arbeit;.

Shen, S. C., Y. C. Chen, F. L. Hsu, and W. R. Lee. 2003. Differential apoptosis-inducing effect of quercetin and its glycosides in human promyeloleukemic HL-60 cells by alternative activation of the caspase 3 cascade. *J Cell Biochem* 89 (5):1044-1055.

Shimada, S., H. Matsuzaki, T. Marutsuka, K. Shiomori, and M. Ogawa. 2001. Gastric and intestinal phenotypes of gastric carcinoma with reference to expression of brain (fetal)-type glycogen phosphorylase. *J Gastroenterol* 36 (7):457-464.

Shimada, S., K. Shiomori, U. Honmyo, M. Maeno, Y. Yagi, and M. Ogawa. 2002. BGP expression in gastric biopsies may predict the development of new lesions after local treatment for early gastric cancer. *Gastric Cancer* 5 (3):130-136.

Shimada, S., S. Tashima, K. Yamaguchi, H. Matsuzaki, and M. Ogawa. 1999. Carcinogenesis of intestinal-type gastric cancer and colorectal cancer is commonly accompanied by expression of brain (fetal)-type glycogen phosphorylase. *J Exp Clin Cancer Res* 18 (1):111-118.

Shin, S. Y., B. R. Chin, Y. H. Lee, and J. H. Kim. 2006. Involvement of glycogen synthase kinase-3beta in hydrogen peroxide-induced suppression of Tcf/Lef-dependent transcriptional activity. *Cell Signal* 18 (5):601-607.

Skurat, A. V., A. D. Dietrich, and P. J. Roach. 2000. Glycogen synthase sensitivity to insulin and glucose-6-phosphate is mediated by both NH2- and COOH-terminal phosphorylation sites. *Diabetes* 49 (7):1096-1100.

Skurat, A. V., and P. J. Roach. 1996. Multiple mechanisms for the phosphorylation of C-terminal regulatory sites in rabbit muscle glycogen synthase expressed in COS cells. *Biochem J* 313 (Pt 1):45-50.

Smith, K. J., K. A. Johnson, T. M. Bryan, D. E. Hill, S. Markowitz, J. K. Willson, C. Paraskeva, G. M. Petersen, S. R. Hamilton, B. Vogelstein, and et al. 1993. The APC gene product in normal and tumor cells. *Proc Natl Acad Sci U S A* 90 (7):2846-2850.

Soyalan, B. 2005. Einfluss von Flavonoiden auf die Glykogenphosphorylase und Glykogensynthase transkription in humanen Tumorzelllinien, Food chemistry and Enviromental Toxicology, Universtity of Kaiserslautern, Kaiserslautern.

Stalmans, W. 1976. The role of the liver in the homeostasis of blood glucose. *Curr Top Cell Regul* 11:51-97.

Strassburg, C. P., Nguyen, N., Manns, M. P. & Tukey, R. H. (1999) 1999. UDPglucuronosyltransferase activity in human liver and colon. *Gastroenterology* 116:149–160.

Strassburg, C. P. N., N. Manns, M. P. Tukey, R. H. 1998. Polymorphic expression of the UDP-glucuronosyltransferase UGT1A gene locus in human gastric epithelium. *Mol Pharmacol* 54 (4):647-654.

Takizawa, Y., T. Morota, S. Takeda, and M. Aburada. 2003. Pharmacokinetics of (-)-epicatechin-3-O-gallate, an active component of Onpi-to, in rats. *Biol Pharm Bull* 26 (5):608-612.

Tamai, K., M. Semenov, Y. Kato, R. Spokony, C. Liu, Y. Katsuyama, F. Hess, J. P. Saint-Jeannet, and X. He. 2000. LDL-receptor-related proteins in Wnt signal transduction. *Nature* 407 (6803):530-535.

Tashima, S., S. Shimada, K. Yamaguchi, J. Tsuruta, and M. Ogawa. 2000. Expression of brain-type glycogen phosphorylase is a potentially novel early biomarker in the carcinogenesis of human colorectal carcinomas. *Am J Gastroenterol* 95 (1):255-263.

Thangapazham, R. L., A. K. Singh, A. Sharma, J. Warren, J. P. Gaddipati, and R. K. Maheshwari. 2007. Green tea polyphenols and its constituent epigallocatechin gallate inhibits proliferation of human breast cancer cells in vitro and in vivo. *Cancer Lett* 245 (1-2):232-241.

Thiel, A., M. Heinonen, J. Rintahaka, T. Hallikainen, A. Hemmes, D. A. Dixon, C. Haglund, and A. Ristimaki. 2006. Expression of cyclooxygenase-2 is regulated by glycogen synthase kinase-3beta in gastric cancer cells. *J Biol Chem* 281 (8):4564-4569.

Thomas, J. A., K. K. Schlender, and J. Larner. 1968. A rapid filter paper assay for UDPglucose-glycogen glucosyltransferase, including an improved biosynthesis of UDP-14C-glucose. *Anal Biochem* 25 (1):486-499.

Tiihonen, J., T. Hallikainen, H. Lachman, T. Saito, J. Volavka, J. Kauhanen, J. T. Salonen, O. P. Ryynanen, M. Koulu, M. K. Karvonen, T. Pohjalainen, E. Syvalahti, and J. Hietala. 1999. Association between the functional variant of the catechol-O-methyltransferase (COMT) gene and type 1 alcoholism. *Mol Psychiatry* 4 (3):286-289.

Torres, M., Yang-Snyder, J. Purcell, SM., Demarais, AA., McGrew, LL., Moon, RT., . 1996. Activities of the wnt-1 class of secreted factors are antagonized by the Wnt-5A class and by a dominant negative cadherin in ealry Xenopus embryo. *J Cell Biol* 133 1123–1137

Vaidyanathan, J. B., and T. Walle. 2003. Cellular uptake and efflux of the tea flavonoid (-)epicatechin-3-gallate in the human intestinal cell line Caco-2. *J Pharmacol Exp Ther* 307 (2):745-752.

van de Werve, G., and B. Jeanrenaud. 1987. Liver glycogen metabolism: an overview. *Diabetes Metab Rev* 3 (1):47-78.

van de Wetering, M. C., J. Korinek, K. Clevers, H 1996. Extensive alternative splicing and dual promoter usage generate Tcf-protein isoforms with differential transcription control properties. . *Mol Cell Biol* 16 745–752.

van der Woude, H., A. Gliszczynska-Swiglo, K. Struijs, A. Smeets, G. M. Alink, and I. M. Rietjens. 2003. Biphasic modulation of cell proliferation by quercetin at concentrations physiologically relevant in humans. *Cancer Lett* 200 (1):41-47.

van der Woude, H., M. G. Ter Veld, N. Jacobs, P. T. van der Saag, A. J. Murk, and I. M. Rietjens. 2005. The stimulation of cell proliferation by quercetin is mediated by the estrogen receptor. *Mol Nutr Food Res* 49 (8):763-771.

van Noort, M., and H. Clevers. 2002. TCF transcription factors, mediators of Wnt-signalling in development and cancer. *Dev Biol* 244 (1):1-8.

Vanhaesebroeck, B., and D. R. Alessi. 2000. The PI3K-PDK1 connection: more than just a road to PKB. *Biochem J* 346 Pt 3:561-576.

Veeriah, S., T. Kautenburger, N. Habermann, J. Sauer, H. Dietrich, F. Will, and B. L. Pool-Zobel. 2006. Apple flavonoids inhibit growth of HT29 human colon cancer cells and modulate expression of genes involved in the biotransformation of xenobiotics. *Mol Carcinog* 45 (3):164-174.

Vogelstein, B., and K. W. Kinzler. 1993. The multistep nature of cancer. *Trends Genet* 9 (4):138-141.

Walgren, R. A., J. T. Lin, R. K. Kinne, and T. Walle. 2000. Cellular uptake of dietary flavonoid quercetin 4'-beta-glucoside by sodium-dependent glucose transporter SGLT1. *J Pharmacol Exp Ther* 294 (3):837-843.

Walle, T. A., T. Browning, A. Reed, S. Walle, U. K. . 2003. Effect of dietary flavonoids on oral cancer cell proliferation: bioactivation by saliva and antiproliferative mechanisms. *Second Annual AACR International Conference Frontiers in Cancer Prevention Research, Phoenix, AZ*.

Waltner-Law, M. E., X. L. Wang, B. K. Law, R. K. Hall, M. Nawano, and D. K. Granner. 2002. Epigallocatechin gallate, a constituent of green tea, represses hepatic glucose production. *J Biol Chem* 277 (38):34933-34940.

Waltzer, L., and M. Bienz. 1999. The control of beta-catenin and TCF during embryonic development and cancer. *Cancer Metastasis Rev* 18 (2):231-246.

Wang, Q., Y. Zhou, and B. M. Evers. 2006. Neurotensin phosphorylates GSK-3alpha/beta through the activation of PKC in human colon cancer cells. *Neoplasia* 8 (9):781-787.

Wang, Y., and P. J. Roach. 1993. Inactivation of rabbit muscle glycogen synthase by glycogen synthase kinase-3. Dominant role of the phosphorylation of Ser-640 (site-3a). *J Biol Chem* 268 (32):23876-23880.

Waterman, M. L. 2004. Lymphoid enhancer factor/T cell factor expression in colorectal cancer. *Cancer Metastasis Rev* 23 (1-2):41-52.

Wolffram, S., M. Block, and P. Ader. 2002. Quercetin-3-glucoside is transported by the glucose carrier SGLT1 across the brush border membrane of rat small intestine. *J Nutr* 132 (4):630-635.

Wolfram, S., D. Raederstorff, M. Preller, Y. Wang, S. R. Teixeira, C. Riegger, and P. Weber. 2006. Epigallocatechin gallate supplementation alleviates diabetes in rodents. *J Nutr* 136 (10):2512-2518.

Woodgett, J. R. 1990. Molecular cloning and expression of glycogen synthase kinase-3/factor A. *Embo J* 9 (8):2431-2438.

———. 1991. A common denominator linking glycogen metabolism, nuclear oncogenes and development. *Trends Biochem Sci* 16 (5):177-181.

Woodgett, J. R., and P. Cohen. 1984. Multisite phosphorylation of glycogen synthase. Molecular basis for the substrate specificity of glycogen synthase kinase-3 and casein kinase-II (glycogen synthase kinase-5). *Biochim Biophys Acta* 788 (3):339-347.

Wright, N. A., and M. Irwin. 1982. The kinetics of villus cell populations in the mouse small intestine. I. Normal villi: the steady state requirement. *Cell Tissue Kinet* 15 (6):595-609.

Xiao, J. H., C. Ghosn, C. Hinchman, C. Forbes, J. Wang, N. Snider, A. Cordrey, Y. Zhao, and R. A. Chandraratna. 2003. Adenomatous polyposis coli (APC)-independent regulation of beta-catenin degradation via a retinoid X receptor-mediated pathway. *J Biol Chem* 278 (32):29954-29962.

Yang, C. S., J. D. Lambert, J. Ju, G. Lu, and S. Sang. 2006. Tea and cancer prevention: Molecular mechanisms and human relevance. *Toxicol Appl Pharmacol*.

Zhou, P., C. Byrne, J. Jacobs, and E. Fuchs. 1995. Lymphoid enhancer factor 1 directs hair follicle patterning and epithelial cell fate. *Genes Dev* 9 (6):700-713.

Ziemienowicz. 2001. Plant selectable markers and reporter genes. *Acta. Physiol. Plant.* 23 (3):363-374.

8 Addendum

8.1 List of Publications

2004

The 12th international conference on polyphenols. 25.08 – 28.08.2004, Helsinki (Finnland)

Melanie Kern, Zeina Tjaden, **Yufanyi Ngiewih**, Nicole Puppel, Frank Will, Helmut Dietrich, Gudrun Pahlke and Doris Marko: Apple polyphenols as inhibitors of the epidermal growth factor receptor (EGFR)

"GDCH-Jahrestagung Chemie 2004", Bonn, 33 deutscher Lebensmittelchemikertag 13.9 - 5.09.2004

Melanie Kern, Zeina Tjaden, **Yufanyi Ngiewih**, Nicole Puppel, Frank Will, Helmut Dietrich, Gudrun Pahlke and Doris Marko: Hemmstoffe des epidermale Wachstumsfaktorrezeptors in Apfelsaftextrakt.

2005

EURO FOOD CHEM XIII. Hamburg 19.05 – 23.05.2005,

Yufanyi Ngiewih, Melanie Kern, Victoria Schreiner, Sandra Jakobs, Gudrun Pahlke, Doris Marko and Gerhard Eisenbrand: Quercetin as a modulator of the Wnt-signalling in human colon.

Yufanyi Ngiewih, Melanie Kern, Victoria Schreiner, Sandra Jakobs, Gudrun Pahlke, Doris Marko and Gerhard Eisenbrand: Quercetin as a modulator of the Wnt-signalling in human colon. *EURO FOOD CHEM* XIII 2005, 2, 525-528.

Melanie Kern, Zeina Tjaden, **Yufanyi Ngiewih**, Nicole Puppel, Frank Will, Helmut Dietrich, Gudrun Pahlke and Doris Marko. Inhibitors of the epidermal growth factor receptor in apple juice extract. *Molecular Nutrition and Food Research* 2005, 49, 317-328.

2006

"Lebensmittelchemiker Regionaltagung Südwest", Karlsruhe, 6-7 März 2006

Yufanyi Ngiewih, Melanie Kern, Gudrun Pahlke, Sandra Jakobs, Doris Marko and Gerhard Eisenbrand. Effects of natural flavonoids and apple constituents on key elements of the Wnt pathway.

Gudrun Pahlke, **Yufanyi Ngiewih**, Melanie Kern, Sandra Jakobs, Doris Marko and Gerhard Eisenbrand: Impact of Quercetin and EGCG on key elements of the Wnt pathway in human colon carcinoma. *Journal of Agricultural and food chemistry* 2006, Vol. 54, No. 19, 7075 – 7082.

Melanie Kern, Gudrun Pahlke, **Yufanyi Ngiewih**, and Doris Marko: Modulation of key elements of the Wnt pathway by apple polyphenols. *Journal of Agricultural and food chemistry* 2006, Vol. 54, No. 19, 7041 – 7046.

2007

International Symposium on Nutrition and Intestinal Health 2007 (NutIntest2007), 28.02 – 01.03.2007

Yufanyi Ngiewih, Gudrun Pahlke, Melanie Kern, Sandra Jakobs, Gerhard Eisenbrand and Doris Marko: Impact of Quercetin, EGCG and apple polyphenols on key elements of the Wnt Pathway in Human Colon Carcinoma Cells.

8.2 Optimization of the dual luciferase reporter gene assay in HEK293 cells (24 well plate format)

Data to figure 23: Transient transfection of HEK293 cells with TOP*flash* and FOP*flash*

TOPflash/pRL-TK	50/5	100/10	200/20	300/30	400/40	500/50
3105-03.06.05	1.28	1.25	2.43	4.17	4.68	6.95
08.06-11.06.05	1.09	2.06	6.21	8.93	11.66	11.58
14.06-17.06.05	1.4	1.6	2.8	3.74	5.74	6.89
MW	**1.26**	**1.64**	**3.81**	**5.61**	**7.36**	**8.47**
STABW	**0.12763**	**0.3317**	**1.70142**	**2.3518**	**3.0712**	**2.19688**

FOPflash/pRL-TK	50/5	100/10	200/20	300/30	400/40	500/50
3105-03.06.05	1.08	1.53	2.04	3.03	3.32	4.00
08.06-11.06.05	1.55	2.08	3.04	3.92	4.84	7.13
14.06-17.06.05	1.15	1.56	2.6	3.44	3.83	4.67
MW	**1.26**	**1.72**	**2.56**	**3.46**	**4.00**	**5.27**
STABW	**0.207**	**0.2525**	**0.4092**	**0.3637**	**0.6316**	**1.3457**

Data to figure 24: Determination of the optimal pRL-TK-vector DNA concentration

TOPflash/pRL-TK	400/40	400/45	400/50	400/55	400/60
Total DNA	**440.00**	**445.00**	**450.00**	**455.00**	**460.00**
05.07-08.07.04a	5.7	5.6	4.9	2.3	2.2
05.07-08.07.04b	3.1	3.5	3.6	3.4	3.2
05.07-08.07.04c	3.3	3.4	3.2	5.2	4.3
MW	**4.03**	**4.17**	**3.90**	**3.63**	**3.23**
STABW	**1.18**	**1.01**	**0.73**	**1.20**	**0.86**

FOPflash/pRL-TK	400/40	400/45	400/50	400/55	400/60
Total DNA	**440.00**	**445.00**	**450.00**	**455.00**	**460.00**
05.07-08.07.04a	3.1	3.9	2.73	2.7	2
05.07-08.07.04b	3.4	3.6	3.1	2.5	2
05.07-08.07.04c	2.1	2.9	3.1	4.28	3.1
MW	**2.87**	**3.47**	**2.98**	**3.16**	**2.37**
STABW	**0.56**	**0.42**	**0.17**	**0.80**	**0.52**

Data to Figure 25: Co transfection of HEK293 cells with TOP*flash*/FOP*flash* (400ng) and pFLAG-CMV5a-Δ45-*β*-Catenin.

TOPflash

β-catenin	0 ng/ml	5 ng/ml	10 ng/ml	15 ng/ml	20 ng/ml	30 ng/ml
0608-090804 a	7.6	23.1	35.7	33	57.9	62.5
0608-090804 b	8.4	28.7	35.1	36.7	74.3	102.6
0608-090804c	8.1	24.3	49.8	67.8	89.7	116.9
0908-120804	8.4	25.6	46	49.5	61	57.2
MW	**8.1**	**25.4**	**41.7**	**46.8**	**70.7**	**84.8**
STABWN	**0.3**	**2.1**	**6.4**	**13.6**	**12.6**	**25.5**

FOPflash

β-catenin	0 ng/ml	5 ng/ml	10 ng/ml	15 ng/ml	20 ng/ml	30 ng/ml
0608-090804a	4.1	4.5	3.7	5.5	6.5	5.9
0908-1208	6.4	6.5	7.2	7.6	6.7	8.4
MW	**5.3**	**5.5**	**5.5**	**6.6**	**6.6**	**7.2**
STABWN	**1.2**	**1.0**	**1.8**	**1.1**	**0.1**	**1.3**

8.3 Optimization of the luciferase reporter gene assay (10 cm Petri dish format)

Data to figure 26A: Determination of the optimal FuGENE 6/TOP*flash* ratio in HEK293 cells (10cm plate)

TOPflash DNA:Fugene 6	5 µg 1:3	1:6	1:9
1406-180605a	274487	344324	246595
1406-180605b	312238	304040	418011
1706-210605a		259526	162953
1706-210605b	620608	369892	133802
MW	**402444**	**319446**	**240340**
STABWN	**155033**	**34633**	**106162**

Data to figure 26B: Determination of the optimal pFLAG-CMV5a-Δ45-*β*-catenin for co-transfection experiments with TOP*flash*/FOP*flash*.

TOPflash beta-catenin Δ45	5 µg 0 µg	0,5 µg	1 µg	2 µg
26/05/2005	187502	4161756	6308530	11594871
02/06/2005	46146	265580	1871318	
MW	**116824**	**2213668**	**4089924**	**11594871**
STABWN	**70678**	**1948088**	**2218606**	**0**

FOPflash beta-catenin Δ45	5 µg 0 µg	0,5 µg	1 µg	2 µg
26/05/2005	86842	160440	311025	405217
02/06/2005	25290		60261	
MW	**56066**	**160440**	**185643**	**405217**
STABWN	**30776**	**0**	**125382**	**0**

Data to figure 27: Determination of the optimal FuGENE 6/plasmid DNA ratio in HCT116 cells with TOP*flash* (10cm plate)

TOPflash	1 µg			2.5 µg			5 µg		
	1:3	1:6	1:9	1:3	1:6	1:9	1:3	1:6	1:9
0306-070605	11764	26415	143355	10858	33625	322983	11236	44425	1001791
0606-100605							44979	64293	296296
MW	**11764.0**	**26415.0**	**143355.0**	**10858.0**	**33625.0**	**322983.0**	**28107.5**	**54359.0**	**649043.5**
STABWN	**0**	**0**	**0**	**0**	**0**	**0**	**16871.5**	**9934**	**352748**

Data to figure 28: Effect of serum on the transfection efficiency in HEK293 cells measured 19h post transfection

TOPflash

FCS	0.0%	10.0%	20.0%
1309-160904	3.2	6.1	6.3
0410-081004	3.4	5	5.40
1110-141004	5.2	10.6	12.6
MW	**3.9**	**7.2**	**8.1**
STABW	0.90	2.42	3.20

FOPflash

FCS	0.0%	10.0%	20.0%
1309-160904	2.1	5.7	4.6
MW	**2.1**	**5.7**	**4.6**

Data to figure 29: Effect of LiCl and SB216763 on the transcriptional activity of Tcf/Lef diven luciferase activity in HEK293 cells after 19h incubation

Renilla normalization

	10 mM LiCl	5 µM SB216763	10 µM SB216763
3008-030904	128.4		
0609-100904	82.7		
2009-240904	115.6		
2709-011004	74.3		
0410-081004	159.5	341.9	1882.9
1110-151004	92.8	244.1	1331.2
1810-221004	102.5	220.7	1168.4
1810-221004	105.6	270.8	1269.6
MW	**107.7**	**269.4**	**1413.0**
STABW	25.42	45.47	277.44

Protein normalization

	10 mM LiCl	5 µM SB216763	10 µM SB216763
3008-030904	263.5		
0609-100904	266.9		
2009-240904	436.4		
2709-011004	382.5		
0410-081004	343.0	235.5	1882.7
1110-151004	264.5	235.3	1391.0
1810-221004	267.6	219.0	1121.2
1810-221004	295.2	244.2	1171.2
MW	**315.0**	**233.5**	**1391.5**
STABW	61.47	9.11	301.19

8.4 Effect on the *β*-Catenin/Tcf/Lef-mediated Transcriptional Activity

Data to figure 30A: Effect of quercetin and SB216763 on Tcf-Lef driven gene transcription in HEK293 cells

TOPFLASH *

Quercetin [µM]	50	25	10	1
17.03.05	157.0		119.0	
24.03.05	164.0		111.0	
14.04.05	217.0		117.0	
09.06.05	208.0	175.0		
07.07.05	167.0	169.0		120.0
18.08.05		137.0		104.0
MW	**182.6**	**160.3**	**115.7**	**112.0**
STABWNA	**24.8**	**16.7**	**3.4**	**8.0**

FOPFLASH

Quercetin [µM]	50	25	10	1
17.03.05			42.0	
31.03.05	76.0		47.7	
14.04.05	82.0		60.0	
09.06.05		102.0	78.0	
07.07.05	83.0	77.0		48.0
18.08.05		134.0		125.0
MW	**80.3**	**104.3**	**56.9**	**48.0**
STABWNA	**3.1**	**23.3**	**13.8**	**38.5**

Topflash	SB216763 10 µM
1012-161204	3589.0
1401-190105	3267.0
2101-260105 a	1534.0
2101-260105 b	1448.0
0402-1002	2760.0
1102-1702	1100.0
1102-1702 a	1143.0
1103-1703	2274.0
1803-2403	1950.0
140405	1341.0
020605	2215.0
090605	1393.0
070705	2529.0
180805	3343
MW	**2134.7**
STABWNA	**825.1**

Fopflash	SB216763 10µM
0701-120105	66.0
1401-190105	123.0
2101-260105 a	96.0
2101-260105 b	131.0
2801-0302a	89.0
2801-0302b	93.3
0402-1002	124.0
1102-1702	92.0
1103-1703	104.0
1803-2403	95.0
090605	84.0
180805	72
MW	**97.4**
STABWNA	**19.3**

Data to figure 30B: Effect of EGCG on Tcf-Lef driven gene transcription in HEK293 cells

TOPFLASH

EGCG [µM]	0.1	1	10	25	50
140705		80.9	80.9	70.00	83
180805	112.0		95.0	100.0	81.0
020905a	81.0	76.0	99.0	86.0	68.0
020905b	111.0	99.0	84.0	91.0	81.0
MW	**101.3**	**85.3**	**89.7**	**86.8**	**78.3**
STABWNA	**14.4**	**9.9**	**7.5**	**10.9**	**6.0**

FOPFLASH

EGCG [µM]	0.1	1	10	25	50
140705		65.0	71.0	53.0	83.0
180805	91.0	108.0	98.0	81.0	84.0
020905	67.0	58.0	70.0	59.0	65.0
020905	73.0	68.0	76.0	73.0	73.0
MW	**77.0**	**74.8**	**78.8**	**66.5**	**76.3**
STABWNA	**10.2**	**19.5**	**11.3**	**11.1**	**7.8**

Data to figure 31A: Effect of AE02 on Tcf-Lef driven gene transcription in HEK293 cells

TOPFLASH

AE02 [µg/ml]	500	400	300	200	100
170305					
240305				98.0	99.0
310305			122.0	93.0	100.0
070405			123.0	139.0	
140405			122.0	130.0	
210405				124.0	
280405		94.0			94.0
020605	109.0	102.0	101.0		
090605	97.0				
180805	116.0	106.0	105.0	84.0	
MW	**107.3**	**100.7**	**114.6**	**111.3**	**97.7**
STABWNA	**7.8**	**5.0**	**9.6**	**20.6**	**2.6**

FOPFLASH

AE02 [µg/ml]	500	400	300	200	100
170305	59				
240305					
310305				32	22
070405		93.0	52	51	
140405		67.0	64	50.5	
210405	57			63	
280405					137
020605	64	56	67.7		
090605	68				
180805		80	73	76	74
MW	**62.0**	**74.0**	**64.2**	**54.5**	**77.7**
STABWNA	**4.3**	**13.9**	**7.7**	**14.6**	**47.0**

Data to figure 31B: Effect of phloretin, phloridzin, epicatechin on Tcf-Lef driven gene transcription in HEK293 cells

TOPFLASH

Phoretin [µM]	10
19.01.05	119.0
26.01.05a	123.0
26.01.05b	
03.02.05	87.0
10.02.05	118.0
MW	**111.8**
STABWNA	**14.4**

FOPFLASH

Phoretin [µM]	10
19.01.05	51.0
26.01.05a	35.0
26.01.05b	38.0
03.02.05	65.0
MW	**47.3**
STABWNA	**11.9**

TOPFLASH

Phloridzin [µM]	50	10
10.02.05	122	
17.02.05	84	
17.03.05	82	
24.03.05	93	
31.03.05a		122
31.03.05b		94
07.04.05		101
14.04.05		89.1
MW	95.25	101.525
STABWNA	15.99	12.55

FOPFLASH

Phloridzin [µM]	50	10
10.02.05	150	
17.02.05	96	
17.03.05	30	
24.03.05		
31.03.05a		43
31.03.05b		43
07.04.05		38.7
14.04.05		46.5
MW	92	42.8
STABWNA	49.07	2.76

TOPFLASH

EC [µM]	100	50
16.12.04	74.0	95.0
26.01.05a		115.0
26.01.05b		82.0
07.04.05	85	91
21.04.05	96	
MW	**85.0**	**95.8**
STABWNA	**9.0**	**12.1**

FOPFLASH

EC [µM]	100	50
16.12.04	66.0	
26.01.05a		31
26.01.05b		36.5
07.04.05	46.5	46.7
21.04.05	52.3	
MW	**54.9**	**38.1**
STABWNA	**8.2**	**6.5**

Data to figure 32A: Effect of quercetin on Tcf-Lef driven gene transcription in HEK293 cells tranfected co transfected with pFLAG-CMV-Δ45-*β*-catenin

TOPFLASH/ beta catenin (Δ45)

Quercetin [µM]	50	25	10	1	0.1
090605	205.0	193.0	145.0		
70705		180.0	137.0	96.0	
270705				102.0	89.0
110805	170.0	173.0	114.0	96.9	102.0
250805	162.0	159.0	96.0		89.0
MW	**179.0**	**175.0**	**118.3**	**98.3**	**93.3**
STABWNA	**18.7**	**14.0**	**20.2**	**2.6**	**6.1**

FOPFLASH/ beta catenin (Δ45)

Quercetin [µM]	50	25	10	1	0.1
270705	4.2	2.9	1.7	1.2	1.2
110805	2.0	2.1	2.0	1.4	1.5
250805	2.2	2.1	2.5	3.0	2.2
MW	**2.8**	**2.4**	**2.1**	**1.9**	**1.6**
STABWNA	**1.0**	**0.4**	**0.3**	**0.8**	**0.4**

TOPFLASH /beta catenin (Δ45)

	SB216763 10µM
090605	124.0
070705	148.0
140705	157.0
MW	143.0
STABWNA	13.9

FOPFLASH /beta catenin (Δ45)

	SB216763 10µM
090605	
070705	1.5
140705	1.5
MW	1.5
STABWNA	0.0

Data to figure 32B: Effect of EGCG on Tcf-Lef driven gene transcription in HEK293 cells tranfected co transfected with pFLAG-CMV-Δ45-*β*-catenin

TOPFLASH/ beta catenin (Δ45)

EGCG [µM]	0	1	10	25	50
140705		98.0	117.0		107.0
040805	102.0	93.0	103.0	93.0	100.0
110805	102.0	96.0	108.0	92.0	91.0
250805	92.0	96.0		89.0	
MW	**98.7**	**95.8**	**109.3**	**91.3**	**99.3**
STABWNA	**4.7**	**1.8**	**5.8**	**1.7**	**6.5**

FOPFLASH/ beta catenin (Δ45)

EGCG [µM]	0	1	10	25	50
140705		1.50	1.80	2.00	2.10
040805	3.40	3.00	3.20	3.10	2.80
110805	1.50	1.30	1.60	1.40	1.20
250805	1.70	1.70	1.60	1.40	0.80
MW	**2.2**	**1.9**	**2.1**	**2.0**	**1.7**
STABWNA	**0.9**	**0.7**	**0.7**	**0.7**	**0.8**

Data to figure 33A: Effect of Quercetin and SB216763 on Tcf-Lef driven gene transcription in HCT116

TOPFLASH	Quercetin [µM]			SB216763 [µM]
	1	10	25	10
230504				149.0
230605	98.0	182.0	391.0	188.0
140705	81.0	205.0	524.0	144.0
MW	**89.5**	**193.5**	**457.5**	**160.3**
STABWNA	**8.5**	**11.5**	**66.5**	**19.7**

FOPFLASH	Quercetin [µM]			SB216763 [µM]
	1	10	25	10
230504				89.0
230605	53.0	74.0	136.0	32.5
140705	51.0	86.0	172.0	40.7
MW	52.0	80.0	154.0	54.1
STABWNA	1.0	6.0	18.0	24.9

Data to figure 33B: Effect of EC, EGCG and phloretin on Tcf-Lef driven gene transcription in HCT116

TOPFLASH

	EC 50µM	EGCG 10µM	Phoretin 10 µM
2101-270105 a	102.0	112.0	140.0
2101-260105 b	103.0	91.0	126.0
2101-260105 c	88.0	104.0	115.0
MW	**97.7**	**102.3**	**127.0**
STABWNA	**6.85**	**8.65**	**10.23**

8.5 Effect on GSK

Data to figure 34A: Effect of quercetin and SB216763 on GSK-3*α* and phospho-GSK-3*α*

GSK-3*α*

	Q_10 µM	Q_25 µM	Q_ 50 µM	Q 75 µM	SB21 _10µM
070405a		72.0	94.9	94.9	
070405b		82.0	61.0	56.0	
210405				161.0	129.0
280405				162.0	
070705	82.0	90.0	70.0	75.0	
140705_1	77.4	75.5	90.0	78.5	
280705					106.0
120807	91.5	87.5	71.5		114.0
180805					118.0
250805					98.6
MW	**83.63**	**81.40**	**77.48**	**104.57**	**113.12**
SD	**5.87**	**6.85**	**12.83**	**41.81**	**10.38**
n	3.00	5.00	5.00	6.00	5.00

Phopho-GSK-3*α*

	Q_10 µM	Q_25 µM	Q_ 50 µM	Q 75 µM	SB21_10 µM
070405a				142.0	
210405	89.0				120.0
280405	52.0		134.0	182.0	
070705_1		66.0	107.0	132.0	
140705_1	48.8	59.4	68.0	72.0	
140705_2	52.6	72.6	60.2	71.9	
120805	89.9	80.7	92.2		155.0
250805					180.0
MW	**66.46**	**69.68**	**92.28**	**119.98**	**151.67**
SD	**18.82**	**7.89**	**26.74**	**42.64**	**24.61**
n	5.00	4.00	5.00	5.00	3.00

Data to figure 34B: Effect of quercetin and SB216763 on GSK-3*β* and phospho-GSK-3*β*

GSK-3*β*

	Q_10 µM	Q_25 µM	Q_ 50 µM	Q 75 µM	SB21 _10µM
070405a		103.0	101.0	98.0	
070405b		94.0	82.0	85.0	
210405					89.0
70705	86.0	83.0	81.0	76.0	
140705	73.5	85.5	91.7	86.8	
280705					138.0
120805	84.0		76.2		122.0
180805					116.0
250805					100.6
MW	**81.17**	**91.38**	**86.38**	**86.45**	**113.12**
SD	**5.48**	**7.85**	**8.87**	**7.82**	**17.00**
n	**3.00**	**4.00**	**5.00**	**4.00**	**5.00**

Phopho-GSK-3*β*

	Q_10 µM	Q_25 µM	Q_ 50 µM	Q 75 µM	SB21 _10µM
070405a		88.0	111.0	83.0	
210405					46.0
280405				85.0	48.4
070705_0	108.0	83.0	101.0	100.0	
140705_1		72.2	60.0	95.3	
140705_2	94.9	83.3	99.0		
280705					32.0
120805	107.0		54.0		30.0
250805					39.0
MW	**103.30**	**81.63**	**85.00**	**90.83**	**39.08**
SD	**5.95**	**5.79**	**23.30**	**7.06**	**7.31**
n	**3.00**	**4.00**	**5.00**	**4.00**	**5.00**

Data to figure 35A: Effect of EGCG on GSK-3*α* and phospho-GSK-3*α*

GSK-3*α*

EGCG	0.1	0.5	1	10	25	50
070405a			70.0	86.0	73.0	
070405b			63.0	83.0	67.0	
210405			107.0		163.0	94.0
280405			126.0	82.0	140.0	139.0
300606_0			80.0	79.0	105.0	88.0
300605_1			121.0	103.0	110.0	120.0
300605_2			126.0	108.0	112.0	91.6
070705_0				68.0	73.0	62.0
140705			63.8	80.9		
210705						93.0
210705_1			66.0	83.0	98.5	80.0
040805	98.0	125.0	107.0			
120805	87.0	96.9	88.0			
180805	104.0	128.0	111.0	112.0	112.0	53.0
250805	82.0	98.6	98.3	87.6	93.9	
MW	**92.75**	**112.13**	**94.39**	**88.41**	**104.31**	**91.18**
SD	**8.70**	**14.43**	**23.02**	**12.87**	**27.58**	**24.88**
n	**4.00**	**4.00**	**13.00**	**11.00**	**11.00**	**9.00**

Phospho-GSK-3*α*

	0.1	0.5	1	10	25	50
070405a				268.0	229.0	
210405			209.0		286.0	175.0
280405			114.0	221.0	256.0	245.0
300605_0			116.0			165.0
300605_1			193.0	247.0	209.0	251.0
040805	147.0	152.0	181.0			
120805	114.0	152.0	285.0			
180805	115.0	161.0		225.0		219.0
250805	120.0		172.6	224.0	271.0	
MW	**124.00**	**155.00**	**181.51**	**237.00**	**250.20**	**211.00**
SD	**13.47**	**4.24**	**54.15**	**18.06**	**27.91**	**35.30**
n	**4.00**	**3.00**	**7.00**	**5.00**	**5.00**	**5.00**

Data to figure 35A: Effect of EGCG on GSK-3*β* and phospho-GSK-3*β*

GSK-3*α*

EGCG	0.1	0.5	1	10	25	50	SB21_ 10µM
070405a			70.0	86.0	73.0		
070405b			63.0	83.0	67.0		
210405			107.0		163.0	94.0	129.0
280405			126.0	82.0	140.0	139.0	106.0
300606_0			80.0	79.0	105.0	88.0	
300605_1			121.0	103.0	110.0	120.0	
300605_2			126.0	108.0	112.0	91.6	
070705_0				68.0	73.0	62.0	
140705			63.8	80.9			
210705						93.0	
210705_1			66.0	83.0	98.5	80.0	
040805	98.0	125.0	107.0				
120805	87.0	96.9	88.0				114.0
180805	104.0	128.0	111.0	112.0	112.0	53.0	118.0
250805	82.0	98.6	98.3	87.6	93.9		98.6
MW	**92.75**	**112.13**	**94.39**	**88.41**	**104.31**	**91.18**	**113.12**
SD	**8.70**	**14.43**	**23.02**	**12.87**	**27.58**	**24.88**	**10.38**
n	4.00	4.00	13.00	11.00	11.00	9.00	5.00

Phospho-GSK-3*β*

EGCG	0.1	0.5	1	10	25	50	SB21_ 10µM
070405a			158.0	158.0	173.0		
210405			190.0				46.0
280405							48.4
300605_0			120.0	131.0	160.0	163.0	
300605_1				145.0	177.0	180.0	
070705_0					146.0	128.0	
140705_1			141.0				
210705					1.6E+02	1.2E+02	
210705_1				142.0			
280705							32.0
040805	97.0						
120805	137.0	150.0	172.0				30.0
180805	145.0	139.0		143.0			
250805	115.0	149.0	130.0	161.0	164.0		39.0
MW	**123.50**	**146.00**	**151.83**	**146.67**	**162.67**	**148.75**	**39.08**
SD	**18.83**	**4.97**	**24.18**	**10.14**	**10.35**	**23.57**	**7.31**
n	4.00	3.00	6.00	6.00	6.00	4.00	5.00

8.6 Effect on *β*-catenin

Data to figure 36: Effect of quercetin on total *β*-catenin and phosphorylated *β*-catenin

Total *β*-catenin

	Q_10 µM	Q_25 µM	Q_ 50 µM	Q 75 µM	SB21_10µM
070405a		130.0	118.0	132.0	
070405b		69.0	75.0	75.0	
210405					
280405	108.0		109.0	101.0	
200505a					
200505b	90.0	119.0	76.0		153.0
020605	49.0	55.0		80.0	
090605			68.0		
230605	132.0		69.9		144.8
070705_0	56.0	77.0	89.0	96.0	
140705	63.9	66.5	96.5	122.0	
040805					158.0
120805	113.0	89.6	74.0		
250805					162.0
MW	**87.41**	**86.59**	**86.16**	**101.00**	**154.45**
SD	**29.49**	**26.04**	**17.06**	**20.59**	**6.42**
n	7.00	7.00	9.00	6.00	4.00

Phospho *β*-catenin

	Q_10µM	Q_25 µM	Q_ 50 µM	Q 75 µM	SB2167 10 µM
020605	171.0	125.0	153.0	134.0	
090606	172.0	190.0			
230607	151.0	144.0	127.0	97.0	29.0
070705_0	80.0	61.0	76.0	75.0	
40805					21.0
120805	60.5	33.0			28.3
180805					26.0
250805					38.0
MW	**126.90**	**110.60**	**118.67**	**102.00**	**28.46**
SD	**47.26**	**56.76**	**31.98**	**24.34**	**5.53**
n	5.00	5.00	3.00	3.00	5.00

Data to figure 37: Effect of EGCG on total *β*-catenin and phosphorylated *β*-catenin

Beta Catenin

EGCG	0.1	0.5	1	10	25	50	SB21_ 10µM
070405a			72.0	74.0			
070405b					52.0		
210405			129.0		60.0	40.0	
280405				81.0	36.0	59.0	
200505b							153.0
230605							144.8
300605			79.0	86.0	61.0	57.0	
070705_0				62.0	41.0		
140705			116.0	58.6			
210705			110.0		42.0	55.0	
040805	113.0	97.0	97.0				158.0
120805		112.0	118.0				
250805							162
MW	**113.00**	**104.50**	**108.17**	**71.90**	**48.00**	**52.75**	**154.45**
SD	**0.00**	**7.50**	**19.61**	**10.58**	**9.62**	**7.50**	**6.42**
n	**1.00**	**2.00**	**7.00**	**5.00**	**6.00**	**4.00**	**4.00**

Phospho Beta catenin

EGCG	0.1	0.5	1	10	25	50	SB21_ 10µM
230605							29.0
300605			115.0	83.0	21.0	36.0	
300605_1			127.0		78.0		
070705_0				66.0	28.0		
210705			98.6	81.8	49.0	25.0	
040805	67.0	96.3	81.0				21.0
120805			84.0				28.3
180805	73.0	90.0	70.0	78.0	72.0	34.9	26.0
250805	81.0	141.0	118.0		41.0	28.0	38.0
100905a	170.0					34.9	
100905b	156.0					34.1	
100905c	134.0						
MW	**113.50**	**109.10**	**90.32**	**75.27**	**47.50**	**31.38**	**28.46**
SD	**41.39**	**22.70**	**19.97**	**6.72**	**21.04**	**4.13**	**5.53**
n	6.00	3.00	7.00	4.00	6.00	6.00	5.00

Data to figure 38: Effect of quercetin and EGCG on nuclear *β*-catenin

Quercetin [µM]

	DMSO	1	10	25	50
13/10/2005	95.45 104.55		104.00	73.00	76.00
01.12.2005	105.10 94.90	90.00	89.60	80.00	94.50
08.12.2005	103.50 96.50	88.00	78.20	66.70	
15.12.2005	97.30 102.70	96.40	69.40	92.90	83.00
12.01.2006	87.40 112.60	94.20	107.00	94.50	98.50
MW	**100.00**	**92.15**	**89.64**	**81.42**	**88.00**
SD	**8.31**	**3.32**	**14.48**	**10.89**	**8.97**

EGCG [µM]

	DMSO	0.1	1	10	25	50	SB216763
29/09/2005	109.20 90.80			114.00	115.00		
07/10/2005	90.80 109.20		108.50	101.00	125.00	47.00	156.50
13/10/2005	79.00 121.00			94.40	98.00		
13/10/2005	93.40 106.60					43.40	
20/10/2005	99.60 100.40	88.70	90.00	88.15			150.00
20/10/2005	83.70 116.30				109.60		
10/11/2005	89.80 110.20	99.40	102.20	127.00			
10/11/2005	87.30 112.70			132.00	78.90		
17/11/2005	97.30 102.70		92.00	69.30	45.00		140.50
17/11/2005	81.10 118.90	77.00	95.30		52.90	46.00	
24/11/2005	86.10 113.90	90.50	86.10	61.90	44.60	48.95	166.70
24/11/2005	108.40 91.60		80.25		42.30	44.20	
MW	**100.00**	**88.90**	**93.48**	**98.47**	**79.03**	**45.91**	**153.43**
SD	**12.29**	**7.98**	**8.85**	**23.71**	**31.76**	**1.98**	**9.55**

Data to figure 39: Effect of EGCG and SB216763 on *β*-catenin transcripts

Sample	Detector	Avg delta Ct	delta Ct SD	delta delta Ct	RQ	RQ Min	RQ Max
DMSO	beta-catenin	3.0963905	0.0172983	0	1	0.975373	1.025249
EGCG 1µM	beta-catenin	3.4379334	0.0182923	0.34154296	0.789197	0.768267	0.810697
EGCG 10µM	beta-catenin	3.6277173	0.0204269	0.5313268	0.691918	0.671074	0.71341
EGCG 0.1µM	beta-catenin	3.3458343	0.012753	0.24944377	0.841221	0.824566	0.858212
EGCG 25µM	beta-catenin	3.748485	0.0228702	0.6520946	0.636356	0.613513	0.660049
SB21 10 µM	beta-catenin	3.1901023	0.0231288	0.09371185	0.937109	0.902249	0.973315

Data to figure 40: Effect of quercetin on *β*-catenin transcripts

Sample	Detector	Avg delta Ct	delta Ct SD	delta delta Ct	RQ	RQ Min	RQ Max
DMSO 1 %	beta-catenin	1.852802	0.116724	0	1	0.710707	1.407051
Quercetin 20 mM	beta-catenin	1.974798	0.308844	0.121996	0.918915	0.372271	2.268254
Quercetin 80 mM	beta-catenin	2.216008	0.281081	0.363206	0.777435	0.341605	1.769313

8.7 Effect on GS

Data to figure 41: Effect of EGCG and SB216763 on GS activity

EGCG 25 µM

Date	0.5h	1h	3h	6h	12h	24h
26.04.06						
						103.60
04.05.06						
						98.30
11.05.06						
				121.00	86.60	
18.05.06						
			110.00		97.90	
31.05.06						
			89.70	120.00	62.20	73.30
13.06.06	97.00	70.00	104.00			
08.08.06						
		80.00				
09.08.06						
	87.00	83.30				
11.08.06						
	103.00	87.00				
15.08.06						
			87.20	111.00		
16.08.06						
						102.00
17.08.06						
			107.00	119.00		82.00
22.08.06						
				146.00	71.80	100.00
24.08.06						
					90.30	
06/12/2006						
		95.00				
03/01/2007						
	121.00					
12/01/2007						
	102.20	74.30				
MW	**102.04**	**81.60**	**99.58**	**123.40**	**81.76**	**93.20**
SD	**11.06**	**8.19**	**9.32**	**11.84**	**12.95**	**11.40**
n	5.00	6.00	5.00	5.00	5.00	6.00

SB216763 10µM

Date	0.5h	1h	3h	6h	12h	24h
11.05.06					120.00	
18.05.06						
		168.00	149.00		153.60	
31.05.06						
				175.00	131.00	
13.06.06						
	199.00	137.00	148.00			
08.08.06						
		297.00				
09.08.06						
	167.00	290.00				
11.08.06						
	148.00	147.00				
15.08.06						
			228.00	229.00		
17.08.06						
			225.00	225.00		132.00
22.08.06						
					175.00	138.00
05/12/2006						
		144.00				
13/12/2006						
						157.00
03/01/2007						
	208.00		144.00	257.00		
07/01/2007						
						158.00
10/01/2007						
						123.00
12/01/2007						
			142.00		173.00	
MW	**180.50**	**197.17**	**172.67**	**221.50**	**150.52**	**141.60**
SD	**24.17**	**68.80**	**38.15**	**29.54**	**22.03**	**13.84**
n	4.00	6.00	6.00	4.00	5.00	5.00

Data to figure 42: Effect of EGCG and SB216763 on the phosphorylation of GS

Phospho GS 15 min

Date	DMSO	EGCG 25µM	SB216763 10 µM
10.11.2006_a	94.00		
	106.00	87.00	46.00
15/11/2006	90.00		
	110.00	135.90	
22/11/2006	95.20		
	104.80	80.95	
28/11/2006	83.00		
	117.00	71.00	31.60
06/12/2006	82.00		
	118.00	97.00	39.00
13/12/2005	98.00		
	102.00	133.30	
16/01/2007	90.00		
	110.00	130.00	34.00
MW	**100.00**	**105.02**	**37.65**
SD	**11.19**	**25.36**	**5.51**
n	14.00	7.00	4.00

Phospho GS 60min

Date	DMSO	EGCG 25 µM	SB216763 10 µM
10/11/2006	92.00		
	108.00	117.00	41.00
16/11/2006	93.00		
	107.00	92.50	33.90
22/11/2006	83.00		
	117.00	88.65	53.83
28/11/2006	71.80		
	128.20	111.00	19.00
06/12/2006	78.00		
	122.00		24.00
13/12/2006	99.00		
	101.00	95.00	48.00
04/01/2007	97.00		
	103.00		49.00
16/01/2007	79.00		
	121.00	92.00	28.00
MW	**100.00**	**99.36**	**37.09**
SD	**16.33**	**10.66**	**11.98**
n	16.00	6.00	8.00

Phospho GS 24h

Date	DMSO	EGCG 1 µM	EGCG 25 µM	SB216763 10 µM
16/11/2006	98.40			
	101.60		108.20	39.10
22/11/2006	83.00			
	117.00	105.00	128.00	38.50
29/11/2006	94.00			
	106.00		111.00	46.60
07/12/2006	100.00			
	100.00	124.00		41.00
14/12/2006	94.00			
	106.00	115.00	102.00	55.00
10/01/2007	89.00			
	111.00	116.00	100.00	40.00
11/01/2007	68.00			
	132.00	108.00	123.00	51.00
MW	**100.00**	**113.60**	**112.03**	**44.46**
SD	**14.68**	**6.65**	**10.30**	**6.03**
n	14.00	5.00	6.00	7.00

Data to figure 43: Effect of EGCG and SB216763 on total GS

Date	DMSO	EGCG 1 µM	EGCG 25 µM	SB216763 10 µM
07/12/2006	88.00			
	112.00	119.00	138.00	383.00
14/12/2006	94.00			
	106.00	140.00	156.00	345.00
10/01/2007	93.00			
	107.00	142.00	152.00	240.00
11/01/2007	81.00			
	119.00	75.00		
17/01/2007	85.00			
	115.00			234.00
20/01/2007	94.00			
	106.00	84.00	139.00	337.00
24/01/2007	91.00			
	109.00	135.00	151.00	403.00
MW	**100.00**	**115.83**	**147.20**	**323.67**
SD	**11.54**	**26.85**	**7.30**	**65.18**
n	14.00	6.00	5.00	6.00

Data to figure 44A: Effect of EGCG and SB216763 on LGS transcripts

LGS (6h)

Sample	Detector	Avg delta Ct	delta Ct SD	delta delta Ct	RQ	RQ Min	RQ Max
EGCG 1µM	liverGS	14.51568	0.4716113	0.1793375	0.8831084	0.1850427	4.214598
EGCG 10µM	liverGS	15.812203	0.18751161	1.4758606	0.3595189	0.1980647	0.6525839

LGS (24h)

Sample	Detector	Avg delta Ct	delta Ct SD	delta delta Ct	RQ	RQ Min	RQ Max
DMSO control	liverGS	15.31534	0.12463336	0	1	0.826842	1.209421
EGCG 10 µM	liverGS	15.29578	0.11573198	-0.01955	1.013644	0.849583	1.209387
EGCG 25 µM	liverGS	15.47835	0.10359465	0.16301	0.89316	0.76259	1.046085
SB216763 10 µM	liverGS	14.35601	0.06322499	-0.95932	1.9444	1.765611	2.141293
EGCG 1 µM	liverGS	15.11299	0.19766417		0.890139	0.484668	1.634822
NTC	liverGS						

Data to figure 44B: Effect of EGCG and SB216763 on MGS transcripts

MGS (6h)

Sample	Detector	Avg delta Ct	delta Ct SD	delta delta Ct	RQ	RQ Min	RQ Max
EGCG 1µM	muscleGS	5.503043	0.04700203	0.313826	0.804506	0.696226	0.929625
EGCG 10µM	muscleGS	6.488787	0.037180193	1.29957	0.406247	0.362352	0.45546

MGS (24h)							
Sample	Detector	Avg delta Ct	delta Ct SD	delta delta Ct	RQ	RQ Min	RQ Max
DMSO control	muscleGS	5.2078996	0.032014396	0	1	0.9523322	1.0500537
EGCG 10 µM	muscleGS	5.5052667	0.046053227	0.2973671	0.8137361	0.758526	0.8729648
EGCG 25 µM	muscleGS	5.5598145	0.01791002	0.3519149	0.7835434	0.762424	0.8052478
SB216763 10 µM	muscleGS	5.315325	0.01680099	0.1074252	0.9282432	0.9047531	0.9523432
EGCG 1 µM	muscleGS	5.5817127	0.024860997	0.3738132	0.77174	0.7409253	0.8038364

Data to figure 45: Effect of quercetin on MGS transcripts

LGS (6h)

Sample	Detector	Avg delta Ct	delta Ct SD	delta delta Ct	RQ	RQ Min	RQ Max
Quercetin 20µM	liverGS	14.134944	0.124662295	-0.2013989	1.1498127	0.7836465	1.6870735
Quercetin 80µM	liverGS	13.736491	0.16853501	-0.5998516	1.5155606	0.9025416	2.544951

MGS (6h)

Sample	Detector	Avg delta Ct	delta Ct SD	delta delta Ct	RQ	RQ Min	RQ Max
Quercetin 20µM	muscleGS	5.8334765	0.01467803	0.6442595	0.6398211	0.6115806	0.6693658
Quercetin 80µM	muscleGS	6.4878325	0.02164198	1.2986155	0.4065161	0.3803395	0.4344944

LGS (24h)

Sample	Detector	Avg delta Ct	delta Ct SD	delta delta Ct	RQ	RQ Min	RQ Max
Quercetin 20µM	liverGS	15.215787	0.20352077	0.27069092	0.8289225	0.4340042	1.5831932
Quercetin 80µM	liverGS	15.166507	0.149226	0.22141075	0.8577263	0.542042	1.3572644

MGS (24h)

Sample	Detector	Avg delta Ct	delta Ct SD	delta delta Ct	RQ	RQ Min	RQ Max
Quercetin 20µM	muscleGS	4.8368206	0.019563992	-0.113061905	1.0815212	1.0183666	1.1485924
Quercetin 80µM	muscleGS	5.414919	0.025599128	0.4650364	0.7244528	0.6696044	0.783794

Data to figure 46A: Effect of EGCG on MGS and LGS transcripts in HepG2 cells

MGS (6h)

Sample	Detector	Avg delta Ct	delta Ct SD	delta delta Ct	RQ	RQ Min	RQ Max
EGCG 1 µM	muscleGS	6.327994	0.018181192	0.08902645	0.9401569	0.88903	0.9942242
EGCG 10 µM	muscleGS	6.2068596	0.025802257	-0.03210783	1.0225049	0.9445007	1.1069514

LGS (6h)

Sample	Detector	Avg delta Ct	delta Ct SD	delta delta Ct	RQ	RQ Min	RQ Max
EGCG 1 µM	liverGS	13.80549	0.20075868	-0.29340744	1.2255313	0.6076539	2.471682
EGCG 10 µM	liverGS	14.021217	0.11866881	-0.077679634	1.0553193	0.7326259	1.5201467

MGS (24h)

Sample	Detector	Avg delta Ct	delta Ct SD	delta delta Ct	RQ	RQ Min	RQ Max
EGCG 1 µM	muscleGS	4.9944453	0.01665157	-0.4066887	1.3256397	1.2594606	1.3952961
EGCG 10 µM	muscleGS	5.2582855	0.031757414	-0.1428485	1.104083	1.0013467	1.2173597

LGS (24h)

Sample	Detector	Avg delta Ct	delta Ct SD	delta delta Ct	RQ	RQ Min	RQ Max
EGCG 1 µM	liverGS	14.298144	0.25228915	-0.441968	1.3584561	0.588778	3.1342938
EGCG 10 µM	liverGS	15.831564	0.19103956	1.0914516	0.46928895	0.2491705	0.8838612

Data to figure 46B: Effect of quercetin on MGS and LGS transcripts in HepG2 cells

MGS (6h)

Sample	Detector	Avg delta Ct	delta Ct SD	delta delta Ct	RQ	RQ Min	RQ Max
Quercetin 20 µM	muscleGS	6.3117623	0.02093278	0.072794914	0.9507943	0.8915124	1.014018
Quercetin 80 µM	muscleGS	6.002098	0.022734378	-0.23686934	1.1784327	1.0988523	1.2637764

LGS (6h)

Sample	Detector	Avg delta Ct	delta Ct SD	delta delta Ct	RQ	RQ Min	RQ Max
Quercetin 20 µM	liverGS	14.218636	0.13220057	0.11973858	0.9203544	0.6128858	1.3820717
Quercetin 80 µM	liverGS	14.376901	0.2432388	0.2780037	0.8247314	0.3805837	1.7872072

MGS (24h)

Sample	Detector	Avg delta Ct	delta Ct SD	delta delta Ct	RQ	RQ Min	RQ Max
Quercetin 20 µM	muscleGS	5.581742	0.017435957	0.1806078	0.8823312	0.8362634	0.9309368
Quercetin 80 µM	muscleGS	5.5280385	0.028761463	0.1269045	0.9157943	0.8382669	1.000492
LGS (24h)							
Sample	Detector	Avg delta Ct	delta Ct SD	delta delta Ct	RQ	RQ Min	RQ Max
Quercetin 20 µM	liverGS	16.65366	0.15158142	1.9135475	0.26543903	0.1562886	0.4508192
Quercetin 80 µM	liverGS	13.183871	0.13352957	-1.556241	2.940866	1.9235283	4.4962645

8.8 Effect on GP

Data to figure 48: Effect of EGCG and SB216763 on GP activity

EGCG 25 µM

Date	0.5h	1h	3h	6h	12h	24h
26.04.06						112.90
04.05.06						77.90
09.05.06	105.50			92.20	80.80	
17.05.06	105.20		93.30	86.90	93.90	
31.05.06			95.70	93.10	84.10	72.30
27.06.06		116.00				
09.08.06		110.00				
19/09/2006	102.00	111.00	85.60			
01/11/2006						93.00
03/11/2006						95.10
08/11/2006						81.20
10/11/2006						107.10
15/11/2006						105.10
22/11/2006	115.70		102.00	99.10		102.10
MW	**107.10**	**112.33**	**94.15**	**92.83**	**86.27**	**94.08**
SD	**5.15**	**2.62**	**5.87**	**4.33**	**5.56**	**13.39**
n	4.00	3.00	4.00	4.00	3.00	9.00
p	**0.032787889**	**3.17618E-06**	**0.062614582**	**0.002175667**	**0.001729753**	**0.172773407**

SB216763 10µM

Date	**0.5h**	**1h**	**3h**	**6h**	**12h**	**24h**
26.04.06						66.20
04.05.06						88.80
09.05.06				100.60	75.90	
17.05.06	106.40	106.00		75.10	103.80	
23.05.06	105.80	111.00	162.00	73.00		
31.05.06			102.90	87.00	83.00	91.60
13.06.06		103.60	103.00			
20.06.06			148.00			
09.08.06	97.20	115.00				
19/09/2006	97.50	125.00				
01/11/2006						89.00
22/11/2006		104.00				
MW	**101.73**	**110.77**	**128.98**	**83.93**	**87.57**	**83.90**
SD	**4.38**	**7.53**	**26.49**	**11.01**	**11.84**	**10.28**
n	4.00	6.00	4.00	4.00	3.00	4.00

Data to figure 49: Effect of EGCG and SB216763 on total GP

GP	24h			
Date	DMSO	EGCG 1 µM	EGCG 25 µM	SB216763 10 µM
16/11/2006	91.30			
	108.70	121.45	113.50	100.50
22/11/2006	85.00			
	115.00		109.00	102.00
29/11/2006	64.00			
	136.00		81.00	115.00
07/12/2006	92.00			
	108.00	95.00	92.00	49.00
04/01/2007	60.00			
	140.00	108.00	54.00	92.00
10/01/2007	94.00			
	106.00	116.00	67.00	79.00
11/01/2007	35.00			
	165.00		96.00	47.00
17/01/2007	71.00			
	129.00		67.00	91.00
20/01/2007	96.00			
	104.00	133.00	110.00	77.70
24/11/2007	87.00			
	113.00	99.00	71.00	72.00
MW	**100.00**	**112.08**	**86.05**	**82.52**
SD	**29.24**	**13.04**	**19.98**	**21.10**
n	20.00	6.00	10.00	10.00

Data to figure 50B: Effect of EGCG on the transcripts of GP after 6h in HT29 cells

BGP (6h)

Sample	Detector	Avg delta Ct	delta Ct SD	delta delta Ct	RQ	RQ Min	RQ Max
DMSO	brainGP	1.5282803	0.0420414	0	1	0.8541997	1.1706865
EGCG 1 µM	brainGP	2.3345928	0.0142396	0.8063126	0.5718416	0.542119	0.6031938
EGCG 10 µM	brainGP	2.4744892	0.0236198	0.946209	0.5189945	0.4750193	0.5670407

LGP (6h)

Sample	Detector	Avg delta Ct	delta Ct SD	delta delta Ct	RQ	RQ Min	RQ Max
DMSO	liverGP	5.684272	0.0598348	0	1	0.7990847	1.2514318
EGCG 1 µM	liverGP	7.1598024	0.0727285	1.4755306	0.3596011	0.2737939	0.4723004
EGCG 10 µM	liverGP	7.0273266	0.0448489	1.3430548	0.3941851	0.3331878	0.4663494

Data to figure 50B: Effect of EGCG on the transcripts of GP after 24h in HT29 cells

BGP (24h)

Sample	Detector	Avg delta Ct	delta Ct SD	delta delta Ct	RQ	RQ Min	RQ Max
DMSO	brainGP	0.24593163	0.0347421	0	1	0.948377	1.054433
EGCG 10 µM	brainGP	0.4859403	0.04648693	0.240009	0.84674	0.788769	0.908972
EGCG 25 µM	brainGP	1.864591	0.014152023	1.618659	0.325638	0.318683	0.332745
SB216763 10 µM	brainGP	0.88783455	0.017612927	0.641903	0.640867	0.623876	0.658321
EGCG 1 µM	brainGP	0.69029236	0.02696105	0.444361	0.73491	0.703141	0.768114

LGP (24h)

Sample	Detector	Avg delta Ct	delta Ct SD	delta delta Ct	RQ	RQ Min	RQ Max
DMSO control	liverGP	5.6536994	0.04055208	0	1	0.940008	1.06382
EGCG 10 µM	liverGP	6.104302	0.055873822	0.450603	0.731737	0.671947	0.796847
EGCG 25 µM	liverGP	5.169576	0.047945168	-0.48412	1.398736	1.300077	1.504881
SB216763 10 µM	liverGP	5.8124065	0.027000958	0.158707	0.895828	0.859676	0.9335
EGCG 1 µM	liverGP	6.1441517	0.042199347	0.490452	0.711802	0.664233	0.762777

MGP (24h)

Sample	Detector	Avg delta Ct	delta Ct SD	delta delta Ct	RQ	RQ Min	RQ Max
DMSO control	muscleGP	13.826332	0.05944484	0	1	0.913301	1.094929
EGCG 10 µM	muscleGP	13.610616	0.047892448	-0.21572	1.16128	1.079457	1.249306
EGCG 25 µM	muscleGP	13.133941	0.026678054	-0.69239	1.61596	1.551511	1.683087
SB216763 10 µM	muscleGP	12.81324	0.03194128	-1.01309	2.018232	1.922242	2.119016

Data to figure 51: Effect of quercetin on the transcripts of GP in HT29 cells after 6h and 24h

BGP (6h)

Sample	Detector	Avg delta Ct	delta Ct SD	delta delta Ct	RQ	RQ Min	RQ Max
DMSO	brainGP	1.5282803	0.0420414	0	1	0.8541997	1.1706865
Quercetin 20 µM	brainGP	2.0272703	0.0145153	0.4989901	0.707602	0.6701299	0.7471694
Quercetin 80 µM	brainGP	2.1276217	0.0318624	0.5993414	0.6600552	0.5857474	0.7437896

LGP (6h)

Sample	Detector	Avg delta Ct	delta Ct SD	delta delta Ct	RQ	RQ Min	RQ Max
DMSO	liverGP	5.684272	0.0598348	0	1	0.7990847	1.2514318
Quercetin 20 µM	liverGP	6.376072	0.0520099	0.6918001	0.6190809	0.5094232	0.7523434
Quercetin 80 µM	liverGP	6.454685	0.0700565	0.7704134	0.5862495	0.4508531	0.7623069

BGP (24h)

Sample	Detector	Avg delta Ct	delta Ct SD	delta delta Ct	RQ	RQ Min	RQ Max
DMSO	brainGP	-0.6399727	0.1042912	0	1	0.7256079	1.3781548
Quercetin 20 µM	brainGP	-0.35392252	0.0212563	0.2860502	0.8201444	0.7682437	0.8755513
Quercetin 80 µM	brainGP	0.68417484	0.0256467	1.3241475	0.3993851	0.3690937	0.4321626

LGP (24h)

Sample	Detector	Avg delta Ct	delta Ct SD	delta delta Ct	RQ	RQ Min	RQ Max
DMSO	liverGP	4.2677255	0.0856001	0	1	0.768541	1.3011668
Quercetin 20 µM	liverGP	4.5688796	0.0333818	0.3011541	0.8116029	0.7324143	0.8993534
Quercetin 80 µM	liverGP	4.9842224	0.0769121	0.7164969	0.6085733	0.4803793	0.7709774

Data to figure 52A: Effect of EGCG transcripts of GP after 6h and 24h in HepG2 cells

BGP (6h)

Sample	Detector	Avg delta Ct	delta Ct SD	delta delta Ct	RQ	RQ Min	RQ Max
EGCG 1 µM	brainGP	3.6636543	0.0138274	0.1404636	0.9072276	0.8694557	0.9466404
EGCG 10 µM	brainGP	3.9738548	0.021393	0.450664	0.731706	0.6851138	0.7814667

LGP (6h)

Sample	Detector	Avg delta Ct	delta Ct SD	delta delta Ct	RQ	RQ Min	RQ Max
EGCG 1 µM	liverGP	3.7452633	0.0436748	0.3037255	0.8101576	0.7083284	0.9266259
EGCG 10 µM	liverGP	3.997619	0.0547063	0.5560811	0.6801472	0.5748224	0.8047707

BGP (24h)

Sample	Detector	Avg delta Ct	delta Ct SD	delta delta Ct	RQ	RQ Min	RQ Max
EGCG 1 µM	brainGP	5.1508718	0.0207906	0.0103531	0.9928495	0.9313527	1.0584068
EGCG 10 µM	brainGP	5.1525016	0.0145723	0.0119829	0.9917285	0.9482635	1.0371858

LGP (24h)

Sample	Detector	Avg delta Ct	delta Ct SD	delta delta Ct	RQ	RQ Min	RQ Max
EGCG 1 µM	liverGP	4.5118995	0.059023	-0.0086336	1.0060023	0.8390042	1.2062403
EGCG 10 µM	liverGP	4.889883	0.0422467	0.36935	0.7741312	0.6798095	0.8815399

Data to figure 52B: Effect of quercetin transcripts of GP after 6h and 24h in HepG2 cells

BGP (6h)

Sample	Detector	Avg delta Ct	delta Ct SD	delta delta Ct	RQ	RQ Min	RQ Max
Quercetin 20 µM	brainGP	3.6179874	0.0192113	0.0947967	0.9364042	0.8826805	0.9933978
Quercetin 80 µM	brainGP	3.9213207	0.013254	0.3981299	0.7588413	0.7285311	0.7904125

LGP (6h)

Sample	Detector	Avg delta Ct	delta Ct SD	delta delta Ct	RQ	RQ Min	RQ Max
Quercetin 20 µM	liverGP	3.745807	0.0620275	0.3042691	0.8098524	0.6692033	0.9800624
Quercetin 80 µM	liverGP	4.159971	0.0343441	0.7184334	0.607757	0.546837	0.6754639

BGP (24h)

Sample	Detector	Avg delta Ct	delta Ct SD	delta delta Ct	RQ	RQ Min	RQ Max
Quercetin 20 µM	brainGP	5.1762433	0.0170076	0.0357246	0.9755417	0.9258259	1.027927
Quercetin 80 µM	brainGP	4.909824	0.0417644	-0.2306948	1.1733999	1.0319599	1.3342255

LGP (24h)

Sample	Detector	Avg delta Ct	delta Ct SD	delta delta Ct	RQ	RQ Min	RQ Max
Quercetin 20 µM	liverGP	5.0131946	0.0528406	0.4926615	0.7107128	0.6041112	0.8361253
Quercetin 80 µM	liverGP	6.0932884	0.0690807	1.5727553	0.3361658	0.2718222	0.4157402

8.9 Effect on cellular Glycogen

Data to figure 53: Effect of EGCG and SB216763 on total GS

DMSO

Date	0.5h	1h	3h	6h	12h	24h
27.04.06						97.80
						102.20
11.05.06		99.65		95.00	87.13	
		100.35		105.00	112.87	
18.05.06		85.00	90.00	95.00	112.00	
		115.00	110.00	105.00	88.00	
24.05.06	95.00	95.00	94.00			
	105.00	105.00	106.00			
01.06.06	97.00	99.00	99.00	99.30	95.00	97.00
	103.00	101.00	101.00	100.70	105.00	103.00
14.06.06	98.70	99.10	99.70	98.50		99.70
	102.30	100.90	100.30	101.50		100.30
21.06.06		92.00				
		108.00				
28.06.06	98.10	95.00				
	100.90	105.00				
MW	**100.00**	**100.00**	**100.00**	**100.00**	**100.00**	**100.00**
SD	**3.15**	**6.98**	**5.85**	**3.63**	**10.56**	**2.15**
n	8.00	14.00	8.00	8.00	6.00	6.00

EGCG 25 µM

Date	0.5h	1h	3h	6h	12h	24h
27.04.06						47.40
05.05.06						67.30
11.05.06						
		94.10		94.90	79.70	
18.05.06						
			88.50	72.00	81.60	
01.06.06						
	105.00	112.00	113.00	96.70	72.90	68.70
14.06.06						
	98.50	82.00	91.10	115.00		85.50
21.06.06						
		108.00				
28.06.06						
	92.40	124.00				
MW	**98.63**	**104.02**	**97.53**	**94.65**	**78.07**	**67.23**
SD	**5.14**	**14.57**	**10.99**	**15.26**	**3.73**	**13.50**
n	3.00	5.00	3.00	4.00	3.00	4.00

SB216763 10µM

Date	0.5h	1h	3h	6h	12h	24h
27.04.06						
						456.50
05.05.06						
						453.00
11.05.06				151.50	218.10	
18.05.06		109.00	146.00	169.50	264.80	
24.05.06	112.80	109.20	174.00			
01.06.06						
	105.00	128.00	134.00		241.00	387.00
14.06.06						
	106.00		159.00	214.00		
MW	**107.93**	**115.40**	**153.25**	**178.33**	**241.30**	**432.17**
SD	**3.47**	**8.91**	**14.89**	**26.27**	**19.07**	**31.97**
n	3.00	3.00	4.00	3.00	3.00	3.00

8.10 Acknowledgments

I would like to express my profound gratitude to the following persons without whom I would not be doing what I am doing today. My family, Papa, Mami, Winie, Bri (your fighter spirit got me to Germany), shushu, Tsi, Tang, Kia, Yo and Joy. When times were hard and I thought I will not make it, the memory of you kept me going.

To you Beri my deepest gratitude. This last year would have been a disaster for me if I did not have you.

I would like to give thanks to Gudrun Pahlke, Prof. Eisenbrand, Prof. Marko and Sandra Jakobs.

Special thanks to the entire family of AG Eisenbrand. Personally I would like to thank Bülent Soyalan, Jochen Zeller and Tamara Weisel, Manuela Goettel and Yvonne Fery for their friendship.

8.11 Curriculum Vitae

PERSONAL DATA

Yufanyi Ngiewih

Born on 30.10.75 in Buea-Fako, Cameroon

Single

SCHOOL CAREER

1983 - 1987	Primary education at the Anglo Arabic Primary School, Bamenda, Cameroon
1987 - 1992	Secondary school education at the Presbyterian Secondary School Mankon (PSS-Mankon), Bamenda, Cameroon
1992-1995	High school education at CASST Bambili and Longla Comprehensive College Mankon, Cameroon

12/1995-10/1997	Human rights activist and member of the Human Rights Defence Group Bamenda, Cameroon
01/1996-01/1997	Preparations for further studies in Germany.
	SUNCOM german language school, Bamenda, Cameroon (Basic- and intermediate level)

UNIVERSITY STUDIES

01/1998-06/1998	German language school at the University of Clausthal“
1998 - 2004	Food chemistry studies at University of Kaiserslautern
10/1998 - 04/2001	Introductory studies in food chemistry, analytical chemistry, biochemistry, anorganic and organic chemistry
12.04.2001	Intermediate state’s Examination
04/2001 - 04/2004	Advanced studies in food chemistry
10/2001-04/2004	Student dogsbody „Institut für Verbundwerkstoffe GmbH Kaiserslautern, Germany“
01/2003-03/2003	Research Internship at the faculty of food chemistry and environmental toxicology, Kaiserslautern, Germany “Influence of selected flavonoids and pteridines on the activity of enzymes of the PDE family”
13.05.2004	Completion of studies in Food chemistry (GPA 1+)
	Diploma Thesis in the department “Molekulare Ernährungsforschung” supervised by Prof. Doris Marko “Effect of Apple components on the gene expression in human cancer cells. (Grade 1 +)

From 05/2004 — Doctoral Thesis at the University of Kaiserslautern "Effect of selected flavonoids and polyphenols on key elements involved in the regulation of the glucose/glycogen homeostasis and the Wnt signalling pathway"

Supervisor: Prof. Dr. Gerhard Eisenbrand Faculty of Chemistry, Department of Food Chemistry and Environmental Toxicology

04/2006-12/2006 — Scholarship granted by the state of Rhineland Palatinate for excellent scientific work "Stipendium im Rahmen des Exzellenz-förderungsprogramms des Landes Rheinland-Pfalz"

8.12 Formulae

y-axis intercept

$$A = \frac{\left(\sum_i y_i\right)\left(\sum_i x_i^2\right) - \left(\sum_i x_i\right)\left(\sum\left(x_i \cdot y_i\right)\right)}{N}$$

Error of y- axis intercept (m_A):

$$m_A = \sqrt{\frac{S\sum_i x_i^2}{(n-2)N}}$$

Slope (B):

$$B = \frac{n\sum_i \left(x_i \cdot y_i\right) - \left(\sum_i x_i\right)\left(\sum_i y_i\right)}{N}$$

Denominator (N):

$$N = \sum_i x_i^2 - \left(\sum_i x_i\right)^2$$

Error of slope (m_B):

$$m_B = \sqrt{\frac{nS}{(n-2)N}}$$

Square sum of error (S): $S = \sum_{i=1}^{n} (y_i - Bx_i - A)^2$

IC_{50}-value: $IC_{50} = \frac{50 - A}{B}$

Error of IC_{50}-value (m_{IC50}): $m_{IC50} = \sqrt{\left(-\frac{1}{B}\right)^2 \cdot (m_A)^2 + \left(\frac{A-50}{B^2}\right)^2 \cdot (m_B)^2}$

Arithmetic mean ($\bar{x}$): $\bar{x} = \frac{\sum_i x_i}{n}$

Standard deviation (σ_{n-1}): $\sigma_{n-1} = \pm\sqrt{\frac{1}{n-1} \cdot \sum_{i=1}^{n} \left(x_i - \bar{x}\right)^2}$

Nalimov outlier: $r = \frac{x^* - \bar{x}}{\sigma_{n-1}} \cdot \sqrt{\frac{n}{n-1}}$ x^*: Testvalue

Outlier criteria :x* = outlier when r >

1.409 at n = 3
1.645 bei n = 4
1.757 bei n = 5
1.814 bei n = 6
1.848 bei n = 7
1.870 bei n = 8

Comparative Ct method: $2^{-[delta][delta]Ct}$

[delta][delta]Ct = [delta]Ct of sample - [delta]Ct of reference